National Library of Canada
Canadian Theses Service
Ottawa, Canada
K1A 0N4

Bibliothèque nationale du Canada
Services des thèses canadiennes

CANADIAN THESES

THÈSES CANADIENNES

NOTICE

The quality of this microfiche is heavily dependent upon the quality of the original thesis submitted for microfilming. Every effort has been made to ensure the highest quality of reproduction possible.

If pages are missing, contact the university which granted the degree.

Some pages may have indistinct print especially if the original pages were typed with a poor typewriter ribbon or if the university sent us an inferior photocopy.

Previously copyrighted materials (journal articles, published tests, etc.) are not filmed.

Reproduction in full or in part of this film is governed by the Canadian Copyright Act, R.S.C. 1970, c. C-30.

AVIS

La qualité de cette microfiche dépend grandement de la qualité de la thèse soumise au microfilmage. Nous avons tout fait pour assurer une qualité supérieure de reproduction.

S'il manque des pages, veuillez communiquer avec l'université qui a conféré le grade.

La qualité d'impression de certaines pages peut laisser à désirer, surtout si les pages originales ont été dactylographiées à l'aide d'un ruban usé ou si l'université nous a fait parvenir une photocopie de qualité inférieure.

Les documents qui font déjà l'objet d'un droit d'auteur (articles de revue, examens publiés, etc.) ne sont pas microfilmés.

La reproduction, même partielle, de ce microfilm est soumise à la Loi canadienne sur le droit d'auteur, SRC 1970, c. C-30.

THIS DISSERTATION
HAS BEEN MICROFILMED
EXACTLY AS RECEIVED

LA THÈSE A ÉTÉ
MICROFILMÉE TELLE QUE
NOUS L'AVONS REÇUE

NL-339 (r.86/06)

Canada

POOLE FRENKEL CONDUCTION IN ANODIC TANTALUM PENTOXIDE

submitted in partial fulfilment of the requirements of a doctorate degree in experimental solid state physics at the University of Ottawa

by Carla J. Miner

1985

© Carla J. Miner, Ottawa, Ganada, 1986.

Permission has been granted to the National Library of Canada to microfilm this thesis and to lend or sell copies of the film.

The author (copyright owner) has reserved other publication rights, and neither the thesis nor extensive extracts from it may be printed or otherwise reproduced without his/her written permission.

L'autorisation a été accordée à la Bibliothèque nationale du Canada de microfilmer cette thèse et de prêter ou de vendre des exemplaires du film.

L'auteur (titulaire du droit d'auteur) se réserve les autres droits de publication; ni la thèse ni de longs extraits de celle-ci ne doivent être imprimés ou autrement reproduits sans son autorisation écrite.

ISBN 0-315-30971-7

TABLE OF CONTENTS

	page
Abstract	i
Preface	ii
Acknowledgements	iv
Table of Symbols	vi
List of Tables and Figures	x
PART I - BACKGROUND	
1. Anodic Oxide Films : An Introduction	1
2. Alternate Conduction Models	13
Contact Limited Conduction : Schottky Barriers	18
Space Charge Limited Conduction	29
Hopping Conduction	42
PART II - THEORY	
1. Poole Frenkel Conduction Theory	59
2. Definition of Experimental Goals	87
PART III - EXPERIMENTS	
1. Sample Preparation and Measurement Techniques	92
2. Results	
The Effect of Device Area	102
The Effect of Oxide Thickness	104
The Effect of Dielectric Constant	107
The Effect of Heat Treatments	115
Current - Voltage - Temperature Behavior	118
3. Summary of Results	126
PART IV - DISCUSSION	
1. Extensions to the Theory	129
2. Intermediately Compensated Donors	130
3. Spatially Non-Uniform Donors	146
4. Conclusions	157
Appendix - The Finite Difference Algorithm	159
References	165

POOLE FRENKEL CONDUCTION IN ANODIC TANTALUM PENTOXIDE FILMS

Abstract:

The current-voltage-temperature (I-V-T) behavior of anodic tantalum pentoxide films was studied as a function of the physical properties of the oxide. Oxide thickness was varied by controlling anodizing conditions, and the oxide dielectric constant was varied by incorporation of nitrogen. A third property, device area, was photolithographically defined. Finally, the absolute level of conductivity was changed by heating the anodized oxide in vacuum or under a reducing atmosphere. While agreement could be obtained between the predictions of standard Poole-Frenkel theory and the I-V behavior observed at any one temperature with the use of arbitrary constants, agreement could not be obtained over a range of temperatures without significant temperature variation in the physical properties of the oxide such as the dielectric constant. The anomalous temperature behavior was explained by extending Poole Frenkel theory to include a transition from uncompensated to partially compensated donor statistics at a critical temperature. The theory was also extended to include spatially nonuniform donor distributions, and thus was able to explain the observed asymmetry in current with respect to zero bias.

PREFACE

This thesis describes a study of conduction in anodic tantalum pentoxide films. Since amorphous thin film oxides have peculiarities all their own, a brief introduction to the factors controlling conduction is given in Part I, section 1. The goal of the investigation was to determine which conduction process was responsible for the dramatic current-voltage (I-V) non-linearity observed for electric field strengths between 10^6 V/m and 10^8 V/m. Included in Part I, section 2 is a summary of the proposed mechanisms other than Poole Frenkel conduction.

Preliminary results indicated that the non-linearity could best be described by the Poole Frenkel theory. The model is based on field assisted ionization of localized impurity states in the band gap. A detailed description of Poole Frenkel conduction comprises Part II. It is necessary to examine the model, in its simple and various modified forms, for its applicability to the anodic oxide device. In the concluding section of Part II, a sequence of experiments is proposed to test the model.

The results of those tests are documented in Part III, along with a description of the measurement and analysis techniques. In Part IV the results are discussed. The major conclusion is that Poole Frenkel theory, as it is presently used, does not adequately describe all of the observed behavior. Specifically, the magnitude of non-linearity as a function of temperature

cannot be reconciled with the measured electrical and optical properties of the oxide. In addition, there is no provision in the model for the degree of I-V asymmetry with respect to zero bias that is observed in some samples.

In ~~Part~~ IV, section 2, it is shown that the two presently used forms of Poole Frenkel theory are valid for certain temperature and doping conditions. The anomalous temperature dependence of I-V behavior shown by the samples studied is evidence of a transition between the two. This analysis allows a physical interpretation of the mechanisms by which nitrogen incorporation and heat treatments affect conduction.

In Part IV, section 3, a model based on spatially non-uniform donor distributions is proposed to account for the I-V asymmetry. Numerical simulations are employed to show that the predictions of the model are consistent with the observed behavior.

ACKNOWLEDGEMENTS

Most of the experiments reported in this work were performed in the Advanced Technology Laboratory of Bell-Northern Research in support of a program to create a new liquid crystal messaging terminal. To multiplex such a display, the voltage contrast threshold of the individual liquid crystal picture elements must be sharpened. Previous research had shown that this would be possible if each picture element were connected to a device with non-linear current-voltage (I-V) characteristics. My main responsibility to the program was to determine the causes and methods of control of I-V non-linearity in the devices proposed for use in these liquid crystal displays.

It is a pleasure to acknowledge two members of the project team with whom I shared the responsibility for the preparation of the devices: Mr. Blair MacLaurin, and Mr. Grant Este. I also wish to acknowledge the contribution of Dr. David Smith of the University of British Columbia, who measured the oxide thickness and index of refraction using the ellipsometer of the Electrical Engineering Department. Special thanks are due to my managers over the course of the project: Dr. David R. Baraff and Dr. Richard W. Streater, for their encouragement and support, and for providing a work environment conducive to research. Much credit is also due Dr. William D. Westwood, who, besides being an invaluable source of information concerning thin films in general

and tantalum thin films in particular, asked the question that proved to be central to this thesis: namely, "What is meant by intermediate compensation?". I would also like to thank Bell-Northern Research for providing me with a post graduate award to enable the completion of this work on a full time basis.

Finally, I must express my loving thanks to my husband Bob and my son Glen for their (usually) uncomplaining forbearance of the consequences of part-time wife and mother.

TABLE OF SYMBOLS

A, a_i, B, b_i, c_i, C, d_i - numerical constants

a - nearest neighbour spacing

A^* - Richardson constant (defined on page 20-21)

c - hop length correction constant (page 47)

D - diffusion coefficient

$\overline{D}$ - electric displacement vector

d - insulator thickness

E - energy

E_c - conduction band energy

E_d - donor (or dopant) energy

E_F - Fermi energy

E_t - trap energy

E_v - valence band energy

f - probability function (used on page 65)

g - ground state degeneracy of an impurity level

h - Planck's constant ($\hbar = h/2\pi$)

h - mesh spacing for numerical simulation

I - current

J - current density

$\mathcal{J}$ - Jonscher's normalized "current" (page 80)

K_{sch} - Schottky conductivity coefficient (page 22)

K_H - Hopping conductivity coefficient (page 47)

K_{pf} or K - Poole Frenkel conductivity coefficient (pages 74-75)

k - Boltzmann constant

m - exponent of r in expressions of E(r) (page 68)

m - specific x value in numerical simulation (eg. mid point)

m_o - free electron mass

TABLE OF SYMBOLS

m^* - effective electron mass

$\hat{n}$ - index of refraction

n - free electron carrier density

n_a - density of unionized acceptors

N_a - total density of acceptors

N_c - conduction band effective density of states

N_c' - effective conduction band density of states (page 31)

n_d - density of unionized donors

N_d - total density of donors

N_d^+ - density of ionized donors

n_{ex} - extrapolated zero bias carrier density (page 137)

n_i - density of traps

n_k - normalizing carrier density (pages 74-75)

n_o - density of Poole Frenkel carriers at zero bias

N_o - constant n_o which is independent of x

n_t - density of occupied traps

N_t - total density of traps

N_t^* - characteristic trap energy density (page 33)

$n_t(E)$ - density of traps / energy (page 33)

$N(E_F)$ - density of electron states at the Fermi energy level

p - density of holes

P - pressure

$\vec{P}$ - dipole moment

$P(\xi)$ - probability of electron emission from donor

q - electronic charge

q_i - ion coordinates

R - hop length

TABLE OF SYMBOLS

r - generalized 3-D radial coordinate

r_{eff} - radial position such that $E_t = E_c - \zeta_{th}$

r_o - shielding length of the Yukawa potential (page 67)

r_p - radial position of the Coulombic potential barrier peak

s - normalized temperature in SCLC theory (page 33)

$s(b)$ - exponent in variable range hopping (page 47)

T - temperature

t, t_i - elapsed time, characteristic times (page 34)

T_g - defect formation temperature (c.f. glass temperature)

T_f - characteristic temperature in SCLC theory (page 33)

T_c - critical temperature (Figure <7>, page 46)

T_o - normalizing temperature in hopping theory (page 46)

u_o - disorder parameter (page 49)

v - electron drift velocity

v_{sat} - saturated electron drift velocity

V - voltage

V_c - crossover voltage (page 30)

V_n - $(E_c - E_F)/q$

V_{in} - in built or internal voltage drop

w - depletion layer thickness

W_D - energy difference between trap states

W_H - hopping activation energy

W_p - polaron hopping energy

x,y,z - generalized coordinates

α - field induced energy barrier lowering (page 62)

β_{sch} - Schottky nonlinearity coefficient (page 22)

β_{pf} or β - Poole Frenkel nonlinearity coefficient (pages 74-75)

TABLE OF SYMBOLS

γ - compensation index (page 75)

δ - Jonscher's normalized "electric field" (page 80)

ϵ - dielectric constant

ϵ_o - permittivity of free space

ζ_a - activation energy

ζ_d - $E_c - E_d$ (i.e. donor energy depth)

ζ_{do} - zero bias ζ_d

ζ_{eff} - effective activation energy (page 63-64)

ζ_t - $E_c - E_t$ (i.e. trap energy depth)

ζ_{th} - thermal energy (i.e. kT)

η - rate of decay of impurity state wave function (page 44)

θ - angle or n/n_t in SCLC theory (page 32)

θ_D - Debye temperature

μ - mobility

ν - frequency (e.g. an attempt to escape frequency)

ξ - electric field

ρ - space charge density

σ - conductivity

τ - carrier lifetime

ϕ - potential barrier

ϕ_m - metal work function

ϕ_o - zero bias potential barrier

χ - electron affinity

ψ - potential

ω - angular frequency

List of Tables and Figures

TABLES

		page
I	Experimental Evidence for Schottky Conduction	28
II	Experimental Evidence for Space Charge Limited Conduction	41
III	Experimental Evidence for Hopping Conduction	58
IV	Experimental Evidence for Poole Frenkel Conduction	85
V	Comparison of Proposed Conduction Formulae	91
VI	Summary of X-Ray Analysis of N_2 Doped Tantalum Films	109
VII	Optical Properties of Anodic Films on N_2 Doped Tantalum	114
VIII	Poole Frenkel Coefficients of Anodic Films on N_2 Doped Ta	114
IX	Summary of Hopping Analysis of Anodic Films on N_2 Doped Ta	114
X	Summary of Poole Frenkel Analysis	145

FIGURES

		after page
<1>	Energy Band Diagram of Metal Semiconductor Contact	18
<2>	Energy Barrier Lowering in Metal Semiconductor Contacts	21
<3>	Theoretical Schottky to Poole Frenkel J-V Transition	23
<4>	Theoretical SCLC to Schottky J-V Transition	24
<5>	Theoretical J-V Behavior for Various Forms of SCLC	33
<6>	Theoretical Current Transients Associated with SCLC	33
<7>	Temperature Dependence of Activation Energy in Hopping	46
<8>	Schematic of the Intra-site Transfer of a Polaron	51

<9> Energy Band Diagram of Poole Frenkel Potential Well 61

<10> Field Dependence of Different Emission Enhancement Ratios 63

<11> Schematic of Truncation Procedure of Ieda et al. 64

<12> Onsager.- Poole Frenkel Emission Enhancement Ratio 66

<13> Comparison of Proposed Models Fitted to J-V Data 87

<14> Outline of Sample Preparation Sequence 92

<15> Typical Anodizing I-V-t Characteristics 93

<16> Mask for I-V-T Test Pattern 95

<17> Mask for Area Test Pattern 95

<18> Typical Transients Seen in I-V Measurements 97

<19> Poole Frenkel Plot for Devices of Various Areas 100

<20> Observed Current as a Function of Device Area 102

<21> Oxide Thickness as a Function of Anodizing Voltage 104

<22> Poole Frenkel Plot for Devices of Various Thicknesses 104

<23> Variation of Poole Frenkel Coefficients with Thicknesses 104

<24> Hopping Analysis of Devices with Different Thicknesses 105

<25> SCLC Analysis of Devices with Various Thicknesses 106

<26> Reflectance Spectra of N_2 Doped Tantalum Oxides 110

<27> Poole Frenkel Analysis of Heat Treated Devices 116

<28> Hopping Analysis of Heat Treated Devices 118

<29> Hopping J-V-T Behavior of Unheated Oxides 119

<30> Hopping J-V-T Behavior of Vacuum Baked Oxides 119

<31> Hopping J-V-T Behavior of Hydrogen Annealed Oxides 119

<32> Temperature Dependence of Low Field Ohmic Conductance 119

<33> Temperature Dependence of Inferred Hop Length 121

<34> Variable Range Hopping Analysis of Ohmic Conductance 121

<35> Poole Frenkel Plot of Unheated Oxides 122

<36> Poole Frenkel Plot of Vacuum Baked Oxides 122

<37> Poole Frenkel Plot of Hydrogen Annealed Oxides 122

<38> Voltage Dependence of Activation Energy 123

<39> β-T Behavior of Unheated Oxides 125

<40> β-T Behavior of Vacuum Baked Oxides 125

<41> β-T Behavior of Hydrogen Annealed Oxides 125

<42> Temperature Dependence of Carrier Density 134

<43> K_{pf}-T Behavior of Unheated Oxides 136

<44> K_{pf}-T Behavior of Vacuum Baked Oxides 136

<45> K_{pf}-T Behavior of Hydrogen Annealed Oxides 136

<46> Voltage Dependence of Carrier Density 137

<47> Temperature Dependence of the Compensation Index 139

<48> Dependence of the Compensation Index on Acceptor Density 142

<49> Energy Band Diagram with Spatially Nonuniform Donors 150

<50> Calculated J-V Plot for Nonuniform Donor Distribution 156

<51> Flowchart of the Finite Difference Algorithm 163

PART I - BACKGROUND

1. ANODIC OXIDE FILMS : AN INTRODUCTION

Early in the development of the science of electrochemistry, it was discovered that if the anode in a simple water electrolysis cell was made from one of a limited number of metals, known as valve metals, oxygen evolution no longer occurred. Instead, uniform layers of oxide were built up on the anode. The name valve metal derives from the observation of strong current rectification in the manner of vacuum tube "valves", for the anodic oxides of Ta, Al, Nb, Zr, Hf and W. Anodic oxides are not restricted however, to these metals. Other metals such as Bi, Sb, Sn and Ti, and semiconductors such as Si, Ge, and GaAs also form stable anodic oxides provided care is exercised in the choice of an electrolyte in which the oxide is relatively insoluble. Thus the anodic oxide studied in this work, tantalum pentoxide, is only one member of a large family of technologically important materials. Likewise, the topic of electronic conduction is only one property among many that interest scientists working with anodic oxides. These other interests are covered in such standard texts as "Anodic Oxide Films" by L. Young (1), and "Electrochemistry at Semiconductor and Oxidized Metal Electrodes" by S. R. Morrison (2).

The intrinsic properties of anodic oxides contribute one main advantage and numerous limitations to a study of electronic

conduction. The advantage is the excellent uniformity of film properties, especially film thickness, as discussed in detail below. The limitations are also dicussed as the topic is progressively narrowed from thin films in general, to amorphous anodic tantalum pentoxide thin films in particular.

Anodic films are uniquely uniform due to the "self-healing" property of anodic film growth. During anodization, thin regions, which are consequently high field regions, experience rapid film growth until any asperity is smoothed out. The uniformity of such films can greatly exceed that attained by other thin film deposition techniques. For example, the intense interference colors of anodic Ta_2O_5 films appear uniform over large areas, as well as on a microscopic scale, even though the eye is capable of discerning changes in optical thickness as small as 10 nm. Because the electric field is nearly constant during oxide film growth, the absolute thickness of the oxide is controlled by the anodizing voltage, and to a lesser degree by the current density and electrolyte temperature (3). Thus for a particular parent metal, one speaks of an anodizing constant relating thickness to voltage. The anodizing constant for Ta for example, ranges from 1.52 to 1.94 nm/V, depending on the crystalline phase and impurity content of the parent metal (4). The ability to grow very thin, uniform films of known thickness is used as a tool, in fact, for sectioning metal samples (5). The enhanced control over material

properties afforded by the anodization process is also of great use in solid state research - especially in conduction studies such as this.

Properties of Thin Films :

Conduction in thin films differs on several points from that usually seen in bulk semiconductors. In the latter, current density is linearly related to electric field through a voltage independent resistivity. However, in films as thin as these (10 nm to 10 μm), high field effects are encountered even at reasonably low voltages. Resistivity becomes decidedly non-linear. In the samples discussed here it drops from a high of 10^7 ohm-m to a low of 10^4 ohm-m as electric field strength approaches the value present during anodizing. The small thickness of the samples and their high resistivity may also allow space charge regions to extend throughout the film's thickness, and thus modify conduction processes greatly (6). For example, current transients with time constants varying up to many minutes are frequently observed as a result of space charge effects (7). A conduction model, space charge limited current (SCLC) is commonly put forward to explain conduction behavior, and thus warrants closer examination in the following section. Electrode to electrode tunnelling will not be discussed since the films considered here are too thick (i.e. >10 nm) for this mechanism to be significant.

In addition, conduction in thin films differs from that in bulk semiconductors because the influence of surfaces is emphasized in the thin sample. To begin with, there are limitations on the theory of electron propagation which become significant in small specimens (8). Besides these geometric effects, one must consider that material parameters of thin films will not necessarily be the same as bulk values (9-11). Finally, as dimensions shrink, contacts become increasingly important. A contact controlled conduction model, Schottky emission, is also discussed in the following section.

Properties of Amorphous Thin Films :

Next, the amorphous nature of the anodic oxide must be taken into consideration. In the first place, it complicates the attempt to model behavior with theories developed for crystalline materials. Also, on the basis of thermodynamic arguments, it can be shown that amorphous materials are, at best, metastable (12). Slow, irreversible drift of characteristics is seen accompanying long term voltage stress (13) and temperature cycling (14). In some cases, there is evidence for a concurrent increase in crystallinity (15). This, too, must be considered in the design and implementation of conduction experiments.

Properties of Anodic Amorphous Thin Films

The anodic amorphous thin film is a system that compounds the idiosyncracies mentioned above with a few more derived from the method in which the film is made. Four features of anodic films are important to consider in a conduction model: 1) the inevitably large impurity level, 2) the frequent occurrence of flaws in the form of microscopic pores and fissures, 3) the possibility of stoichiometry variations throughout its thickness, and 4) the predisposition of these films to carry current ionically rather than electronically.

1) The predominant impurities in anodic films formed in aqueous electrolytes are water (or OH) (16) and to a lesser or greater degree, depending on anion size, the electrolyte itself (17). At one extreme, anodizing in phosphoric acid leads to considerable phosphorus incorporation in the outer half of the film as detected by Auger and XPS (X-ray Photoelectron Spectroscopy) profiling (18). The two halves show quite different chemical properties (e.g. etch rates) (19), structural properties (e.g. rates of recrystallization under electron beam irradiation) (20) and optical properties (e.g. optical constants) (21). To limit this effect, the films studied in this work were anodized in dilute citric acid. The large size of the citric acid anion is such that electrolyte incorporation is unlikely. Auger and SIMS (Secondary Ion Mass Spectroscopy) analysis did not detect a carbon component traceable to the electrolyte. Water, which was

likely present, would not be detected by this analysis technique.

Other impurities from the parent metal or surface contamination can enter the oxide during growth. Early work with bulk Ta foil (99.9% pure) was particularly susceptible to metallic impurities. References to the related effect of cleaning procedures on oxide resistivity can also be found (22). The work described here deals with oxides grown on Ta thin films sputtered from 99.999% pure targets and subsequently processed under clean room conditions.

2) A major concern with metallic impurities is their firmly established connection with flaws and anomalous conduction behavior (23-25). This is the second feature of anodic oxides to be considered. Vermilyea demonstrated flaw controlled conduction by electrochemically decorating current carrying filaments distributed across the sample (26). Recent work with high resolution TEM (Transmission Electron Microscopy) has confirmed the importance of much smaller defect sites (as small as 10 nm across) to catastrophic breakdown, and field induced recrystallization (20). Flaw conduction was shown to be responsible for the rectification that was previously thought to be characteristic of oxide coated valve metals (27). Surfaces polished prior to oxide growth (22) and counter electrodes evaporated at oblique angles (27) were shown to reduce leakage currents in accordance with a model of flaw dominated conductivity. The possibility of flaw conduction must be

recognized, and hopefully eliminated from the samples used before conduction models are examined. One must determine whether the observed conduction takes place uniformly through the whole film or only at local flaws where physical properties can be dramatically different from what can be measured macroscopically.

A series of tests were proposed (28) to identify nominally flaw free films: current density - voltage characteristics should be nearly symmetric with respect to zero bias, and should be independent of device area, and ambient moisture level. This last criterion arises from the historical use of gold as a counter electrode. This metal tends to bridge flaws in the oxide and reduce the effect of flaws on conduction, and yet leave a void into which water may penetrate and alter charge injection from the contact (28). Strongly adherent metallizations, as are used in this study, are not expected to be affected by atmospheric moisture in this way.

3) The third consequence of anodic oxidation is the belief that the film has a varying stoichiometry throughout its thickness (29). Tracer experiments determined that both the oxygen and the metal move from the respective interfaces to a line approximately in the center of the film where successive layers of oxide form (30). During anodization, both species of ions are en route through the stoichiometric oxide to the center line; when anodization is halted these ions are frozen in place. One expects that the outer layer is oxygen rich and the inner layer is oxygen

deficient. The effect can be reduced by holding the anodizing voltage constant until current density has dropped to levels associated with electronic conduction alone. This practice was observed in this work.

The variation in stoichiometry is expected to alter I-V behavior in the finished device. A conduction model described by Sasaki (31) claims that the variation is large enough for the formation of a p-i-n diode. The model proposed in this work relies on the existence of a spatially non-uniform donor density distribution, which may be related to the stoichiometry variations. The donor density distributions are studied by comparing the behavior of films seeing various heat treatments, which are thought to change the composition profile (32).

Concerning the final feature of anodic films, ionic conduction in its own right is a possibility since field strengths used for conductivity measurement may be as large as those used during anodization. Also anodization takes place at room temperature, but conductivity tests may be done at elevated temperatures where ionic conduction will be enhanced. One of the major sources of poor reproduciblity and long term drift in amorphous materials is thought to be ionic transport. The scope of this work does not include ionic processes. In these experiments, therefore, field strengths were kept relatively low, and electrical behavior was periodically checked against control samples which had not been voltage stressed up to that point.

Properties of Amorphous Anodic Tantalum Oxide Thin Films:

Restricting the topic under discussion to anodic tantalum pentoxide itself brings out a few more points that must be considered when comparing conduction data from various laboratories. Small differences in anodizing behavior and oxide properties such as index of refraction are noted when different phases of Ta are used (33). Bulk Ta foil is polycrystalline body centered cubic (b.c.c. or α-Ta) whereas sputtered and evaporated thin films may be b.c.c. or an impurity stabilized tetragonal phase, β-Ta (34). High oxide conductivity is often associated with sputtered b.c.c. films which tend to be highly stressed and exhibit poor film to substrate adhesion and high oxide flaw density (35,36).

Although, as noted before, metallic impurities in bulk Ta affect conductivity levels by introducing flaws, the bulk properties of the sputtered Ta film and its nominally flaw free anodic oxide may be altered by reactive sputtering. Intentional (or inadvertant) doping can occur by the incorporation of gases such as N_2, O_2, H_2, and CH_4, into the Ta during deposition, which then become part of the oxide during growth (37-39). Thus the cleanliness and base pressure of the sputtering system are important factors. Deliberate additions of N_2 into the sputtering atmosphere can lead to the deposition of nitrogen doped Ta, Ta_2N or TaN films and the subsequent growth of tantalum oxy-nitride

dielectrics. The procedure becomes a novel method of changing the oxide properties to test the conduction models proposed (40,41).

An additional experimental variable that affects conduction is the practice of heat treating the oxide after growth. This may operate by driving off water (42), inducing crystallinity (15), diffusing counter electrode material into the oxide (43), or modifying the Ta-Ta_2O_5 interface (14). This interface is normally abrupt in the anodic film. Physical analysis has shown that the interface width is less than 2 nm (44). In thermally grown oxides, the oxygen concentration decreases throughout the layer (45). It has been proposed by Smyth et al (14) that the interface in the thermally treated anodic oxide is substantially broadened. They attribute the latter to the propensity of tantalum to dissolve oxygen at elevated temperatures. This effect is reduced when thin films of tantalum or tantalum nitride are used, since their capacity to store the dissolved oxygen is reduced (38,39). The types of heat treatments reported vary from the nominally untreated films, to those with photolithographically defined counter electrodes (T_{max} = 150°C), to those which are baked under high vacuum, air or N_2 atmospheres at temperatures up to 400°C where crystallization begins. Here we report quantitative changes in impurity densities caused by vacuum baking (T_{max} = 150°C, P = 10^{-4} Pa), and hydrogen annealing (T_{max} = 350°C in flowing 10% H_2-N_2 mixtures).

From theoretical considerations it is clear that a contact

limited conduction process is more likely in a thin film than in a thick one. Therefore it would not be surprising if some conduction models apply to certain ranges of thicknesses and not to others. In the following section film thickness will be noted with any experimental observations from the literature. Film thickness is limited in anodic Ta_2O_5 by the onset of what is inaccurately known as field recrystallization. At that point current is diverted from the growth of normal amorphous oxide to breakdown sites where small crystallites form, and progressively displace the pre-existing oxide (46). Many reseachers study films which approach that thickness (approximately 500 nm), whereas the samples used here are nominally 50 nm thick.

Finally, because Ta_2O_5 has a large band gap and is amorphous, the density of states at the Fermi energy within the band gap may be non-zero. This can lead to various forms of hopping conduction (47) such as are dicussed in Part II.

Summary :

To conclude, the relatively simple fabrication and well controlled macroscopic properties of the anodic oxide makes it an attractive choice of subject matter in the study of conduction in amorphous materials. The thinness of the film allows the investigation of high field and space charge related phenomena. The possibility of interference from contact and surface related phenomena is recognized, as is the possibility of long term stability problems due to the amorphous nature of the film. An anodic oxide has unique properties derived from its method of growth: e.g. the high and variable impurity level, and a stoichiometry which may vary throughout the film thickness. Electronic conduction, representative of the oxide in general, must be distinguished from flaw dominated and ionic processes. The study is aided by the facility to modify conduction behavior in a controlled manner by 1) the choice on anodizing parameters, 2) the formation of doped oxides on reactively sputtered tantalum, and 3) the use of various heat treatments after growth.

2. ALTERNATIVE CONDUCTION MODELS

Previous Approaches:

Investigations of anodic oxides have usually been undertaken in the context of an intended application. For example, material aspects have been studied in conjunction with the use of these films as decorative or protective finishes (48). They have also been studied as a means by which thin film resistors may be trimmed and stabilized (49). More important is the wide use of anodic oxides of tantalum and aluminum in electronic devices. Some examples of these devices are capacitors (50), MOS structures (51-53), electroluminescent displays (54), and thin film transistors (55,56). Work in these areas has concentrated on reducing conduction and defects, and improving a-c dielectric properties. Thus capacitance and dissipation factor receive considerable attention in the literature.

This thesis addresses the high field conduction properties of anodic tantalum pentoxide, where current density rises rapidly with increasing voltage. Because the usefulness of many thin oxide devices is limited by excessive conduction in that regime, this topic has been dealt with in a number of theoretical and experimental papers. In contrast to earlier applications, however, the non-linearity of high field conduction in anodic tantalum oxide has recently become a desired attribute. Tantalum pentoxide MIM (Metal - Insulator - Metal) devices have been used

as non-linear resistors for threshold control in liquid crystal displays (57). Because the material used in this study has been optimized for the latter application, it should be noted that it has higher conductivity than the type of tantalum oxide generally described in the literature. Also note that some of the work cited in this section deals with gas phase anodized and sputtered Ta_2O_5, as well as other anodic oxides. The conduction behavior of SiO_x, a more distantly related amorphous oxide which is usually evaporated, is also described for comparison.

Conduction Models:

In this section three high field conduction models are discussed: contact limited conduction, space charge limited conduction, and hopping conduction. These are the main alternatives to the conduction model advocated here; namely Poole Frenkel theory. These are not competing models in the sense that one is right and the others are wrong, but rather each has a range of applicability depending on such parameters as oxide thickness, temperature, electric field strength, impurity density and contact characteristics. In general terms, the proposed models differ in one of three characteristics: mobility is either high and crystal like, or low and phonon assisted; conduction is either contact or bulk limited; and the charge carriers are either electrons or holes. Quantitative estimates of these physical properties of Ta_2O_5 vary widely depending on the

conduction model used to explain the observed behavior.

For example, a mobility of $2x10^{-11}m^2/V-s$ (58) has been estimated for Ta_2O_5 from a space charge limited conduction model, yet an interpretation of similar data based on Poole Frenkel theory has yielded a value of $7.5x10^{-3}m^2/V-s$ (59). Hall effect measurements would resolve the discrepancies. However, even if a sample could be made without the usual underlayer of unanodized Ta, conductivity is non-ohmic at the current levels necessary for Hall voltage measurement. To the author's knowledge, other techniques such as photo-Hall (60), EBIC (Electron Beam Induced Current)(61) or time of flight measurements (62) have not been attempted with Ta_2O_5. Theoretical approaches to estimating mobilities are severely hampered by the general lack of information about oxide band parameters. All that has been reported about Ta_2O_5, for instance, is its band gap of 4.6 eV (63,64). In amorphous materials the concept of a uniquely defined mobility and a band gap is replaced by that of the mobility gap (65). Over a narrow range of energies corresponding to the band edges in crystalline semiconductors, mobility drops precipitously from values comparable to the single crystal (i.e. $\mu > .001\ m^2/V-s$) to very low, but non-zero values in the gap (i.e. $\mu << .001\ m^2/V-s$). There is, therefore, a dichotomy among conduction models: those advocating low mobility transport via localized states in the gap without excitation to the conduction band, and those proposing activated processes with high mobility

transport through extended states in the conduction band. Both Poole Frenkel and Schottky conduction assume the latter condition, while hopping conduction is based on the former. Space charge limited conduction is often found in low mobility materials, but as such does not specify the mode of carrier transport.

Another distinction among the models is the importance attached to the contacts. If the current limiting step in conduction is the passage of charge carriers across a potential barrier at the interface, it is a fundamentally different problem from one where the resistance of the interior of the material dominates. The former should be sensitive to choice of electrode material, while the latter should have identical electrical behavior in both bias polarities. Unfortunately, these distinctions are not as clear as one would hope. The existence of surface states can pin the Fermi energy at a particular level irrespective of electrode material (66), while the symmetry of so-called bulk conduction assumes homogeneity throughout the dielectric, and the absence of internal electric fields, both questionable assumptions.

Unless otherwise noted, the dominant charge carrier is assumed to be the electron. While this is not an uncommon assumption, it should be noted that the matter has yet to be settled conclusively. As mentioned, Hall effect measurements of carrier type are not possible. Some supporting evidence is

present in the form of the cold cathode behavior of Ta_2O_5 in electroluminescent devices (54). Light emission is dependent on the injection of hot electrons from the oxide into the semiconductor. The energy distribution of these electrons has been reported recently by O'Clock and Feisil (67). Also, extensive scintillation studies of tantalum anodizing behavior near breakdown have led to a successful impact ionization theory, based on the assumption of electron injection from the electrolyte and rapid removal from the oxide (68). The model also requires holes to be deeply trapped and deduces from experimental data a hole mobility of $10^{-11} m^2/V\text{-}s$. Furthermore, short circuit photocurrent experiments by Hoenig reported by Thomas (69) point to electron conduction. On the basis of additional photoconductivity results, Thomas proposes a Fermi energy level 1.4 eV below the conduction band, and thus n type conductivity. In contrast, Gubanski and Hughes show that SCLC in Ta_2O_5 is strongly affected by choice of counter electrode material, and conclude that they are observing hole injection (70). This contradicted the previous SCLC data for Ta_2O_5. Both observations could be reconciled if like in Nb_2O_5 (71), hole and/or electron injection in Ta_2O_5 may also be favoured by certain sample preparation methods.

Contact Limited Conduction - Schottky Barriers

Theory of Barrier Formation:

The process of supply or extraction of charge carriers at the contacts may be the rate determining step in the passage of current from one electrode to the other (72). Interfacial potential barriers similar to that shown in Figure <1> can arise as a result of the thermodynamic requirement that the Fermi energies of the two materials align upon contact. This is accomplished by the transfer of electrons between the two; the flow being from the material with the lower work function (defined as the energy difference between the vacuum level and the Fermi level) to that with the higher work function. In the metal the work function is denoted $q\phi_m$, whereas in the insulator the work function is the sum of the electron affinity $q\chi$, and the separation of the Fermi energy and the conduction band, qV_n. The final position of the conduction band in the insulator with respect to the metal Fermi energy is directly related to the respective work functions and the density of surface states which can supply (or take up) a portion of the transfer electrons. Those electrons not coming from (or ending up in) the surface states are extracted from (or injected into) the bulk of the insulator forming a depletion (or accumulation) layer adjacent to the metal interface. The doping density of the insulator will determine how far the layer will extend into the bulk of the

Figure <1> Energy Band Diagram of Metal Semiconductor Contact

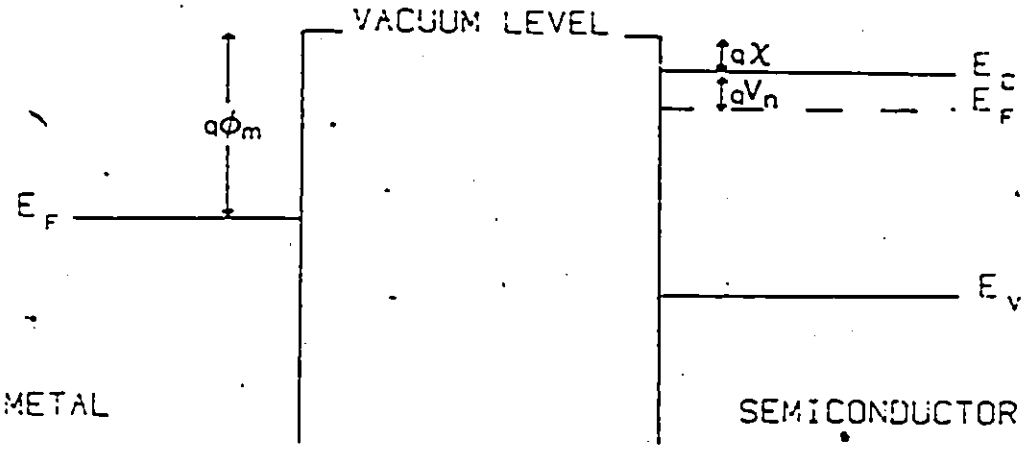

a) The vacuum levels of the metal and the semiconductor determine the relative positions of the Fermi energy level in each when the two are widely spaced.

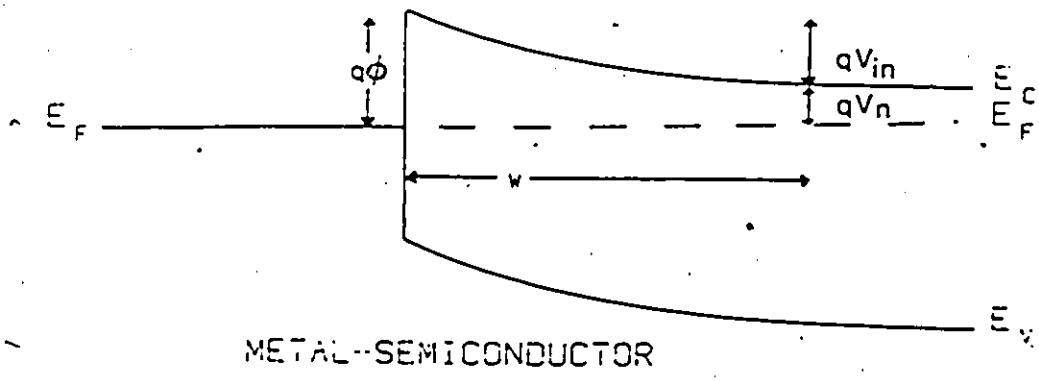

b) Upon contact, the Fermi energies align due to a flow of electrons from the material with the smallest work function into that with the largest work function. Thus, a potential barrier of height $q\phi = q(\phi_m - \chi)$ and a depletion region of width w are created.

insulator. In imperfect insulators with semiconductor-like doping densities the layer is a few tens of nanometers thick, whereas the very low carrier concentrations of normal insulators will often force this region to extend completely from one side of the sample to the other. This latter configuration is known as the Mott or punch-through Schottky barrier. The electric field, ξ, in the normal insulator sample is uniform and equal to the ratio of the sum of the applied voltage, V, plus the internal depletion voltage, V_{in}, (for dissimilar opposing contact metals) to sample thickness, d. i.e.

$$\xi = \frac{V + V_{in}}{d} \qquad <1>$$

In imperfect insulators and semiconductors, on the other hand, both the electric field, which has a maximum at the interface, and the depletion/accumulation layer thickness, w, increase with increasing reverse bias as given by: (72)

$$w = \sqrt{\frac{2\varepsilon\varepsilon_o}{q N_d} (V_{in} + V - kT/q)} \qquad <2>$$

and

$$\xi_{max} = \frac{2}{w} (V_{in} + V - kT/q)$$

$$= \sqrt{\frac{2q N_d}{\varepsilon\varepsilon_o} (V_{in} + V - kT/q)} \qquad <3>$$

where ε = high frequency dielectric constant

N_d = impurity density

T = temperature

The size and voltage dependence of this layer's width may be inferred from the bias behavior of capacitance. In extreme cases, insulators with large interfacial defect or impurity concentrations, and/or sufficiently high surface state densities, exhibit features of both the semiconductor-like depletion layer, which can quickly respond to changes in bias, and the normal insulator, whose carrier concentrations respond relatively slowly due to deep trapping and/or space charge effects. The combination can lead to some interesting history effects and other non-equilibrium behavior as described by Simmons and Nadkarni (73) that will not be considered here.

Current - Voltage - Temperature Behavior:

The emission of carriers over the barrier at the metal interface is analogous to the case of the well known vacuum diode. By considering the distribution of electrons in the metal with energies sufficient to surmount the barrier and trajectories in the appropriate direction, one arrives at the Richardson relationship between J, the current density and T, temperature. Modifications must be made in insulators and semiconductors to take into account the carrier effective mass (72).

Thus:

$$J = A^{*} T^{2} \exp(-q\phi/kT) \qquad \langle 4 \rangle$$

$$A^* = \frac{4\pi q m^* k^2}{h^3} \qquad \text{<5>}$$

where $q\phi$ is the barrier height

m^* is the effective mass

A^*, the effective Richardson coefficient, can be further adjusted to take into consideration quantum mechanical reflection, tunnelling probabilities, and optical phonon backscattering, but its value remains on the same order of magnitude as the free space value of 1.2×10^6 $A/(m^2K^2)$.

The current density - voltage behavior of the Schottky barrier is not immediately obvious in this expression because the barrier height is also voltage dependent. Consider the detailed Figure <2>. A carrier at a distance x from the interface experiences a force due to the depletion region field, any externally applied field, ξ, and an "image force" due to an induced charge located in the metal at -x. As shown in the figure, the fields have the net effect of lowering the barrier under appropriate bias conditions. The amount of barrier lowering is derived by differentiating an expression that gives the energy of the charge as a function of distance from the interface given by:

$$E(x) = E_c - \frac{q^2 x}{4\pi\varepsilon\varepsilon_o (2x)^2} - q\xi x \qquad \text{<6>}$$

Figure <2> Energy Barrier Lowering in Metal Semiconductor Contacts

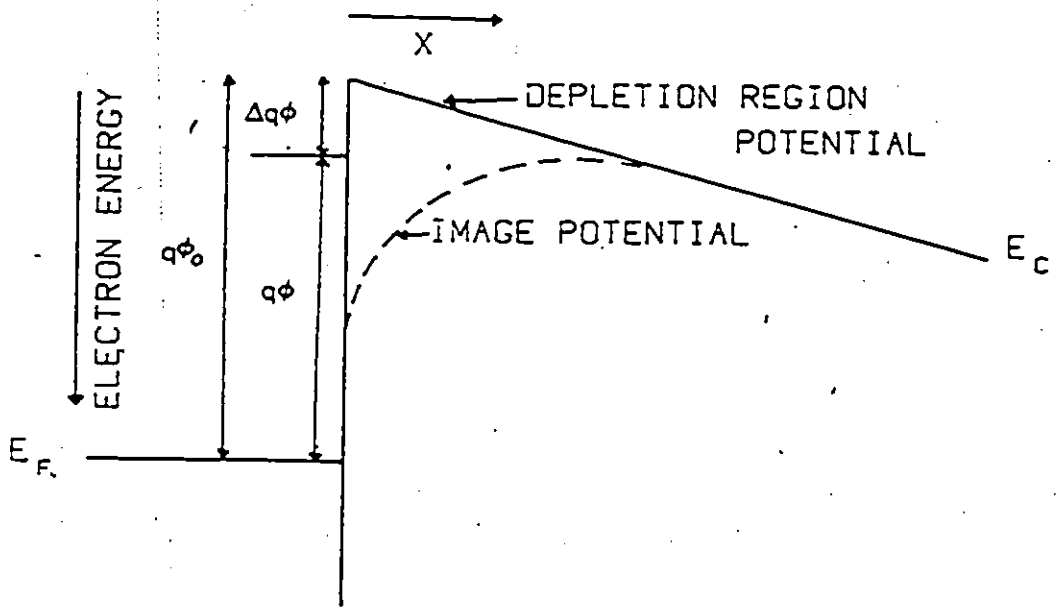

The detailed picture of the metal-semiconductor interface must take into account the image force arising from electrons in the metal which take up positions mirroring any fixed charges in the semiconductor depletion region. The potential energy for carriers in the semiconductor is the sum of the depletion region potential (approximately linear in x on this scale) and a Coulombic image force potential which varies as 1/x. The peak height of the barrier to current flow is reduced by an amount $\Delta q\phi$. An external applied field of the appropriate polarity increases the slope of the depletion potential, and in turn further lowers the interfacial barrier.

the energy has a maximum at

$$x = \sqrt{\frac{q}{16\pi\varepsilon\varepsilon_o\xi}} \qquad <7>$$

with the value

$$E_{max} = E_c - \sqrt{\frac{q^3\xi_{max}}{4\pi\varepsilon\varepsilon_o}} \qquad <8>$$

Since the $(E_c - E_{max})$ is equal to $\Delta q\phi$, equation <8> leads to the expanded J-ξ expression for both the Schottky barrier at the reversed biased imperfect insulator (semiconductor-like) metal contact of doping density N_d, and thickness d:

$$J = A^*T^2\exp(-\frac{q\phi_o}{kT})\exp\left[\frac{q}{kT}\sqrt{\frac{q\xi_{max}}{4\pi\varepsilon\varepsilon_o}}\right] \qquad <9>$$

$$= A^*T^2\exp(-\frac{q\phi_o}{kT})\exp\left[\frac{q}{kT}\sqrt{\frac{q}{4\pi\varepsilon\varepsilon_d}\sqrt{\frac{2qN_d(V_{in}+V-\frac{kT}{q})}{\varepsilon\varepsilon_o}}}\right]$$

and the punch-through barriet in normal insulators:

$$J = A^*T^2\exp(-\frac{q\phi_o}{kT})\exp\left[\frac{q}{kT}\sqrt{\frac{q\ (V_{in}+V)}{4\pi\varepsilon\varepsilon_o d}}\right] \qquad <10>$$

or recast in terms of current density, J, and voltage, V:

$$J = K_{sch}\exp(\beta_{sch}\sqrt{V}) \qquad <11>$$

where

$$K_{sch} = A^*T^2\exp(-\frac{q\phi_o}{kT}) \qquad <12>$$

and

$$\beta_{sch} = \frac{1}{kT}\sqrt{\frac{q^3}{4\pi\varepsilon\varepsilon_o d}} \qquad <13>$$

assuming V_{in} is small compared to V

Hybrid Theories:

Contact barriers surely exist in almost all metal-insulator-metal systems. It is apparent therefore that in a normal insulator the effects of the contacts are usually overshadowed by those of the highly resistive bulk. Occasionally for less resistive materials, narrow depletion layer contact barriers can form which have appreciable influence on the conductivity of the sample for certain ranges of voltages and temperatures. Simmons (74) examined in detail the theoretical characteristics of a metal-imperfect insulator-metal system where the resistances of the contacts and the bulk were similar. Current flow over the barrier followed the normal Schottky equation <9>, where the electric field was calculated to take into consideration the uneven division of the voltage between the contact and the bulk. He found that for low voltages, current rose very steeply with increasing bias when most of the voltage was dropped over the narrow depletion layers. At higher voltages the influence of the bulk became increasingly dominant until the J-V curves were essentially identical with normal Poole Frenkel curves. This is shown schematically in Figure <3>. There is a transition between a low field, thickness independent behavior to a high field Poole Frenkel behavior which is strongly dependent on sample thickness.

In a similar fashion Frank and Simmons (75) discussed the effect of space charge on contact controlled conduction. In the

Figure <3> Theoretical Schottky to Poole Frenkel J-V Transition

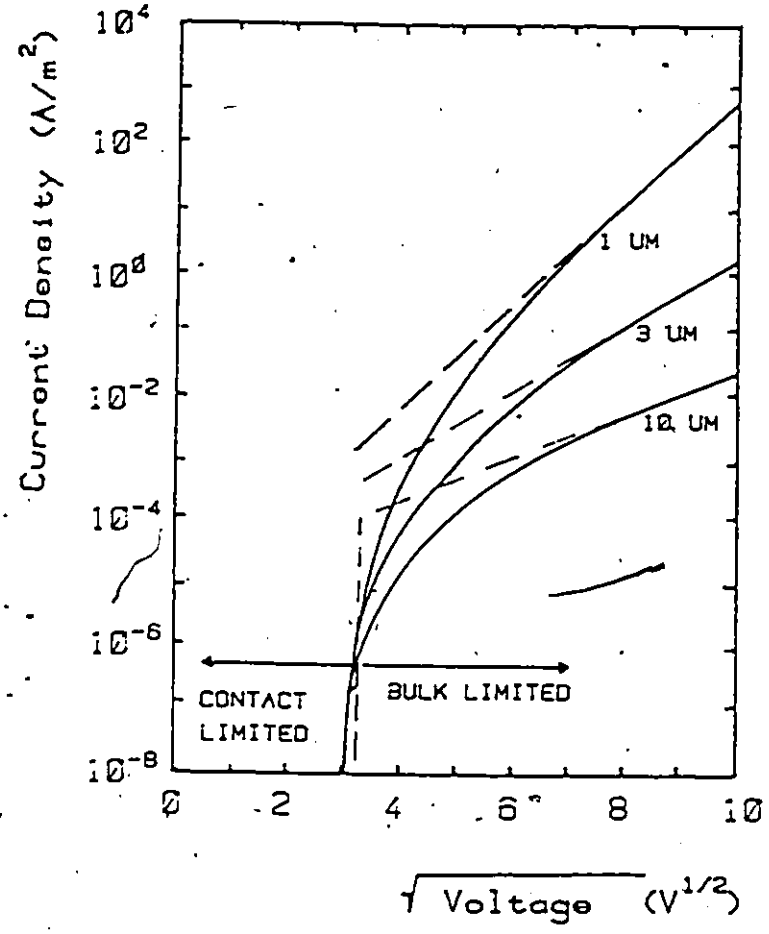

Plotted is the theoretical current density - voltage (J-V) behavior of metal-insulator-metal devices with three different insulator thicknesses, d. The low field behavior, for voltage below ~10 V is dominated by Schottky emission over a potential barrier at the cathode and is therefore independent of d. The high field behavior is dominated by Poole Frenkel emission from donors in the insulator bulk and exhibits an asymptotic slope proportional to $1/\sqrt{d}$ on this type of plot. From Simmons (74)

case where the work function of the metal contacts is less than that of the insulator, injecting contacts are formed. Current passes from one electrode to the other over a potential maximum in the interior which is also known as a virtual cathode. As current increases, the size of the accumulation region shrinks in accordance with SCLC (space charge limited conduction) theory. Eventually, the supply of carriers from the emitting contact is unable to keep up with the extraction of carriers from the accumulation region. At that point the virtual cathode becomes coincident with the real cathode and contact limited conduction takes over. The I-V curves for a variety of combinations of barrier heights, carrier mobilities and concentrations were calculated. The common features were a low voltage, bulk controlled regime where current rises steeply, and a high voltage, thickness independent regime which asymptotically approaches the usual Schottky behavior. A schematic diagram of the typical behavior is given in Figure <4>.

Pulfrey, Shousha and Young (76) made a theoretical study of conduction behavior for a range of insulator properties. They were able to identify major regions on a graph of current density versus the product of donor density and sample thickness where either Poole Frenkel, Schottky or space charge limited conduction dominated.

Figure <4> Theoretical SCLC to Schottky J-V Transition

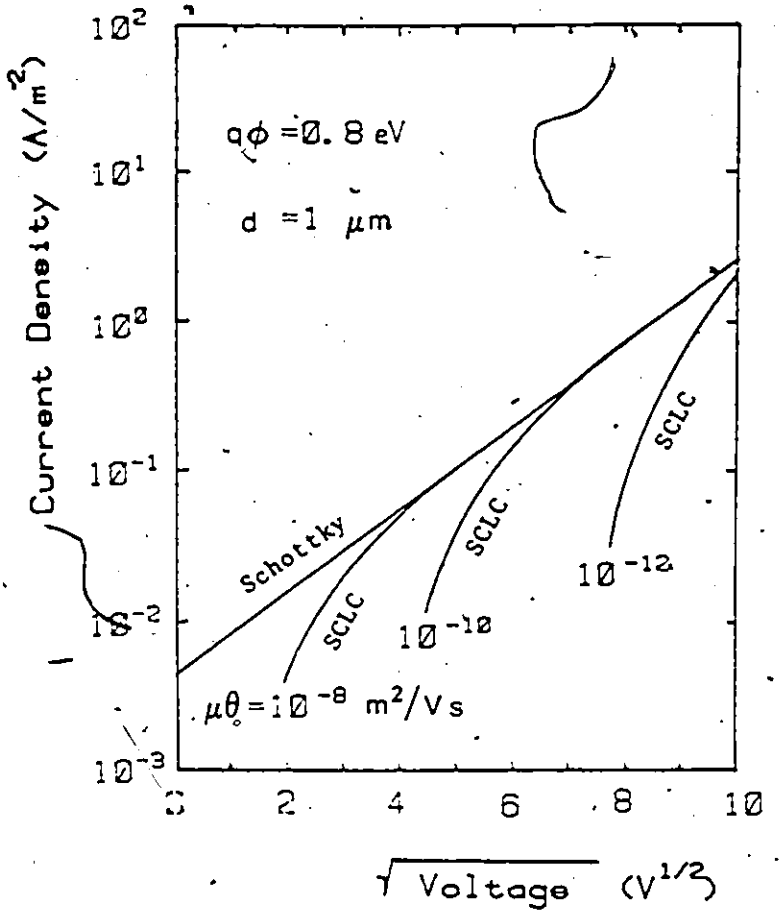

Plotted is the theoretical current density - voltage (J-V) behavior of 1 μm thick metal-insulator-metal devices showing a transition between space charge limited conduction (SCLC) at low voltages to Schottky emission over the interfacial barrier of height $q\phi$. When either mobility, μ, or the ratio of the densities of carriers to occupied traps, θ, is reduced the upper voltage limit of the SCLC dominated range increases. From Frank and Simmons (75)

Experimental Evidence:

Unambiguous identification of Schottky barrier controlled conduction is hampered by the close similarity of its I-V-T (current - voltage - temperature) behavior to that of Poole Frenkel conduction. Thus many experimental results, initially reported as exhibiting Schottky behavior have been subsequently re-interpreted as Poole Frenkel conduction and vice versa. Additional tests are required. For instance, if a strong contact work function dependence is established, then Poole Frenkel conduction can be ruled out. This has been done by Hacskalyo for very thin (2.7 to 8.3 nm) Al_2O_3 films with Zn, Sn and Au contacts (77). Flannery and Pollack have also compared I-V-T characteristics of very thin (2.4 nm) plasma anodized Ta_2O_5 films with Au contacts (78) with similar behavior reported by Namba on 14 nm thick, wet anodized Ta_2O_5 with Al contacts (79). Good agreement with the Schottky model was obtained. In addition, the values of the physical parameters estimated from low temperature tunnelling currents agreed with those derived from the high temperature Schottky curves. C.Mead, working with ZnO_1 was able to relate the voltage intercept on the ln(I) vs $\sqrt{V}$ curve to the theoretical contact potential difference (80).

Simmons' predicted transition from Schottky to Poole Frenkel I-V behavior upon increasing bias has been convincingly demonstrated in a number of systems. In SiO_x for instance,

Hartman, Blair and Bauer (81), Hirose and Wada (82), Inagaki, Adachi and Nitta (83), and Stuart (84,85) have presented data showing the characteristic steeply rising, thickness independent behavior at low bias, diverging into ln(I)vs $\sqrt{V}$ behavior with slopes dependent on thickness. In Ta_2O_5 the effect is more elusive. Matsumoto (86) presented a probable example, but only after subtracting the effects of a shunt resistance from the data. P.L.Young (87) on the other hand, only saw this phenomenon in abnormally conductive Ta_2O_5 films.

Less clear examples, with no corroborating work function evidence, can be tentatively assigned to Schottky conduction on the basis of three tests. First, the temperature dependence of the I-V characteristics should predict a barrier height consistent with that given another technique such as photoconductivity. Second, strong rectification should occur when dissimilar contacts are used. Third, punch-through conditions must be consistent with the doping levels and insulator thickness observed. Under these criteria, the rectifying 6 nm evaporated aluminum oxide sample of Antula (88) is probably exhibiting Schottky conduction. Antula was also able to show agreement with Schottky predictions on the changes in conductivity when a known quantity of dopant was electrochemically drawn into the film. Likewise, the thinnest of the Ta_2O_5 films studied by O'Clock (89) exhibited ln(I) vs $\sqrt{V}$ behavior that can be attributed to Schottky emission. Note that this was not the conclusion drawn in that

work. An error had been made in the value of the dielectric constant and the correct value does in fact give good agreement with theory.

As one final example, Pulfrey et al. (90) attributed the ln(I) vs $\sqrt{V}$ characteristics demonstrated by wet anodized Ta_2O_5 with Au or In contacts to Schottky conduction for the Ta positive polarity. The other polarity also showed ln(I) vs $\sqrt{V}$ behavior, but with a slope more in line with Poole Frenkel predictions. Interestingly, the application of a high voltage stress removed the rectification, increased conductivity by several orders of magnitude and the ln(I) vs $\sqrt{V}$ slope for both polarities became the "Schottky" value. As will be explained in a following section the nonrectifying behavior is more likely to be due to Poole Frenkel conduction. The re-interpretation of Pulfrey's and other workers' "Schottky" behavior will be discussed there.

Table I summarizes some of the experimental evidence for Schottky emission in insulators, emphasizing its predominance in thin films.

TABLE 1

Experimental Evidence for Schottky Conduction

DEVICE STRUCTURE	THICKNESS (nm)	EVIDENCE	REF.
$Ta-Ta_2O_5-Au$	2.4	J-V (Ta +ve)	78
$Al-Al_2O_3$ { Zn, Sn, Au }	2.7 to 8	J-V-Ø metal	77
$Si-Si_3N_4-Al$	8	J-V	91
Al-mica-Al	5	$Ø_{J-V}=Ø$ photo	92
Al { GeO_2-Al, Al_2O_3-Al, polymerized silicon oil-Au }	<10	J-V	93
Al-GaSe-Au (single crystal)	60	$Ø_{J-V}=Ø$ photo	94
$Al-Al_2O_3-Al$	6 and 17	J-V doping	88
$Ta-Ta_2O_5-Au$	9	J-V	89

PART I - BACKGROUND

Space Charge Limited Conduction

Theory:

One of the frequently called upon conduction models in the study of anodic oxide films is space charge limited conduction - SCLC. This model considers the injection of electrons and/or holes into the dielectric in a manner analogous to a vacuum diode. In this model, a limitless supply of carriers is available at one electrode. These are injected into the material until the space charge that is built up repels new additions of charge. The flow of current is therefore dependent on the balance between the injection rate, as determined by the voltage, and the extraction rate, as determined by the carrier mobility and insulator thickness. A much abbreviated summary of the results will be presented here as a basis for comparison with Poole Frenkel conduction. The interested reader is referred to the definitive work on the subject by Lampert and Mark (95) for the details.

The development of the I-V relationships for SCLC begins with the trap free insulator of thickness d, dielectric constant ϵ, carrier concentration n, and mobility μ. In later discussions, traps of varying energy depths, and then hole currents and recombination centers will be added. Neglecting diffusion currents, the relation between current density J and electric field ξ is given by:

$$J = n q \mu \xi \qquad \langle 14 \rangle$$

Poisson's equation gives us:

$$\vec{\nabla} \cdot \vec{D} = \rho(x,y,z) \qquad \text{<15>}$$

But for d c current conditions,

$$\vec{D} = \varepsilon\varepsilon_o\xi \qquad \text{<16>}$$

therefore, in one dimension

$$\frac{d\xi}{dx} = \frac{n(x)\,q}{\varepsilon\varepsilon_o} \qquad \text{<17>}$$

$$J = \varepsilon\varepsilon_o \frac{d\xi}{dx}\,\xi\mu \qquad \text{<18>}$$

Upon integration, with $\xi(0)=0$, we have:

$$\xi(x) = \sqrt{\frac{2\,J\,x}{\varepsilon\varepsilon_o\,\mu}} \qquad \text{<19>}$$

$$V(x) = \int_o^d \xi(x)\,dx = \sqrt{\frac{8\,J\,d^3}{9\varepsilon\varepsilon_o\mu}} \qquad \text{<20>}$$

$$J = \frac{9\varepsilon\varepsilon_o\mu V^2}{8\quad d^3} \qquad \text{<21>}$$

Note that below a threshold voltage the current density due to drift of thermally generated carriers, n_o, i.e. the ohmic component, overshadows the SCLC component. Setting the two components equal,

$$J = \frac{q\mu n_o V_c}{d} = \frac{9\varepsilon\varepsilon_o\mu V_c^2}{8\quad d^3} \qquad \text{<22>}$$

yields the crossover point voltage V_c.

$$V_c = \frac{8\,n_o q d^2}{9\,\varepsilon\varepsilon_o} \qquad \text{<23>}$$

Expressed in another way, SCLC is dominant only if the injected carriers can transit the sample before they are

thermally relaxed.

If there are traps present in the dielectric, they will reduce the amount of space charge current by immobilizing a portion of the injected carriers. The occupancy of the trap level is given by:

$$n_t(x) = \frac{N_t}{1 + \frac{1}{g} \exp\left[\frac{E_t - E_F(x)}{kT}\right]} \qquad <24>$$

and the free electron density is given by:

$$n(x) = N_c \exp\left[\frac{E_F(x) - E_c}{kT}\right] \qquad <25>$$

where n_t - density of occupied traps

N_t - density of traps

g - degeneracy factor (= 2 for singly charged donors)

E_c - conduction band energy

E_t - trap energy

E_F - Fermi energy

N_c - conduction band effective density of states

For clarity, let

$$N_c' = \frac{N_c}{2} \exp\left[\frac{E_t - E_c}{kT}\right]$$

$$= \frac{N_c}{2} \exp\left[\frac{-\zeta_t}{kT}\right] \qquad <26>$$

therefore, combining <24> and <26>

$$n_t(x) = N_t \left[1 + \frac{N_c'}{n(x)}\right]^{-1} \qquad <27>$$

Note that for shallow traps, i.e. E_F below E_t,

$$n_t(x) \cong N_t \frac{n(x)}{N_c'} \qquad \text{<28>}$$

$$\frac{n(x)}{n_t(x)} = \frac{N_c'}{N_t} = \theta, \text{ independent of V} \qquad \text{<29>}$$

Thus for shallow traps

$$J = \frac{9\varepsilon\varepsilon_o\theta\mu V^2}{8 \quad d^3} \qquad \text{<30>}$$

But for deep traps where E_F is above E_t

$$n_t(x) \cong N_t \; ; \; \theta = 1 \qquad \text{<31>}$$

and

$$J = \frac{9\varepsilon\varepsilon_o \mu V^2}{8 \quad d^3} \qquad \text{<32>}$$

This is just as in the trap free case (equation <21>, page 30). Thus one would expect that if the Fermi energy were made to pass through the energy level of a trap, through increased injection, for instance, then current density should increase rapidly from the shallow trap regime, where $J \propto \theta V d^{-3}$, to the trapped filled conditions of equation <32>. Since $n(x)/n_t(x) = \theta$ can be very small (for example 10^{-7}), the increase in current density can be very dramatic. The transition points between ohmic and shallow trap conditions, shallow and trap filled regimes, are used to estimate the thermally generated carrier density, and the trap density.

Exponents of V higher than 2 are possible, if the traps have an exponential energy distribution of the form

$$n_t(E) = N_t^* \exp\left[\frac{E - E_c}{kT_f}\right] \qquad \langle 33 \rangle$$

where $n_t(E)$ = trap density / unit energy

T_f = a characteristic temperature

N_t^* = a characteristic trap density / unit energy

It can be shown that for these conditions (96)

$$J = q\mu N_c \left[\frac{\varepsilon\varepsilon_o}{qN_t kT_f}\right]^s \frac{V^{s+1}}{d^{2s+1}} \qquad \langle 34 \rangle$$

where $s = T_f/T$

Two carrier injection arises from the arrangement of an electron injecting cathode, a hole injecting anode and a suitable density of recombination centers in between. The theoretical treatment is more involved (97), but leads to four distinct J-V regimes: a low field ohmic region, a V^2 region, then VCNR (voltage controlled negative resistance), followed by a high current region where:

$$J \propto \tau\varepsilon\varepsilon_o\mu_p\mu_n \frac{V^3}{d^5} \qquad \langle 35 \rangle$$

where τ = an average carrier lifetime

μ_p = hole mobility

μ_n = electron mobility

The full range of expected SCLC J-V behavior is sketched in Figure <5>.

One further identifying feature of SCLC is the characteristic current transient as shown in Figure <6>. This subject has been

Figure <5> Theoretical J-V Behavior for Various Forms of SCLC

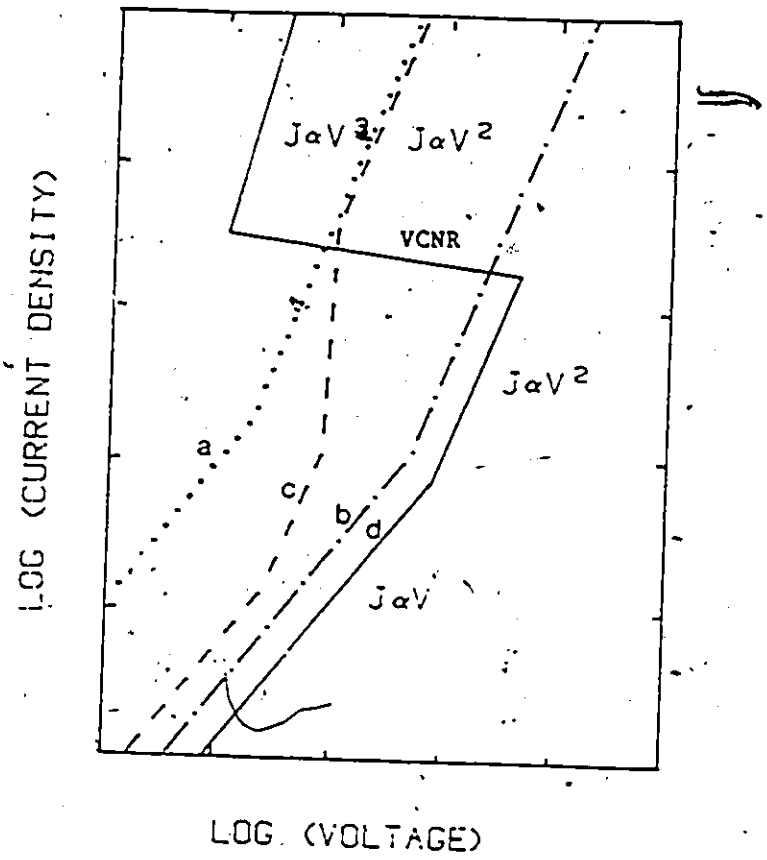

Theoretical current density - voltage (J-V) behavior of the various forms of space charge limited conduction (SCLC) is shown in this graph. In the simple, trap free, single carrier SCLC, low field ohmic $J \alpha V$ and higher field SCLC $J \alpha V^2$ regimes are seen (a). When shallow traps are present both the ohmic and SCLC relations hold as before, but at much reduced current levels (b). Deep traps, on the other hand, can have J-V behavior identical to the trap free case. However, because the Fermi level shifts with increased injection, a trap may be considered shallow at low voltage and deep at higher voltage. Consequently its J-V behavior can show a nearly vertical transition between shallow $J \alpha V^2$ and deep $J \alpha V^2$ relations (c). In the case where injection occurs at both electrodes, ohmic, then simple $J \alpha V^2$ behavior is followed by voltage controlled negative resistance (VCNR) and finally a high current $J \alpha V^3$ regime. From Lampert and Mark (95).

Figure <6> Theoretical Current Transients Associated with SCLC

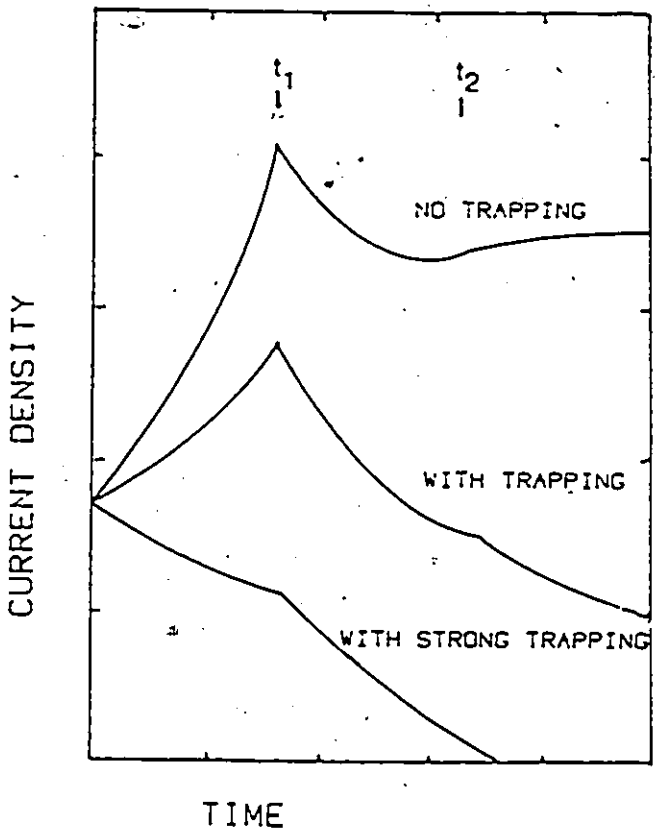

The space charge in an insulator takes a finite period of time to establish its final distribution. As a result, the transient behavior of current with time takes on the characteristic form shown. Current at t = 0 tends to a value equal to approximately one half its steady state value. Also it will overshoot the steady state mark by up to 21% before finally decreasing. In the presence of trapping, the transient is overlaid with a general decrease proceeding with time. For strong trapping the overshoot can be completely obscured. From Lampert and Mark (95).

dealt with in detail by Lampert (98), Many and Rakavy (99), and Lindmayer (100). An explanation is given below based upon the treatment of Lampert (98). The transient is composed of three portions: the initial rise stage from t=0 to t_1 (when the injected charge uniformly fills the volume between the cathode and the charge front which has not yet reached the anode); the relaxation stage from $t=t_1$ to t_2; and the steady state stage for $t>t_2$. The analysis of the initial rise stage is particularly simple, since the electric field is a linear function of distance between the cathode and the charge front (space charge is uniform), and is constant between the charge front and the anode (zero space charge). Also, the analysis yields quantitative estimates of both the magnitude and time of current overshoot.

The current density in the initial rise time period is the sum of conduction and displacement terms. The conduction term is, in turn, made up of drift and diffusion terms, but the diffusion term can be neglected for insulators, and for moderate electric field strengths (101). Thus

$$J(x,t)=q\mu n(x,t)\xi(x,t)+\frac{\partial}{\partial t}\varepsilon\varepsilon_o\,\xi(x,t) \qquad \langle 36\rangle$$

From Poisson's equation n(x,t) can be evaluated, i.e.

$$q\,n(x,t)=\varepsilon\varepsilon_o\frac{\partial}{\partial t}\xi(x,t) \qquad \langle 37\rangle$$

$$J(x,t)=\varepsilon\varepsilon_o\left[\mu\,\xi(x,t)\frac{\partial}{\partial t}\xi(x,t)+\frac{\partial}{\partial t}\,\xi(x,t)\right] \qquad \langle 38\rangle$$

Current density is the same throughout the thickness of the

sample, therefore it can be averaged over x from the cathode to the anode. Thus:

$$J(t) = \frac{\varepsilon\varepsilon_o}{d}\left[\mu\int_o^d \xi(x,t)\,\partial\,\xi(x,t) + \frac{\partial}{\partial t}\int_o^d \xi(x,t)dx\right]$$

$$= \frac{\varepsilon\varepsilon_o}{d}\left[\frac{\mu\,\xi^2(d,t)}{2} + \frac{\partial V}{dt}\right]$$

$$= \frac{\varepsilon\varepsilon_o\mu}{2d}\,\xi^2(d,t) \qquad \text{<39>}$$

assuming $\xi(0) = 0$, and V is constant.

If J is evaluated at the anode (x = d) during the initial rise time, then the only component is the displacement term because the charge front has not yet reached the anode. Therefore, combining <36> and <39>

$$\frac{\partial\,\xi(d,t)}{\partial t} = \frac{\mu}{2d}\,\xi^2(d,t) \qquad \text{<40>}$$

which can be integrated from t=0 to t to yield

$$\frac{1}{\xi\,(d,0)} - \frac{1}{\xi\,(d,t)} = \frac{\mu\,t}{2d} \qquad \text{<41>}$$

but since $\xi(d,0) = V/d$

$$\xi\,(d,t) = \frac{1}{\frac{d}{V} - \frac{\mu t}{2d}} = \frac{V}{d}\left\{\frac{1}{1-t/2t_o}\right\}, \qquad \text{<42>}$$

where $t_o = d/v = d^2/\mu V$ is the transit time in the absence of

space charge effects. It is obvious that the electric field at the anode (which is the same as that at the leading front) is larger than the steady state value of V/d, and grows with time. Substitution of this result into <39> gives an expression for current density in the intial rise time

$$J(t) = \frac{\varepsilon\varepsilon_o \mu V^2}{2d^3}\left[\frac{1}{1- t/2t_o}\right]^2 \qquad <43>$$

Note that J(0) is equal to

$$\frac{\varepsilon\varepsilon_o \mu V^2}{2d^3}$$

which is slightly less than one half of the steady state value calculated on page 30 (equation <21>).

To calculate the amount of current overshoot, note that it occurs when the transit of the leading front is complete at t_1. Therefore:

$$\int_o^{t_1} \mu \xi (d,t)\partial t = d \qquad <44>$$

$$= \frac{2 \mu t_o V}{d} \ln\left(1 - \frac{t_1}{2t_o}\right)^{-1}$$

which implies

$$t_1 = 2t_o (1 - 1/\sqrt{e}) = .787\ t_o \qquad <45>$$

Therefore, evaluating <43> at t_1 gives,

$$J(t_1) = 1.21\ J(t>>t_o) \qquad <46>$$

In a similar fashion, the relaxation stage has been examined with typical results shown in Figure <6> following page 33.

Hybrid Theories:

A number of theoretical papers combine SCLC with one or more other effects. As mentioned, Frank and Simmons (75) studied the effect of Poole Frenkel trap depth lowering on the transition between contact controlled conduction and SCLC. Later Edwards and Jones extended the work to a variety of trap energy distributions (102). Nicolet (103) and later Sworakowski (104) both attended to the problem of spatially non-uniform trap distributions. In general, however, the predictions hold that for some range of current and voltage and for some s, the researcher should observe:

$$J \propto \frac{V^{s+1}}{d^{2s+1}} \qquad \langle 47 \rangle$$

Experimental Evidence:

Good examples of SCLC in a variety of insulators can be found in Lampert and Mark's book (95) on the subject. An early report of SCLC in an anodic oxide was made by Hickmott (71). $J \propto V^3/d^5$ behavior, typical of two carrier SCLC was observed in anodic Nb_2O_5 if the counter electrode was a high work function metal: e.g. gold, while $J \propto V^2$ behavior, corresponding to one carrier injection was found with a low work function material: e.g. indium. Electrode dependent behavior was also reported for this material by Sciri and Chabicovsky (105), although they saw one carrier SCLC with evaporated Au electrodes and Poole Frenkel characteristics if the gold electrodes were sputtered. The full

range of expected two carrier SCLC behavior, including VCNR was seen by Taylor and Lalevic (106) in TiO_x. A report on Al_2O_3 by Mason and Nathoo (107) shows complex behavior, complicated by drift, which has certain features similar to SCLC.

In Ta_2O_5, however, most of the well documented observations have come from researchers at the University College of North Wales. The point in mentioning this fact is that the experimental method of preparing the oxide is common to all these papers. In 1973, Aris and Lewis (58) reported work done on thick oxides (160 to 500 nm), formed by anodization in phosphoric acid. They observed current rectification, with the anodic (Ta positive) polarity yielding much higher currents than the cathodic (Ta negative) polarity. Above a voltage threshold, and for films thicker than 200 nm, J was proportional to V^2d^{-3}. The low voltage behavior was attributed to a Poole Frenkel trap emptying mechanism. The forward bias currents were analyzed with a Schottky model, although as will be shown later, a Poole Frenkel model is just as appropriate. The analysis yields a value for the (high frequency) dielectric constant which they incorrectly use for determining the mobility in the reverse SCLC regime where the static dielectric constant should have been used. The error amounts to just under a factor of 5: therefore, the order of magnitude of effective mobility is essentially unchanged at $10^{-15}m^2/V\text{-}s$. A slightly different value is deduced from the shape of the charging current transients. Effective mobility is the

product of 0 from equation <29> and the true mobility. From their estimate of trap depth energy (.44 eV) and density (in excess of 10^{24} m^{-3}), the true mobility is calculated to be $10^{-11}m^2/V\text{-}s$. This is much lower than the electron mobility quoted in other sources (59) and is, in fact, inconsistent with transport in extended states.

Their coworkers, Jones and Hughes, (11) prepared oxides in the same manner on sputtered Ta films (b.c.c. phase). The J-V curves appear the same, showing a rapid rise due to Poole Frenkel trap emptying, followed by a $J \alpha V^2 d^{-3}$ region for the Ta electrode positively biased. They correct the mistake with respect to dielectric constant, and determine a trap density of $10^{25} m^{-3}$ and an effective mobility of $10^{-16} m^2/V\text{-}s$. The transient response agreed with these values.

The third paper from the group then appeared, authored by Gubanski and Hughes (70). The only change in structure is the use of gold counter electrodes instead of aluminum ones. In the course of their temperature studies they discovered that the films were rectifying and space charge dominated when freshly prepared - but exhibited low leakage symmetric ln(J) vs $\sqrt{V}$ behavior after being heated in vacuum. In fact, the original characteristics could be restored by re-exposure to the atmosphere. They attributed the change to oxygen diffusion. However, as mentioned previously, moisture is also a likely culprit. The significance they drew from this behavior was that

if conduction was controlled by conditions at the anode, then, contrary to previous assumptions, the SCLC observed was actually hole injection. A note that can be added as proof is the similarity between the mobility calculated by these workers and that deduced from anodization studies by Kadary and Klein ($10^{-10} m^2/V\text{-}s$) (68). A final observation was that TSC (thermally stimulated current) scans of both the rectifying and nonrectifying samples had high temperature regions where the sense of current flow was opposite to convention, indicating non-uniform internal fields.

A summary of the experimental evidence for SCLC is given in Table II. This presentation of the data highlights the very low mobilities usually observed, and the association of SCLC with anodic oxide films thicker than 100 nm.

TABLE II

Experimental Evidence for Space Charge Limited Conduction

DEVICE STRUCTURE	THICKNESS (nm)	EVIDENCE	Nt (m^{-3})	μ ($m^2/V-s$)	REF.
Ta-Ta_2O_5-Al	160-510	$J \alpha V^2$, J-t	10^{24}	10^{-16}	58
Ta-Ta_2O_5-Au	300-500	$J \alpha V^2$, J-t			70
Ta-Ta_2O_5-Al	300	$J \alpha V^2$, J-t	10^{24}	10^{-16}	11
Al-Al_2O_3-Al -Au	50-130	$J \alpha V^2$, J-t			107
Ta-Ta_2O_5-NiCr:Au	500	$J \alpha V^2$	10^{24}		108
Nb-Nb_2O_5-Au	160	$J \alpha V^2$	10^{25}		105
Ti-TiO_2-Cr	2000	$J \alpha V^3$, VCNR			106
Nb-Nb_2O_5-Au -In	100-270	$J \alpha V^3 d^{-5}$ $J \alpha V^2$			71
Ta-Ta_2O_5-NiCr-Au	190-350	$J \alpha V^2$	10^{24}		109
Si-V_2O_5-Au	160	$J \alpha V^2$	10^{19}	10^{-8}	110

Hopping Conduction

Theory:

As the name suggests, hopping conduction describes the process by which carriers move through an insulator or semiconductor via a discrete number of jumps between localized states. The distinction between such a process and Poole Frenkel conduction, where carriers also "hop" from one localized state to another, is that the true hopping carrier never reaches the conduction (or valence) band. Its mobility is much lower, usually less than 10^{-4} m^2/V-s. Both electrons and holes can hop. In addition, the combination of an electron and the polarization induced potential well that surrounds it, known collectively as the polaron, can also hop. Polarons only form in those ionic lattices where the electron is moving sufficiently slowly that the lattice has time to distort in response to the charge. Also, since to move a polaron, the lattice distortion around the electron is dragged along, the effective mass of the hopping entity is larger. Both these effects limit polaron hopping to low mobility materials. The two types of hopping - that of electrons along a band of localized states at the Fermi energy, and that of polarons - will be discussed in this section. The aim will be to produce the appropriate J-V-T (current density - voltage - temperature) equations. The study of hopping and polarons is much more extensive than can be covered here. Extensive reviews

covering additional topics such as the frequency dependence of conductivity, and the optical properties of systems of hopping carriers are found in "Electronic Processes in Noncrystalline Materials" by N. F. Mott, and E. Davis (47).

i - Variable Range Hopping :

Low Field Behavior:

The Fermi energy of the non-degenerate semiconductor or insulator lies within the band gap between the valence and conduction bands. The band gap of a perfect crystal is characterized by the lack of allowed electron states, whereas within the band gap of an amorphous material or a heavily doped and compensated semiconductor a small but non-zero number of states are present. Thus in a perfect crystal carriers must be activated to the appropriate band to participate in conduction. The electrons within a kT or so of the Fermi energy in an amorphous or highly doped sample, however, are able to hop from one allowed state to another without necessarily reaching the conduction band. As expected, the principles that govern the two processes are quite different. A distinction can also be made between the hopping conductor, and a metallic sample which also has allowed states at the Fermi level. In contrast to metallic samples, the states at the Fermi energy in an amorphous semiconductor or insulator which exhibit hopping conduction are

too few to overlap significantly. It is the overlap which leads to the formation of extended states and gives rise to band-like conduction properties.

Consider an insulator with a distribution of localized states at the Fermi energy. The probability of a successful hop depends on the energy difference, W_D, between the origin and destination state, and the overlap of the wave functions of the two states. To quantify the overlap, let the potential in the vicinity of a localized state be given by: (111)

$$\Psi(r) = \Psi_o \exp(-\eta r) \qquad \text{<48>}$$

where $\eta = \sqrt{\frac{2 m^* \zeta_d}{\hbar}}$

ζ_d - the ionization energy of the state

m^* - the effective mass of the carrier

For the materials being studied here the radius of the localized states, given by $1/\eta$, is on the order of a few tenths of nanometers. In this notation the overlap factor in the hopping probability is given by $\exp(-2\eta R)$; where R is the hopping distance. If we compare hopping to the analogous process of ion diffusion then it is possible to define a diffusion coefficient D for hopping: (112)

$$D = \nu R^2 \exp\left(-\frac{W_D}{kT}\right) \exp\left(-2\eta R\right) \qquad \text{<49>}$$

where ν is the attempt - to - escape frequency (which some authors have set to the lattice vibrational frequency of $10^{12} s^{-1}$ (47)).

Mobility may then be ascertained by use of the Einstein relationship $\mu = qD/kT$.

$$\mu = \frac{q\nu R}{kT} \exp\left(\frac{-W_D}{kT}\right) \exp\left(-2\eta R\right) \qquad \langle 50 \rangle$$

and thus

$$J = nq\,\mu\xi$$

$$= q^2 \nu R^2\, \xi N(E_F)\, \exp\left(-\frac{W_D}{kT} - 2\eta R\right) \qquad \langle 51 \rangle$$

where $n = N(E_F)\, kT$

The minimum spacing of energies in the band of localized states has been estimated by Mott (111) to be

$$W_{min} = \frac{3}{4\pi\, R^3 N(E_F)} . \qquad \langle 52 \rangle$$

At low temperatures, all transitions will be to states separated by this value, so that

$$J = q^2 \nu R^2\, \xi\, N(E_F) \exp\left(-2\eta R - \frac{3}{4\pi R^3 N(E_F) kT}\right) \qquad \langle 53 \rangle$$

Clearly, the exponential has a maximum when

$$2\eta = \frac{9}{4\pi R^4 N(E_F) kT} \qquad \langle 54 \rangle$$

or

$$R = \sqrt[4]{\frac{9}{8\eta\pi N(E_F) kT}} \qquad \langle 55 \rangle$$

If it is assumed that conduction is dominated by these optimal jumps, then

$$J = q^2 \nu R^2 \xi N(E_F) \exp\left(-\frac{8\eta R}{3}\right) \quad <56>$$

$$= q^2 \nu R^2 \xi N(E_F) \exp-\left[\frac{T_o}{T}\right]^{\frac{1}{4}} \quad <57>$$

where $$T_o = \frac{18.1\ \eta^3}{N(E_F)k} \quad <58>$$

This is known as the Mott law for variable range hopping. The numerical prefactor in <58> varies from 5 to 20 depending on the averaging technique used.

At high temperatures, the limitation on successful hops will not be the supply of thermal energy, but rather the overlap factor $\exp(-2\eta R)$. Under these conditions the observed activation energy will be W_{max}, which is equal to the mean spread in energies within the band of localized states. The hallmark of variable range hopping is, therefore, an Arrhenius plot of $\ln(J/V)$ vs $1/T$ which is not linear. A typical example is shown in Figure <7>. The activation energy derived from such a plot decreases continuously as temperature decreases, and the low temperature behavior is better fitted with $\ln(J/V)$ set equal to a linear function of $T^{-\frac{1}{4}}$. Because the low temperature behavior is so distinctive it is most often used to test the applicability of the model to experimental data.

Related low temperature hopping conduction models have been proposed. For instance, if the density of states at the Fermi

Figure <7> Temperature Dependence of Activation Energy in Hopping

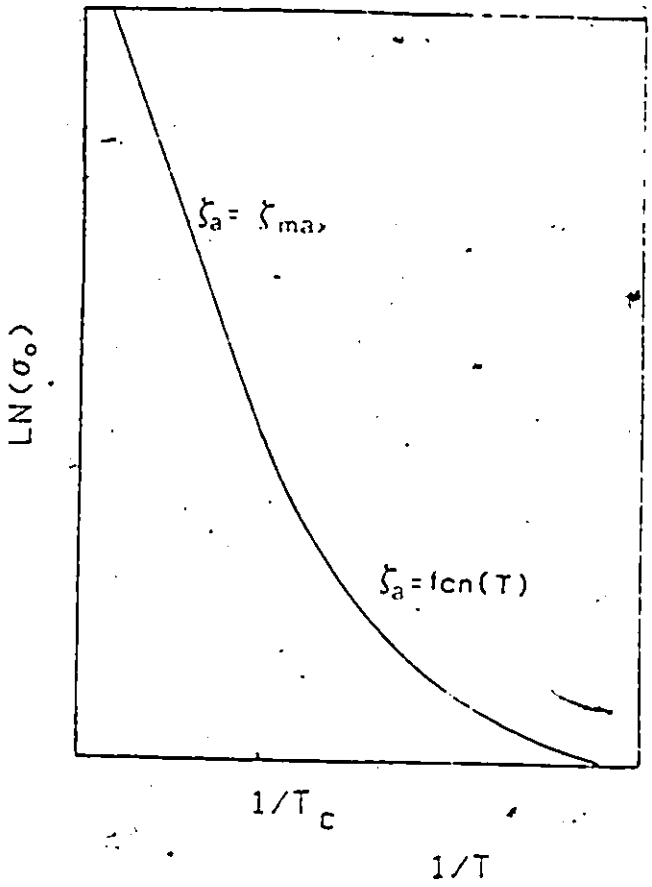

The activation energy of conductivity in a system exhibiting variable range hopping is a constant at high temperatures when the carrier hops between nearest neighbours of a fixed energy separation, $\zeta_{a\ max}$. Below a transition temperature, T_c, the carrier may not posses sufficient energy to make a transition to these sites, and will instead be forced to find a more distant site whose energy separation is smaller. Thus the observed activation energy drops at low temperature.

energy is allowed to vary with energy, analysis has shown (113):

$$\ln \sigma \propto T^{-s(b)} \qquad <59>$$

$$s = \frac{b+1}{b+4} \qquad <60>$$

where $$N(E) \propto |E-E_F|^b \qquad <61>$$

Note that for b=0 (constant density of states), Mott's hopping law is recovered. In the experimental work accompanying this analysis, an exponent of .40 ± .05 was found for a number of amorphous semiconductors including Si, GaAs, GaP, and InP.

It has also been pointed out that for films whose thicknesses are comparable, or less than, the hop distance, conductivity becomes thickness dependent, and s(b) of equation <59> approaches 1/3 (114-116).

High Field Behavior:

So far hopping has only been shown to produce ohmic behavior. The model has been extended to higher electric fields (117-122). It is assumed that for each jump of length R the electron picks up an amount of energy qξR. The effective activation energy is then W-qξR and current density is

$$J = K_H \xi \exp\left(\frac{cq\xi R}{kT}\right) \exp -\left[\frac{T_o}{T}\right]^{\frac{1}{4}} \qquad <62>$$

where $K_H = \frac{q^2 \nu R^2 n}{kT}$

c is a constant less than unity introduced by Pollak

and Riess (119) to take into account that the path from one site to another has only a component exactly parallel to the field. Their percolation methods gave a typical value of c to be .17.

At medium field strengths a significant number of transitions are made "upstream", against the electric field. For those jumps the barrier is increased. The net current density is given by (117,118,120,121):

$$J = 2 K_H \xi \exp-\left[\frac{To}{T}\right]^{\frac{1}{4}} \sinh \left\{\frac{q\xi R}{kT}\right\} \qquad \langle 63 \rangle$$

Shklovskii (121,122) and Hill (117) both extended the work to high fields. In Shklovskii's treatment

$$J \alpha \exp \left[\frac{q\xi R}{kT}\right]^{1/1+\nu} \qquad \nu \approx 0.9 \qquad \langle 64 \rangle$$

Hill on the other hand, finds that at higher fields, the electron gains enough energy to reach the conduction band, and thus no longer qualifies as a true "hopping" carrier. In fact, his treatment shows that the differences between hopping conduction and Poole's law for field assisted ionization of closely spaced donors become negligible as ξ increases. Poole's law will be discussed in Part II as an extension to Poole Frenkel conduction.

In all of these treatments, R is temperature dependent. At low temperature the electron must hop a longer distance to find a site that differs by only the small amount of thermal energy

available, whereas at high temperature, the electron can jump to any of the nearest neighbours. Thus R should decrease with increasing temperature.

ac Conductivity:

Although the temperature and field dependences of hopping conduction should suffice to distinguish between hopping and the other conduction models proposed for Ta_2O_5, most researchers rely upon on further signature: that is, the ac conductivity $\sigma(\omega)$ at low frequencies (10^{-3} to 10^{5} Hz) for hopping conduction is found to be proportional to ω^{s} where $0.8 < s < 1$. The derivation of the detailed expression is found in reference 123. The main result is quoted below to permit the evaluation of experimental evidence from the literature, even though the ac properties of the films in this study were not examined in any depth.

$$\sigma(\omega) \sim 2.5q^2\, kT\omega \left(\frac{n}{u_o}\right)^{2\eta-5} \left\{\ln\left(\frac{\nu}{\omega}\right)\right\}^4 \qquad <65>$$

where n = hopping carrier density

η = overlap parameter (equation <48>, page 44)

u_o = disorder parameter

ν = phonon frequency ($10^{12}\ s^{-1}$)

For low frequency measurements, Mott estimates the frequency dependence of $(\ln(\nu/\omega))^4$ to be approximately $\sim \omega^{-.2}$ yielding an s of .8.

In contrast, the high frequency conductance was found to be (124)

$$\sigma(\omega) = \left(\frac{\pi q \omega n}{u_o}\right)^2 \hbar\, \eta^{-5} \left\{\ln\left(\frac{\Psi_o}{\hbar\omega}\right)\right\}^4 \qquad \langle 66 \rangle$$

where Ψ_o was defined in equation <48> page 44.

An ω^2 response is often found in insulators and semiconductors. However, other phenomena can also give rise to an ω^2 response (e.g. series resistance), so that the high frequency response is not conclusive evidence for hopping conduction.

ii - Polaron Hopping

Low Field Behavior:

Because polaron hopping is completely analogous to electron hopping, the basic equations describing J-V-T behavior is the same as in equation <51> page 45, repeated here.

$$J = q^2 \nu R^2 \xi N(E_F) \exp\left[-\frac{\zeta_a}{kT} - 2\eta R\right] \qquad <51>$$

In this case however, the nature of the hopping carrier, the polaron, contributes to the form and temperature dependence of the hopping activation energy ζ_a(125-127). In the hopping of the polaron, there are two energies to be considered: that needed to form the polaron, W_p, and that needed to overcome any energy difference between the origin and the destination states, W_D. To calculate W_p, let the distortion energy of an ion be expressed in terms of a displacement from an equilibrium position q_1. A parabolic expression with the value of zero at the minimum might be:

$$E_I(x) = A\,(x-q_1)^2 \qquad <67>$$

Let a second ion have a similar energy form, but a minimum value of W_D i.e.

$$E_{II}(x) = A\,(x-q_2)^2 + W_D \qquad <68>$$

These two sites are shown schematically in Figure <8>.

Figure <8> Schematic of the Intra-site Transfer of a Polaron

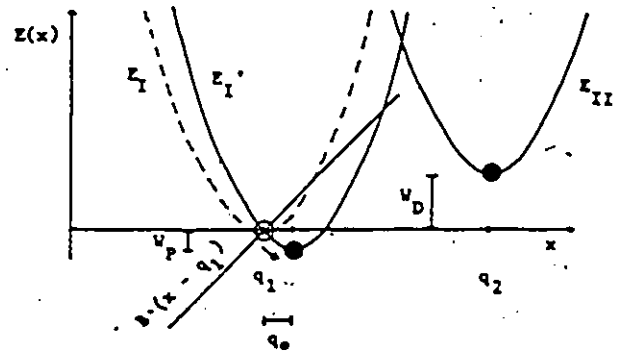

Any displacement of ions I and II from their equilibrium positions (q_1 and q_2) results in a parabolic increase in each of their potential energies E_I and E_{II}. The equilibrium energies of the two sites differ by W_D.

Adding an electron to site one contributes an energy $B\cdot(x - q_1)$, creating a polaron with total energy E_I'. The activation energy for the formation of the polaron is W_P.

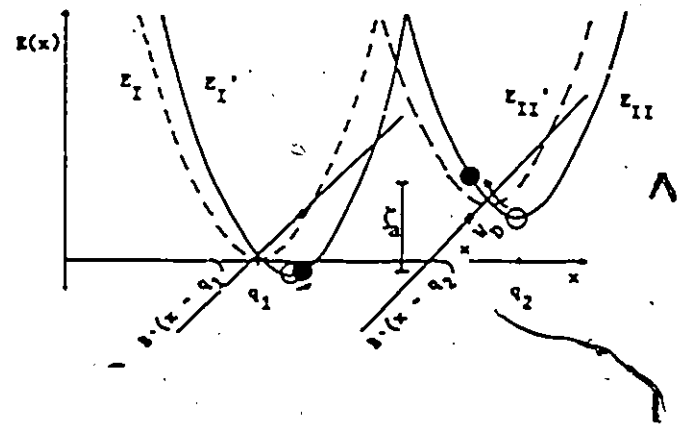

For electron transfer to occur the electron energy on site I, $B\cdot(x - q_1)$, must equal that on site II, $B\cdot(x - q_2) + W_D$.

A suitable configuration can be formed by allowing both ions to distort. The optimal distortion, shown here, has an activation energy of ζ_a.

Now if an electron were placed adjacent to the first ion, its energy expression becomes:

$$E_I'(x) = A(x-q_1)^2 - B(x-q_1) \qquad <69>$$

which has a minimum at:

$$(x-q_I) = \frac{B}{2A} = q_0 \qquad <70>$$

Thus the amount of energy required to produce a system of an electron and a distorted lattice is:

$$W_P = E_I'(q_0) - E_I(q_0) = \frac{B^2}{4A} = Aq_0^2 \qquad <71>$$

Although it may require W_P to create a polaron, it takes somewhat less than that value to shift the polaron from one lattice site to another. The necessary condition is that the electron have the same energy in both sites. i.e.

$$B(x-q_1) = B(x-q_2) + W_D \qquad <72>$$

The energy required to produce the distortion of the lattice corresponding to this configuration is:

$$\zeta_a = A(x-q_1-q_0)^2 = A(x-q_1-\frac{W_D}{B})^2 \qquad <73>$$

The energy of site one with $(x - q_1) = q_0$

The energy of site two with $(x - q_2)$ as in equation <72>

ζ_a, as defined by this equation, has a minimum when

$$(x-q_1) = \frac{q_0}{2} + \frac{W_D}{2B} \qquad <74>$$

Therefore:

$$\zeta_a = A\left(\frac{W_D}{2B} - \frac{q_0}{2}\right)^2 + A\left(\frac{q_0}{2} - \frac{W_D}{2B}\right)^2 \quad \text{<75>}$$

$$= 2A\left\{\left(\frac{W_D}{2B}\right)^2 + \frac{q_0 W_D}{2B} + \frac{q_0^2}{4}\right\}$$

$$= \frac{Aq_0^2}{2} + \frac{W_D}{2} + \frac{AW_D^2}{2B} \quad \text{<76>}$$

let $W_H = \zeta_a(W_D = 0) = Aq_0^2/2$, then

$$\zeta_a = W_H + \frac{W_D}{2} + \frac{W_D^2}{16 W_H} \quad \text{<77>}$$

Note that the energy to shift a polaron in the absence of W_D, i.e. W_H, is one half of the energy required to create the polaron. From known values of W_p, polaron hopping energies of on the order of .5 eV can be estimated (126).

The transfer of the electron can be made in two ways: adiabatically, and nonadiabatically.

1) Two conditions must hold for the adiabatic case: the excited state where a polarization well exists for both sites (Figure<8>) must persist long enough, and the separation between the wells must be small enough that the electron makes many passes back and forth between the sites. This resonance lowers ζ_a further below $W_p/2$ (125). The J-V-T expression <51> (page 45) becomes:

$$J = \frac{q^2 \nu a^2 \xi n}{kT} \exp\left(-\frac{\zeta_a}{kT}\right) \quad \text{<78>}$$

Note that the closely spaced ions imply that the overlap factor, $\exp(-2\eta R) = 1$, and that $R=a$, where a is the nearest

neighbour separation.

2) In the nonadiabatic case, the electron transition is not probable, therefore the resonance effect is negligible. Also, the overlap factor must be retained. Therefore equation <51> remains unchanged.

Schnakenberg (127) has examined the temperature dependence of the hopping activation energy when more than one type of phonon (acoustic and optical) are involved. His analysis predicts a change in ζ_a from $\sim W_H + W_D/2$ (equation <76>, page 53) to W_D as temperatures drop below $\Theta_D/2$. Θ_D is the Debye temperature, which ranges in oxides similar to Ta_2O_5 between 400 and 800 K. W_D itself is estimated to be on the order of kT (118).

High Field Behavior:

As in electron hopping, conductivity becomes nonohmic when the polaron picks up an energy $q\xi R$ which is an appreciable fraction of the hopping activation energy. Therefore, using the same arguments, for moderate fields:

$$J(\xi) = \frac{J(0)\ \sinh\left(\frac{cqR\xi}{2kT}\right)}{\frac{cqR\xi}{2kT}} \qquad <79>$$

and for high fields:

$$J(\xi) = J(0)\ \exp\left(\frac{cqR\xi}{kT}\right) \qquad <80>$$

As mentioned before, c is a number to take into account that

not all jumps are exactly parallel with the field. Also, as mentioned before, $R_{}$ is temperature dependent, decreasing to the limit of nearest neighbour spacing as temperature increases. In some work it is evident that the number of sites "passed over" at room temperature can be substantial - in a variety of transition metal ion glasses Austin and Sayer found the hopping distance appeared to be 4 to 17 times the intersite spacing (118). They attributed this to the enhancement of the local electric field around the site due to fluctuations in the local well depths.

Experimental Evidence:

Hopping conduction is well documented in amorphous semiconductors (113, 114, 116, 128-130), heavily doped single crystals (131-134) and transition metal oxide single crystals (135). In this section, the emphasis is on those materials most similar to Ta_2O_5. Only two examples of hopping conduction in Ta_2O_5 itself are found. Both cases rely heavily upon the examination of the frequency dependence of ac conductivity. In Savinova's study (136) σ was found to be proportional to ω^s where $s = .95$ - for frequencies between 10^{-1} and 10^3 Hz, and temperatures between 300 and 400 K. Bryksin et al. (137) also examined the ac conductivity of Ta_2O_5. In the range of 1 to 10^5 Hz, s was found to be .95 at room temperature but somewhat smaller at higher temperatures. Thus variable range hopping was inferred. Bryksin et al. also looked at the temperature and field dependence of dc conductance. Mott's law, equation <57> was observed for an extended temperature range (77 - 400 K) and equation <62> relating electric field and conductance was observed for ξ between 2 and 3.8×10^8 V/m. A characteristic hop length of 1.81 nm, independent of temperature, was calculated from the data. The number of sites participating was also calculated to be on the order of 10^{26} m^{-3}.

Also note worthy are the examples of SiO_x studied by Frost and Jonscher (138), and the Cr_2O_3 studied by Barbe and Herman

(139). In both cases, the ac conductivity indicated hopping, while the dc behavior was best analyzed using the Poole Frenkel model. These models are compatible, since the ac behavior is controlled by the easiest transition, whereas the dc behavior is controlled by the hardest transition (140).

The experimental evidence for hopping conduction in Ta_2O_5 and related compounds are summarized in Table III.

TABLE III

Experimental Evidence for Hopping Conduction

DEVICE STRUCTURE	THICKNESS (nm)	EVIDENCE	REF.
Ta-Ta_2O_5-C	200	$\sigma \sim \omega^{.95}$	136
Ta-Ta_2O_5-{Ag, Al, acid}	175	$\sigma \sim \omega^{.95}$ $\ln\sigma \sim T^{-\frac{1}{4}}$ $\ln\sigma \sim \xi$ (limited range)	137
Si-Cr_2O_3-Al	100	$\sigma \sim \omega^{.95}$ LF $\sigma \sim \omega^2$ HF	139
Sc-Sc_2O_3-In	10-15	$\sigma \sim \omega$ $.5 \leq s \leq 1$	141
Au-$(V_2O_5)(P_2O_5)$-Au		$\sigma \sim \omega$ $.73 \leq s \leq .86$ $\zeta a = fcn(T)$	142
Au-SiO_x-Au	220-420	$\sigma \sim \omega^{.6}$	143-144
Al-AlN-Al	125	$\sigma \sim \omega^{.93}$	145
{Al, Ti}-Si_3N_4-{Al, Ti}	120	$\ln\sigma \sim T^{-\frac{1}{4}}$	146
Al- biotite mica -Au	10^5	$\ln\sigma \sim T^{-\frac{1}{4}}$ $\ln\sigma \sim \xi$ $\zeta a = fcn(T)$	147
Au-{NiF_2, FeF_3}-Au	500	$\ln\sigma \sim T^{-\frac{1}{4}}$ $\zeta a = fcn(T)$	148

PART II - THEORY

1. POOLE FRENKEL CONDUCTION THEORY

In this section a detailed Poole Frenkel conduction theory will be presented. To begin with, simple one dimensional analysis will be put forward, followed by an extension to three dimensions. Then field enhanced ionization of non-Coulombic potential wells will be discussed. This will set the stage for a description of the current density - voltage - temperature (J-V-T) behavior expected when Poole Frenkel barrier lowering controls conductivity. Although this thesis is concerned only with dc conductivity, field enhanced barrier lowering is of concern in the interpretation of DLTS (Deep Level Transient Spectroscopy) (149,150), FATSIC (Field Assisted Thermally Simulated Ion Current) (151), photoconductivity (152,153) and ac conductivity (154) results, as well. As in the discussions of alternate conduction models, this section will conclude with a description of the various hybrid models that combine the Poole Frenkel effect with other conduction models, and with a summary of the experimental evidence for Poole Frenkel conduction reported in the literature.

Poole Frenkel Barrier Lowering - One Dimensional Analysis:

Poole Frenkel conduction arises from the interaction between a large electric field and the potential well surrounding a donor or an acceptor. The term donor (or acceptor) is meant precisely. By definition, a donor is charged when empty and neutral when filled. There are other configurations, for example, traps, which do not experience Poole Frenkel barrier lowering because they are charged when full and neutral when empty. The reason for this distinction will become clear in the following discussion. First, consider as Frenkel did in 1938 (155), the isolated donor in a crystalline semiconductor. Solid state theorists have shown that the behavior of an electron in the vicinity of the donor may be described with surprising accuracy by making slight modifications to the predicted behavior of an electron near a singly charged positive ion (156). Because the escaping electron sees an attractive force due to the net positive charge on the ionized donor, the potential well is Coulombic, as in the hydrogen atom. However an effective electron mass and an effective dielectric constant are used to take into consideration the other core electrons between the positive ion and the electron under study. Furthermore, these constants are characteristic of the matrix, not the source of the imperfection, which may be an impurity atom or misplaced host atom, because the orbit of the extra electron encompasses many host atoms. The orbital frequency of the extra electron is such that the core electrons are not polarized.

Therefore the dielectric constant used in the model is the high frequency one. An appropriate measure of the high frequency dielectric constant is the square of the index of refraction. This distinction is particularly important in Ta_2O_5 which has a low frequency dielectric constant of 21 to 29 (157) and a high frequency dielectric constant of 4.4 to 5 (158). In fact, this can be used to distinguish between electronic Poole Frenkel barrier lowering and an analogous process which enables ions to move from potential well to potential well under the influence of an electric field (159-161). In the latter case, the low frequency dielectric constant is appropriate.

Thus a modified Coulomb's law gives the shape of the potential well surrounding an arbitrary imperfection as:

$$E(r) = \frac{q^2}{4\pi\varepsilon\varepsilon_o r} \qquad \text{<81>}$$

As shown in Figure <9a>, this form of potential implies a spherically symmetric barrier of height $\zeta_d = E_c - E_d$ to an electron attempting to escape from the vicinity of the impurity into the conduction band. The superposition of an applied electric field, as shown in Figure <9b>, distorts the potential barrier, and reduces its height for trajectories with a component parallel to the field. If the field is applied in the positive x direction, then the total potential energy of the electron is given (in 1 dimension) by

Figure <9> Energy Band Diagram of Poole Frenkel Potential Well

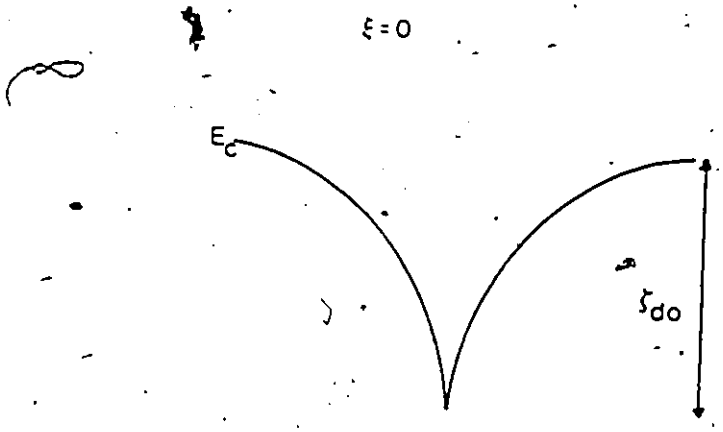

(a) The potential well formed around a donor has a spherically symmetric shape defined by Coulomb's law.

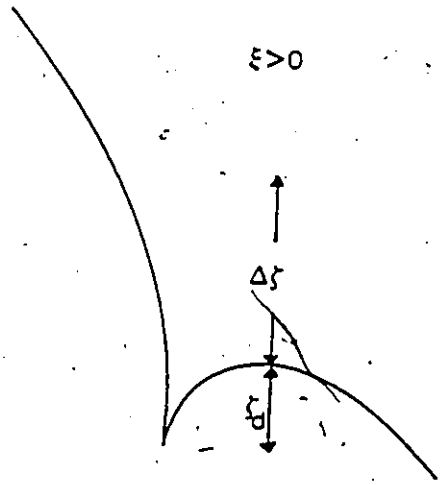

(b) An external electric field can distort the potential well, making it easier for the electron to escape in the field direction. The amount of barrier lowering $\Delta\zeta$ is proportional to the square root of applied electric field.

$$E(x) = E_c - \frac{q^2}{4\pi\epsilon\epsilon_o x} - q\xi x \qquad \langle 82 \rangle$$

Differentiating with respect to x locates the peak in the positive x direction

$$x_p = \sqrt{\frac{q}{4\pi\epsilon\epsilon_o \xi_{max}}} \qquad \langle 83 \rangle$$

which implies a barrier lowering of

$$\Delta\zeta_d = \sqrt{\frac{q^3 \xi}{\pi\epsilon\epsilon_o}} = \alpha \qquad \langle 84 \rangle$$

Thus in this one dimensional analysis the enhancement in emission probability, $P(\xi)$ over the zero field probability, $P(0)$ is:

$$\frac{P(\xi)}{P(0)} = \exp\left(\frac{\alpha}{kT}\right) \qquad \langle 85 \rangle$$

Poole Frenkel Barrier Lowering - Three Dimensional Analysis:

There is an obvious difficulty with this simple theory: emission is enhanced for all trajectories with a component aligned with the field. Many researchers have considered this aspect (65,162-165). Equation <82> is replaced by

$$E(r,\theta) = -\frac{q^2}{4\pi\epsilon\epsilon_o r} - q\xi r\cos\theta \qquad \langle 86 \rangle$$

where θ = the angle between the escape trajectory and the field direction.

By differentiating $E(r,\theta)$ with respect to r and setting the result to zero, the angle dependent barrier lowering can be

evaluated:

$$\Delta\zeta_d = \sqrt{\frac{q^3 \xi \cos\theta}{\pi\epsilon\epsilon_o}} = \alpha\sqrt{\cos\theta} \qquad \langle 87 \rangle$$

In order to obtain the total emission enhancement ratio different methods of spatial averaging over all θ were used by the different researchers. Connell et al. (162) used an exact numerical method.

Hartke (163) integrated over the "forward hemisphere" (i.e. for $-\pi/2 < \theta < \pi/2$). Emission into the "reverse hemisphere" was considered to be unaffected by the electric field. This approach yields:

$$\frac{P(\xi)}{P(0)} = \left[\frac{kT}{\alpha}\right]^2 \left[1 + \left(\frac{\alpha}{kT} - 1\right) \exp\left(\frac{\alpha}{kT}\right)\right] + \frac{1}{2} \qquad \langle 88 \rangle$$

Note that the "1/2" term is the constant term arising from the "reverse hemisphere" emission. See Figure <10>

Jonscher (65) set the reverse term to zero - implying no reverse emission. Hill (164) proposed that an appropriate approximation would be to let the barrier at $(r, \pi-\theta)$ in the "reverse" direction be increased by the same amount that the barrier at (r, θ) had been decreased. The resultant expression is:

$$\frac{P(\xi)}{P(0)} = 2\left(\frac{kT}{\alpha}\right)^2 \left[\left(\frac{\alpha}{kT}\right)\cosh\left(\frac{\alpha}{kT}\right) - \sinh\left(\frac{\alpha}{kT}\right)\right] \qquad \langle 89 \rangle$$

Ieda et al. (165), on the other hand, introduced the concept that given the availability of thermal energy ζ_{th} in the form of

Figure <10> Field Dependence of Different Emission Enhancement Ratios

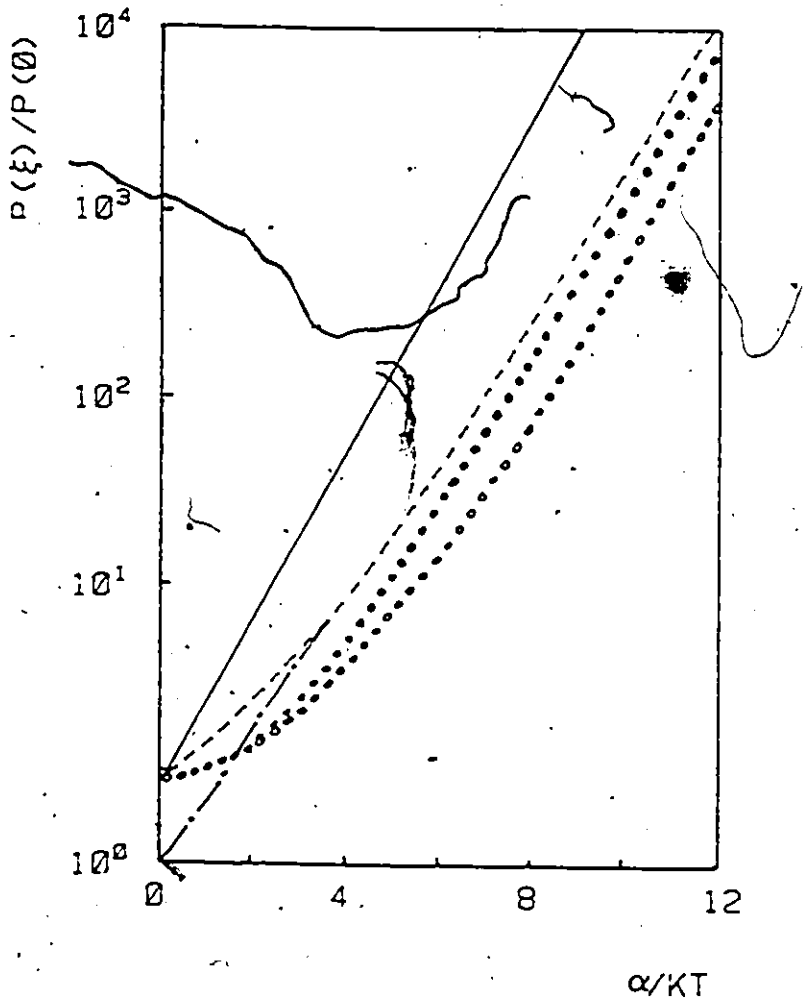

In this diagram the Poole Frenkel emission enhancement ratio is plotted against the dimensionless parameter α/kT (defined on page 62) for the following models:

———	one dimensional	equation <85>	page 62
- - - -	Hartke	<88>	63
—·—	Hill	<89>	63
·····	Ieda et al.	<91>	64
•••••••	Onsager/Pai (one step process)	<93>	65

Note that the slopes of these plots are the same for $\alpha/kT > 5$, corresponding to a voltage of 0.6 V for the devices considered here.

Figure <11> Schematic of Truncation Procedure of Ieda et al.

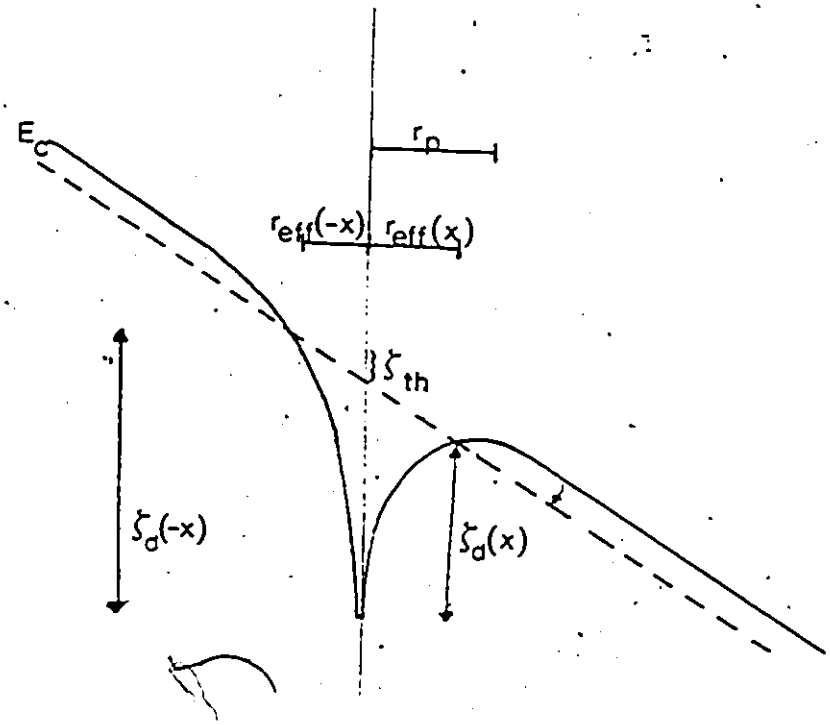

In the procedure of Ieda et al. (165) the edge of the Coulombic potential well is set to be where the energy of the escaping electron is within ζ_{th} of the conduction band. In this manner an effective radius, r_{eff}, and an effective donor depth $\zeta_d(d)$ can be defined for all trajectories.

lattice phonons, the carrier need only reach within ζ_{th} of the band edge to be considered ionized. This assumption permits the definition of an effective potential well depth, $\zeta_{eff}(\theta)$ for all carrier trajectories as shown in Figure <11>. It is then possible to integrate over all θ in a simple manner. Two regimes become apparent. At low fields the carrier is ionized before reaching the peak of the barrier, so that the enhancement ratio is:

$$\frac{P(\xi)}{P(0)} = 2\zeta_{th}\ \frac{kT}{\alpha^2}\ \sinh\left[\frac{\alpha^2}{4kT\zeta_{th}}\right] \qquad <90>$$

But at high fields, the radial position of the peak of the barrier, $r_p(\theta)$ is within $r_{eff(\theta)}$ for some portion of the "forward hemisphere", so that:

$$\frac{P(\xi)}{P(0)} = \left[\frac{kT}{\alpha}\right]^2\left[\left(\frac{\alpha}{kT} - 1\right)\exp\left(\frac{\alpha}{kT} - \frac{\zeta_{th}}{2kT}\right) - \frac{\zeta_{th}}{kT}\exp\left[\frac{-\alpha^2}{2kT\zeta_{th}}\right] + \exp\left[\frac{\zeta_{th}}{2kT}\right]\right] \qquad <91>$$

Equations <88-89>, <91> and <93> are compared against the one dimensional equation <85>, page 62 on Figure <10>. Note that for high electric fields the slopes of the enhancement ratio vs $\sqrt{\xi}$ curves are identical. Only at low fields are differences evident. Also, each of the three dimensional approaches characteristically produce near ohmic behavior at very low fields.

So far, all of the Poole Frenkel conduction models have expressed the emission enhancement ratio in terms of the barrier

height alone. The implication is that the nature of the escape process has little effect on the observed electrical behavior. In contrast, the Onsager approach (166-169) explicitly considers the three dimensional diffusion process (Brownian motion) in the presence of a specified potential. The equation to be solved is:

$$\frac{\partial f}{\partial t} = \frac{kT}{q}\,\mu\,\mathrm{div}\left[\exp\left[\frac{E(r,\theta)}{kT}\right]\mathrm{grad}\; f\,\exp\left[\frac{-E(r,\theta)}{kT}\right]\right] \qquad \text{<92>}$$

where $E(r,\theta)$ is given by equation <86> page 62

f is the probability function

μ is mobility

The solution in the case of the electron originating at a donor for steady state is:

$$\frac{P(\xi)}{P(0)} = \frac{J_i\left(i\frac{\alpha}{kT}\right)}{\frac{i\,\alpha}{2kT}} \qquad J_i = \text{Bessel function of first order.} \qquad \text{<93a>}$$

$$= 1 + \frac{1}{2!}\left(\frac{\alpha}{2kT}\right)^2 + \frac{1}{2!3!}\left(\frac{\alpha}{2kT}\right)^4 + \frac{1}{3!4!}\left(\frac{\alpha}{2kT}\right)^6 + \cdots \qquad \text{<93b>}$$

The subsidiary assumptions are:

i) carrier is delocalized if $r > \frac{1}{2}\left[\frac{q^2}{4\pi\epsilon_0\epsilon kT}\right]$

ii) $\exp\left[\frac{q\,\xi r\cos\theta}{kT}\right] \rightarrow 1$ for $r < \frac{1}{2}\left[\frac{q^2}{4\pi\epsilon_0\epsilon kT}\right]$

iii) negligible screening

iv) negligible overlap of adjacent potential wells

Pai (167) considered the ramifications to the Poole Frenkel conduction situation. His results are also shown on Figure <10>.

A simple formula which replicates equation <93b> for ξ in the range of 10^6 to 10^9 V/m is given by Adamec and Calderwood (168):

$$\frac{P(\xi)}{P(0)} = .531 \left[\frac{kT}{\alpha}\right]^{.75} \exp\left[\frac{\alpha}{kT}\right] \qquad \text{<94>}$$

The Onsager formulation is especially useful in describing the electric field dependence of recombination events where the electron and hole are initally separated (166, 167, 169, 170). The change in boundary conditions has a profound effect on the field dependence of the enhancement ratio, as shown in Figure <12>. The high field $\ln\{P(\xi)/P(0)\}$ linear in $\sqrt{\xi}$ behavior is lost and instead the enhancement ratio tends to saturate at high fields. There is one situation that might be encountered in an insulator to which this form may apply. Suppose the carrier begins its escape from a neutral trap within the Coulombic potential well (171,172). The Onsager formulation for initially separated charges must be used. Plans et al. (171) call this the two step process, and find experimental evidence for it in the case of the release of photogenerated carriers in TSC (Thermally Stimulated Current) spectra.

Poole Frenkel Barrier Lowering - Non-Coulombic Potentials:

At this point, it could be noted that field enhanced emission need not be restricted to Coulombic potentials. Other potentials such as the screened Coulombic (173-177) and those of

Figure <12> Onsager - Poole Frenkel Emission Enhancement Ratio

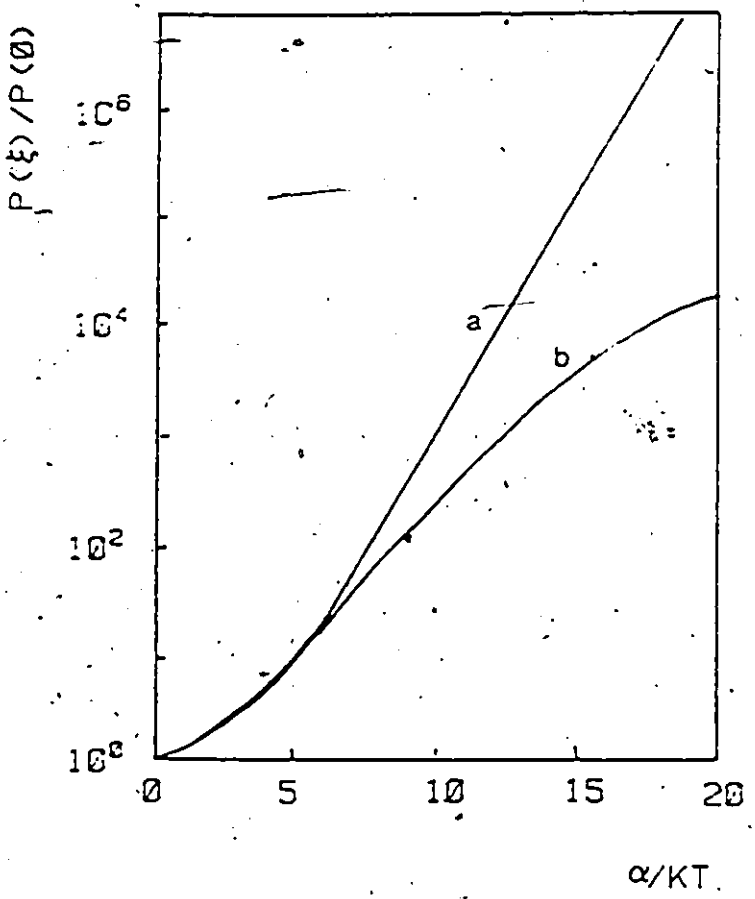

The field dependence of the emission enhancement ratio predicted by the Onsager model is compared for the one and two step processes. In case (a) the electron begins its escape from the center of the potential well, while in case (b) the electron starts its second step of the escape process from a distance of 1.5 nm away from the center. α/kT which is proportional to $\sqrt{\xi}$ was defined on page 62. From Pai (167)

the form $E(r) \propto Ar^{-m}$ have been considered (172, 174-176, 178-179). While strictly speaking the resulting conduction formulae are not "Poole Frenkel-like" in nature, it is instructive to consider them here for comparison.

The screened Coulombic or Yukawa potential (173-177) has been studied in the context of donor ionization. The potential energy of the electron in the vicinity of the donor has the form:

$$E(r,\theta) = \frac{q^2}{4\pi\epsilon\epsilon_o r} \exp\left[\frac{-r}{r_o}\right] + q\xi r\cos\theta \qquad \text{<95>}$$

where r_o is the shielding length.

As in conventional Poole Frenkel analysis, the energy equation <95> is differentiated with repect to radius and set equal to zero to locate the barrier extrema. In this case, however, the process must be done numerically. Martin et al. (173) presented analysis that showed that the Yukawa potential only deviates significantly from the Coulombic potential when r_o is less than 10 nm. Kahnt and Schirrmeister (177) give theoretical enhancement ratio curves for a range of electric fields, screening lengths, dielectric constants and temperatures. They present an estimate of the screening length:

$$r_o = \sqrt{\frac{kT_g \epsilon\epsilon_o}{q^2 N_d^+}} \qquad \text{<96>}$$

where T_g is the temperature at which the defects were formed

N_d^+ is the density of charged donors

Although this expression was proposed for glasses, it can serve as a first order approximation for amorphous Ta_2O_5. Given the material properties of Ta_2O_5, equation <96> implies that in excess of $10^{22}\ m^{-3}$ charged defects are required to reduce the screening length to less than 10 nm. Thus consideration of the Yukawa potential is necessary only when donors are dense and shallow (i.e. charged at room temperature). The strong temperature dependence of conductivity in Ta_2O_5 demonstrates that conduction is not dominated by shallow levels, and thus the Yukawa potential can be safely approximated by the Coulombic one.

Another class of potentials that has been considered (172, 174-176, 178-179) is of the form:

$$E(r) = A\, r^{-m} \qquad <97>$$

where A is a constant, or slowly varying function of r

This yields a one dimensional field induced barrier lowering of the form:

$$\frac{P(\xi)}{P(0)} = \exp\left(\frac{m+1}{kT}\left[\frac{A^{1/m} q \xi}{m}\right]^{m/m+1}\right) \qquad <98>$$

Marshall and Miller (179) also used a truncation procedure similar to what Ieda et al. (165) used with the Coulombic potential in order to extend the work to three dimensions.

The Coulombic potential is the special case where m=1. Other exponents are also physically meaningful:

i) m=2 corresponds to the dipole potential energy:

$$E(r,\phi) = \frac{-q\vec{P}\cos\phi}{4\pi\varepsilon\varepsilon_o r^2} \qquad \langle 99 \rangle$$

which may arise from a complex of two oppositely charged centers (173), or from a dipolar molecular impurity(180). In this case the amount of barrier lowering is dependent on the angle between $\vec{\xi}$ and $\vec{P}$.

ii) m=3 is the quadrupole potential energy which may arise from lattice strain around a substitutional isovalent impurity (172).

iii) m=4 is the polarization potential which has been used to describe that around neutral traps (173).

Two other potential wells with similar field dependent enhancement ratios have been considered. They are the system of multiple overlapping Coulombic wells (164), and the square well (173,181). Both lead to Poole's law (155,164):

$$\frac{P(\xi)}{P(0)} = \exp(B\xi) \qquad \langle 100 \rangle$$

where B is a constant

To summarize, the field enhanced ionization of a deep impurity in a semiconductor or an insulator has a variety of theoretical forms governed by the assumed shape of the potential well. The most general form is $E(r)=Ar^{-m}$ which leads to an enhancemant ratio that increases exponentially as ξ to the

exponent of $m/(m+1)$ for $1 \leq m < 4$. Only the Coulombic form ($m=1$) expected for simple donors or acceptors leads to the Poole Frenkel effect. The screened Coulombic or Yukawa potential should be used at high charge densities. By correctly taking into account the possibility of emission in all directions, ohmic behavior is predicted at low field strengths with the Coulombic potential. At high field strengths, however, all Coulombic forms approach the simple one dimensional form, i.e.:

$$\frac{P(\xi)}{P(0)} = \exp\left[\frac{\alpha}{kT}\right] = \exp\left[\frac{1}{kT}\sqrt{\frac{q^3\xi}{\pi\varepsilon\varepsilon_o}}\right] \qquad <85'>$$

In this work, therefore, the various conduction models will be tested in the high field regime. The low field behavior does not yield much additional information, as was noted by Hrivnak (176). The primary reason being that the close similarity between the various three dimensional Poole Frenkel models at low fields precludes distinguishing which model is most appropriate.

PART II - THEORY

Current - Voltage - Temperature Behavior :

Electric field enhanced emission will lead to electric field dependent carrier concentration and thus nonohmic current - voltage behavior if and only if the source of carriers is a partially ionized donor (or acceptor) level. In the following discussion, the expressions relating current to voltage in the presence of Poole Frenkel barrier lowering will be derived.

In the most general system containing acceptors and donors, the expression for charge neutrality is (182):

$$n + n_d + N_a = p + n_a + N_d \qquad \langle 101 \rangle$$

where n = the density of free electrons

N_d = the density of donors

n_d = the density of un-ionized donors

p = the density of free holes

N_a = the density of acceptors

n_a = the density of un-ionized acceptors

Let us consider an n type material. This implies that p and n_a are negligible. Now

$$n = N_c \exp\left[\frac{E_F - E_c}{kT}\right] \qquad \langle 102 \rangle$$

where N_c = the conduction band effective density of states

E_F = the Fermi energy

E_c = the conduction band energy

Also

$$n_d = \frac{N_d}{1 + \frac{1}{g}\exp\left[\frac{E_d - E_F}{kT}\right]} = \frac{N_d}{1 + \frac{N_c}{2n}\exp\left[\frac{-\zeta_d}{kT}\right]} \qquad <103>$$

where E_d = the donor energy level

$\zeta_d = E_c - E_d$, the donor activataion energy

g = ground state degeneracy of the impurity level (= 2).

For the sake of brevity, let:

$$N_c' = \frac{N_c}{2}\exp\left[\frac{-\zeta_d}{kT}\right] \qquad <104>$$

Therefore, from <102>

$$n = N_d - N_a - \frac{N_d}{1+\frac{n}{N_c'}}, \qquad <105>$$

which yields a quadratic expression in n:

$$n^2 + n(N_c' + N_a) - N_c'(N_d - N_a) = 0 \qquad <106>$$

with a physically acceptable solution

$$n = -\frac{1}{2}(N_a + N_c') + \frac{1}{2}\left((N_c' + N_a)^2 + 4N_c'(N_d - N_a)\right)^{1/2} \qquad <107>$$

This formula has two simple approximations as described below.

CASE I - Uncompensated Donors

Let N_a be very small. In addition, let $N_d >> N_c$ to ensure that these levels are partially ionized for Poole Frenkel barrier lowering to be significant. In this case equation <107> has an approximation of

$$n \cong \sqrt{N_c N_d} = \sqrt{\frac{N_c N_d}{2}} \exp\left[\frac{-\zeta_d}{2kT}\right] \qquad <108>$$

And in the presence of Poole Frenkel barrier lowering in the high field limit where from page 62:

$$\Delta\zeta_d = \sqrt{\frac{q^3\xi}{\pi\varepsilon\varepsilon_o}} \qquad <84>$$

Thus

$$n = \sqrt{\frac{N_c N_d}{2}} \exp\left[-\frac{\zeta_{do}}{2kT}\right] \exp\left[\frac{1}{2kT}\sqrt{\frac{q^3\xi}{\pi\varepsilon\varepsilon_o}}\right] \qquad <109>$$

The progression from carrier density to current density can now be made. In well behaved crystalline semiconductors, the relationship between electric field and current density is linear with the constant of proportionality being the product of carrier density, mobility and the electronic charge. Therefore the high field behavior of a semiconductor containing donors (or acceptors) is expected to be of the form:

$$J = n q \mu \xi \qquad <110>$$

and thus

$$J = \mu q \sqrt{\frac{N_c N_d}{2}}\, \xi \exp\left[\frac{-\zeta_{do}}{2kT}\right] \exp\left[\frac{1}{2kT}\sqrt{\frac{q^3 \xi}{\pi \varepsilon \varepsilon_o}}\right] \qquad \langle 111 \rangle$$

This may be recast in terms of the experimental parameters: current density, J, and voltage, V:

$$J = K_{pf}\, V \exp(\beta \sqrt{V}) \qquad \langle 112 \rangle$$

where

$$K_{pf} = \frac{n_k q \mu}{d} \exp\left[\frac{-\zeta_{do}}{2kT}\right] \qquad \langle 113 \rangle$$

$$\beta = \frac{1}{kT}\sqrt{\frac{q^3}{4\pi \varepsilon \varepsilon_o d}} \qquad \langle 114 \rangle$$

d = insulator thickness

$$n_k = \sqrt{\frac{N_c N_d}{2}}$$

CASE II - Partially Compensated Donors

In this case let the acceptors remain, but in smaller numbers than that of the donors. Furthermore, let $N_a >> N_c'$. This condition allows expansion of the square root in equation <107> as follows:

$$n = -\frac{N_a}{2} + \frac{N_a}{2}\left\{1 + \frac{4N_c'(N_d - N_a)}{N_a^2}\right\} \qquad \langle 115 \rangle$$

or

$$n = \frac{N_c'(N_d - N_a)}{N_a} \qquad \langle 116 \rangle$$

$$= \frac{(N_d - N_a)}{2N_a} N_c \exp\left[\frac{-\zeta_{do}}{kT}\right] \qquad \langle 117 \rangle$$

Therefore in the presence of Poole Frenkel barrier lowering,

$$n = \frac{(N_d - N_a)}{2N_a} N_c \exp\left[\frac{-\zeta_{do}}{kT}\right] \exp\left[\frac{1}{kT}\sqrt{\frac{q^3 \xi}{\pi \varepsilon \varepsilon_o}}\right] \qquad \langle 118 \rangle$$

which implies

$$J = \mu q \frac{(N_d - N_a)}{2N_a} N_c \xi \exp\left[-\frac{\zeta_{do}}{kT}\right] \exp\left[\frac{1}{kT}\sqrt{\frac{q^3 \xi}{\pi \epsilon \epsilon_o}}\right] \quad \text{<119>}$$

The β that arises from this situation is

$$\beta = \frac{1}{kT}\sqrt{\frac{q^3}{\pi \epsilon \epsilon_o d}} \quad \text{<120>}$$

which is twice the one in equation <114>

Also K_{pf} differs from that in equation <113>, and is instead:

$$K_{pf} = \mu q \frac{(N_d - N_a) N_c}{2d N_a} \exp\left[\frac{-\zeta_{do}}{kT}\right] \quad \text{<121>}$$

In this work, a compensation index γ is adopted to relate the true barrier lowering $\Delta\zeta_d$ to the slope of the $\ln(J/V)$ vs $\sqrt{V}$ curve, hereafter defined to be β. That is

$$\beta = \frac{\alpha}{\gamma kT \sqrt{d}} \quad \text{<122>}$$

$$= \frac{1}{\gamma kT}\sqrt{\frac{q^3}{\pi \epsilon \epsilon_o d}} \quad \text{<123>}$$

Where $\gamma = 1$ in partially compensated semiconductors

or $\gamma = 2$ in uncompensated semiconductors

Other cases may be envisioned involving impurity sites that experience Poole Frenkel barrier lowering; e.g. N_a may be allowed to increase further to surpass N_d, but then the original equation <102> must be rewritten for p-type material. In these and other cases analogous expressions can be derived. Simmons (6) and Mark

and Hartman (183) have examined these and have found no new forms of the basic carrier concentration equations. The contribution of Yeargan and Taylor (184) was to point out that since β is derived from an approximation at the extremes of the permitted population of partially compensating acceptors, then γ should vary between 1 and 2.

Recall from the discussion of punch-through Schottky barriers that the Schottky β, which is the slope of a ln(J) vs $\sqrt{V}$ plot (equation <13>, page 22), has a value exactly equal to the slope of a similar curve for Poole Frenkel conduction if γ were 2. This has lead to difficulties in distinguishing the two conduction models, especially since the uncompensated case where γ does equal 2 was not originally considered (74,183,185). This issue was brought to a head when data was published that appeared to have a Schottky-like β (82) even up to thicknesses of 4 μm, and even when dissimilar contact materials were used. To reconcile the apparently contact controlled J-V behavior with otherwise bulk controlled characteristics, an argument was waged in the literature between the various camps of Jonscher, Hill and associates at Chelsea College (65, 138, 154, 185-187); Simmons and his students (6, 73-75, 188, 189); Mark and Hartman (183); and Yeargan and Taylor (184), until the explanation was found in semiconductor carrier statistics.

PART II - THEORY

Modifications and Hybrid Theories:

The task remains to test the theory for its validity in the application to anodic Ta_2O_5 films. Although the above simple theory is derived for an isolated donor in a crystalline semiconductor, it is used to explain the behavior of imperfect amorphous insulators. There is considerable irony in the observation that Poole Frenkel conduction has been rarely reported in crystalline materials (190-196). Jonscher (197) offers an explanation. At the electric field strengths required to significantly increase free carrier concentrations through Poole Frenkel barrier lowering, avalanche breakdown has already occurred in a crystalline solid. Amorphous materials also exhibit avalanche breakdown, but at correspondingly higher fields due to the shortened mean free path of the electron. Nevertheless, the use of single crystal concepts to model amorphous behavior is one assumption of this simple picture of Poole Frenkel conduction that must be examined in detail.

First then, the question must be asked - what parts of the theory survive the transfer from a single crystal to an amorphous solid and what parts must be abandoned? The extensive work with amorphous and liquid semiconductors of the last two decades has established that the basic band structure of the amorphous semiconductor differs from that of the single crystal only in the diffuse nature of the band edges (198,199). There is no longer a precisely defined band gap in the amorphous solid. Instead, a

continuum of states exists within the "band gap", which are characterized by rapidly decreasing mobility as the energy separation from the approximate band edges increases. Thus, the electronic propagation that takes place in the conduction band may be safely described with single crystal concepts.

The smeared-out band edges do make the concept of a precisely defined activation energy, ζ_a, suspect, however. An electron thermionically emitted from an impurity site does not reach the conduction band after a specific energy gain - but rather it becomes more and more mobile as its energy increases. A spread of activation energies would intuitively seem more appropriate. Fortunately, thermally stimulated conduction and photoconductivity experiments have indicated that in some amorphous materials at least, activation energies are well defined (69,200).

A second concept that can be questioned is that of mobility. In many materials, amorphous (201) and single crystal (202), the electron drift velocity saturates at high electric fields. After that point, mobility is undefined and equation <110>, page 73, must be replaced by:

$$J = nq\, v_{sat} \qquad \text{<124>}$$

Thus:

$$J \propto \exp\sqrt{cV} \qquad \text{<125>}$$

Note that current density has a field dependence through carrier density alone. Jonscher (65) points out that this is

equivalent to saying that the escaped electron travels to the next nearest site downstream where it is recaptured. In contrast, the simple theory is dependent on the electron spending a mean free time in the conduction band. Under saturated velocity conditions, one observes a linear relationship between ln(J) and $\sqrt{V}$ rather than ln(J/V) and $\sqrt{V}$ as predicted by simple theory. This point has been missed by many workers who have used ln(J)- $\sqrt{V}$ relationship indiscriminately. To the author's knowledge the behavior of drift velocity in Ta_2O_5 has not been investigated (203).

One final objection to raise is how does the behavior of an isolated donor relate to the behavior of an assembly of them in a real material with edges and contacts? Are the electrons extracted and replenished through the contacts with little or no expenditure of voltage? The only contact capable of supplying carriers upon demand without significant assistance of an applied electric field is the true ohmic one. Its behavior may be mimicked however by a process by which electrons tunnel directly into deep levels adjacent to the contact with subsequent excitation to the conduction band (65). Interestingly, exactly this kind of interfacial tunnelling was the mechanism proposed to explain the frequency behavior of tantalum oxide capacitors (204). If the contacts' influence is significant, then one of the hybrid models which combine Poole Frenkel conduction with injecting (76) or blocking (74) contact behavior must be used.

On a different level, the Poole Frenkel effect has been combined with other emission mechanisms. For instance, Hill proposed that the distorted barrier becomes narrow enough at high fields to permit quantum mechanical tunnelling from the donor core to the conduction band (164). Using the Wentzel-Kramers-Brillouin (W.K.B.) tunnelling approximation, he was able to reduce a rather complicated expression to a two variable system which allows the plotting of experimental J-ξ data for a range of temperatures on a single graph. J and ξ are combined into a new variable, $\vartheta = J\,T^{-n}\exp(\xi_d/kT)$ where n = 3 or 4. Poole Frenkel mechanisms are identified when ϑ is a hyperbolic function of $\delta = \beta\sqrt{\xi}\,/kT$. This model accounts for the decreased sensitivity to changing temperature at low temperatures due to the increased dominance of tunnelling in that regime, and for the often seen ohmic behavior at low fields. Experimental data for SiO_x were shown to agree with the theory's prediction for a large temperature range.

Martin et al. (173) and Vincent et al. (181) have extended Hill's work by incorporating phonon assisted tunnelling over Coulombic, and non-Coulombic wells. In these models, the carrier is thermally excited to a psuedo-state partway up within the well, from which point it may more easily tunnel into the conduction band. For all these models, the effects become more noticeable at lower temperatures.

PART II - THEORY

Experimental Evidence :

The most convincing examples of Poole Frenkel conduction have three characteristics in common: $\ln (J/V)$ is proportional to $\sqrt{V}$ and J-V behavior is essentially independent of both electrode work function and bias polarity. Silicon nitride, as studied by Brown et al. (205), and Sze (206) fits the description. In Sze's study, concurrent ohmic and tunnelling components were also identified via temperature dependences. Brown used the wide latitude permitted in the preparation of this material to check the predicted variation in conduction with d and ϵ. He notes that the observed β's tended to be 10% higher than was calculated from independent measurements of d and ϵ. In both studies β was analysed with $\gamma = 1$.

Silicon oxide has also yielded some convincing examples of Poole Frenkel conduction - although not always recognized as such. The work of Hartman, Blair and Bauer (81) is a case in point. Nonrectifying $\ln(J)$ vs $\sqrt{V}$ behavior was obtained for four different metal contacts and for thicknesses varying from 1 to 10 μm. A Schottky emission interpretation was discarded on the unfavourable comparison of the deduced barrier height and the one observed directly with photoresponse techniques. Other internal inconsistencies were found with the model. However, they also discarded the Poole Frenkel theory, as it was then known, because the β appeared to be Schottky like. This is, of course,

permissible when $\gamma = 2$. Their data also shows a classic example of the low bias transition from Schottky emission to Poole Frenkel conduction which was not described theoretically for another two years (74). The results of Hirose and Wada (82) on SiO_2 are similar. They originally interpreted it as Poole Frenkel conduction, but this view fell into disfavour (84) because the deduced ε was much larger than the accepted value. In fact, the agreement is very good when the uncompensated donor model ($\gamma = 2$) is used. The work of Johansen (207) on SiO_2 is often cited for his attempt to reconcile apparent bulk conduction with Schottky like β's. He proposed, (with some expressed misgivings) that Schottky emission could be taking place from islands of "metallic" silicon in the interior of the insulator. Ironically he also mentions the effect of compensation, but misquotes it, and thus expected a β twice as large as the "normal" one, and four times as large as the one he observed.

Extensive research has been performed on SiO_x more recently. A.K. Jonscher and his colleages have been particularly active in this area (12, 65, 138, 154, 185-187). The three mentioned criteria of Poole Frenkel conduction were demonstrated for an exceptionally wide range of bias conditions in the paper of Jonscher and Ansari (187) ... but for dark currents only. Low levels of light intensity increased the current by a temperature insensitive amount proportional to $\sqrt{V}$. They came to the conclusion that the light was capable of altering the equilibrium

electron distribution present in the donor sites. The resulting J-V behavior would therefore appear anomalous, but could be brought back into agreement with Poole Frenkel predictions with the use of an effective temperature higher than that of the lattice. Many subsequent papers from this group explore the dynamic J-V behavior, and TSC (thermally stimulated current) properties of SiO_x that exhibit Poole Frenkel conduction. Table IV reviews some of the experimental evidence for Poole Frenkel conduction in SiO_x, Si_3N_4, and other materials.

The evidence for Poole Frenkel conduction in tantalum pentoxide generally is not as good. Early work with a variety of metal counter electrodes demonstrated large changes in conductivity, but no clear work function dependence (208). Flaw conduction may have been at fault as metal foil was used. Mead (209) had also shown ln(J) vs $\sqrt{V}$ behavior and analysed it as Poole Frenkel conduction, but calculated an erroneous dielectric constant. This was pointed out by Schug (210), who re-examined the data in terms of $\gamma = 2$. Many other examples since these early ones have been documented. Often data is quoted for one polarity only - the other one being subject to too much drift (209). An interesting observation in this respect is that of Pulfrey, Shousha, and Young (76). Their tantalum oxide films were rectifying until a large voltage was applied in the "drifty" polarity, after which point the films became nonrectifying and obeyed a Schottky law. It is likely that the "before" case

resulted from a contact barrier that was removed by the voltage stress, after which uncompensated Poole Frenkel conduction due to the bulk was seen.

The compensation index γ, has been observed by the various workers to be equal to either 1 or 2 (within 23%). Intermediate values have not been documented prior to the work reported in this thesis. Angle and Talley see $\gamma = 1$ for thermal oxides and $\gamma = 2$ for anodic oxides of similar thickness and conductivity (51). Matsumoto (86) changed $\gamma = 1$ behavior to $\gamma = 2$ behavior by vacuum baking the anodized tantalum oxide, whereas P.L.Young (211) sees γ go from 2 to 1 with a more gentle heating of r.f. sputtered films. And finally, Gubanski and Hughes (70) fail to see Poole Frenkel conductivity at all unless their tantalum oxide is thoroughly dried. These examples and others of Poole Frenkel conduction in Ta_2O_5 are also reviewed in Table IV.

TABLE IV

Experimental Evidence for Poole Frenkel Conduction

DEVICE STRUCTURE	THICKNESS (nm)	EVIDENCE	COMPENSATION RATIO, γ	RECTIFICATION RATIO	REF.
$Ta-Ta_2O_5-Al$	50-100	$J \sim \exp(\beta\sqrt{V})$	~1 anodic ~2 thermal	<10	51
$Ta-Ta_2O_5$ {Al, Au}	300-500	$J \sim \exp(\beta\sqrt{V})$	~2	10-100	69
$Ta-Ta_2O_5-Au$	87	J-V-T	~2		209
$Ta-Ta_2O_5-Al$	340	$J \sim \exp(\beta\sqrt{V})$	~1 unheated ~2 heated		86
$Si-Ta_2O_3-Al$	70	$J \sim \exp(\beta\sqrt{V})$	~2		52
$Ta-Ta_2O_5-Au$	27-81	$J \sim \exp(\beta\sqrt{V})$	~1	<2	89
$Ta-Ta_2O_5-Al$	80	J-V-T	~1	<2	59
$Ta-Ta_2O_5$ {Au, Al}	14-240	$J-V-\phi_m$	~2 as is ~1 dried		211
$Al-Al_2O_3-Al$	40	J-V-doping	~1	1	88
$Si-Cr_2O_3-Al$	100	J-V	1.05		139
Si, Mo / Si_3N_4 / {Al, Cr}	60-600	J-V-T d, ε, Ø	.9	<2	205
$Si-Si_3N_4-Al$	350	J-V	~1	1	212
$Si-Si_3N_4$ {Au, Mo}	110-290	J-V	fcn(T)	1	206
$Si-Si_3N_4-Al$	100	J-V-T	~1		213
$Si-Si_3N_4-Al$	100	J-V-T		1	214
$Al-SiO_x-Al$	250-590	J-V-T	~2	~1	138
$Al-SiO_x-Al$	100-1000	J-V	~2	~1	207
$Al-SiO_x$ {Al, Cu, Mg, Ti}	300-1400	$J-V-\phi_m$	~2	~1	187

TABLE IV (Cont'd)

Experimental Evidence for Poole Frenkel Conduction

DEVICE STRUCTURE	THICKNESS (nm)	EVIDENCE	COMPENSATION RATIO, γ	RECTIFICATION RATIO	REF.
Au-SiO_x-Au	100-300	J-V	~1 doped ~2 undoped	~1	215
Al-SiO_x-Al	500	J-V-T	~1		216
Ti-TiO_x-Au	20-60	J-V	~1	1	217
Mo-MgO-electron beam	5-20	J-V-T	1		196
Au {CdO _ P_2O_5 / ZnO} {Au / Ag}	$1.2-4.5\times10^4$	J-V-T-ϕ_m	1	1	161
Au {CdO _ P_2O_5 / ZnO} Au	$1.3-2.1\times10^4$	J-V-ϕ	2	1	160
Si-Si_3N_4-Al	150	J-V-T-ε	1	-	218
Si / Al } SiO_2-Si	50-120	J-V-T-d	.96-1.23	fcn(T)	219
Ag-phthalocyanine-Ag	200-2200	J-V-T-d	1	1	220
Al / Zn / Sn } GeS-Al	50-500	J-V-ϕ	~1 or 2	1	221
Cd-CdSe-Se	5.5	J-V	1	1	193
Al / In / Ag } CdTe { Al / In / Ag	723-1165	J-V-T-d-ϕ	2		222
In / Au } CdF_2 { In / Au	.5-1mm	J-V-T-ϕ		1	223
Au / Al } AlN-Si	100-300	J-V-T	1	1	195
Bi / Au } FeF_3 / NiF_2 { Au	500	J-V-T-ϕ	1	1	148
Au-hexamethyl disiloxane - Au	800	J-V-T			224
Au-polymethyl pentene - Au	5×10^4	J-V-T	1	1	225
Al-polystyrene - Ag	60-350	J-V-T-d	2	1	226

2. DEFINITION OF EXPERIMENTAL GOALS

Now that all of the major contenders have been put forward with appropriate supporting evidence, it remains to be seen which conduction model most closely describes the electrical behavior of the Ta_2O_5 films used in this study. All four models predict the existence of a high field regime where current density rises rapidly and superlinearly with increasing voltage. In fact, all four can be made to fit the J-V behavior observed here - for a restricted range of currents and with appropriate choice of values for the disposable parameters in each J-V expression. This is shown in Figure <13> for a typical set of J-V data. The restricted range is understandable, even expected, because more than one conduction mechanism may be operative in each voltage region. Fortunately the disposable parameters do remain open to examination. The main thrust of the work described here is the comparison of the predicted and observed J-V behavior using independently determined values of the material properties that make up these disposable parameters. The addition of the variable, temperature, allows tests of self consistency as well. For example, the value of a physical property may be inferred from J-V behavior at room temperature and from J-T behavior at constant voltage. The properties involved, such as the dielectric constant or film thickness should have little or no temperature

Figure <13> Comparison of Proposed Models Fitted to J-V Data

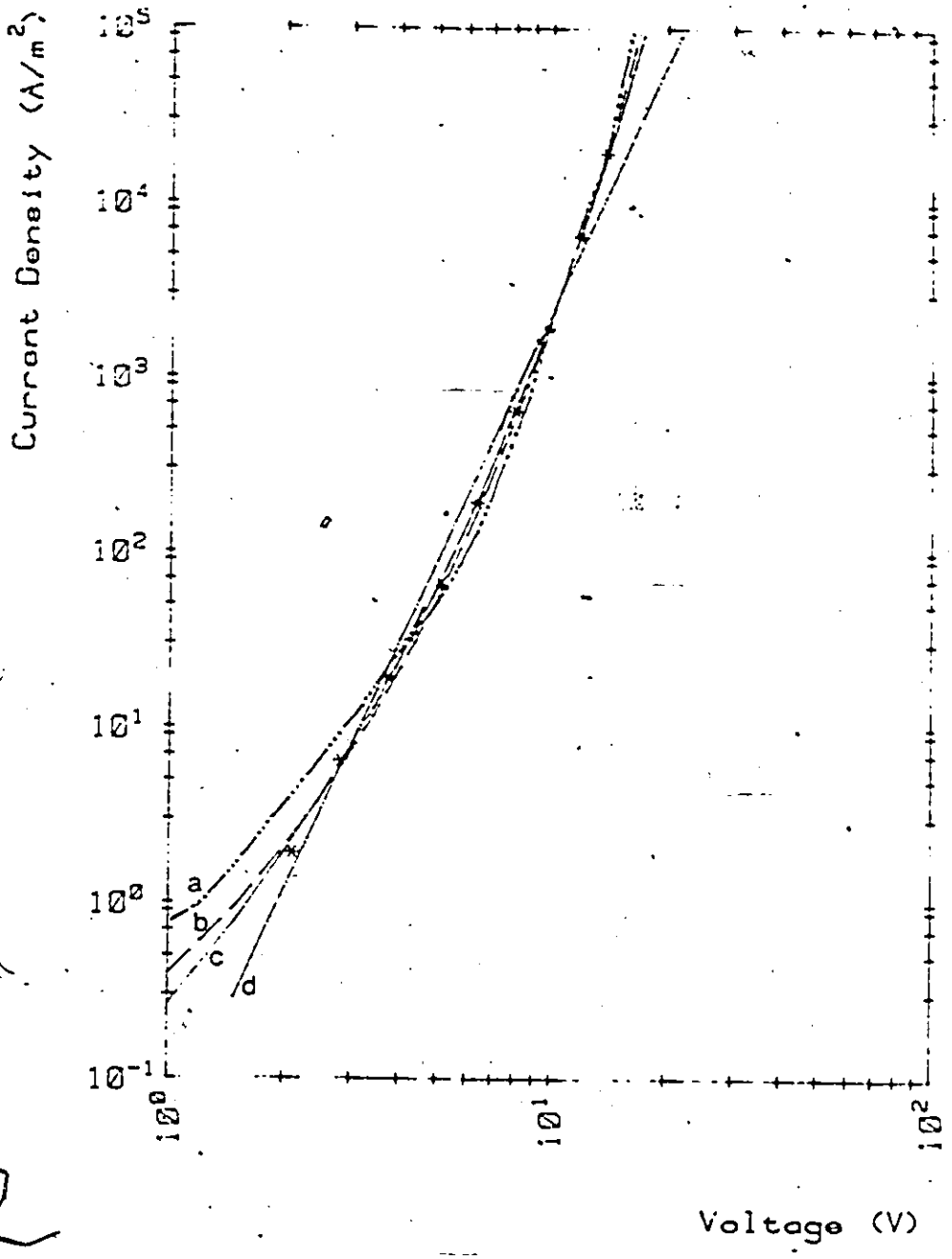

Typical J-V data is plotted here and compared to least squares fits to four conduction models: (a) Hopping, (b) Poole Frenkel, (c) Schottky barrier, and (d) Space charge limited conduction

or voltage dependences in the ranges covered, and so the two inferred values should be the same. Table V presents the J-V-T expressions for Schottky, SCLC, Hopping and Poole Frenkel conduction with the temperature and voltage independent parameters condensed into the single constants the measurements are able to determine. Table V is found on page 91.

An experimental goal that must be achieved prior to J-V study is the exclusion of flaw dominated conduction. The method of sample preparation is designed to reduce flaws. Should they occur, the following test, as recommended by Schwartz and Gresh (28), will set a maximum limit on their size and density. In this experiment, devices are made with areas ranging over three orders of magnitude. The very smallest of the devices, 4 μm by 4 μm in area, are still large compared to the flaws now thought to control catastrophic breakdown (>10 nm in diameter) (20), but the flaws which invalidated much of the early work in anodic conduction would be identified by this test. In addition, flaws in anodized tantalum pentoxide thin films often cluster along the edges of tantalum electrode where etching may leave burrs or promote local lifting of the metal from the substrate. Thus flaw conduction usually depends on device "perimeter" rather than area, and can be identified in this manner.

Once current density has been proven valid, the other geometric property of the device, oxide thickness, can be studied. The thickness dependence of SCLC, $J \propto d^{-(2s+1)}$, where

the exponent, $-(2s+1)$, is uniquely related to the exponent, $s+1$, relating J to V^{s+1}, is significantly different from that of Schottky or Poole Frenkel conduction where $J \propto \exp(\text{constant}/\sqrt{d})$ or Hopping where $J \propto \exp(\text{constant}/d)$. Therefore devices with a range of thicknesses were tested. The range is not extensive, only 40 to 65 nm, primarily because the experimental evidence and the proposed hybrid models have suggested that a transition from one conduction mechanism to the other may be expected as thickness is increased.

In all models conduction is dependent on the dielectric constant which of course varies with frequency. In SCLC, the low frequency, or static dielectric constant is important. For the devices used here, the measurement of capacitance and oxide thickness allows this value to be calculated. For Poole Frenkel and Schottky conduction equations, the high frequency dielectric constant is required. This was calculated from the index of refraction of the oxide, which was obtained by a combination of reflectance spectrophotometry and ellipsometry techniques (41). In hopping conduction both dielectric constants enter into the calculation of the radius and energy of the polaron. To explore further the relationship between the optical and electrical properties of the oxide, the dielectric constant of the oxide was varied in a controlled manner by nitrogen doping the parent tantalum film. The pertinent electrical parameters could be then checked to see if they varied in the fashion predicted.

The values of mobility and carrier concentration and the details of the interface properties do remain inaccessible in all but the hopping conduction model. Hopping is unique in that all parameters are accessible, and are in many ways interdependent (e.g hop length and impurity density). Thus only in a hopping analysis can the absolute level of conductivity be compared to model predictions. Large changes in the overall conductivity are attained through heat treatments while other properties may be unaltered. So, even though the physical cause for these changes cannot be quantified for some of the models, annealing does provide very fertile ground for testing these theories over extended conductivity ranges.

TABLE V

Comparison of Proposed Conduction Formulae

Contact Limited Conduction - Schottky Barriers

$$J_{sch} \propto T^2 \exp\left[\frac{-q\phi_o}{kT}\right] \exp\left[\frac{B}{2kT}\sqrt{\frac{V}{d}}\right] \quad \text{<126>}$$

Space Charge Limited Conduction - SCLC

$$J_{sclc} \propto \exp\left[\frac{-\zeta_{do}}{kT}\right]\left[\frac{V^{s+1}}{d^{2s+1}}\right] \quad \text{<127>}$$

Thermally Activated Hopping Conduction

$$J_{thop} \propto \frac{V}{d} \exp\left[\frac{CVR}{Td}\right] \exp\left[\frac{-W}{kT}\right] \quad \text{<128>}$$

Variable Range Hopping Conduction

$$J_{vhop} \propto \frac{V}{d} \exp\left[\frac{CVR}{Td}\right] \exp\left[\frac{-T_o}{T}\right]^{\frac{1}{4}} \quad \text{<129>}$$

Poole Frenkel Conduction

$$J_{pf} \propto \left[\frac{V}{d}\right]^n \exp\left[\frac{-\zeta_{do}}{\gamma\, kT}\right] \exp\left[\frac{B}{\gamma kT}\sqrt{\frac{V}{d}}\right] \quad \text{<130>}$$

PART III - EXPERIMENTS

1. SAMPLE PREPARATION AND MEASUREMENT TECHNIQUES

Sample Preparation:

The samples of Ta_2O_5 used in this study were prepared with the basic process sequence shown in Figure <14>. The details of this process are described below. First, soda lime or borosilicate glass substrates 2 inches square were thoroughly degreased and rinsed in accordance with standard thin film techniques. Either a dc diode, or planar magnetron sputtering system as previously described in the literature (227,228) was then loaded with a number of these substrates, and pumped to a base pressure of 10^{-4}Pa before the diffusion pump was throttled and high purity argon, the sputtering gas, was admitted into the chamber. After a short pre-sputter period to remove the layer of the target which was exposed to the atmosphere, an etch stop layer of tantalum pentoxide was reactively sputtered in oxygen from a 99.999% pure Ta target. Without breaking vacuum a shutter was then put in place between the target and the substrates and the target was sputtered in pure Ar, or an Ar/N_2 mixture until the stoichiometry of the target was stable. Then the shutter was removed and the substrates were coated with a nominally 200 nm thick layer of tantalum or tantalum nitride. In a few of the earlier experiments, the etch stop layer was formed by depositing a 50 nm Ta layer and converting it to an oxide thermally. The tantalum layer to be anodized was then deposited in the same

Figure <14> Outline of Sample Preparation Sequence

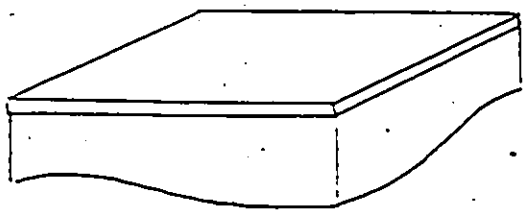

(a) Clean glass substrates are coated with a layer of Ta_2O_5

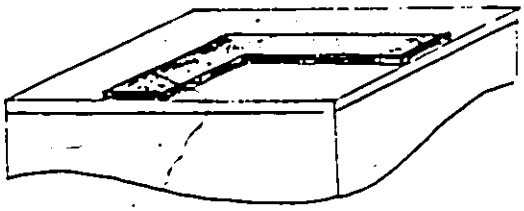

(b) Ta or TaN_x then is sputtered and photolithographically defined.

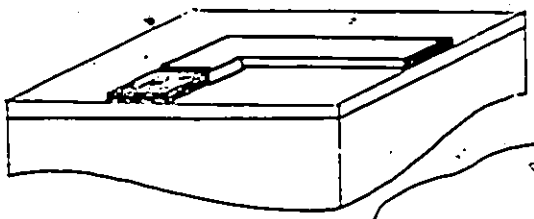

(c) The metal is partially converted to an oxide by anodization in a weak citric acid electrolyte.

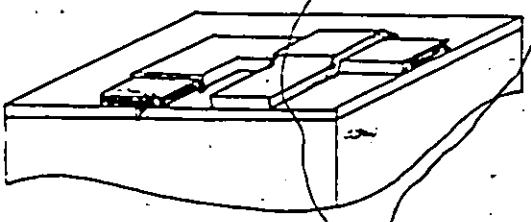

(d) Then a layer of Cr is evaporated and photolithographically defined into strips that intersect the oxide coated tantalum at right angles.

fashion as just described. Next, this tantalum was photolithographically defined into the required base electrode pattern. The etch stop layer of Ta_2O_5 protected the glass substrate from chemical attack in this step.

Anodization of the oxide took place at room temperature in a 0.1% solution of citric acid monohydrate in de-ionized water. A constant current of 10 A/m^2 from a Keithley constant current source was passed through the sample, causing oxide growth, and a linear rise in voltage. When the voltage reached a pre-set limit (30 V, unless otherwise stated) the voltage was held constant until the current had fallen to 10 mA/m^2. The behavior of anodizing current and voltage with time is shown schematically in Figure <15>. The sample was then carefully rinsed in boiling de-ionized water to remove all surface traces of electrolyte.

The top contact metal used in these experiments was electron-beam evaporated chromium. It was also defined photolithographically. The oxide coated tantalum lines and the chromium lines intersect each other at right angles, minimizing the error in area that could be possible through registration difficulties.

During the course of the study both dc diode and magnetron sputtering were used to deposit the first two layers. The latter technique is an improvement on the diode system, featuring a magnetic field to confine the secondary electrons to the target region thus increasing the sputtering rate. As mentioned in the

Figure <15> Typical Anodizing I-V-t Characteristics

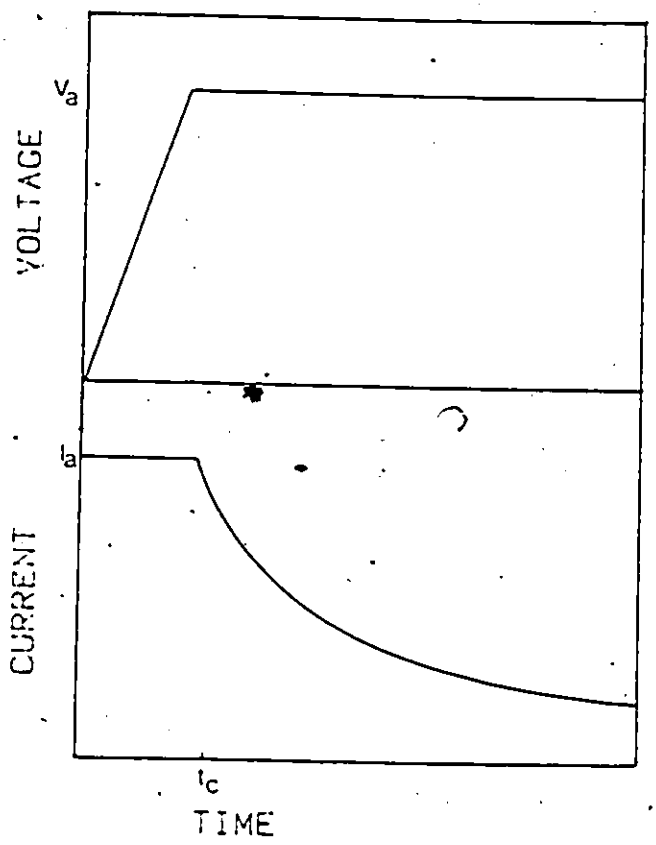

Formation of the anodic oxide uses both galvanostatic and potentiostatic modes. First a constant current is passed through the cell, causing oxide growth and a linear rise in voltage. Once the desired voltage is reached, it is held constant while current falls as 1/time. The process is halted when current has reached levels that can be attributed to electronic conduction alone. For the samples in this study total anodizing times were 3-5 mins.

introduction, the residual gas pressures and impurity levels associated with an individual sputtering system do play an important role in determining the characteristics of the anodic oxide to be formed on the deposited tantalum. This observation was indeed substantiated in our work. Even though the Poole Frenkel nonlinearity coefficient β, which is related to insulator dielectric constant and thickness (defined in equation <122>, page 75), was reproducible from system to system, the conductivity coefficient, K_{pf}, indicative of a doping concentration, was found to be several orders of magnitude lower in oxides formed on magnetron sputtered tantalum, as compared to diode sputtered films.

Four electrode patterns, each designed for a specific type of measurement, were used in this investigation. For optical measurements, broad areas of oxides of different thicknesses were required. For this purpose, centimeter wide tantalum electrodes with a common contact to the anodizing electronics above the electrolyte meniscus were photodefined. Thus the area and appropriate anodizing current could be determined accurately. Also, regions of flawed tantalum that may be present at the edges of the substrate could be avoided. Any such flaw, scratch or pinhole would have thwarted precise control of anodizing parameters, because oxygen evolution there would have short circuited oxide growth. In any case, those samples showing bubbles, or abnormal anodizing I-t behavior were dropped from the

experiment. Three other patterns were designed for conductivity measurements. One, shown in figure <16>, featured ten devices of each of four different areas with provision made for easy simultaneous access to each device with an edge connector. It was primarily used in the J-V-T experiment. Figure <17> shows an enlarged view of the area test pattern, used to determined the area - current relationship. The fourth pattern featured an array of 32 by 32, 12.5 μm square devices, for the purpose of generating statistics on device characteristic uniformity.

Measurement of Optical Properties :

Two parameters that enter the conduction formulae are oxide thickness, d, and index of refraction, $\hat{n}$, (as the square root of the high frequency dielectric constant). The first is particularly difficult to measure by simple step height techniques because the oxide grows both above and below the plane of the unanodized metal. In addition the oxide is very chemically stable, complicating attempts to etch a step while preserving the substrate surface.

The method chosen was a combination of reflectance spectrophotometry and ellipsometry. In the former, the reflectance of the oxide coated metal was measured from 187 nm (the cut-off of the quartz optics) to 1000 nm (beyond the position of the zero-th interference peak) in a Perkin - Elmer 3330 Spectrophotometer (kindly made available by the Optical

Figure <16> Mask for I-V-T Test Pattern

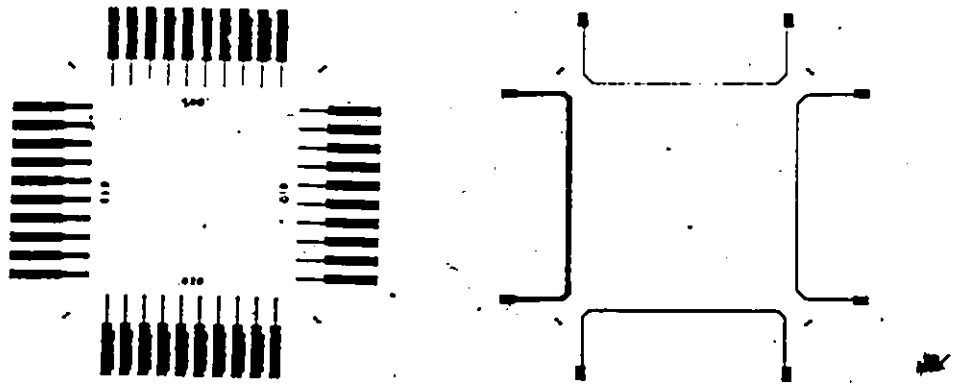

The mask for the tantalum (a) and chromium (b) levels are shown above. When these patterns are overlapped, 40 devices are formed, 10 of each of the following dimensions: .005" = 125 µm, .010" = 250 µm, .020" = 500 µm, .040" = 1000 µm square.

Figure <17> Mask for Area Test Pattern

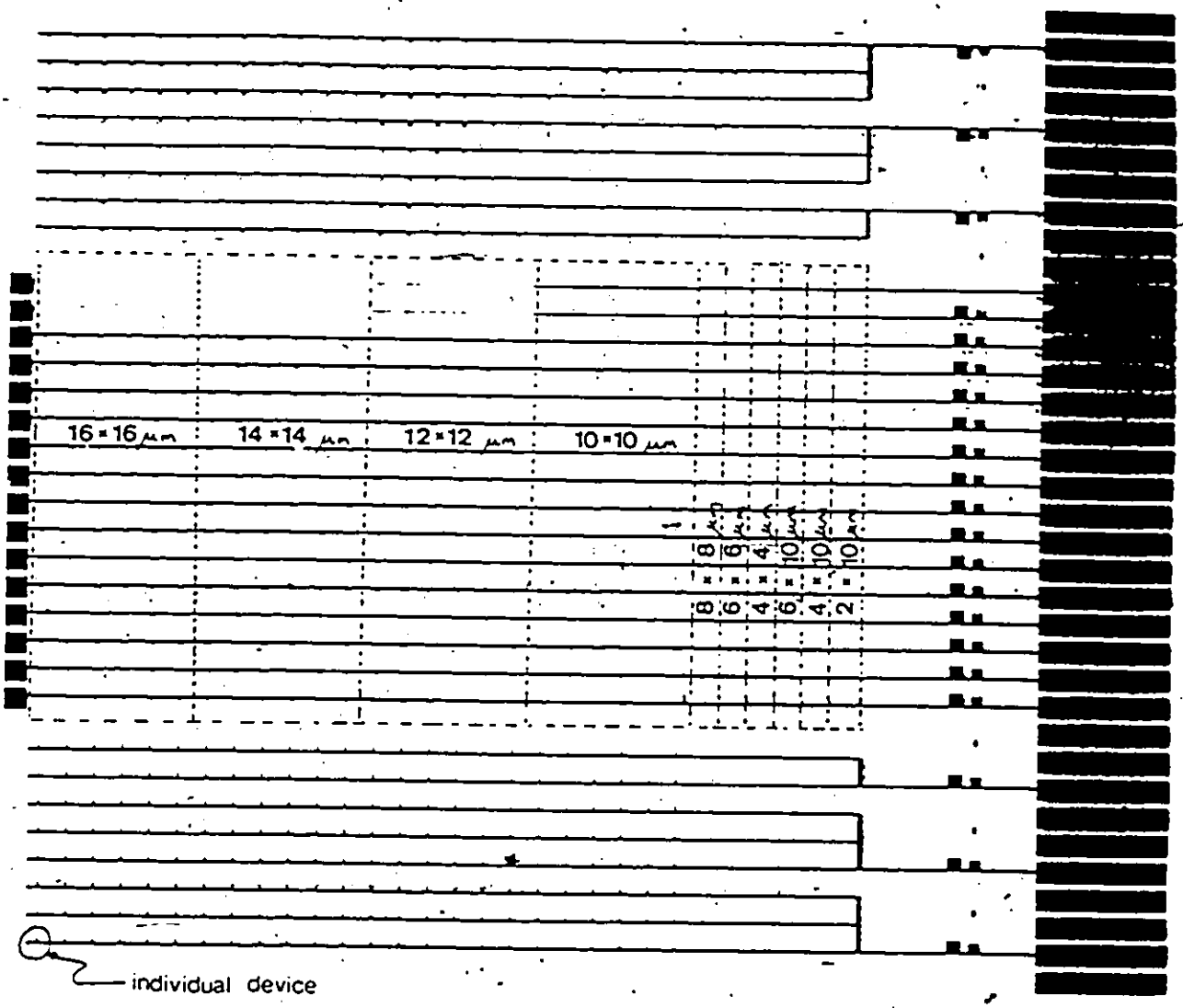

The tantalum level of the area test pattern is shown above at 3.25x. Devices are formed at the crossover of chromium electrodes (not shown) and the oxide coated tantalum lines connected at right angles to the main tantalum electrodes running from right to left in this diagram. The numbers on the diagram refer to the width of the Ta and Cr lines (respectively) making up the devices in each block outlined with the dotted lines.

Physics Department of the National Research Council of Canada). The positions of the peaks are related to the product of the index of refraction, $\hat{n}$, and the oxide thickness, d (229,230). Thus a dispersion curve in terms of $\hat{n}d$ can be constructed for the entire wavelength range. To separate these two variables, more information is required. Either transmission spectra or a measurement of either $\hat{n}$ or d at a single frequency would suffice. The first option is unavailable: the ever present metal underlayer is opaque; therefore the second option was pursued. Representative samples, including those of the various nitrogen doping concentrations, were prepared and analysed at 632.8 nm (He-Ne laser) by ellipsometry at the Electrical Engineering Department of the University of British Columbia by Dr. David Smith. In this method (231) the absolute phase and amplitude of the light reflecting from a given surface are measured for both the components parallel and at right angles to the plane of incidence. The extra variable permits the independent determination of both $\hat{n}$ and d at the one wavelength and thus provides a reference point to scale the dispersion curve determined from the reflectance data.

Measurement of Electrical Properties:

Current - voltage (I-V) measurements were made using a Keithley constant current source (0.1 nA to 10 mA) and a Keithley electrometer (input impedance $10^{14}\ \Omega$). Shielding of the

electrometer, the constant current source cables and the sample holder was required to reduce electrical noise. The measurement error in current is ± 0.5% (or .05 nA, whichever is larger); in device size is ± .25μm; and in voltage is ± 1 mV. The typical device responded to the first application of a constant current in a manner that saw the voltage rise gradually with an estimated time constant of 1 to 5 seconds. Thereafter, the I-V characteristics could be reproduced, provided the highest bias previously reached was not exceeded. The test procedure, therefore, consisted of increasing the current through the device until the maximum desired level had been reached, then reducing the current in steps and allowing for capacitive discharge before measurements of voltage were made. In this way, true steady state behavior could be determined. A recorder trace of typical charging and discharging phenomena may be seen in Figure <18>. In general the range of I-V data is limited by noise in the low current region (< .05 nA), and drift at high fields (V_a > 80% of the anodizing voltage).

In the J-V-T experiment the test limit was kept to a very conservative 15% of the anodizing voltage to eliminate possible drift. In this experiment three out of the 10 devices of a given size on the mask (Figure <16>) were measured at a time. Note that area independence of current density was checked at room temperature. The J-V behavior was re-examined after each temperature excursion and compared to control samples which had

Figure <18> Typical Transients Seen in I-V Measurments

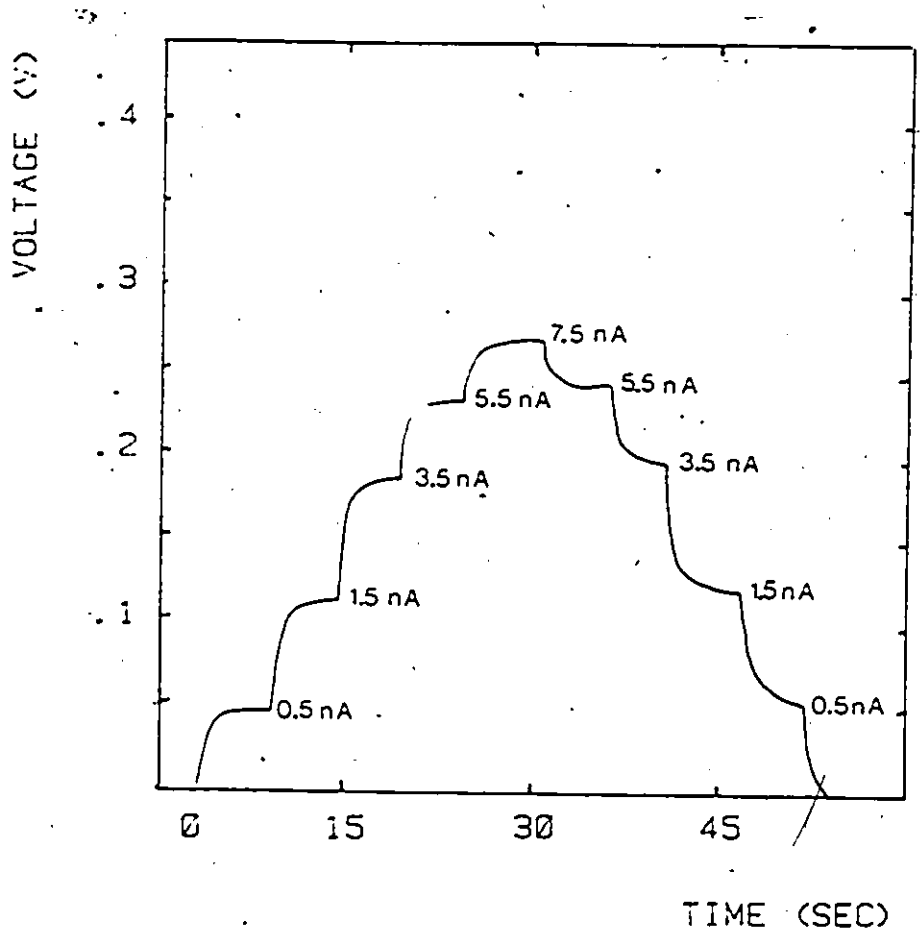

A strip chart recording of voltage vs time is reproduced here showing the transients associated with changing the current flowing through the device to the values indicated. A time constant of the order of seconds and slight hysteresis is evident. Measurements are typically made on the descending bias steps.

been temperature cycled, but not voltage stressed, and to samples seeing no temperature or voltage stress. The vacuum baked and unheated samples exhibited no detectable changes throughout the experiment. The hydrogen annealed samples however did exceed the drift limit of $\Delta I > 3\%$ after the 360 K temperature run and were therefore analysed over a more narrow temperature range.

The problem of control of temperature during J-V-T measurements was studied. A cooling system based on cold nitrogen gas boiled-off from liquid nitrogen (a Delta-type environmental chamber) proved to have too short a thermal time constant. The voltage across a device passing a constant current fluctuated wildly whenever a new "blast" of cold nitrogen was admitted into the chamber. A compressor based refrigeration unit combined with forced air heating was much slower in attaining set points, but could hold that temperature with smaller fluctuations. With the proper choice of thermal mass attached to the substrate, temperatures at the substrate could be kept within at least .2 K (the measurement limit of a chromel/alumel thermocouple - voltmeter combination), or more importantly, within the limit of the measurement of voltage across the device, a more sensitive criterion. Icing and/or condensation problems were avoided by one of two methods: an ambient of dry nitrogen inside the test chamber, or a thorough drying bake at 80°C prior to low temperature runs.

A slightly different approach was followed in testing the 32

by 32 array of 12.5 μm square devices. This mask was the primary tool in the investigation of the thickness and nitrogen doping dependences of J-V behavior. Testing of the entire array was performed by a Rockwell Aim 65 microcomputer, interfaced to an x-y stage, digitally controlled voltage source, instrumentation amplifier (unity gain, 10^{14}ohm input impedance) and digital voltmeter. A test voltage was applied to each device individually, and current (i.e. the voltage drop across a precision resistor) was recorded after a software determined settling period. Uniformity and reproducibility of J-V behavior were evaluated on a routine basis in this manner throughout the duration of the project. Well over one thousand substrates of 1024 devices each were mapped. Uniformity and reproducibility were understandibly functions of processing parameters. However, in the absence of serious processing problems the following statistics were typical: 1 or 2 devices would be shorted due to particulate contamination prior to anodization, or due to electrostatic discharge, up to 5 would be open due to microcracks where the chromium top metallization steps up over the Ta_2O_5 covered tantalum electrode; and the remainder would show a 3σ standard deviation in current for a given voltage of < 3% on a given substrate of 12.5 μm square devices, and < 5% within a fabrication run of 5 to 25 substrates. As mentioned previously, larger differences did appear between the magnetron and dc diode sputtered based Ta_2O_5. By careful measurement of line widths

using a Nanoline automatic dimension measurement system it was determined that uniformity on a substrate was photolithography limited. For the smaller devices, such as are found on the area test pattern (Figure <17>), these tolerances of ± .25 μm imply larger standard deviations of up to 13%, as was observed. Of the 1024 devices on a substrate, 64 were tested with a more substantial range of voltages, so that the appropriate conduction models could be determined.

Finally, a least squares fit to the J-V data was made with functions appropriate to the various models. A typical set of data and the Poole Frenkel fit is given in Figure <19>. There is a range of voltages covering four orders of magnitude of current density where the $\ln(J/V)$ vs $\sqrt{V}$ plot is near ideal. The magnitude of J-V asymmetry with respect to zero bias is also typical. Obviously, there is a K_{pf} for each polarity. Not so obvious is that there is also a slightly different β for each polarity, even though the physical parameters making up β have no apparent bias dependence. This observation is not in accordance with Poole Frenkel theory, and will be discussed fully in Part IV. For this preliminary analysis, an average of the two β's is used.

The high field forms of the Poole Frenkel and hopping conduction equations, appropriate to the fields actually used, were fitted to the data for all but the J-V-T experiment. Thus the K_{pf} and β quoted correspond to equations <113>, <121> and <123> found on pages 74 and 75. It was unnecessary to resort to

Figure <19> Poole Frenkel Plot for Devices of Various Areas

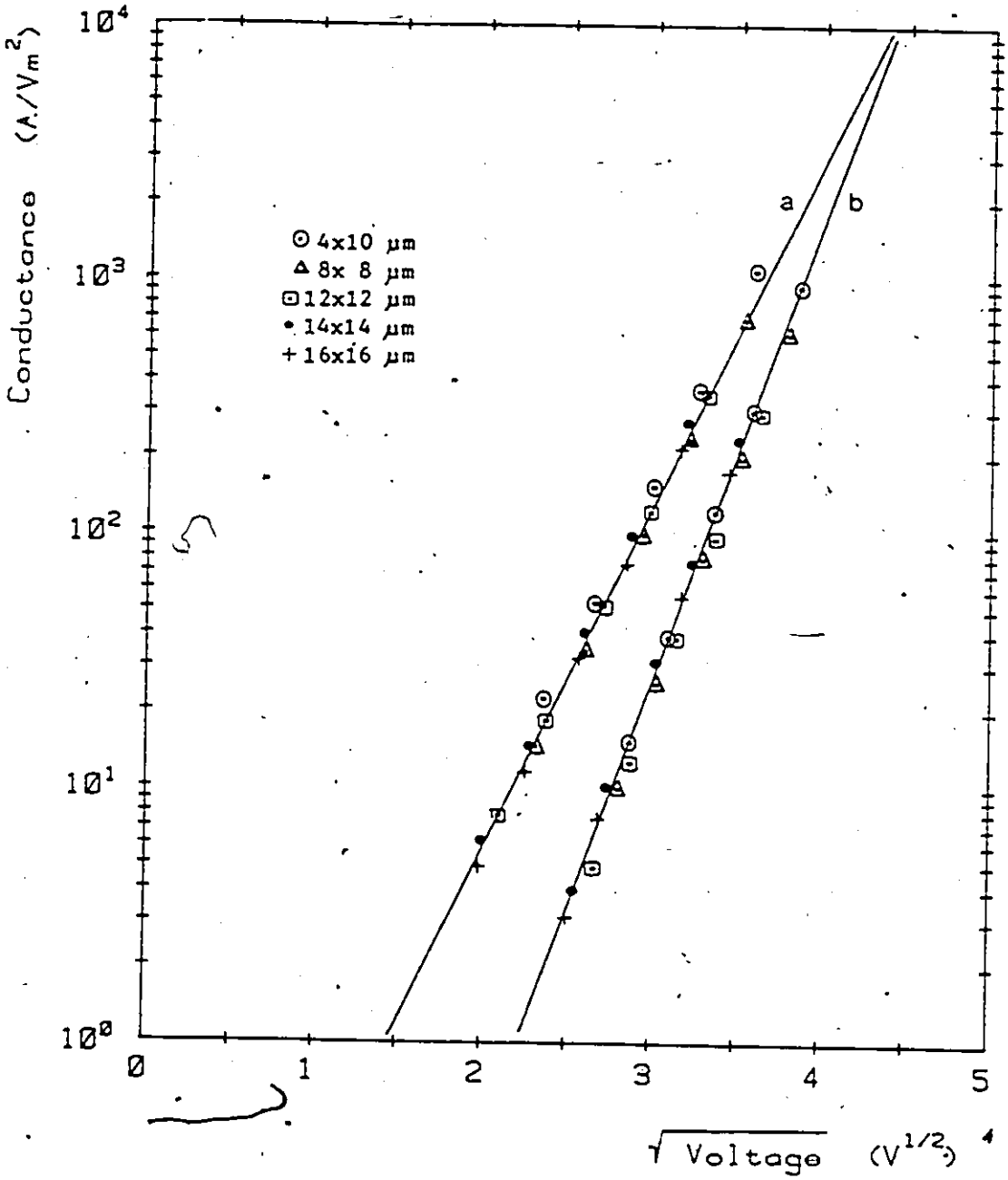

A Poole Frenkel plot of current density/voltage vs the square root of voltage is shown for devices with the nominal areas indicated. For clarity the errors bars have been omitted. The relative error in current is + 0.5%, in area is + 0.5 μm^2, and in voltage is + 1 mV.

line (a) - cathodic polarity (Ta positive with respect to Cr)
line (b) - anodic polarity (Ta negative with respect to Cr)

the less common forms of field induced barrier lowering. No integral values of m in the relationship:

$$\frac{J}{V} \propto \frac{\mu n_o}{d} \exp\left[c\xi^{m/m+1}\right] \qquad \text{<98'>}$$

could be selected to fit the data with any higher accuracy than the Poole Frenkel model (m = 1). The most accurate fits yielded non-integer values of m, close to m = 1, which were not independent of temperature, oxide thickness and dielectric constant. Because the Poole Frenkel fit is satisfactory for the experimental range of these properties, and in addition permits a physical interpretation of the fitting parameters, it will be the only barrier lowering model discussed in subsequent sections. Likewise, the hop length is calculated from equation <80> (page 54). In the J-V-T experiment the limited voltage range necessitates the use of a full 3 dimensional approach - such as the Onsager formulation (equation <93a>, page 65).

2. RESULTS

The Effect of Device Area :

To establish whether current could be described in terms of current density, I-V data were obtained for current levels from 5 nA to 555 nA for devices ranging in size from 4 μm x 4 μm to 250 μm x 500 μm. Five substrates of undoped β-Ta were used (in two different oxide thicknesses) and one each of the 0.6, 0.9, and 1.2 sccm N_2 doped Ta. The generous number of devices available of each size on the area test pattern (32 of the smaller sizes and 128 of the larger) permitted the estimation of the mean deviation in conductivity levels for a particular size of device at 10% to 14%. A few size categories showed anomalously large deviations and thus were not included in this analysis. This is attributed to difficulties with photolithography in the very smallest sized devices and poor step coverage of the chromium over the oxide coated tantalum in certain areas of the substrates.

The data presented in Figures <19&20> are representative of the given device sizes for a particular substrate of 30 V thick undoped oxide devices. Similar behavior was observed with the nitrogen doped and 40 V thick undoped devices. As can be seen in Figure <20>, conductivity for a fixed voltage (and thus fixed electric field) scales with area. The error bars shown are the 3σ deviations for all devices tested of that size. Figure <19> is a

Figure <20> Observed Current as a Function of Device Area

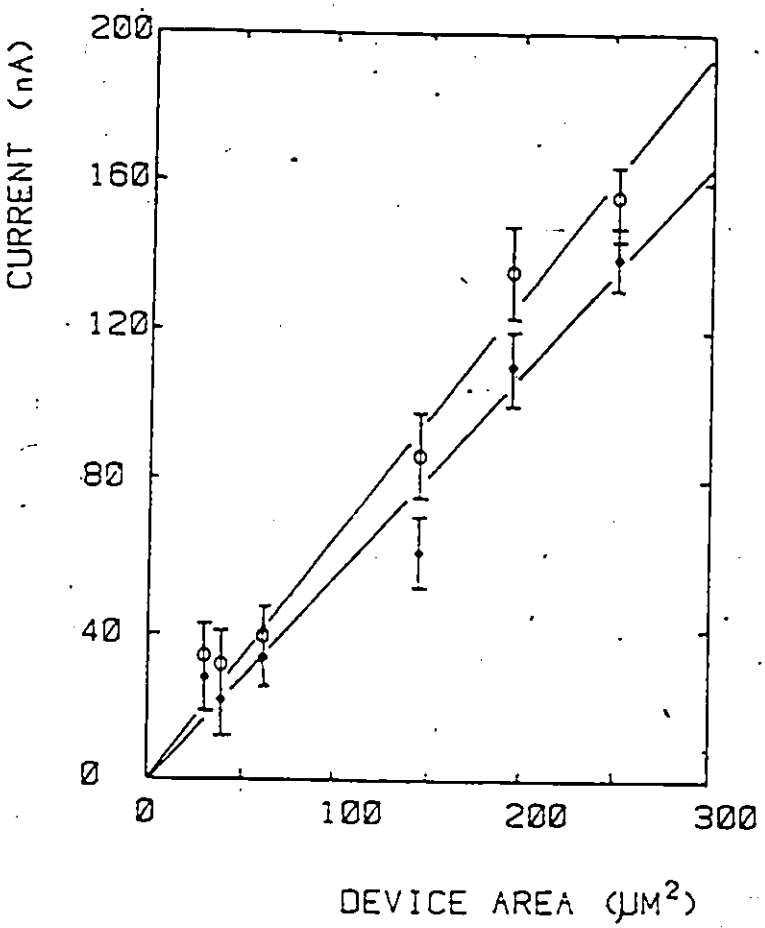

The currents interpolated from the data given in Figure <19> for a voltage of 10 V anodic bias (•) and 8 V cathodic bias (o) are plotted against the device area. The error bars on current represent 3σ deviations for all the devices tested of that particular size.

Poole Frenkel plot of the J-V data for these devices. The logarithm of the ratio of current density to voltage is plotted against the square root of voltage. The J-V data of the devices whose areas vary by more than a factor of six, can be seen to fall on the same curve, confirming that current does scale with area. The largest devices, not plotted, did not fall on this line. For the currents used in the test, only ohmic behavior was observed, presumably because the Poole Frenkel regime had not yet been entered at that bias. The currents required to produce comparable electric fields in devices of this size can be estimated to be approximately 100 μA, two orders of magnitude higher than the arbitrarily chosen current limit for this test.

Although this test conforms to that set out by Schwartz and Gresh to identify nominally flaw free films, it is actually verifying that conduction is uniform on the scale of microns. However, there is the additional evidence in the morphology of the oxide observed at 20,000 times magnification in the scanning electron microscope. The oxide appears uniform and featureless. Thus it is concluded that conduction in these devices is not dominated by flaws such as fissures and micropores.

PART III - EXPERIMENTS

The Effect of Oxide Thickness :

Once confident that the flaw free conditions can be assumed to exist in the oxides under investigation, we can proceed to examine the effect of oxide thickness. In this experiment, three anodizing voltages (25, 30 and 35 V) were chosen to give samples of three different oxide thicknesses. The standard 32 x 32 pattern was used to give a large number of devices for testing. At the same time, an optical test pattern sample was prepared with anodizing voltages from 15 to 55 V, in 10 V increments.

The ellipsometry results were fitted well with a model consisting of a single homogeneous layer. Figure <21> is a plot of the measured oxide thickness as a function of anodizing voltage. The offset, which appears to indicate no oxide formation until -2 V is measured, is not unusual. It can be explained by the existence of a native oxide. Moreover, only the absolute value of oxide thickness is required for the following analysis of conduction behavior.

The J-V behavior of these films is diagrammed in Figure <22>. These data fit the Poole Frenkel relationship, $-\ln(J/V) \sim \sqrt{V}$, for over 4 orders of magnitude of current density in the anodic (Ta positive) bias and a somewhat reduced range for the cathodic (Ta negative) bias. In addition, β, the Poole Frenkel nonlinearity coefficient defined in equation <123>, page 75 is observed to be proportional to $d^{-\frac{1}{2}}$ as predicted (Figure <23b>),

Figure <21> Oxide Thickness as a Function of Anodizing Voltage

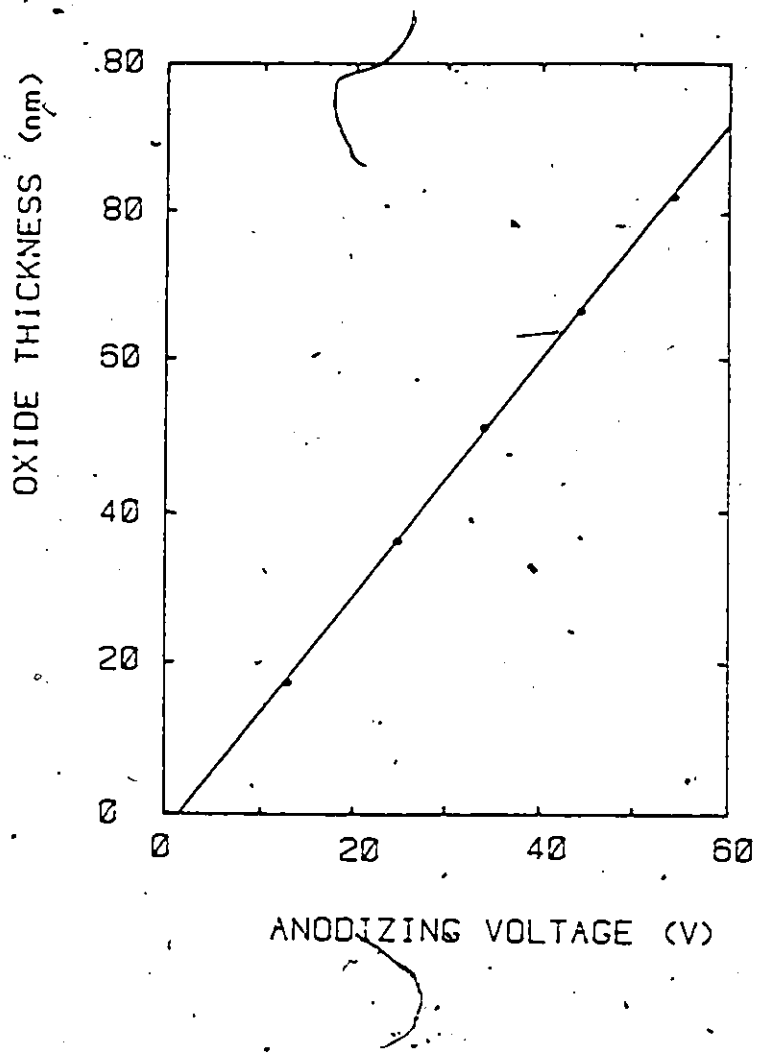

Oxide thickness is determined by the anodizing voltage used. The relationship is shown here for β phase of thin film Ta. The calculated anodizing constant is 1.96 nm/V. The absolute error in thickness as determined by ellipsometry is ± 0.5 nm, while the error in voltage is estimated to be ± 0.1 V.

Figure <22> Poole Frenkel Plot for Devices of Various Thicknesses

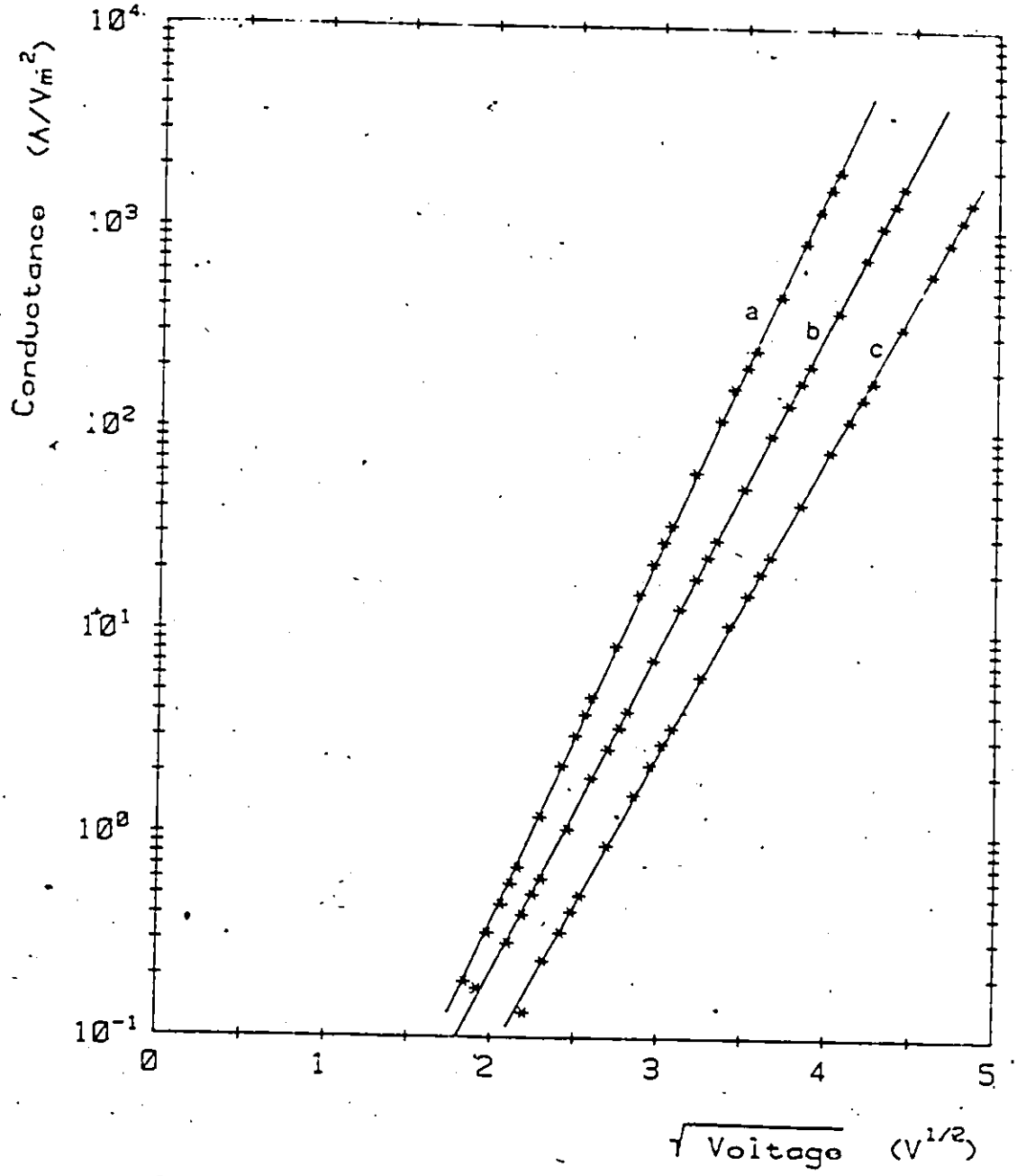

a) Anodic conductance (i.e. current density / voltage for the Ta positive bias) is shown here for three different oxide thicknesses. The curves should be linear on this plot format if 1-D Poole Frenkel conduction is dominant. Three different thicknesses were obtained by the choice of the following anodizing voltages: (a) 25 V, (b) 30 V, (c) 35 V. As in Figure <19>, following page 100, the error bars have been omitted for clarity. The total relative error in conductance is 4% and in voltage is less than .001%.

Figure <22> Poole Frenkel Plot for Devices of Various Thicknesses

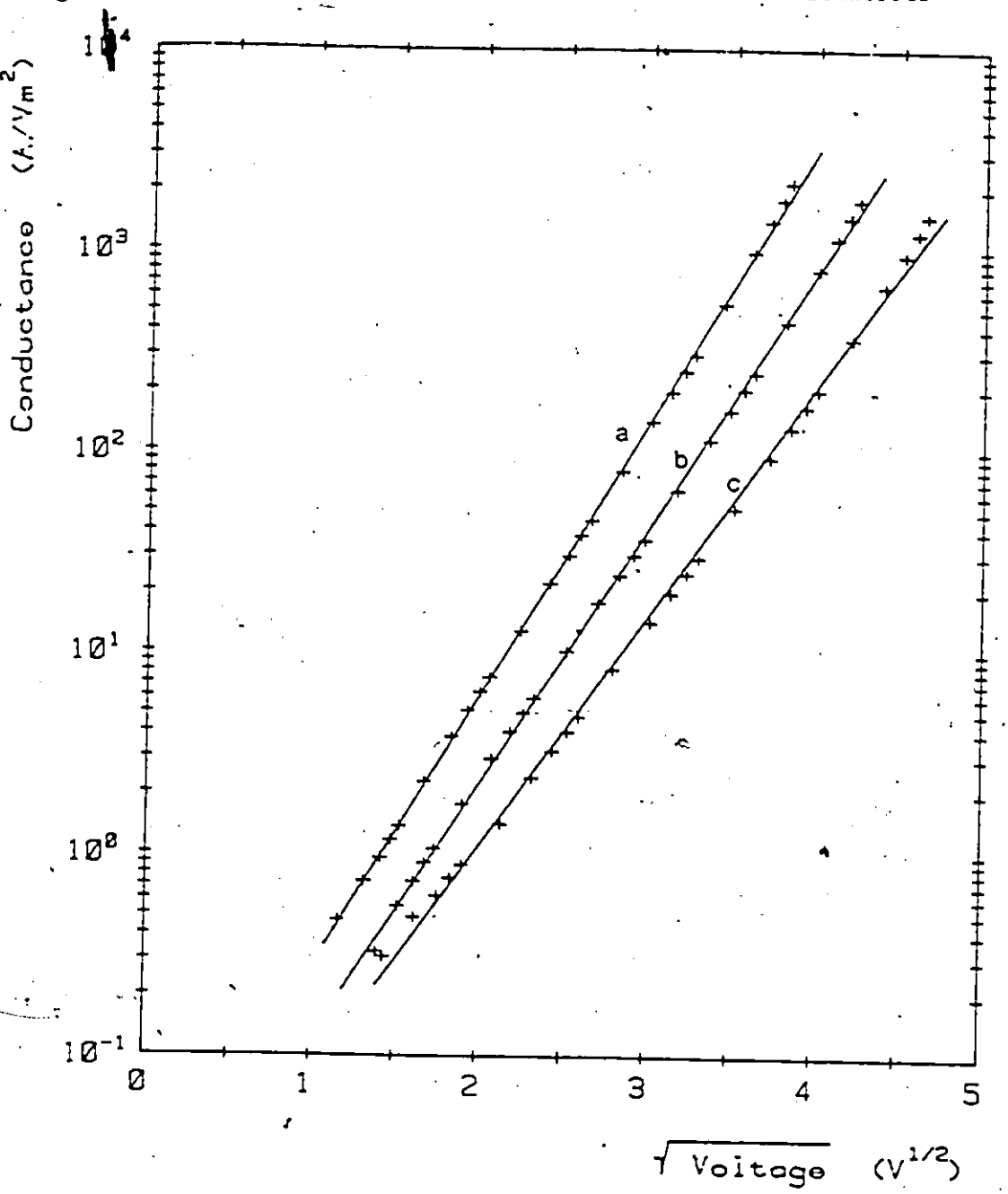

b) The cathodic conductance for the same devices as shown in part a) of this figure is plotted against $\sqrt{\text{voltage}}$. For voltages in excess of 50% of the anodizing voltage, a small excess current is observed for this bias polarity. This phenomenon has been observed by other workers (13, 90), and is believed to be caused by the onset of high field ionic conduction. Also seen in curve (c) is the predicted deviation at low fields due to three dimensional effects. (a) 25 V oxide, (b) 30 V oxide, (c) 35 V oxide

Figure <23> Variation of Poole Frenkel Coefficients with Thickness

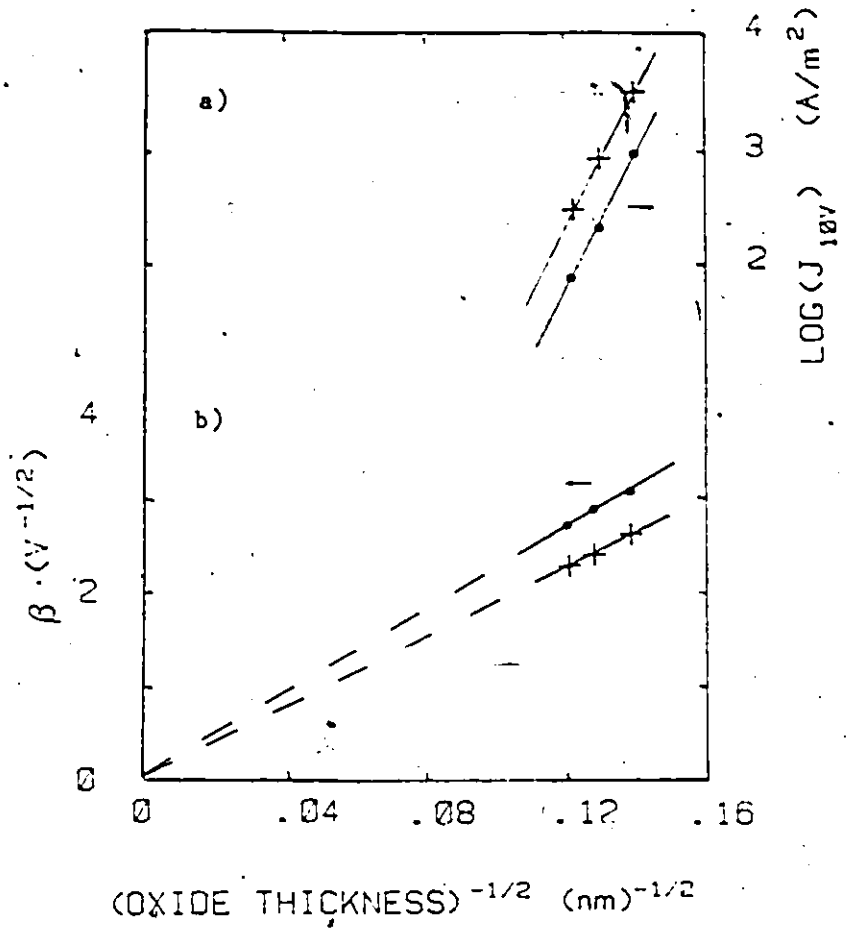

In upper part, the logarithm of current density for a bias of 10 V from Figure <22>, is shown to be a linear function of (oxide thickness)$^{-\frac{1}{2}}$. In the lower part, the Poole Frenkel nonlinearity coefficient, β, is shown to be proportional to (oxide thickness)$^{-\frac{1}{2}}$. The error bars on β of 0.03% are statisically derived for a Student's T confidence limit of 95%. Both relationships should hold if Poole Frenkel conduction is dominant. • - anodic bias (Ta positive), + - cathodic bias (Ta negative).

and current density at a set voltage (10 V is chosen for Figure <23a>) is observed to be an exponential function of $d^{-\frac{1}{2}}$, as predicted in equation <112>, page 74. These relations would also hold for Schottky punch-through conditions, equations <12> and <13>, page 22.

The analysis of the data with respect to the high field hopping model is shown in Figure <24>. The fit is only adequate for conductance greater than 500 Ω/m^2. As discussed on page 54, the slope of the ln(J/V) vs V curve in that region is theoretically equal to: $\frac{cqR}{kTd}$

where c is equal to 0.17

R is the hop length

d is the oxide thickness

For all these curves, R is calculated to be 5.2 $\pm$ .2 nm. This is large compared to the value of 1.81 nm found by Bryksin et al. (137) for Ta_2O_5. If the hop length corresponds to the inter-impurity separation, as might be expected at high temperature, then N_d can be estimated to be on the order of

$$\left[\frac{4\pi R^3}{3}\right]^{-1} = 1.8\times10^{24}\ m^{-3}$$

This is within the range of values for Ta_2O_5 derived from other methods. (See for instance Table II, page 41). Thus hopping conduction cannot be ruled out by these observations.

In contrast, the thickness dependence of J-V behavior predicted for both the imperfect insulator - metal contact and

Figure <24> Hopping Analysis of Devices with Different Thicknesses

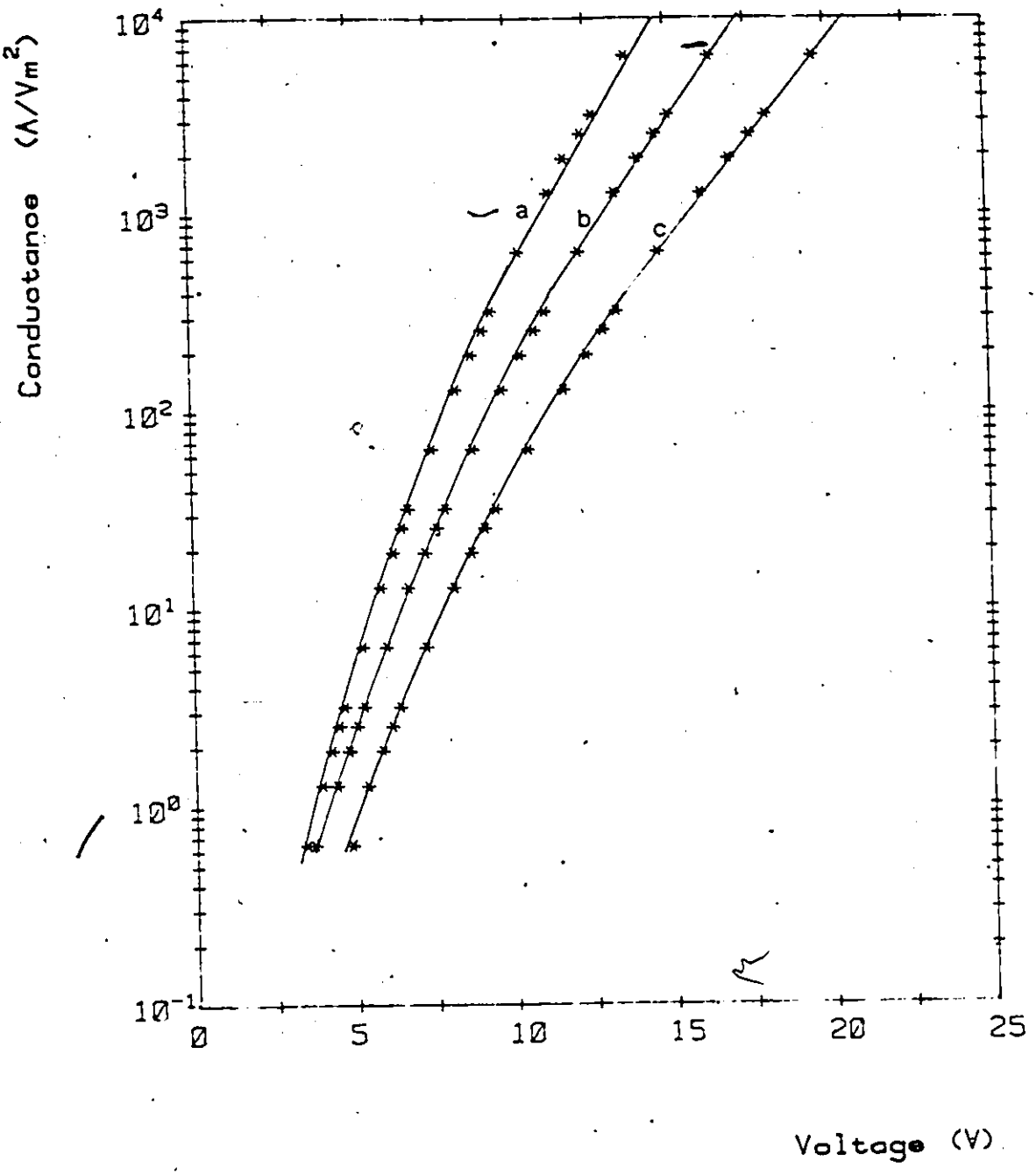

When the hopping model is applied to J-V data covering an extensive range of voltages satisfactory agreement is only attained for the highest voltages. Only in that region does conductance (J/V) increase exponentially with electric field as per equation <128>, page 91. (a) 25 V oxide, (b) 30 V oxide, (c) 35 V oxide

the space charge limited conductor cannot be reconciled with the data. The former predicts no thickness dependence, (equation <9>, page 22), while the other predicts the existence of an unique s such that $J \alpha V^{s+1}$ and $J \alpha d^{-2s+1}$ (equation <37>, page 34). Figure <25> presents an analysis of the J-V data within the standard SCLC model. The s derived from the straightest portion of the J(V) plot is 5.5, while s predicted from J(d) is 3.3.

The conclusion of this experiment is that the space charge limited conduction, and the imperfect insulator - metal Schottky barrier models are not appropriate to these films, whereas either punch-through Schottky barrier emission or hopping or Poole Frenkel conduction might be occurring.

Figure <25> SCLC Analysis of Devices with Various Thicknesses

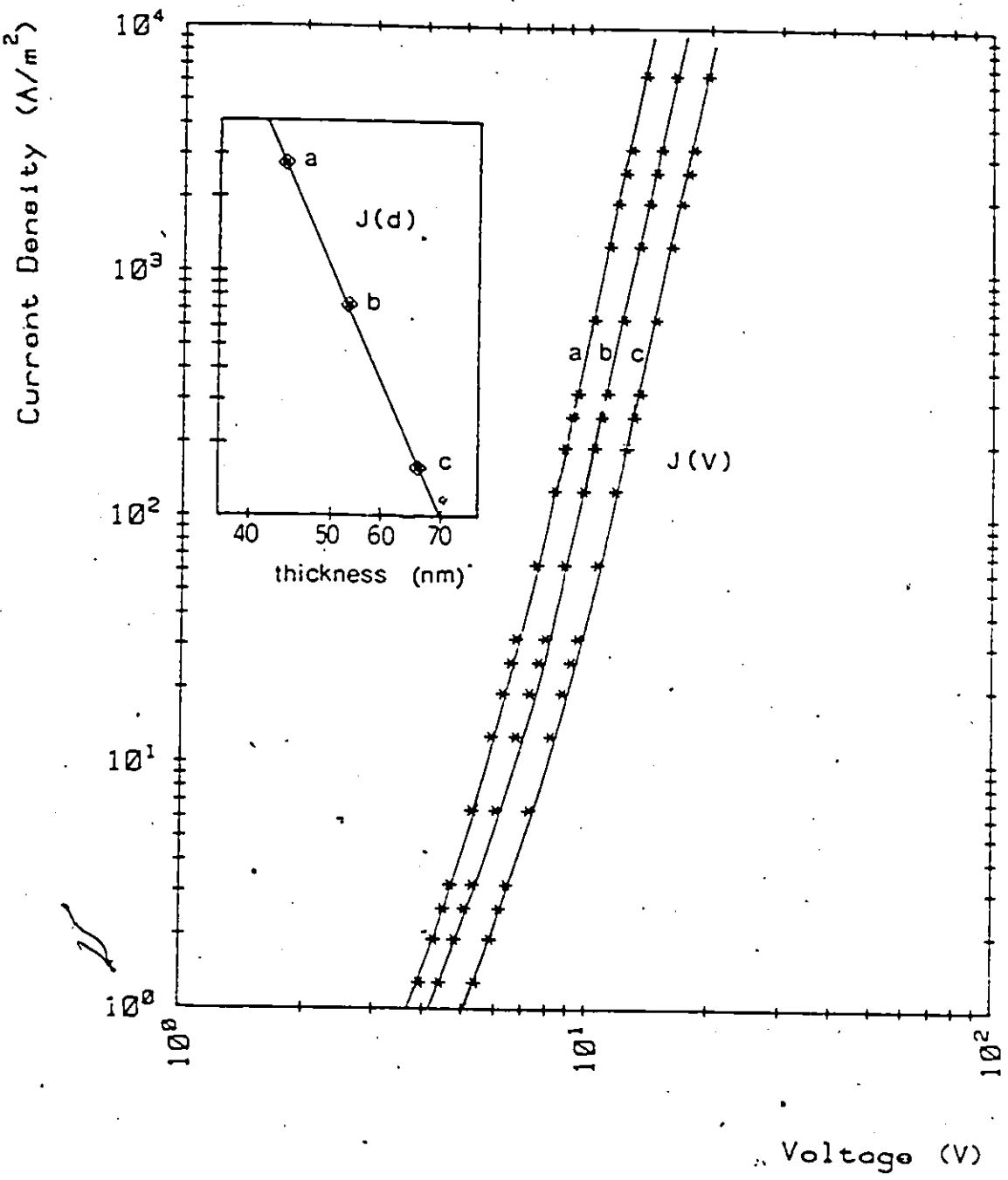

If space charge limited conduction were dominant, then these power law plots of current density vs voltage and current density vs oxide thickness (inset) would be linear with exponents of s+1 and -(2s+1) respectively. The calculated exponents are 6.5 ± 0.1 and -7.6 ± 0.1 for J > 100 A/m^2, and are thus inconsistent with an unique s. As before the error in J is less than 4% and V is 1 mV. (a) 25 V oxide, (b) 30 V oxide, (c) 35 V oxide

The Effect of Dielectric Constant :

Small amounts of nitrogen added to the argon used to sputter the tantalum deposited for these experiments had a dramatic effect on both the metal and the anodic oxide properties subsequently formed on it. As the nitrogen flow into the dc diode sputtering chamber was increased the metal resistivity first dropped from the undoped value of ~2.0 ohm-m to a minimum of ~0.8 ohm-m at 0.3 sccm (standard cubic centimeters per minute) of ultra pure nitrogen. Between 0.6 and 0.9 sccm, the resistivity rose to a plateau at ~3.5 ohm-m. Beyond the plateau, resistivity rose steadily to insulator like values at 1.5 sccm. These results appear to be typical of diode sputtered tantalum, and are in good agreement with the findings of Gerstenberg (37). A smooth transition in crystallographic phase from undoped β-Ta to f.c.c TaN at 1.5 sccm N_2 was observed with wide film Debye Scherer techniques. The intermediately doped films were composed of b.c.c. Ta near the resistivity minimum, and a mixture of Ta_2N, Ta_4N_5 and Ta_5N_6, throughout the plateau region. The two latter phases were not observed by Gerstenberg, but have been reported by Terao (232) for nitrided evaporated tantalum films. The magnetron sputtered tantalum films also went through a similar sequence of phases in good agreement with the literature (233).

To study the changes in oxide properties, three nitrogen flowrates were chosen to compare with the undoped β-Ta based

oxides. These were 0.6, 0.9 and 1.2 sccm. For comparison, note that the argon flowrate was 8 sccm. The interplanar spacings observed are compared to literature values (232-234) in Table VI. The use of flow rate to charactertize the nitrogen content of the films can be justified. Given the deposition rate, and the sticking coefficient of nitrogen to tantalum, analysis has shown that all of the nitrogen entering the chamber is gettered by the film, and is not merely pumped away. These particular flowrates were chosen because they span the range of tantalum nitride that forms useful oxides. At flowrates above 1.2 sccm the nitride became so highly resistive that the voltage dropped in the lines leading from the contact above the electrolyte meniscus down to the device area would significantly reduce the thickness of the oxide formed furthest from the contact. In the range between no N_2 and .6 sccm of N_2, b.c.c. Ta was deposited. These samples did not yield good quality oxides. The anodizing behavior showed evidence of frequent breakdown events during growth, and the interference colors of the oxide were murky and greyed rather than clear and intense, as if containing numerous light scattering centers. Under I-V test, these films were unable to support current in the Poole Frenkel-range without catastrophic breakdown.

Table VI

Summary of X-Ray Analysis - Observed and Reported Interplanar Spacings

Observed Interplanar Spacing vs. N_2 Flowrate (sccm)				Reported Interplanar Spacing vs. Nitride Composition			
none	0.6	0.9	1.2	tetr. β-Ta	h.c.p. Ta_2N	tetr. Ta_5N_6	tetr. Ta_4N_5
?.260 (nm)				.267 (nm)			
		.258				.259	
				.250			
		.248	.248				.249
?.244	.247	.247		.248	.247		
						.244	
	.233	.233			.233		
.232				.232			
.226				.225			
		.220				.219	.216
.214				.214			
.207				.207			
		.152	.152				.152
.143				.144			
	.140				.140		
.132				.133			
		.130	.130				.130
.116				.117			
.098				.101			
		.097					.096

Deduced Composition:

β-Ta	Ta_2N	Ta_2N+ Ta_4N_5+ Ta_5N_6	Ta_4N_5

? indicates poor correlation between observed and reported spacings. Systematic errors due to film shrinkage is suspected. The sum of all other errors in observed values are estimated to be less than 0.5%.

For each nitrogen doping level one substrate was processed with the area test pattern, one with the optical measurement pattern and between 4 and 8 with the standard 32 x 32 test pattern of 12.5 μm square devices in each of two thicknesses.

The reflectance spectra of the oxides are shown in Figure <26>, where the 30 V oxide of each sputtering condition is compared. The reflectance maxima and minima are shifted to shorter wavelengths and the range of amplitude of the interference effects at high frequencies is reduced with the increasing nitrogen content. In practical terms, the first observation means that the doped films "look ten volts thinner", than the undoped films anodized at the same voltage; and the second gives them their less intense colors. In more theoretical terms, it can be concluded that the effect of nitrogen is to reduce the product of the index of refraction and oxide thickness, $\hat{n}d$, and to shift the onset of strong absorption to longer wavelengths. Thomas's photoconductivity study of nitrogen doped tantalum oxide (63) confirms the observation that the absorption edge shifts to longer wavelengths with increasing nitrogen.

The same samples were examined with ellipsometric techniques. The reduction in the product of index of refraction and insulator thickness with doping was shown to be due to a drop in the index of refraction of 10%, as well as a 20% decrease in the thickness of the films prepared at the same anodizing

Figure <26> Reflectance Spectra of N_2 Doped Tantalum Oxides

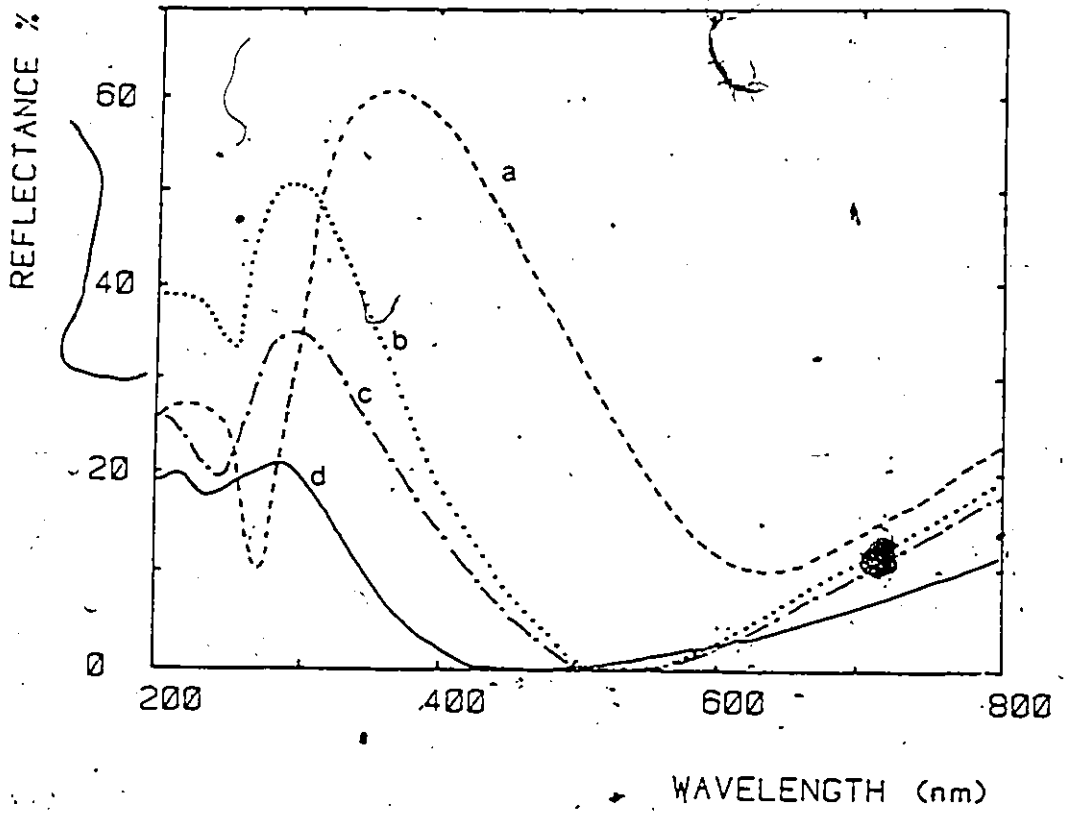

The amount of light reflected from the oxide coated metal as a function of wavelength is determined by interference effects, and absorption near the band gap. Both are related to the complex index of refraction in the oxide and its parent metal and both are shown by these plots to be affected by nitrogen in the tantalum film. The reflectance curves here are for tantalum sputtered with the following nitrogen flowrates: (a) none, (b) 0.6 sccm, (c) 0.9 sccm, (d) 1.2 sccm. The x-ray composition analysis for these films is given in Table VI.

voltage. The optical constants determined are listed in Table VII. The observed effect of nitrogen on the anodizing constant is in qualitative agreement with that seen by Kamei and Matsuzaki (19). The undoped Ta_2O_5 in this experiment is apparently not typical of the β-Ta based oxides reported previously. The index is almost 10% below literature values (52), and has an imaginary component as well, contrary to common experience. The latter implies absorption at the wavelength used in the ellipsometry. This unexpected absorption is thought to be a consequence of the optimization of the oxides used in this study for the MIM-LCD, which requires much higher levels of conductivity than the usual capacitor application. This point will be discussed in Part IV.

Electrical characterization began with the verification of the expected area and thickness dependences of current. Then J-V data was collected for 64 devices on each of 4 to 8 substrates and Poole Frenkel coefficients were determined in the standard fashion and are given in Table VIII. Analysis using a hopping model is given in Table IX and will be discussed shortly. Under the Poole Frenkel model the main conclusions are that the doped films showed lower conductivity (i.e. smaller K), and greater non-linearity (i.e. larger β). Now that both d and ε ($\varepsilon = \hat{n}^2$) are known for each film, the expected β may be calculated directly. The ratio of β calculated for $\gamma = 1$ to the observed slope of the $\ln(J/V)$ vs $\sqrt{V}$ curves, gives the compensation index γ (as defined in equation <122>, page 75). All three doped films exhibit

"normal" Poole Frenkel β's ($\gamma = 1$), conforming to a model of compensated donors, even though ϵ itself varies from 2.99 to 3.45. These β's are inconsistent with the Schottky model. The β of the undoped film is also not Schottky-like, and if Poole Frenkel-like, can only be reconciled with a compensation index between 1 and 2. Interestingly, Thomas also proposes a compensating role for nitrogen in reducing an absorption feature at 2.1 eV that he observed in undoped films, but could not resolve in films made on tantalum with as little as 2% nitrogen (63).

Thus under the Poole Frenkel analysis it can be concluded that nitrogen in the oxide has the effect of compensating the donors responsible for conductivity. This explains the larger non-linearity and lower conductivity of the electrical characteristics, and the reduced absorption observed in the ellipsometric study of the optical properties on these films.

The hopping model also leads to the interpretation that nitrogen doping causes a decrease in the number of impurities. This leads to the observed increase in hop length, and decrease in overall conductivity. The values of the hop length given in Table IX do require comment, however. Devices with the highest nitrogen doping exhibit an inferred hopping length of 18.5 nm. This is surprisingly large, and not in agreement with Bryksin's value of 1.81 nm (137). In fact, in most experimental examples of hopping in a range of materials the hop length is on the order of

.5 to 5 nm. To be able to make a conclusion regarding the appropriateness of the hopping model even in the light of these longer than normal hop lengths, an estimate of the activation energy is required.

TABLE VII

Optical Properties of Anodic Films on N_2 Doped Tantalum

N_2 Flowrate	None	0.6 sccm	0.9 sccm	1.2 sccm
$\hat{n}$ -($Ta_2O_xN_{5-x}$)	1.9-j.06	1.86	1.75	1.73
d(nm)(30 V film)	56.2	43.8	44.8	44.0

-measured by ellipsometry at 632.8nm, relative error = ±1%

TABLE VIII

Poole Frenkel Coefficients of Anodic Films on N_2 Doped Ta
(30 V film)

N_2 Flowrate	None	0.6 sccm	0.9 sccm	1.2 sccm
β ($V^{-\frac{1}{2}}$)	4.2 ± .4	6.4 ± .4	8.5 ± .1	8.8 ± .9
K (A/Vm^2)	7.26×10^{-6}	3.42×10^{-11}	8.77×10^{-13}	1.78×10^{-11}
γ	1.5 ± .3	1.2 ± .2	.9 ± .1	.9 ± .2

-calculated from J(V) and data of Table VII
-absolute error in log (K) is less than .5

TABLE IX

Summary of Hopping Analysis of Anodic Films on N_2 Doped Ta

N_2 Flowrate	None	0.6 sccm	0.9 sccm	1.2 sccm
R(nm)	5.4 ± .4	5.2 ± .3	9.3 ± .1	18.5 ± .9

-inferred from J(V) and data of Table VII

PART III - EXPERIMENTS

The Effect Of Heat Treatments:

As reviewed in the introduction, heat treatments have been shown to make large changes in the level of conductivity in anodic Ta_2O_5. The use of heat treatments was advocated in this study to see if a conduction model could be demonstrated for a range of conductivity levels and whether it could identify the causes of those changes. Furthermore, heat treatments were shown to affect the compensation index γ of those films exhibiting Poole Frenkel conduction, as documented in Part II. This was particularily interesting since the γ determined for our undoped samples was 1.5 - midway between the usually observed values of 1 or 2. This corresponds to intermediately compensated donor statistics. That is, these samples are neither uncompensated, nor are they in the regime where partial compensation is said to occur. This was the first report of a significant departure from 1 or 2 conditions, even though intermediate values had been theoretically predicted by Yeargan and Taylor in 1968 (184). It was important to determine whether these films could be pushed into one of the two more well known regimes.

Two types of heat treatments were tried. One consisted of baking the samples with quartz lamps under high vacuum (10^{-4}Pa) just prior to the deposition of the chromium top metallization. The maximum temperature reached is estimated to be 150°C. This would be very effective in removing water from the oxide, a

likely impurity. The second method was designed to enhance oxygen vacancies, another proposed source of donors. The samples were placed in a tube furnace at 350°C for 1 hour in a flowing stream of 10% H_2 in N_2. The samples were heated to this temperature and cooled down while in the reducing atmosphere.

The J-V-T pattern (Figure <16>) was used. Five substrates from a common sputtering run were processed with each heat treatment and studied over a range of temperatures. Later experiments compared the J-V behavior of vacuum baked and nominally unheated devices on a larger number of 32 by 32 array substrates. The later experiments confirmed the room temperature observations quoted below.

The heat treatments were effective in changing the overall level of conductivity, as shown in Figure <27>. This graph compares the three types of devices at 251 K. This temperature is chosen for illustration purposes only. At this temperature all three sample types exhibit relatively simple J-V behavior. The low field effects that are seen will be discussed in the next section. As can be seen, the conductance of the vacuum baked samples was approximately an order of magnitude greater than samples which saw no heat treatment. The hydrogen annealed samples showed a thousandfold increase in conductivity. These changes were stable provided the samples were kept and tested under a dry nitrogen ambient. As already mentioned, the stability of the hydrogen annealed samples degraded in the upper range of

Figure <27> Poole Frenkel Analysis of Heat Treated Devices

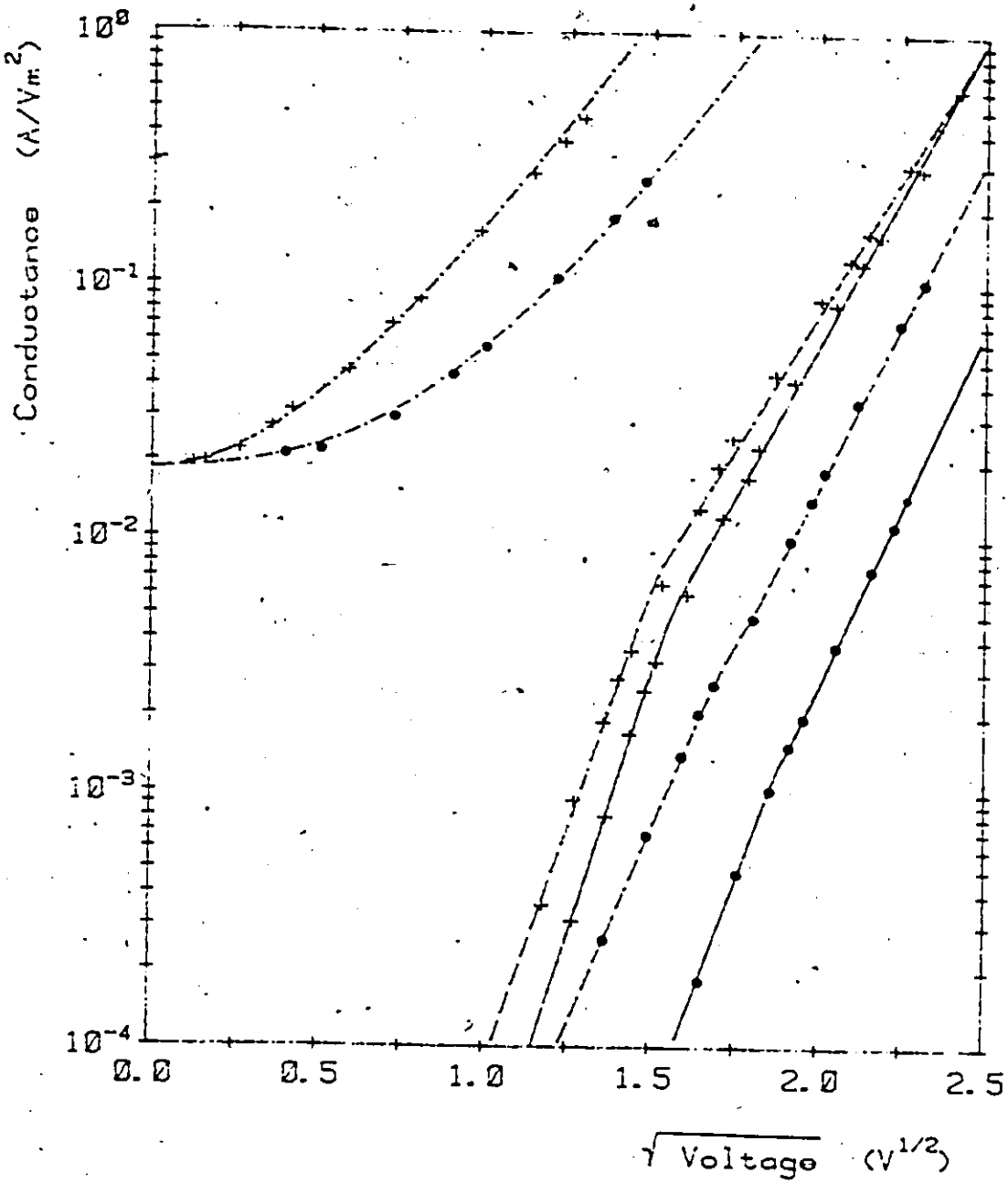

Heat treatments of various types are shown to have an effect on the Poole Frenkel behavior of anodic tantalum oxides. The solid lines connect the anodic (•) and cathodic (+) J-V data for the unheated oxides. The dashed lines similarily connect the vacuum baked J-V points. Note that both the anodic (•) and cathodic (+) currents have been increased by the heat treatment. Hydrogen annealing increases current by an even larger amount as seen by the data connected by the dash-dot line. Cathodic currents (+) for the hydrogen annealed devices remain larger than anodic currents (•). The lines used here to guide the eye do have physical significance as will be explained in later portions of this thesis.

J-V-T testing ($T > 360$ K).

The Poole Frenkel interpretation of the data is discussed first. All samples showed $\ln(J/V)$ vs $\sqrt{V}$ behavior for electric field strengths in excess of 3×10^6 V/m. As expected, β did indeed drop in the vacuum baked samples to the $\gamma \cong 2$ condition. Thus either the number of acceptors has been decreased, or the number of donors has been increased. An intuitive suggestion is that water loss during baking is associated with a decrease in the density of a water related acceptor. The hydrogen annealed samples showed a β of 3.12 $V^{-1/2}$ at 251 K - much too low to be reconciled with the index of refraction and the oxide thickness measured prior to heat treatment. It is unclear whether these have been changed by the anneal. That is to say, the hydrogen annealed samples did not show any change in the appearance of the interference colors of the exposed oxide adjacent to the chromium coated devices, and yet the capacitance and dissipation factor of tantalum capacitors were shown by Vermilyea (15) and later Smyth et al (14) to be quite different after annealing, even though in those instances also, the interference colors were not changed. Smyth developed a model to explain the frequency dependent behavior of the annealed capacitor in terms of a blurring of the metal - oxide interface: his so-called conductivity profile. These studies support the suspicion that the transport properties of hydrogen annealed samples can no longer be described with the macroscopic parameters determined for unheated samples.

An analysis of the data was also made with the hopping model (Figure <28>). The hop length at 251 K inferred was 10.3 nm for the unheated samples, 9.4 nm for the vacuum baked samples, and 9.0 nm for the hydrogen annealed samples. The relative error in these values arising from measurement tolerances and sample nonuniformity is 5%. If nearest neighbour hopping can be assumed (a reasonable assumption in the temperature range under consideration) then these results imply that the impurity concentration is lowest in the unheated samples, and highest in the hydrogen annealed samples. Therefore water would be a poor candidate for the impurity responsible for a hopping type conduction. From these results it is not clear whether the magnitude of the change in impurity density and thus hop length is sufficient to explain the large increases in conductivity in the heat treated samples. One other parameter that may have changed is the activation energy which will be examined in the next section.

Current - Voltage - Temperature Behavior:

The extra variable of temperature was used to check the Poole Frenkel and hopping models for internal consistency, and to quantify the differences between the three types of samples studied in the last section. It also brought unexpected insights into asymmetry and compensation effects.

The J-V behavior of the three types of samples - unheated,

Figure <28> Hopping Analysis of Heat Treated Devices

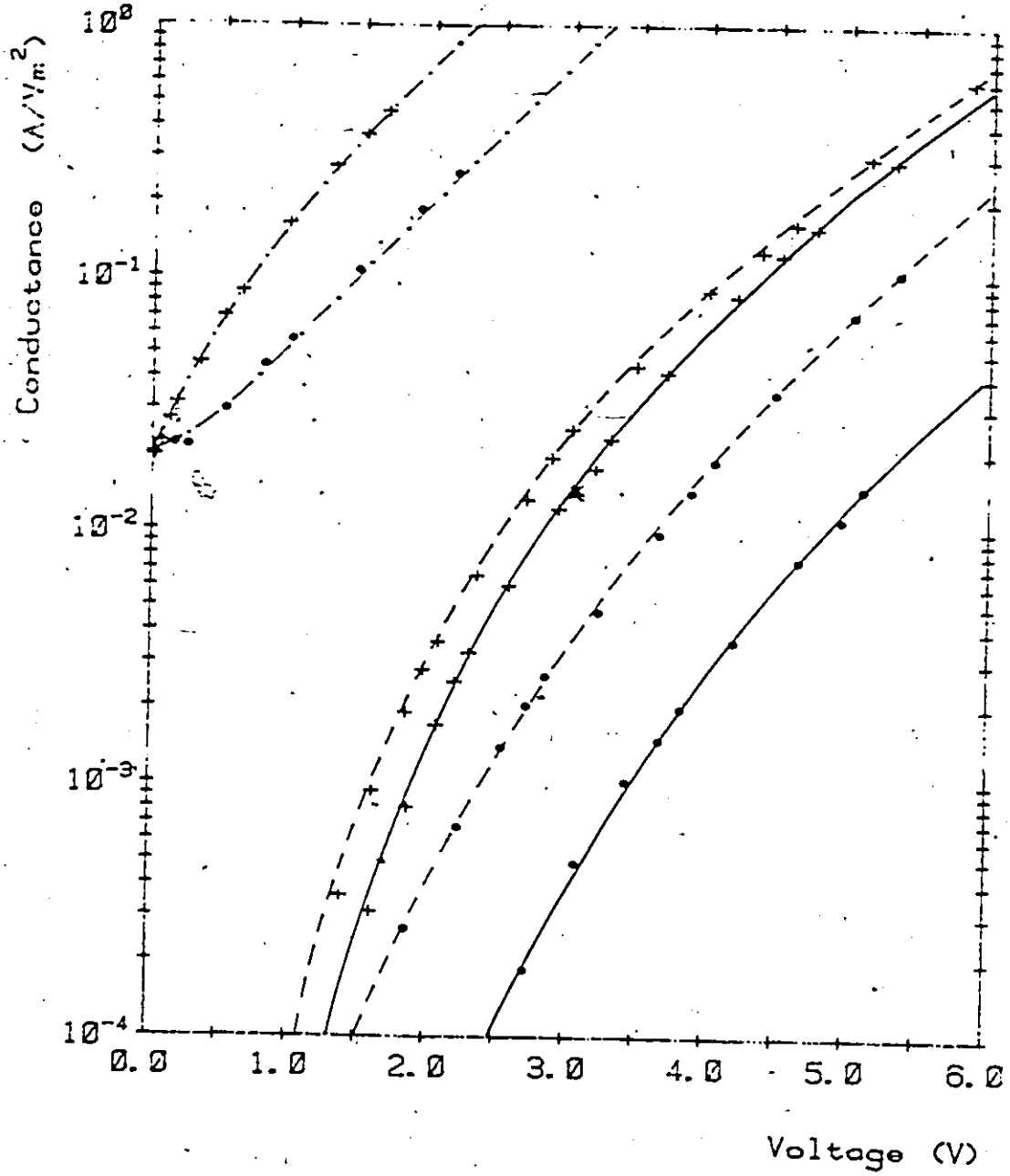

The data of Figure <27> are replotted in the format expected to produce linear plots at high fields if hopping conduction were dominant. As before, the solid, dash and dash-dot lines correspond to the unheated, vacuum baked, and hydrogen annealed oxides, respectively; also (•) denote anodic polarity, and (+) denote the cathodic polarity J-V points. In this figure however, the shape of the lines used has no physical significance. Only the anodic hydrogen annealed line approaches the $J \alpha \exp(V)$ form expected by equation <128>, found on page 91.

vacuum baked, and hydrogen annealed, was investigated over the range of -55°C to 145°C. Within this range conductivity changed by almost eight orders of magnitude.

In this section, analysis of the data will be attempted with the activated hopping, variable range hopping and Poole Frenkel models.

a) Thermally Activated Hopping:

The restricted voltage range and wide temperature variation brought to light a low field ohmic region. This is seen in the hopping plots Figures <29-31> and more clearly in the Poole Frenkel plots Figures <35-37>, pg 122. Both hopping and the three dimensional Poole Frenkel models predict the existence of such a region. From an Arrhenius plot of conductance (J/V) in the voltage independent region vs 1/T, Figure <32>, an activation energy may be calculated. For both the vacuum baked and unheated samples an activation energy of $\zeta_a = 0.86 \pm 0.04$ eV was deduced. The hydrogen annealed samples, on the other hand, exhibited an activation energy of $\zeta_a = 0.69 \pm 0.05$ eV.

With these values of ζ_a it is now possible to calculate the absolute level of conductance predicted by the thermally activated hopping conduction model. Recall equation <51> derived in Part I, page 45, repeated here in an appropriate format:

$$J = \frac{q^2 \nu R^2 n}{dkT} V \exp\left(-\frac{\zeta_a}{kT} - 2\eta R\right) \qquad \text{<51'>}$$

Figure <29> Hopping J-V-T Behavior of Unheated Oxides

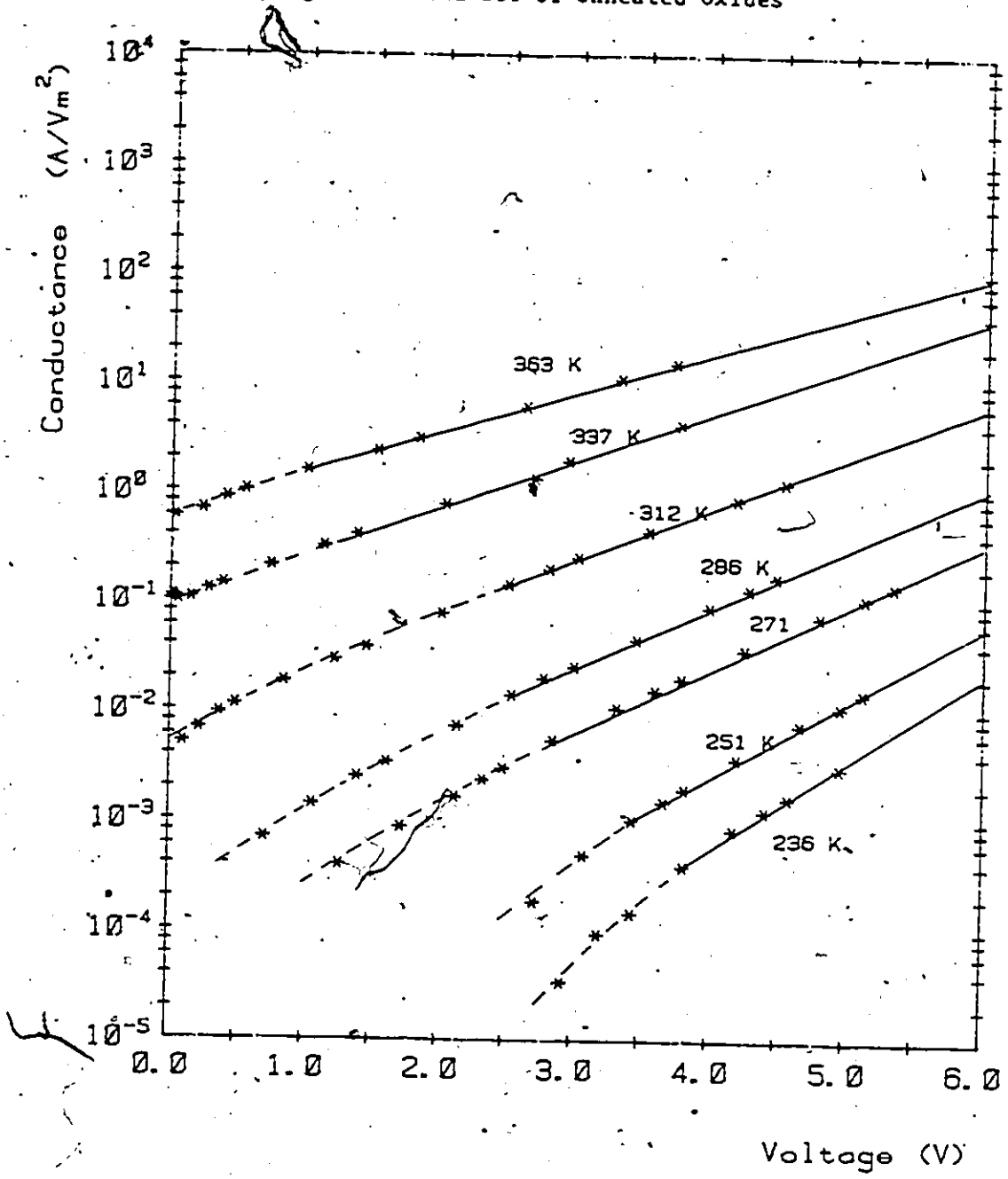

a) On this plot anodic J-V data are shown for a range of temperatures. The estimated errors have been discussed in Figure <22>, following page 104. The solid lines are least square fits to equation <128>, page 91. The lower than expected conductance at low voltages (where data points are connected by dashed lines) is not explained by the hopping theory.

Figure <29> Hopping J-V-T Behavior of Unheated Oxides

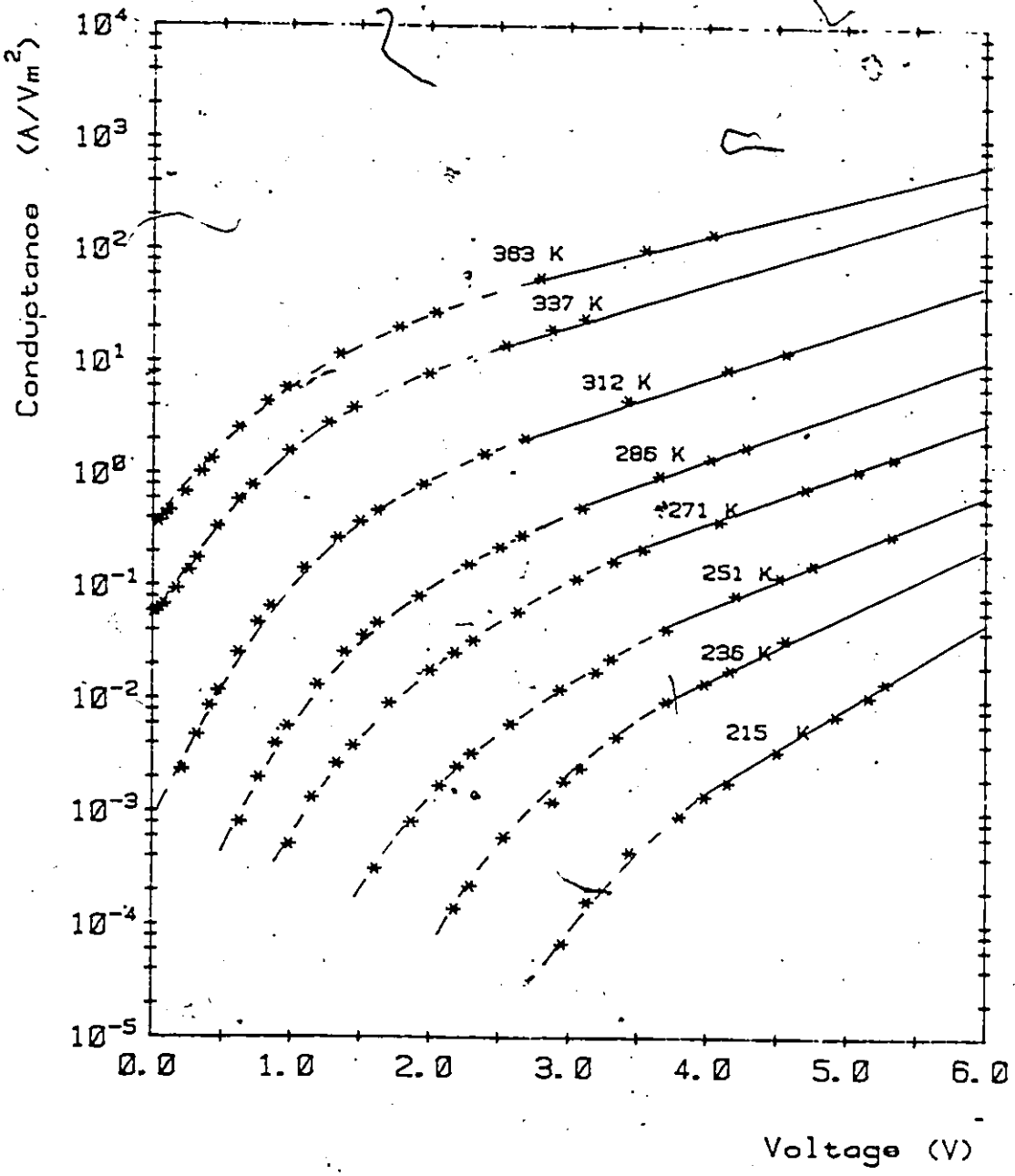

b) Cathodic J-V data is shown as a function of temperature in a format expected to produce straight lines if hopping conduction were dominant. As in the a) part of the figure, linear behavior is only observed at high voltages. The deviation from theory is more significant in this polarity.

Figure <30> Hopping J-V-T Behavior of Vacuum Baked Oxides

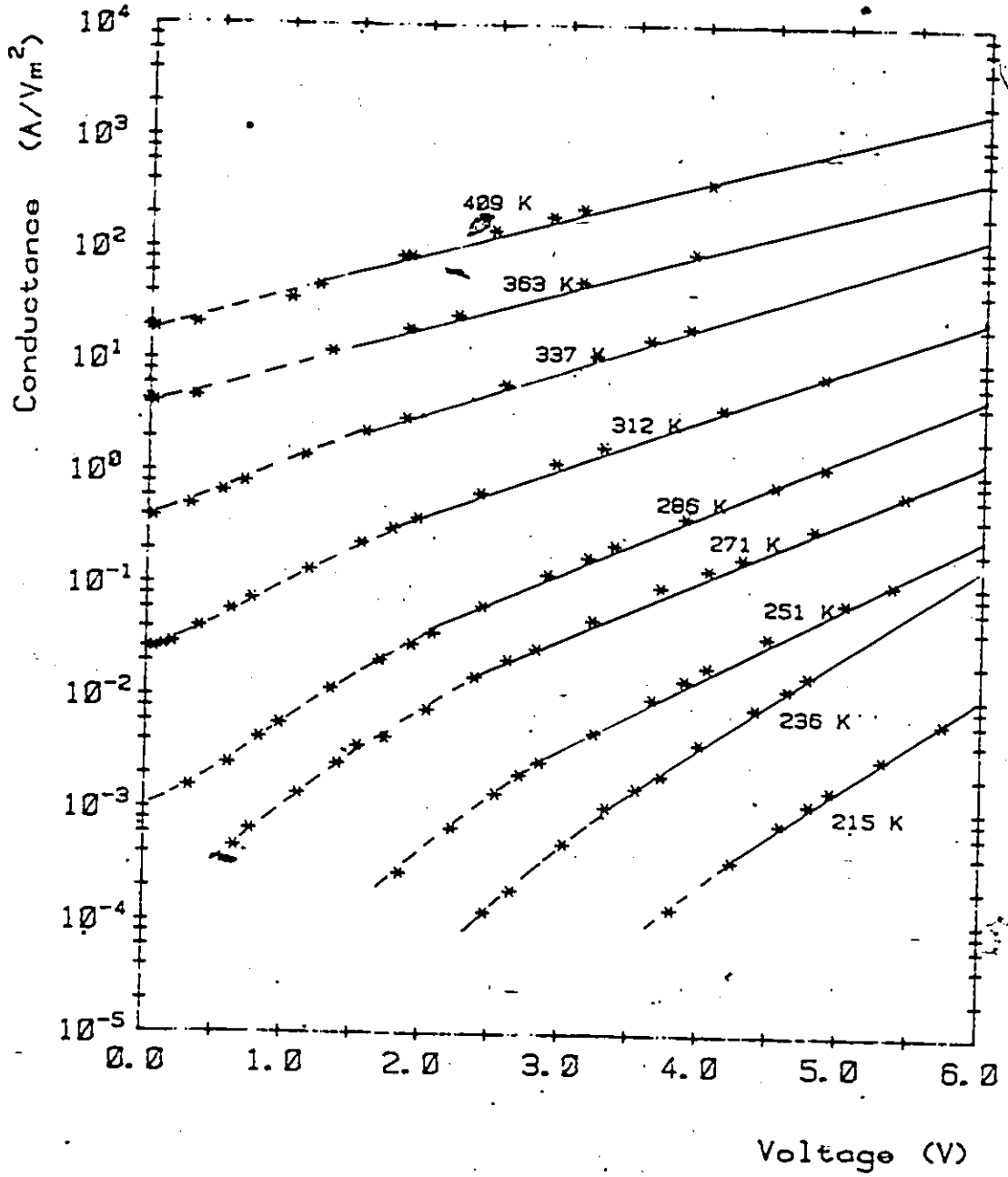

a) On this plot anodic J-V data are shown for a range of temperatures. The solid lines are least square fits to equation <128>, page 91. The hopping model does not explain the dashed portion of the curves.

Figure <30> Hopping J-V-T Behavior of Vacuum Baked Oxides

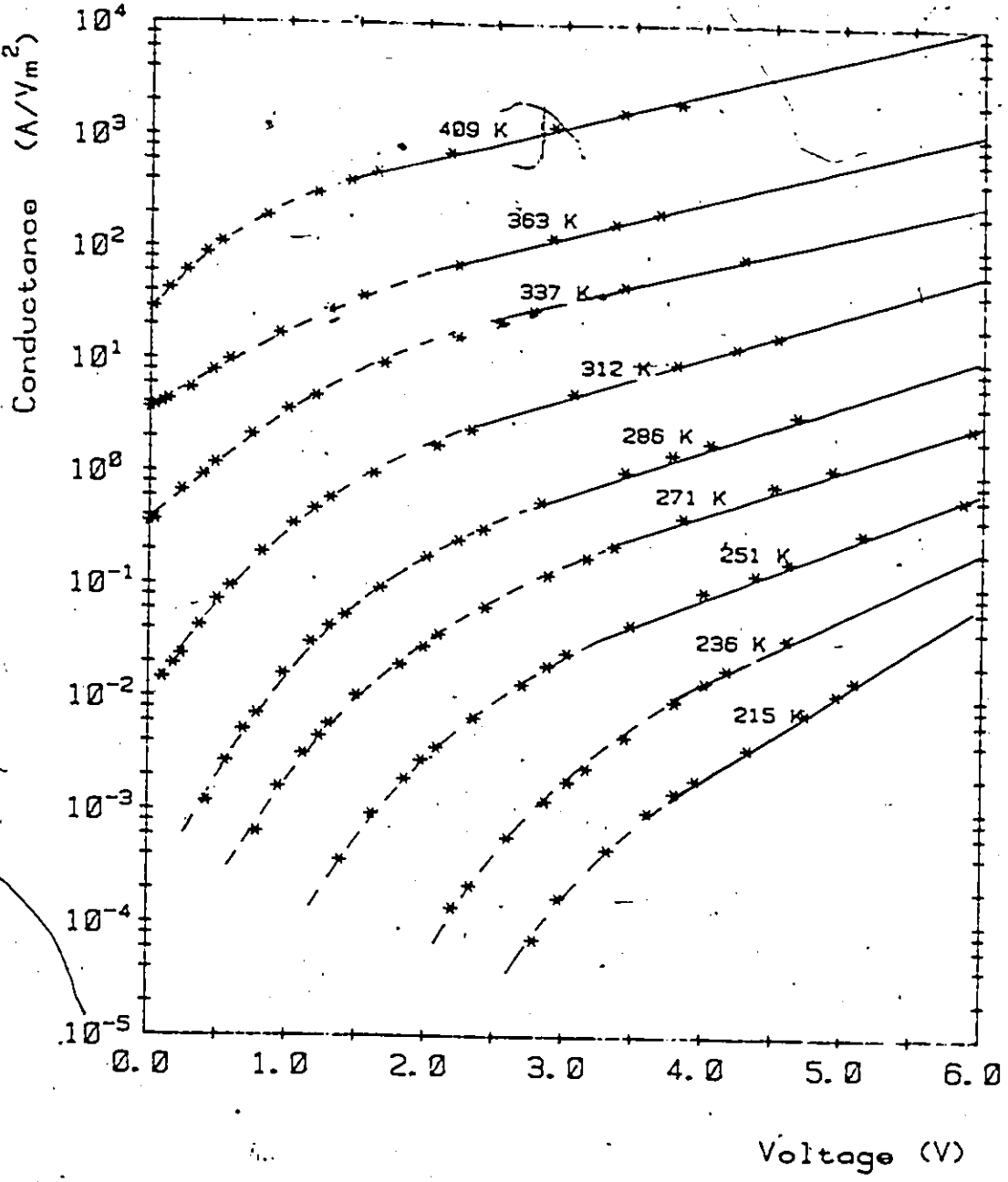

b) On this plot cathodic J-V data are shown for a range of temperatures. The solid lines are least square fits to equation <128>, page 91. The hopping model does not explain the dashed portion of the curves which deviate more strongly in this polarity.

Figure <31> Hopping J-V-T Behavior of Hydrogen Annealed Oxides

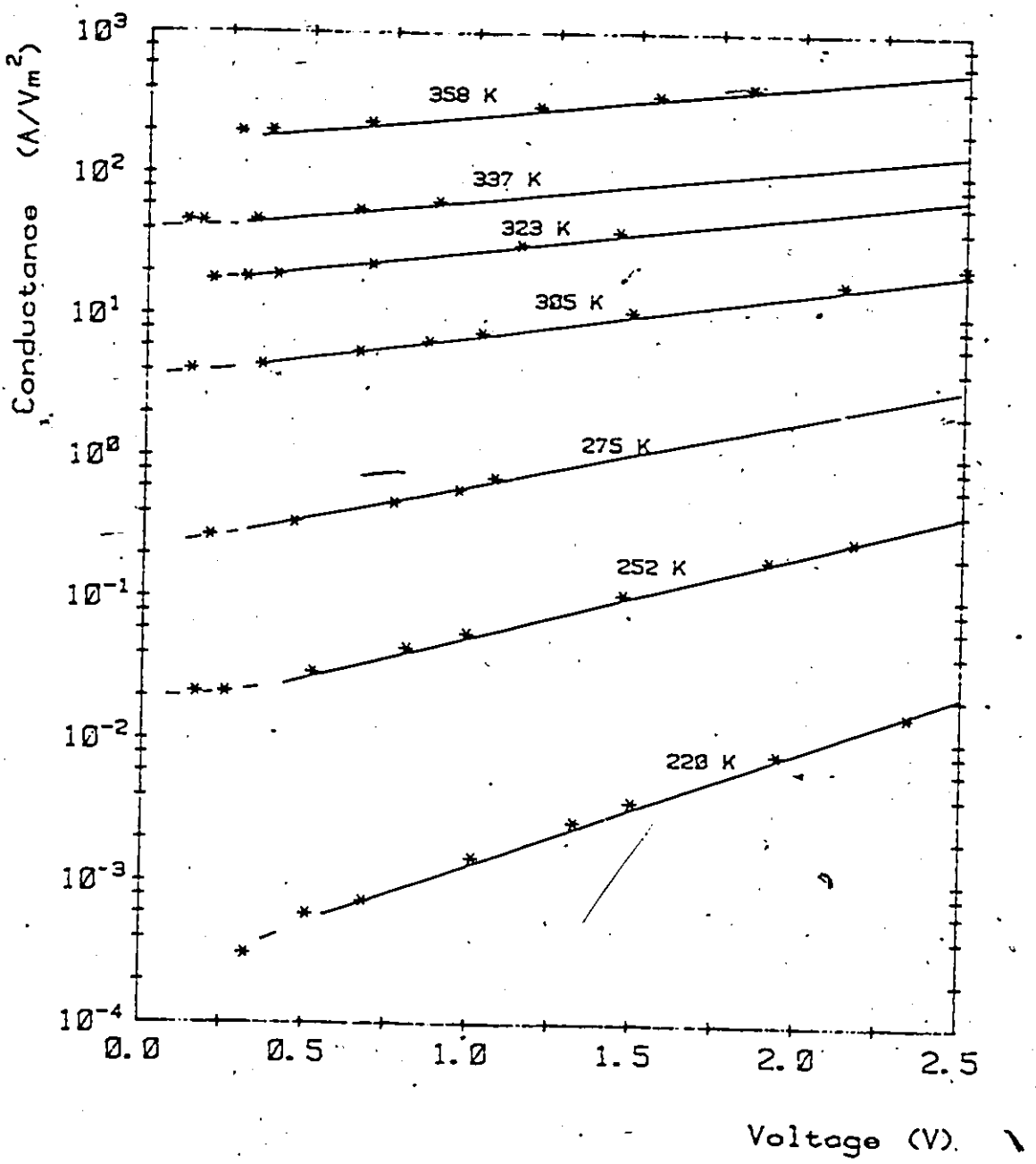

a) On this plot anodic J-V data are shown for a range of temperatures. The solid lines are least square fits to equation <128>, page 91. Note that the fit to the hopping theory prediction of a straight line is significantly better than that exhibited by either the unheated or vacuum baked samples.

Figure <31> Hopping J-V-T Behavior of Hydrogen Annealed Oxides

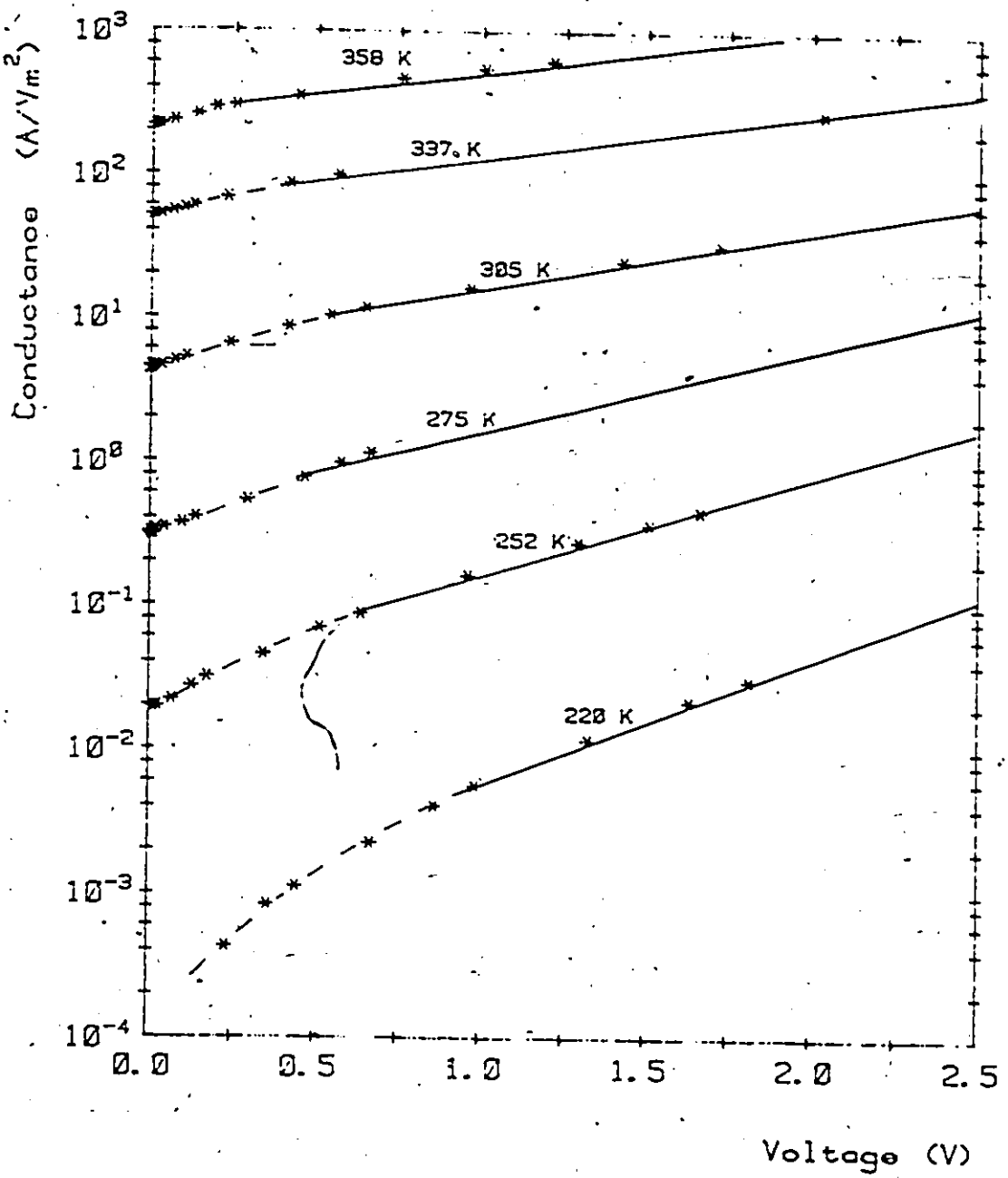

b) On this plot cathodic J-V data are shown for a range of temperatures. The solid lines are least square fits to equation <128>, page 91. The fit to the hopping theory prediction of a straight line degrades at low bias, as observed in the unheated and vacuum baked oxides.

Figure <32> Temperature Dependence of Low Field Ohmic Conductance

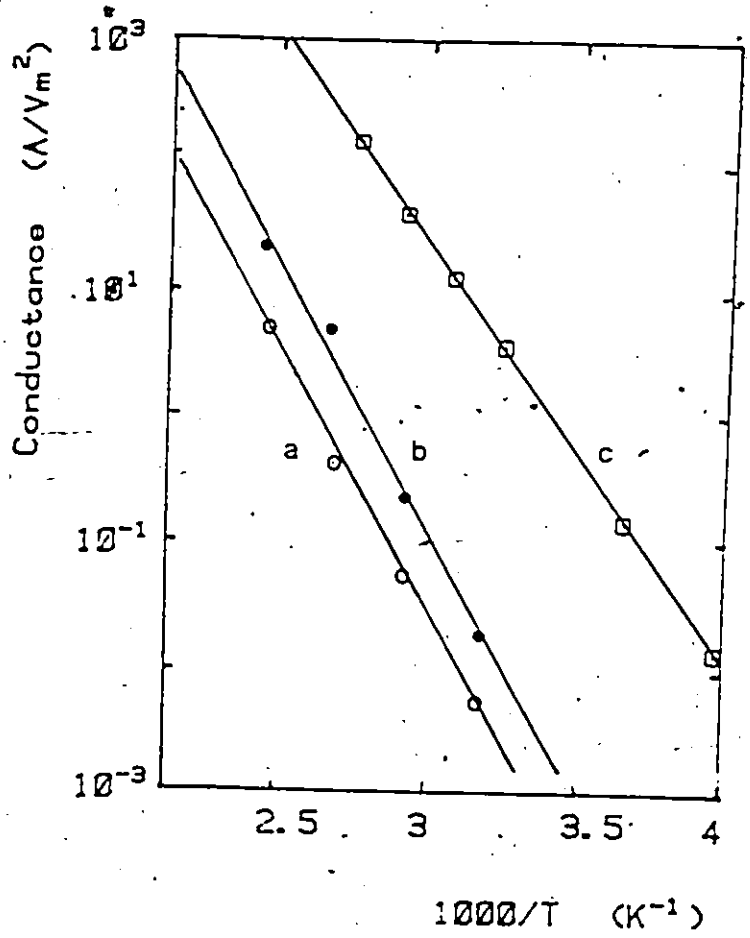

Temperature behavior of the ohmic conductance at zero bias for the (a) unheated, (b) vacuum baked, and (c) hydrogen annealed samples. The calculated activation energies are 0.86 ± .04 eV for the vacuum baked and unheated samples, and 0.69 ± .05 eV for the hydrogen annealed case.

Take as an example the data from Figure <30> for the vacuum baked samples. The following parameters from equation <51'> have been evaluated at 312 K:

$(J/V) = 2.65\times10^{-2}$ A/(V-m^2) - observed at low bias

$\zeta_3 = 0.86$ eV - from Figure <32>

$d = 54.7$ nm - measured by ellipsometry

$R = 8.4$ nm - inferred from J-V dependence

$\nu = 10^{12} - 10^{13}$ s^{-1} - physical property of solids

$\exp(-2\eta R) < 1$ - the overlap factor

Let us assume nearest neighbour transitions which permits the upper limit of the overlap factor can be taken. This also allows n to be estimated 4.0×10^{23} m^{-3}. Substitution in equation <51'> gives a predicted (J/V) value of less than 3.7×10^{-4} A/(V-m^2), 70 times smaller than what is observed.

No improvement is made by allowing for hop lengths, R, in excess of the inter-impurity spacing, a. For instance, suppose that the carriers hop to the next nearest neighbour, i.e. R = 2a. Then the estimate of n would increase to 3.2×10^{24} m^{-3}, helping to increase the estimated value of J/V, but at the same time the overlap factor will drop to below 3.4×10^{-4} (assuming that $1/\eta < a/2$; i.e. impurity wave functions do not overlap). The net result is that the predicted J/V in this case must be less than 1×10^{-6}A/(V-m^2), over four orders of magnitude too small.

Similarly, the optimized predictions of J/V, assuming nearest neighbour hopping, for the unheated and hydrogen annealed

samples at this temperature are 24 and 14 times too small, respectively. These optimized values are over estimates, since experimental evidence shows that R has not yet reached a high temperature limit (Figure <33>), and thus the overlap factor must be retained. Therefore it is concluded that pure thermally activated hopping is unable to explain the observed J-V-T behavior.

b) Variable Range Hopping:

Figure <33> suggests that the Mott theory for variable range hopping should be considered, even though the experimental temperature range is higher than is usually considered appropriate for this mechanism. An additional argument against variable range hopping is the apparent temperature independence of the observed activation energy. In fact, a plot of the low field conductance vs. $T^{-\frac{1}{4}}$, as per equation <57>, page 46, repeated below also gives a straight line. This equation states that for low bias and low temperature conditions:

$$J/V = \frac{q^2 \nu R^2 N(E_F)}{d} \exp -\left[\frac{T_o}{T}\right]^{\frac{1}{4}} \qquad <57>$$

$$T_o = \frac{18.1\ \eta^3}{N(E_F)k} \qquad <58>$$

The values of T_o can be calculated from the slopes of the curves plotted in Figure <34>. These are 6.6, 15.5, and 4.8 $\times 10^{10}$ K for the unheated, vacuum baked and hydrogen annealed samples respectively. They compare poorly with the value of 10^6 K

Figure <33> Temperature Dependence of Inferred Hop Length

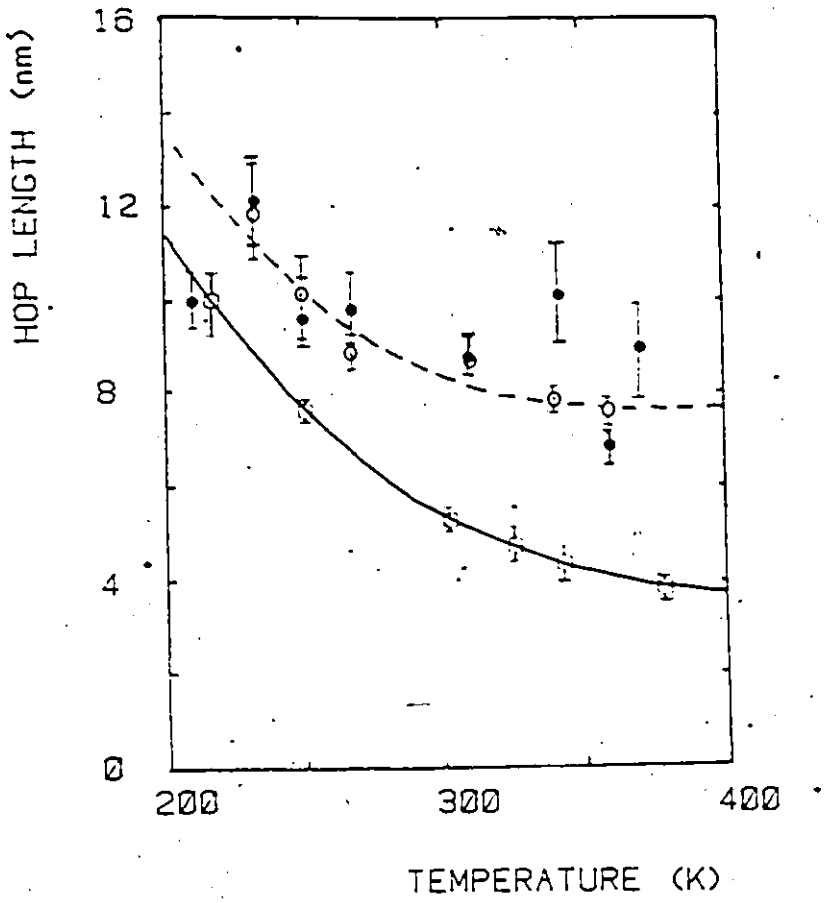

If hop lengths, R, calculated from the data of Figures <29-31> (following page 119) for the unheated o, vacuum baked •, and hydrogen annealed □ samples are plotted against temperature, then a rough tendency towards smaller hop lengths at higher temperature is observed. Only in the case of the hydrogen annealed oxides can a monotonically decreasing function be drawn through all data points. As before, the error bars on R represent a statistically derived Student's T confidence limit of 95% on the results of the linear regression.

Figure <34> Variable Range Hopping Analysis of Ohmic Conductance

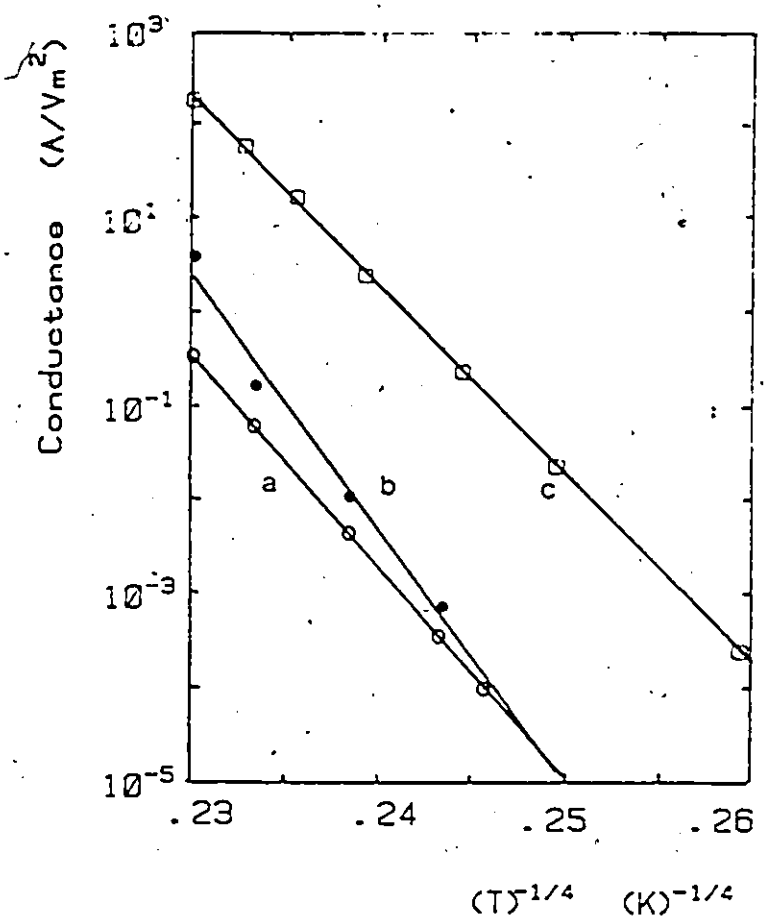

The variable range hopping equation <57>, page 46, predicts that the low field ohmic conductance decreases exponentially as $T^{-\frac{1}{4}}$, as shown in this graph. The three curves shown are for o - unheated, • - vacuum baked, and □ - hydrogen annealed samples. As is discussed in the text, however, the slopes and intercepts of these lines predict physically unacceptible hop lengths.

deduced by Bryksin for Ta_2O_5 (137). Note that the intercepts of the plots on Figure <34> yield an estimate of $N(E_F)$. For the vacuum baked sample, for instance, $N(E_F)$ is found to be 5.3×10^{35} $(J\text{-}m^3)^{-1}$, corresponding to a room temperature density of states at the Fermi level of 2.2×10^{15} m^{-3}. With this value, and the T_o estimate, $1/\eta$ can be estimated. For the vacuum baked device example $1/\eta$ = 25 nm, an exceptionally large value. It is three times the hop length, and is incompatible with the assumptions of hopping conduction. Therefore both the activated and variable range hopping theories must be discarded as possible explanations of the observed J-V-T behavior in these films.

c) Poole Frenkel Conduction:

In general, when the J-V data is plotted in Poole Frenkel format (i.e. $\ln(J/V)$ vs $\sqrt{V}$), each curve has up to 3 distinct segments. These can be seen in Figures <35-37>. The first segment is the low field ohmic region whose activation energy has already been calculated. The next segment is most distinct in the cathodic (Ta negative) polarity in the vacuum baked and unheated samples, but is also present in the anodic (Ta positive) polarity for certain temperatures. It is linear on these Poole Frenkel plots, but with a larger slope than that of the third segment. The third segment is the Poole Frenkel region identified in the previous experiments. A number of conduction models, such as the three dimensional Poole Frenkel models, Poole Frenkel conduction

Figure <35> Poole Frenkel Plot of Unheated Oxides

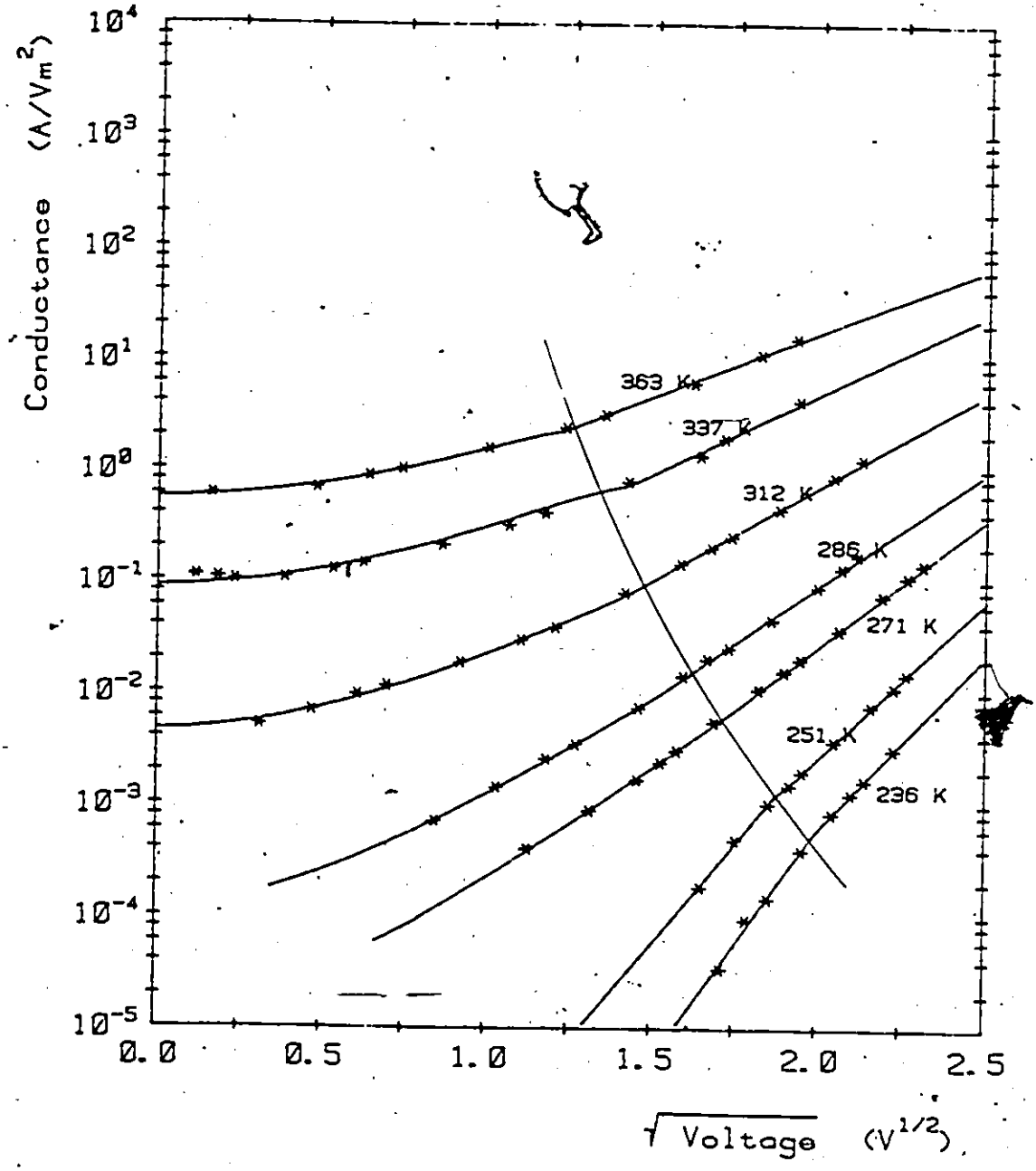

a) This is a Poole Frenkel plot for the anodic bias of the unheated oxides with temperature as a parameter. The estimated errors have been discussed in Figure <22>, following page 104. The solid lines are least square fits to the form predicted by the Poole Frenkel theory discussed in Part IV. The low field behavior is strongly influenced by 3-D effects and thus is curved on this type of plot. The high field behavior for points to the right of the dividing line exhibits a gradual change in slope due to a rise in compensation index when a sufficient number of donors have been ionized.

Figure <35> Poole Frenkel Plot of Unheated Oxides

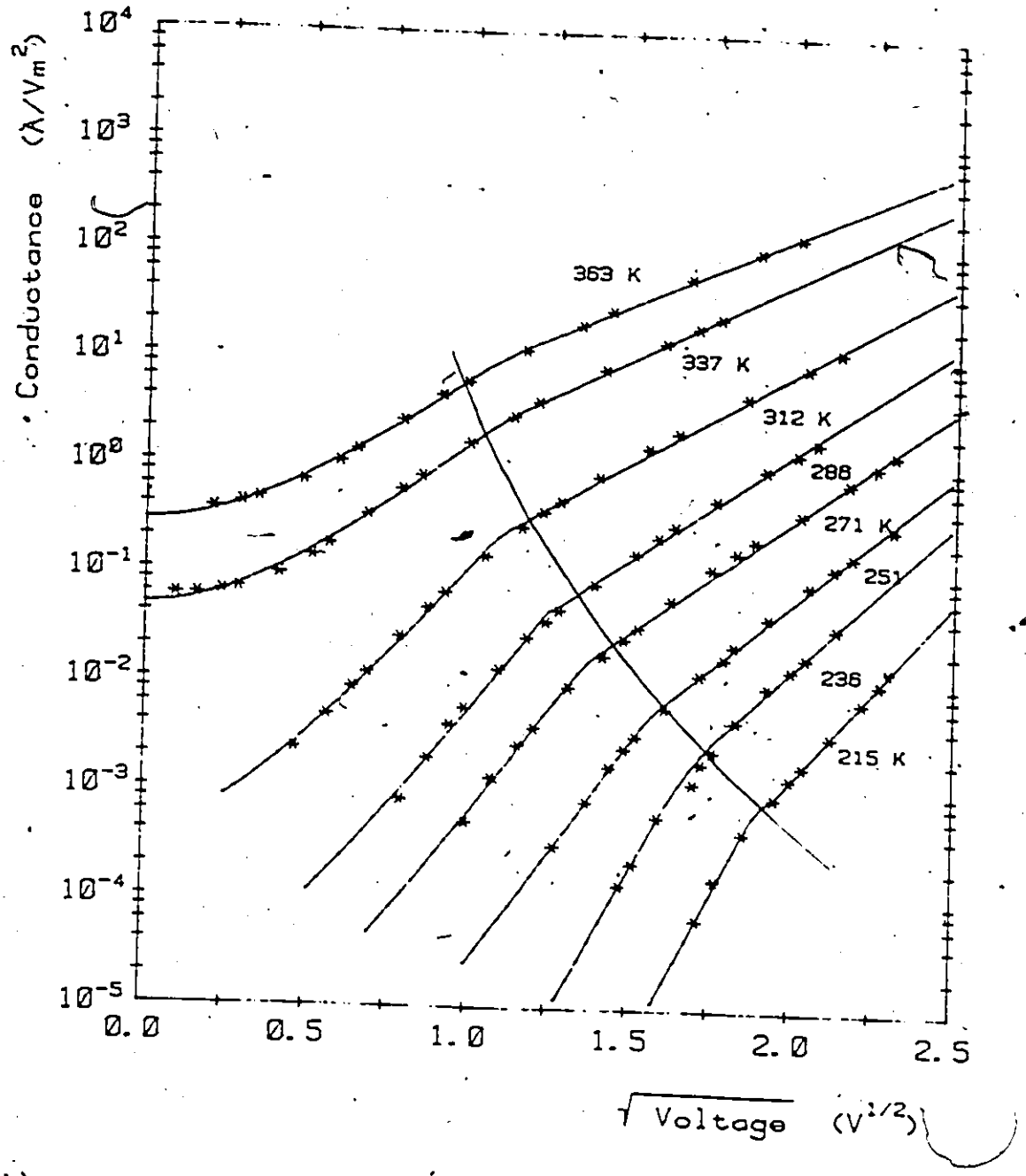

b) This graph shows the corresponding J-V-T curves for the cathodic bias. The transition between the two compensation regions is more distinct than in the anodic case, but in fact occurs at approximately the same current density for both biases. The behavior can also be fitted with the extended Poole Frenkel theory of this thesis.

Figure <36> Poole Frenkel Plot of Vacuum Baked Oxides

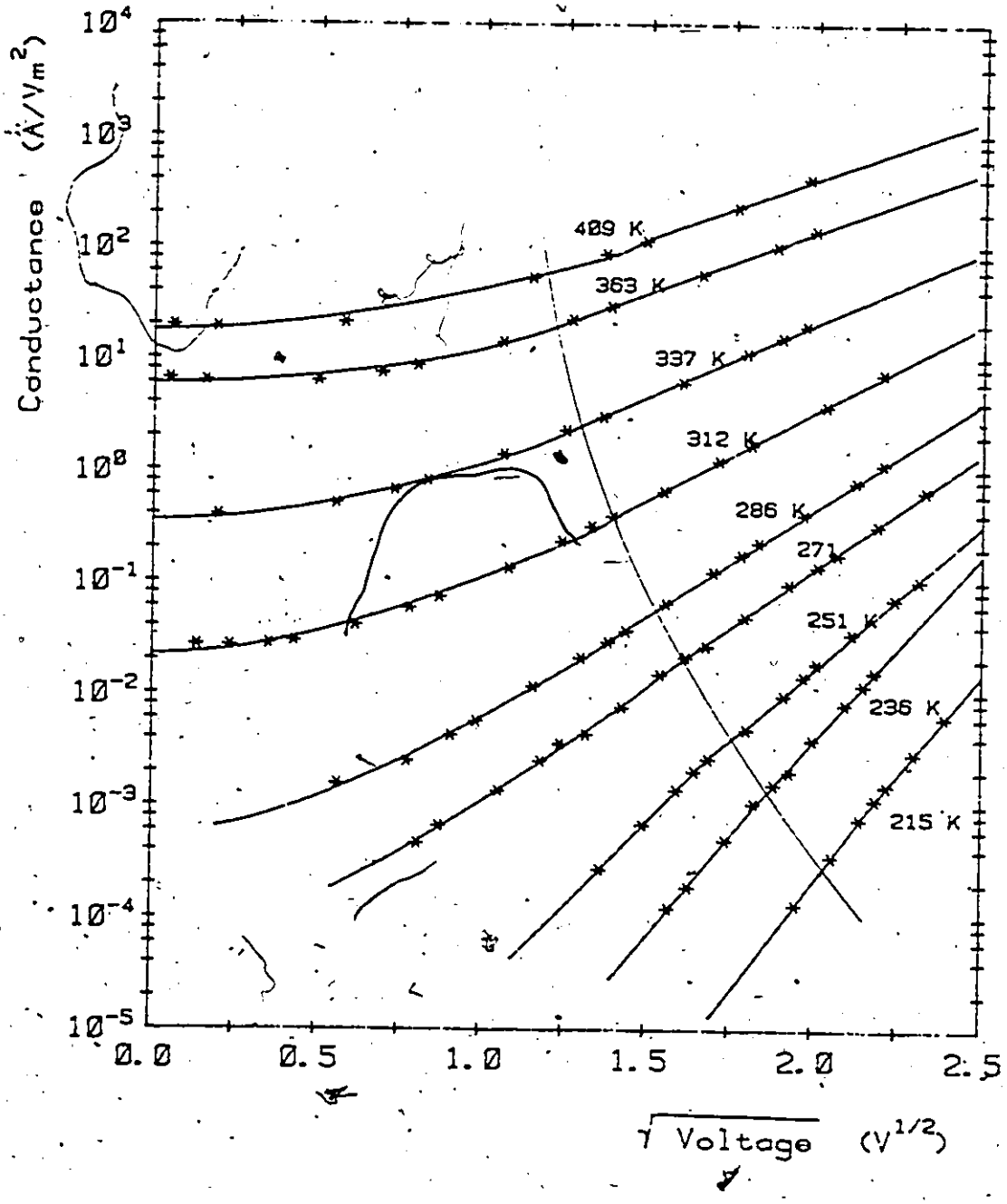

a) The anodic J-V-T behavior of the vacuum baked samples is shown in the same format as given in Figure <35> for the unheated oxides. Temperature is given as a parameter. Low field effects and the mid-field change in slope to the right of the dividing line are also apparent.

Figure <36> Poole Frenkel Plot for Vacuum Baked Oxides

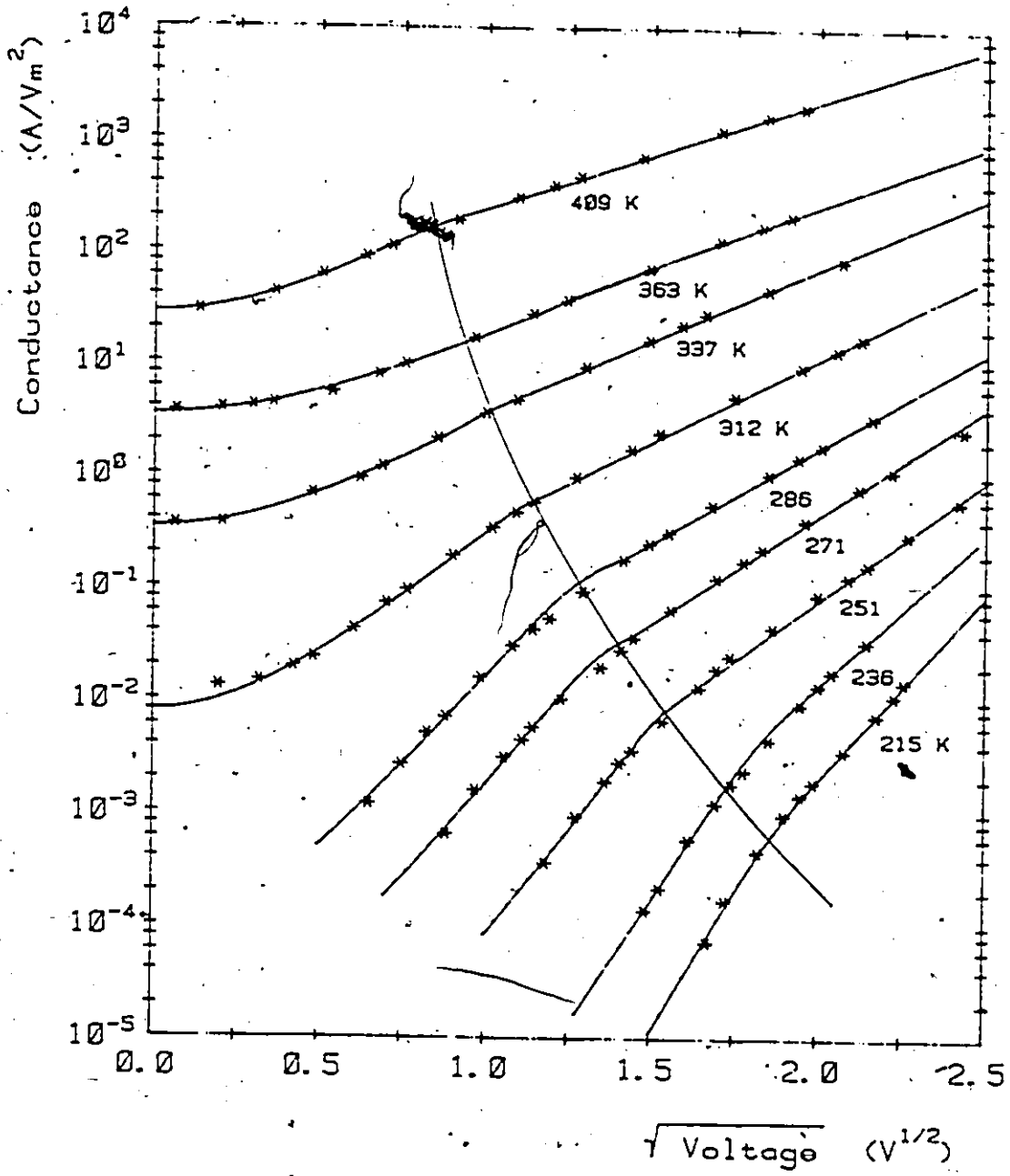

b) The cathodic J-V-T plots for the vacuum baked samples are shown here. The shape of the J-V-T curves for the two biases are more similar to each other for the vacuum baked samples than for the unheated oxides.

Figure <37> Poole Frenkel Plot for Hydrogen Annealed Oxides

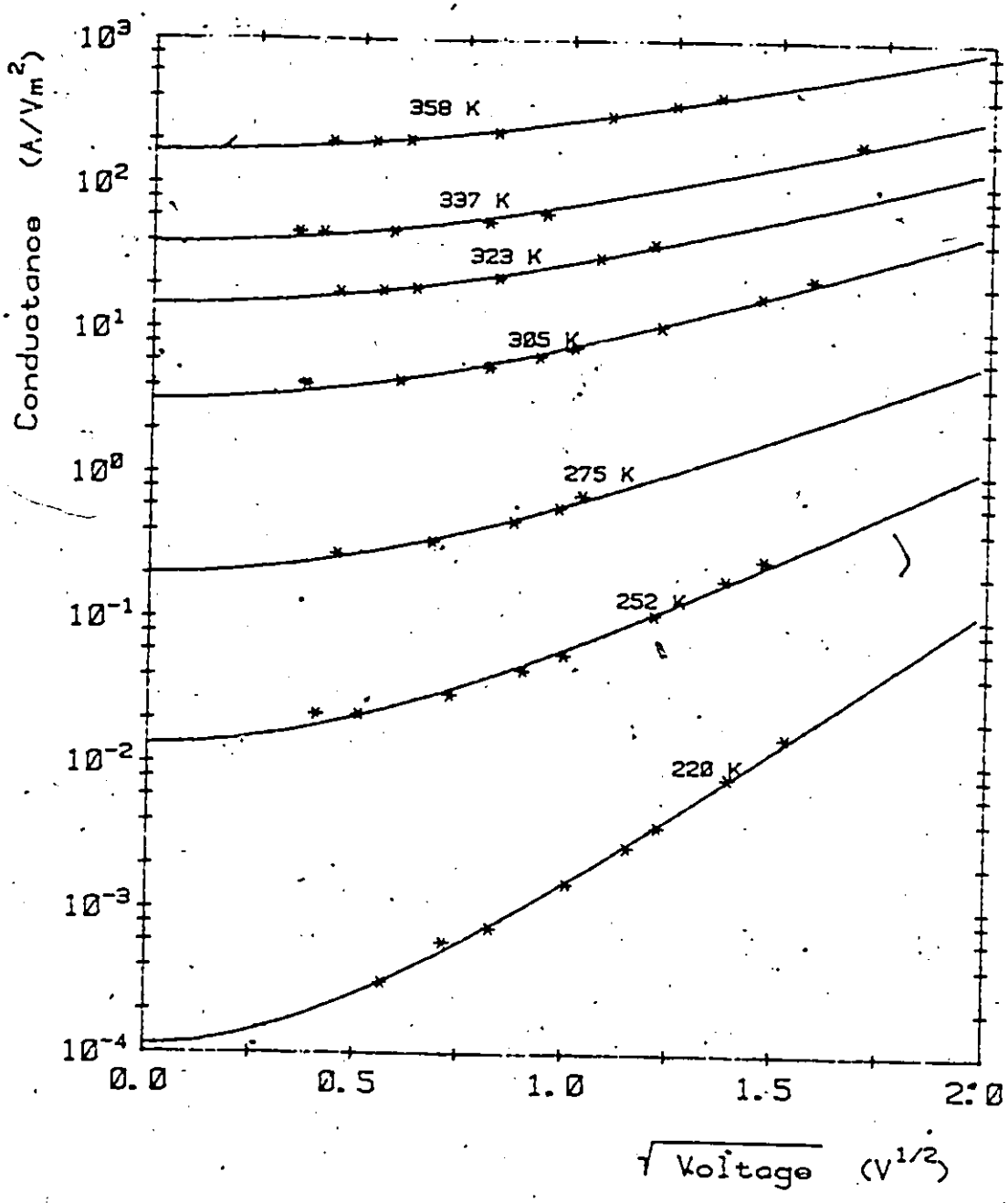

a) For all temperatures the current density in hydrogen annealed oxides is much larger than for the same bias applied to unheated or vacuum baked samples. The anodic bias is shown here. The solid lines are fits to the 3-D Onsager-Poole Frenkel model. No mid-field change in slope is observed within the experimental range.

Figure <37> Poole Frenkel Plot for Hydrogen Annealed Oxides

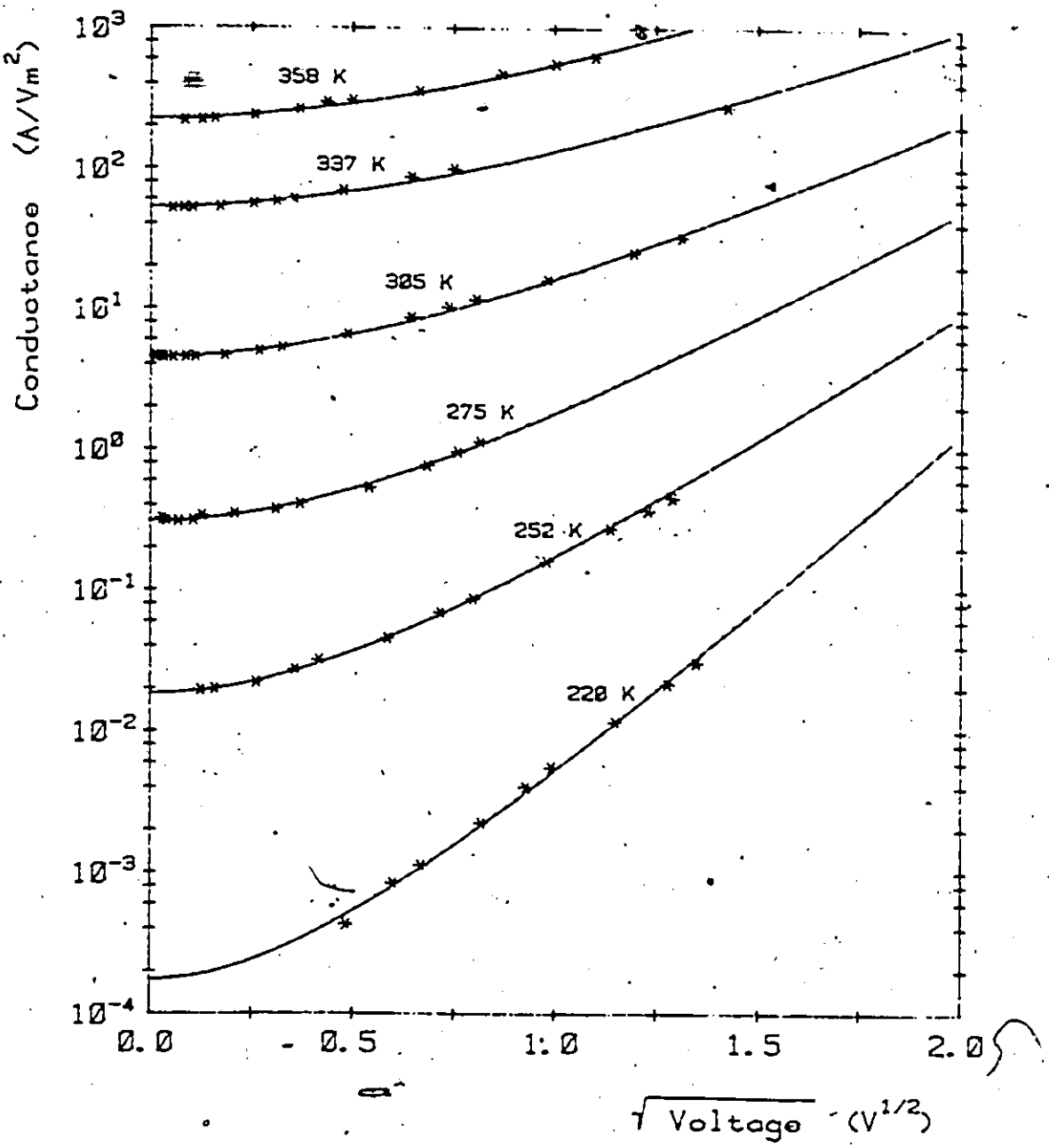

b) The cathodic J-V-T behavior is shown here for the hydrogen annealed samples. The shape of the curves is similar to that of the anodic bias and can be satifactorily fitted to the Onsager-Poole Frenkel model.

involving a second donor level, or a Schottky contact barrier in series with the Poole Frenkel dominated bulk, were applied to the second segment, without success. The least squares algorithm used to draw the solid lines on Figures <35-37> is guided by the conduction model described in Part IV. All regions are fitted to a Poole Frenkel form, with a smooth change in compensation index at a critical voltage. For low voltages it is necessary to consider the three dimensional emission process.

This discussion shall concentrate on the highest field region which should correspond to one dimensional theory. If Poole Frenkel conduction were operative, then one should observe an activation energy for conductance, ζ_a, that decreases with increasing voltage. This is precisely what is seen in Figures <38>. One complication in extracting these values from the experimental J-V-T data was that the data was collected as voltage for a set current, while current for a set voltage is required for the activation energy analysis. Therefore for each point in Figure <38> interpolated values of J(V) were used. Analysis was not carried out for voltages in the ohmic or transition regions. In the high field region the decrease in observed activation energy depth is proportional to the square root of applied voltage as predicted from equation <84>, page 62. The constant of proportionality is nearly the same for both polarities, and for both the vacuum baked and the unheated samples, even though conductivity is an order of magnitude higher

Figure <38> Voltage Dependence of Activation Energy.

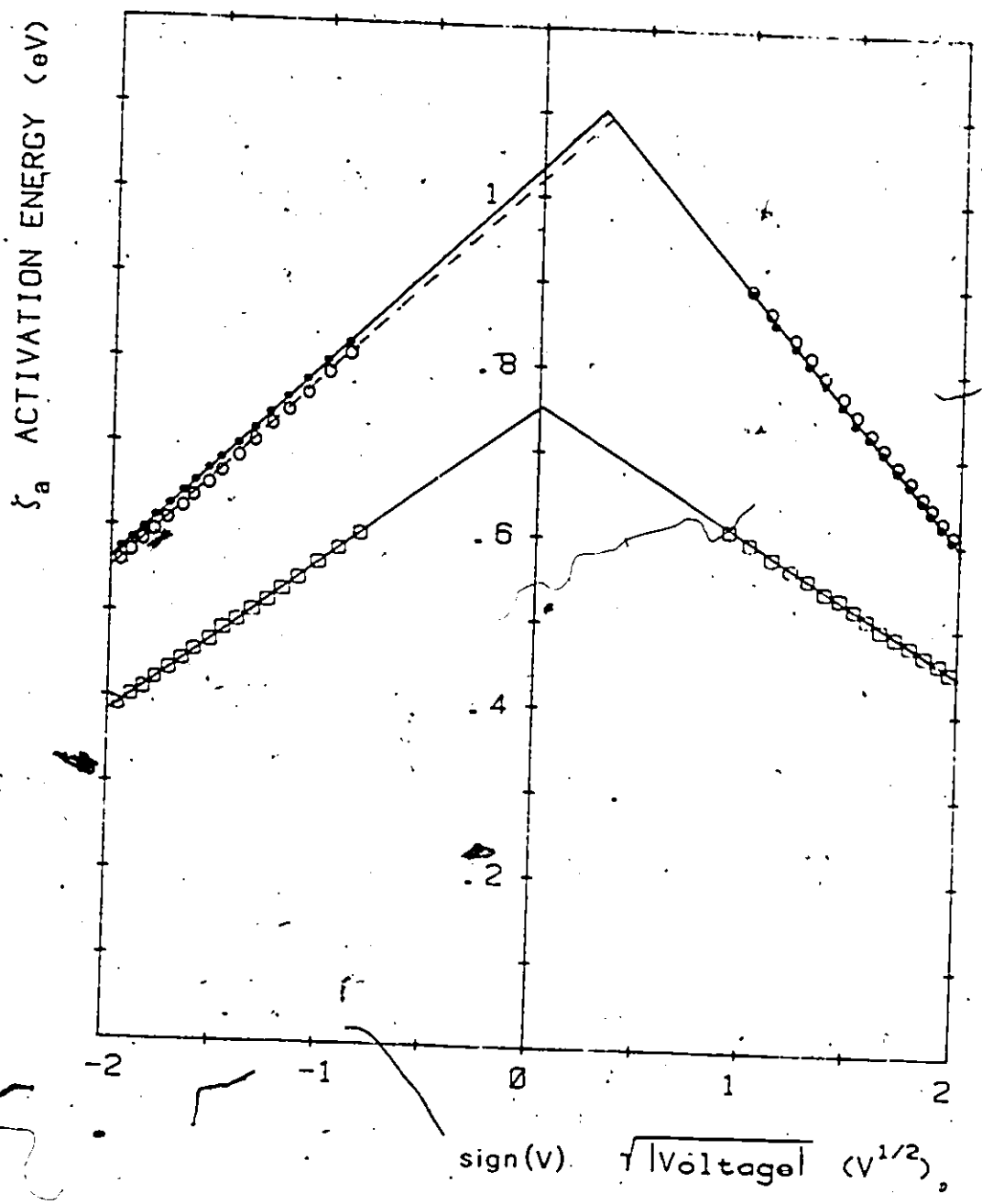

When the activation energy, $\zeta_a(V)$, is calculated from the slopes of experimental ln(J/V) vs. 1/T plots at equally spaced voltage points it is found to decrease linearly as the square root of voltage. Such behavior is characteristic of Poole Frenkel conduction. Near identical behavior is observed for both the unheated (o), and vacuum baked samples (•), even though the magnitude of conduction in the two types of samples differed by a factor of 10. The activation energy for hydrogen annealed samples also decreases linearly with the square root of applied voltage, but both the slope and intercept differ from those observed for unheated and vacuum baked oxides. (□)

in the vacuum baked samples. An asymmetry with respect to zero bias is apparent for these two types of samples. In the hydrogen annealed samples, on the other hand, the asymmetry is absent. The slope of the ζ_a vs $\sqrt{V}$ line was also less at .17 $\pm$ .01 eV/$V^{\frac{1}{2}}$. Thus it would appear that the vacuum baked and unheated samples do experience identical Poole Frenkel barrier lowering operating on the same level. Hydrogen annealing appears to create a new shallower level. These lines do not extrapolate to the correct zero bias activation energies because the one dimensional approach leads to an over estimate of ζ_a.

In the section describing the nitrogen doping experiments, the room temperature nonlinearity coefficient β, was extracted from the J(V) data. Then the compensation index, γ, was calculated as a ratio of the constant

$$\frac{1}{kT}\sqrt{\frac{q^3}{\pi\epsilon\epsilon_o d}}$$

to β, the observed slope of the experimental ln(J/V) vs $\sqrt{V}$, curves. Independently measured values of the pertinent physical parameters enabled accurate calculation of β. In a similar fashion, γ may also be calculated from the slope of the experimental ζ_a vs $\sqrt{V}$ plots. That is

$$\frac{\Delta\zeta_a}{\Delta\sqrt{V}} = \frac{1}{k\gamma}\sqrt{\frac{q^3}{\pi\epsilon\epsilon_o d}} = \beta T \qquad \langle 131 \rangle$$

Thus it may seem possible to calculate γ from J(T) as well as J(V). However, when this is tried, the inferred γ is 0.6 $\pm$ 0.1

for both the vacuum baked and unheated samples. This is inconsistent with the previously calculated γ's of 2 and 1.5 respectively. Even for the hydrogen annealed samples, where there is some doubt as to c and d, a similar discrepancy is found when the slope $\Delta\zeta_a/\Delta\sqrt{V}$ is compared to the product of β and T.

Consider the temperature dependence of β itself (Figures <39-41>). A similar calculation shows β rises much too rapidly with decreasing temperature to be consistent with the γ's calculated at room temperature, or for any other γ between 1 and 2. These graphs do suggest the eventual answer to the dilemma... above room temperature β does follow a proper $\gamma = 2$ line (as is dotted in on the Figure), consistent with independent measurement of c and d. Intution might suggest that at lower temperatures γ is dropping to the $\gamma = 1$ state, causing a rise in β. Part IV will back up intuition with a detailed theory of the intermediately compensated semiconductor, which predicts this effect.

At this point however, the conclusion must be made that standard Poole Frenkel theory is unable to explain the observed J-V-T behavior.

Figure <39> β-T Behavior of Unheated Oxides

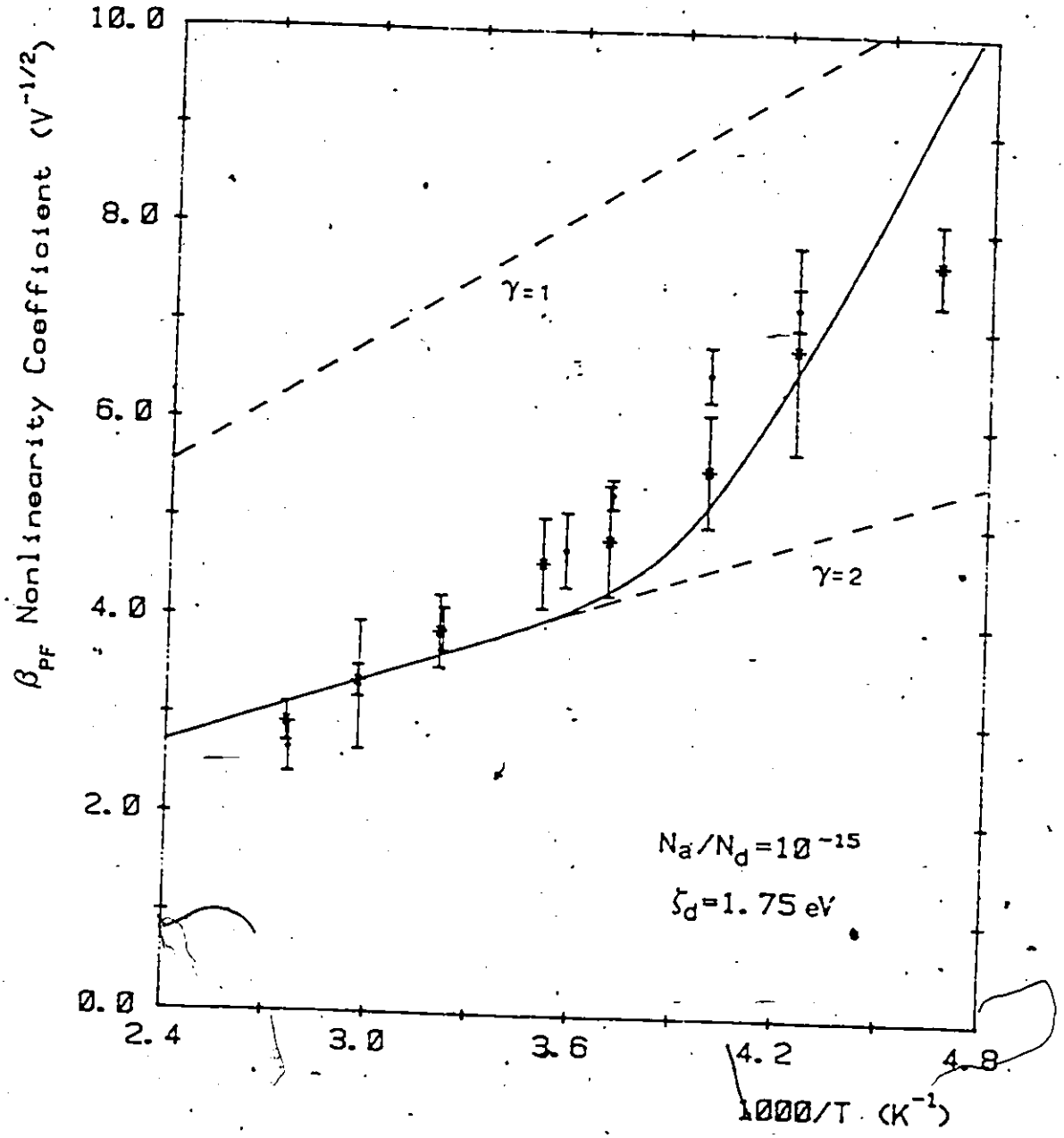

The temperature dependence of β for the unheated oxides is shown here for the anodic (•) and cathodic (*) polarities. Error bars correspond to a Students' T 95% prediction interval. Clearly the data departs fom the γ = 2 line predicted by standard theory. The solid line is the prediction of the extended Poole Frenkel theory proposed in part IV of this thesis. The critical fitting parameters are indicated in the insert, and all others are found in Table X, page 145.

Figure <40> β-T Behavior of Vacuum Baked Oxides

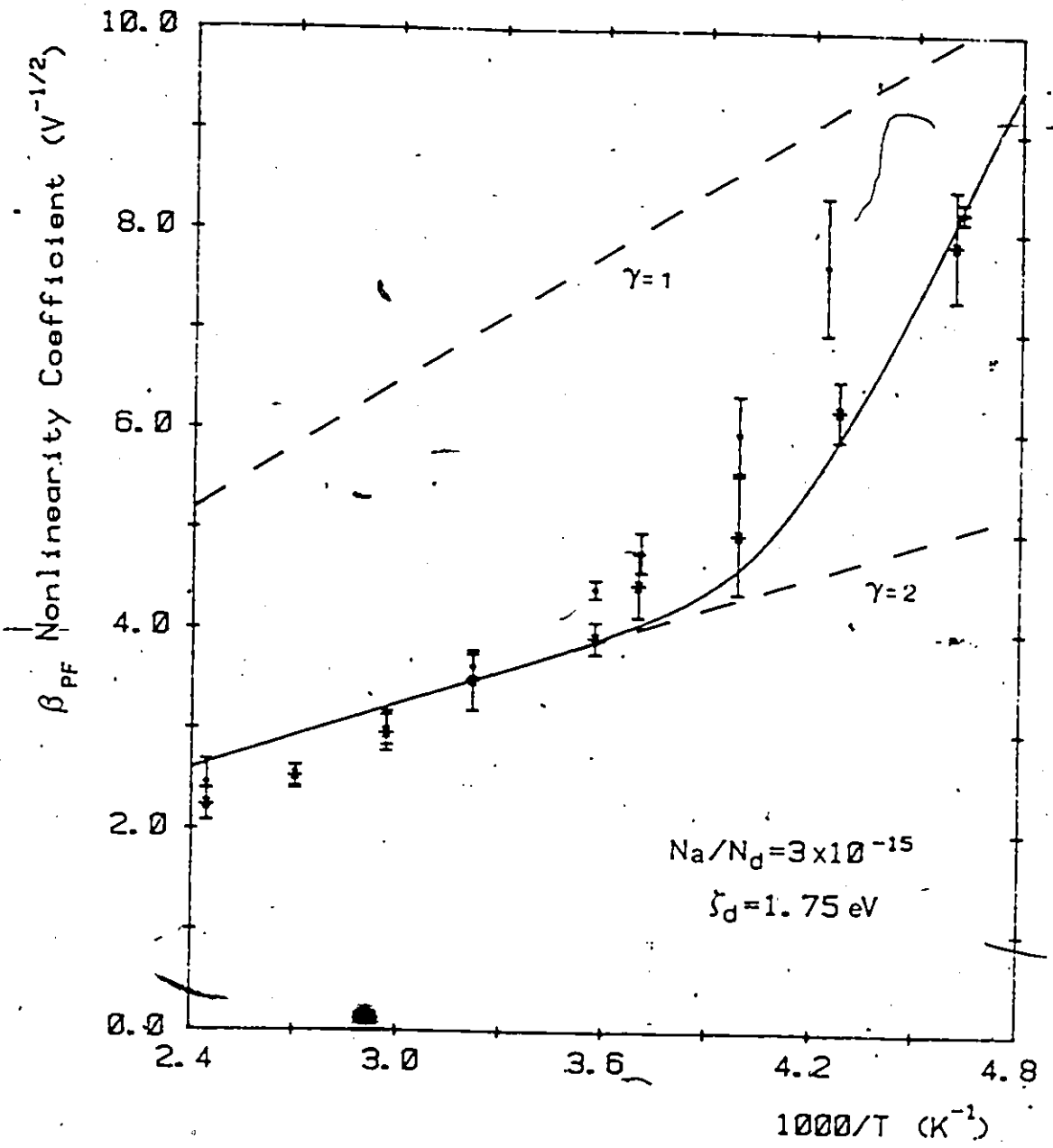

The β's of the vacuum baked oxides show similar temperature behavior to the unheated samples (Figure <39>), even though the room temperature value of β lies closer to the $\gamma = 2$ line in this case. (•) - anodic bias (*) - cathodic bias. To produce the solid curve shown, the ratio of N_a/N_d was increased over that used in Figure <39> by a factor of 3.

Figure <41> β-T Behavior of Hydrogen Annealed Oxides

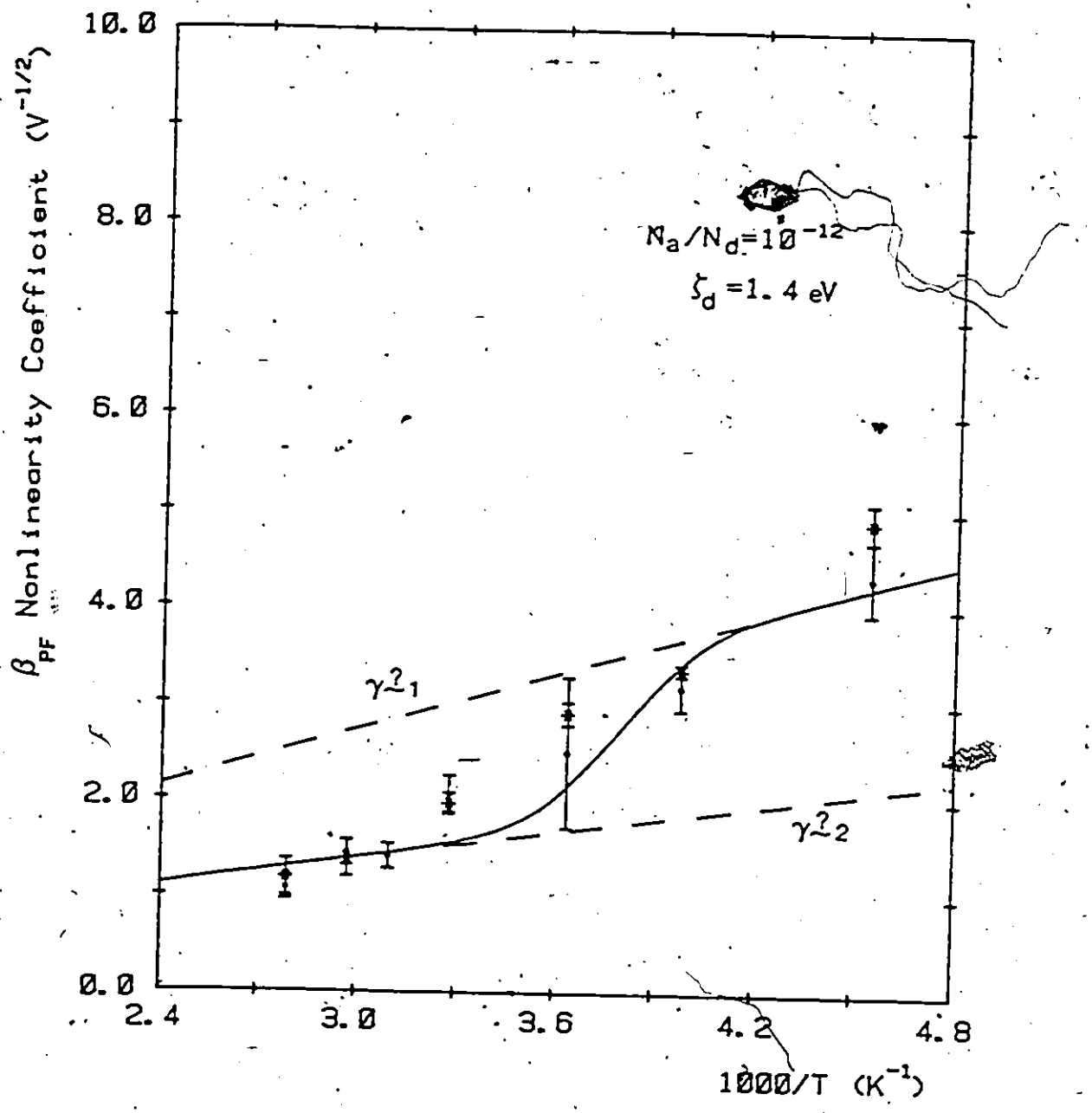

β's for the hydrogen annealed samples are plotted against reciprocal temperature. Values of $\hat{n}$ and d can be chosen to fit the observed β at one temperature, but as in Figures <39> and <40>, standard theory cannot fit all temperatures simultaneously. Even though β is much lower than what can be estimated from pre-anneal $\hat{n}$ and d values, perhaps it is also exhibiting a transition from $\gamma = 1$ to $\gamma = 2$ conditions. If so, the appropriate fitting parameters are those indicated in the insert and in Table X.

3. SUMMARY OF RESULTS

The matter rests at an impasse. Standard Poole Frenkel conduction theory cannot be carried any further. However, the results which have been explained by the existing theory can be summarized thus far.

1) Current is distributed uniformly down to the scale of microns. Flaw dominated conduction is considered unlikely.

2) Current density and the nonlinearity coefficients depend upon insulator thickness in the manner predicted by the punch through Schottky barrier emission, hopping and Poole Frenkel conduction. In contrast, the predictions of imperfect insulator-metal Schottky barrier emission and Space Charge Limited Conduction (SCLC) were not upheld.

3) Independent measurements of ϵ and d, which permit the calculation of a theoretical β, show that "normal" Poole Frenkel conduction occurs in three different tantalum oxy-nitride compositions. Their compensation index is one, in line with the theory that nitrogen compensates the donor operative in the undoped films. The undoped film, on the other hand, showed a room temperature compensation index of 1.5, which is permitted by the theory of Yeargan and Taylor (184), but has not been reported prior to this work. It corresponds to a condition dominated by intermediately compensated donors, where neither partial

compensation nor uncompensated donor statistics can be applied.

In both cases, Schottky conduction is ruled out.

Analysis of the J-V behavior of the nitrogen doped devices also puts hopping conduction in an unfavourable light because the inferred hop lengths are much larger than what is normal for this conduction mechanism.

4) By vacuum baking the undoped sample, conductivity can be increased and its Poole Frenkel compensation index can be brought up to approximately 2. Under the Poole Frenkel model it is concluded that vacuum baking decreases the number of acceptors - possibly by removing water from the film. Hydrogen annealing, on the other hand, creates a new shallower donor - possibly related to oxygen vacancies. The magnitude nonlinearity coefficient, β, of the hydrogen annealed sample cannot be explained by the Poole Frenkel model on the basis of physical parameters measured before annealing. The hopping model, on the other hand, has no difficulty explaining the nonlinearity of the hydrogen annealed sample. It also implies that vacuum baking and hydrogen annealing increases the number of impurities (of a shallower energy depth in the case of the hydrogen annealed samples), causing the hop length to decrease and conductivity to increase.

5) Low field ohmic and a second "Poole Frenkel - like" conduction regime were found at very low field strengths. The only slightly rectifying nature of the ohmic behavior limits the magnitude of any postulated pre-existing internal field such as

would result from contact metal work function differences. The shape of the low field ohmic region is correctly predicted by the Onsager - Poole Frenkel model.

6) The nature of the asymmetry in the high field region is such that the extrapolated peak in the activation energy vs $\sqrt{V}$ plots is shifted in the direction of the anodic polarity in both the unheated and vacuum baked samples. This supports result 4) that the vacuum baked and unheated samples differ in the number of donors and acceptors, not the type of donor. The hydrogen annealed samples were shown to have symmetric activation energy behavior.

7) Using the temperature dependences of the zero bias conductance and the voltage dependence of current density it was shown that the hopping models all predict conductances well below the observed values. This evidence, combined with the exceptionally large hop lengths, and the generally poor J-V fits lead to the dismissal of the hopping model.

8) Discrepances were found in the inferred values of the physical parameters that make up β estimated from temperature dependences, and field dependences. The standard Poole Frenkel model is unable to explain these results. An extension to the theory is proposed in the following section to resolve the difficulty.

1. EXTENSIONS TO THE THEORY

Introduction:

The analysis has shown that standard Poole Frenkel conduction theory has been successful in predicting the functional dependences of J-V data on such physical properties as thickness and dielectric constant. It has also been able to present a consistent picture with regards to the compensating effects of nitrogen doping and heat treatments. But two problems remain. The first, and the most disturbing problem is that one cannot use the standard Poole Frenkel theory to predict unique values for such physical parameters as Y, the compensation index, from both the J(V) and the J(T) data. This problem manifests itself most clearly in the temperature dependence of ρ. It rises too steeply with decreasing temperature. The second problem is that the J-V data is asymmetric; cathodic currents exceed the anodic currents, but the Poole Frenkel model, being strictly a bulk phenomenon, has no provision for this effect. In this section, the Poole Frenkel conduction theory is extended to include explanations for both the anomalous J-V-T behavior and the asymmetry of current with respect to zero bias.

2. INTERMEDIATELY COMPENSATED DONORS:

The anomalous J-V-T data, which gives us different estimates for the physical parameters depending on how the data is analysed, is the crux of the problem. Analysis at any one temperature gives reasonable estimates for all the disposable parameters in the Poole Frenkel conductivity expression. It is the attempt to analyse the behavior at all temperatures simultaneously that leads to the inconsistency. Therefore it is a valid question to ask if there really is a problem. Could the measurements be in error? The answer to this question is "not likely". Adequate calibration of temperature, current and voltage measuring devices, the strict use of controls to check for drift, and the fact that a large number of devices have been tested over a span of many fabrication runs limits the possibility for error. The possibility becomes even more remote when the literature is consulted. Similar anomalous J-V-T behavior has been reported, but not explained, by Jonscher (65) working with SiO_x, by Sinha and Smith (213) also working with SiO_x, by Brown et al (205) working with Si_3N_4, and by Meaudre and Meaudre (215) also in SiO_x. Temperature dependent dielectric constants and/or thickness have been suggested. However, the anomaly described in this thesis appears to be the furthest from theory yet seen. Therefore even the most generous estimates of temperature dependences in ε

and d are simply insufficient to bring the data in line. Fortunately, these temperature dependences are not required to fully explain the J-V-T data reported here and in the literature. In the first extension to the theory presented below, a simple model is derived from within the framework of the Poole Frenkel model to fit the J-V-T behavior based on the existence of partly partially compensated donors within the Ta_2O_5.

One way to explain the J-V-T results is to find a smooth variation with temperature in γ, the only other parameter left in β whose temperature independence has not been verified. Intuitively, it is not hard to understand why this can occur. The degree of compensation, and thus γ must be a function of temperature because the ratio of ionized donors to ionized acceptors is not the same for all temperatures. When temperature is increased the number of ionized donors increases whereas the number of ionized acceptors remains the same since they were all ionized to begin with. Clearly then, the ratio of ionized donors to ionized acceptors increases with heating, making the insulator less "compensated". Thus γ must increase from 1 to 2. This magnitude of change is sufficient to fit the observed values of β in the results presented here.

A detailed analysis will be presented in this section to show that the transition between $\gamma = 1$ and $\gamma = 2$ conditions occurs gradually over the observed temperature range. Recall from Part II, pages 71-75 that γ arose from the relationship between the carrier density and the donor density. The starting assumption was charge neutrality. Free holes and unionized acceptors were neglected. This gave equation <107>.

$$n = -\tfrac{1}{2}(N_a + N_c') + \tfrac{1}{2}\left\{(N_c' + N_a)^2 + 4\,N_c'\,(N_d - N_a)\right\}^{\frac{1}{2}} \qquad <107>$$

where n = density of free electrons

N_d = density of donors

N_a = density of acceptors

$N_c' = \frac{N_c}{2} \exp\left[-\frac{\zeta_d}{kT}\right]$

N_c = conduction band density of states

ζ_d = donor energy depth

Standard theory assumed that if $N_d >> N_c' >> N_a$ (i.e. donors are uncompensated) then only the $4 \cdot N_c' (N_d - N_a)$ term in equation <107> was retained, and therefore the carrier density became:

$$n = \sqrt{\frac{N_d N_c}{2}} \exp\left[-\frac{\zeta_d}{2kT}\right] \qquad <108>$$

Thus $\gamma = 2$

Similarly, if $N_d >> N_a >> N_c'$ (i.e. donors are partially compensated) then it was possible to expand the square root to second order and cancel the two terms in $(N_a + N_c')$.

This left the expression:

$$n = \frac{(N_d - N_a)}{2N_a} N_c \exp\left[-\frac{\zeta_d}{kT}\right] \quad \text{<118>}$$

Thus $\gamma = 1$

In contrast, the analysis presented in this section is concerned with the situation where the donors are neither uncompensated nor partially compensated. In effect, the donors are intermediately compensated. Mathematically speaking, these conditions prevail when:

$$.4\ N_c'(N_d - N_a) < (N_c' + N_a) < 40\ N_c'\ (N_d - N_a)$$

and thus neither of the simplifying assumptions used in the derivation of equation <108> and <118> is valid. When the donor and acceptor densities are in the intermediately compensated regime, the temperature dependence of the carrier density must be calculated directly from <107>.

In the computation of values of equation <107> care must be taken to ensure that round off error does not adversely affect accuracy. For example, if $(N_c' + N_a)^2$ is more than 10^9 times larger than $4 \cdot N_c'\ (N_d - N_a)$, then a formulation of equation <107> exactly as written will return an incorrect value of zero when executed on the Apple //e computer. This is due to the nine digit limit of accuracy. Under these particular circumstances n is the difference between two nearly equal numbers. Therefore the expansion of the square root employed in the derivation of

equation <118> is not only valid under certain circumstances, it is necessary to preserve accuracy. Happily, the range of impurity concentrations where the full formula must be used instead of the expanded form lies within the range where the computation of the full formula is accurate. A similar problem in the computation of equation <107> is the limited dynamic range of the computer. Only numbers in the range of 10^{-38} to 10^{+38} may be manipulated. This problem can be easily circumvented by factoring out a common multiple of, say, 10^{10} from N_a, N_d, and N_c' prior to calculation.

The behavior of this function over the temperature range used in the J-V-T experiment is shown in Figure <42> for a range of acceptor densities. Several features of the plot can be described.

1) For all donor to acceptor ratios greater than 10^{21}, a transition is made between two linear ln(n) vs 1/T curves differing in slope by approximately a factor of two. The high temperature portion corresponds to equation <108> with slope equal to $\zeta_d/2k$, while the low temperature portion corresponds to equation <118> with slope equal to ζ_d/k.
2) The larger the acceptor density, the higher the temperature at which the transition begins.
3) An alternate choice of donor density simply displaces the curves vertically.
4) The donor to acceptor ratios may seem exceptionally large. Why should such a seemingly insignificant number of

Figures <42> Temperature Dependence of Carrier Density

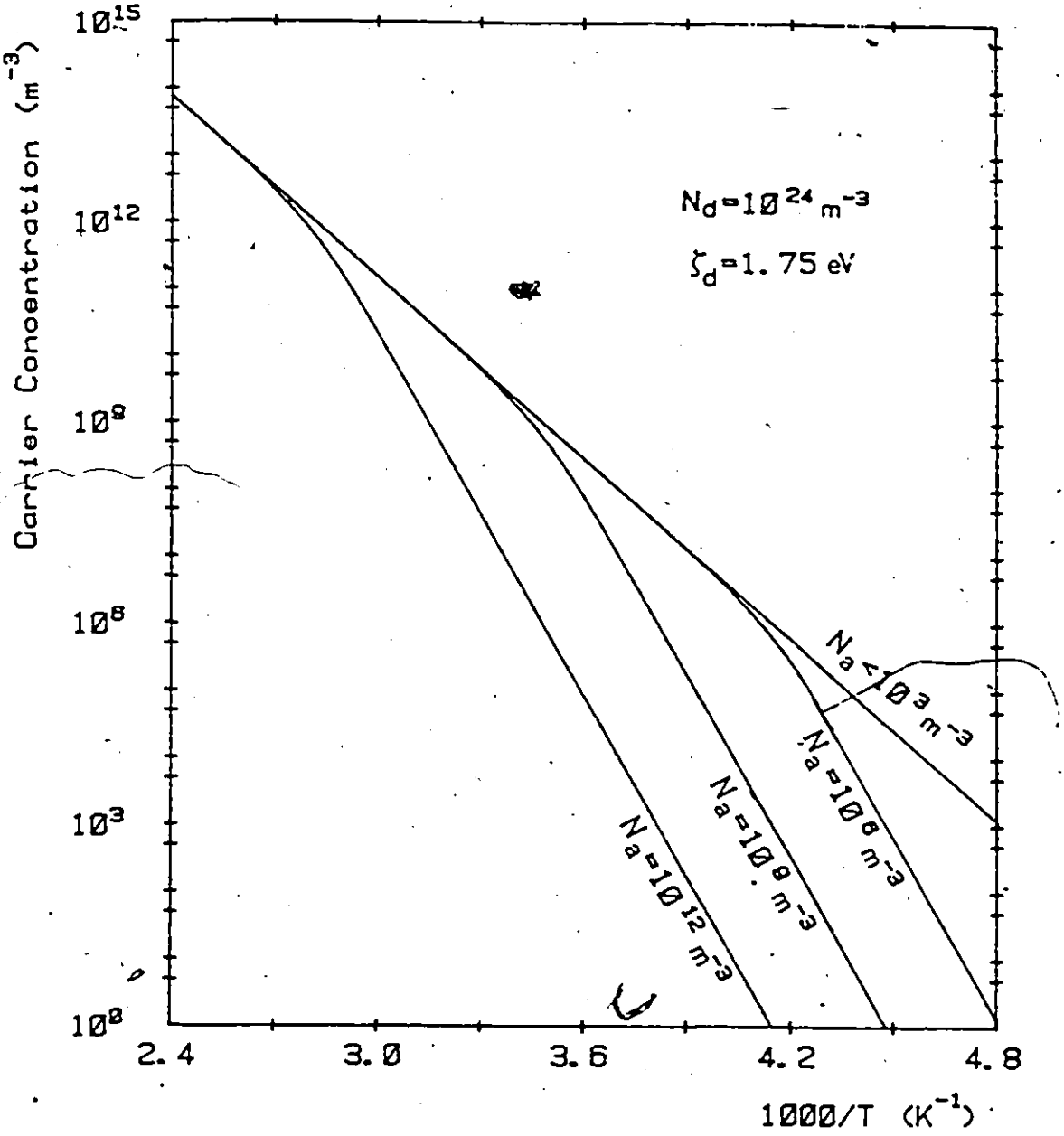

Carrier density, as described by equation <107>, page 72, is plotted here against reciprocal temperature with acceptor density as a parameter. The impurity densities and activation energies are indicated in the inset. They are the same as those used for fitting the unheated oxides.

acceptors be so important? In fact, the number of ionized donors and ionized acceptors are comparable. For example, for T = 300 K, $N_d = 10^{24}$, $N_a = 10^9$, and $\zeta_d = 1.75$ eV, the number of ionized donors is only 5.1×10^9, and thus the material is indeed partially compensated. If, on the other hand, ζ_d were only 0.5 eV, then the donor to acceptor ratio must be below 100 to exhibit a transition in this temperature range. In short, the deeper the donors are, the fewer acceptors needed to compensate them.

5) The acceptor activation energy has no influence on the form of the plot provided $E_F - E_a$ is greater than 2kT. This was contained in the assumption that the material was n-type, and therefore that all of the acceptors were ionized.

6) The calculation is only valid up to the point where $E_d - E_F$ becomes less than 2kT. This was contained in the assumed validity of the Boltzmann relationship between carrier density and donor activation energy. All of the calculations shown in this thesis have been verified to be within the range of Boltzmann statistics.

The temperature dependence of carrier concentration with differing donor to acceptor ratios shown here is nothing startling. Similar graphs can be found in the text "Semiconductor Statistics" by Blakemore (235), and Hall data showing experimental evidence of the transition can be found (236). What

is new is the application to the Poole Frenkel situation.

In the Poole Frenkel situation both β_{pf}, the nonlinearity coefficient, and K_{pf}, the conductivity coefficient, are affected by the degree of compensation. The Poole Frenkel conductivity coefficient, K_{pf}, in either of the two asymptotic doping regimes is equal to:

$$K_{pf} = \frac{\mu q}{d} n_o(T) \qquad <132>$$

where $n_o(T)$ is the carrier concentration in the absence of Poole Frenkel barrier lowering.

Thus in previous applications of standard Poole Frenkel theory plots of K_{pf} vs 1/T were presumed to be linear with slope equal to $\zeta_d/\gamma k$. Data and predictions of standard theory are given in Figures <43-45>. In both the vacuum baked and unheated examples the standard theory tends to overestimate K_{pf} in the low temperature range. Under the model described here, the decrease in K_{pf} below the values predicted by standard theory is due to the transition from uncompensated to partially compensated donor statistics as temperature decreases. It might be expected that these K_{pf} plots should be identical to those of n(T) in Figure <42> except for a vertical displacement to account for the $\mu q/d$ multiplicative factor. Although such a fit to the data (given in Figure <43> only) shows the desired drop at low temperatures, this curve also deviates from the observed data. The trouble is that K_{pf} is not exactly as given in equation <132>

Figures <43> K_{pf}-T Behavior of Unheated Oxides

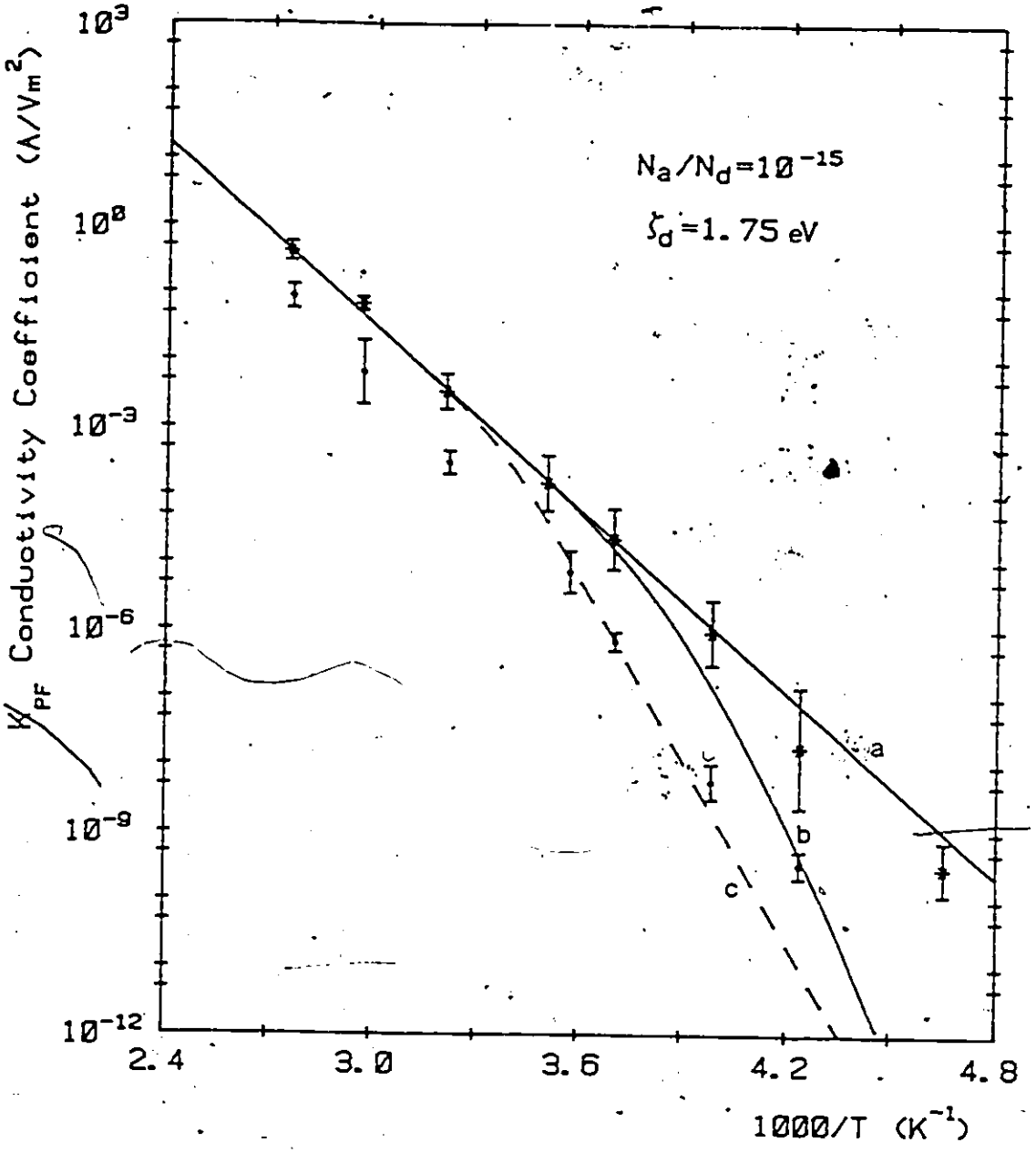

This graph shows the large variation in the observed K_{pf} values over the temperature range examined. Standard theory is unable to fit the low temperature K's which fall below the prediction, a). The curve b) drawn for the same fitting parameters used for the β-T fit (Figure <39>, page 125) correctly predicts the deviation, and falls between the anodic (•) and cathodic (*) points. Neglect of the voltage dependence of compensation leads to the dashed curve c).

Figure <44> K_{pf}-T Behavior of Vacuum Baked Oxides

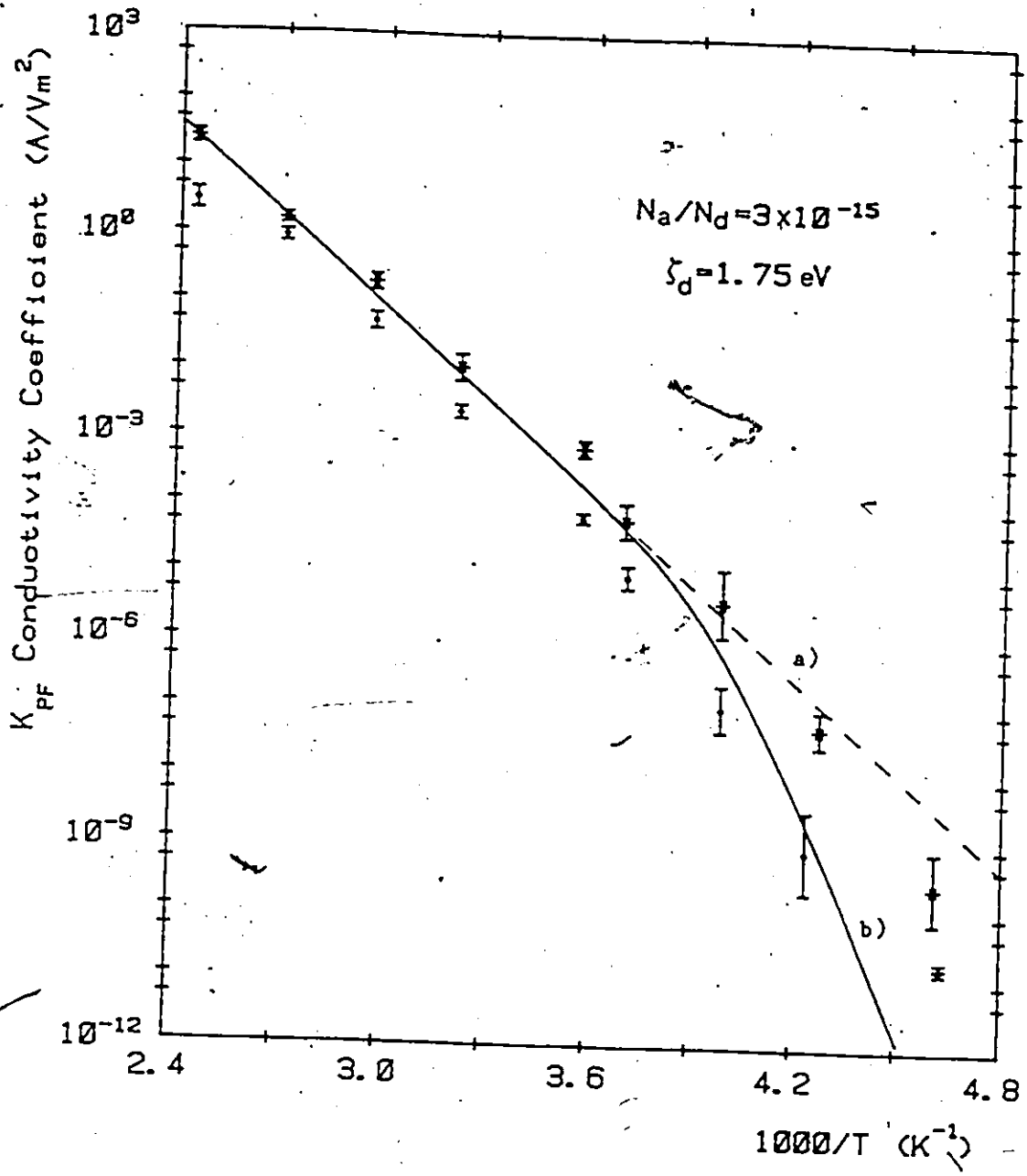

The K_{pf}-T behavior of the vacuum baked samples show even more clearly the low temperature deviation from standard theory a). The predictions of the extended Poole Frenkel theory, b), using the fitting parameters from the β-T curve, Figure <40>, page 125 falls between the anodic (•) and cathodic (*) points. As in the previous Figure, the error bars are the 95% Student's T intervals.

Figure <45> K_{pf}-T Behavior of Hydrogen Annealed Oxides

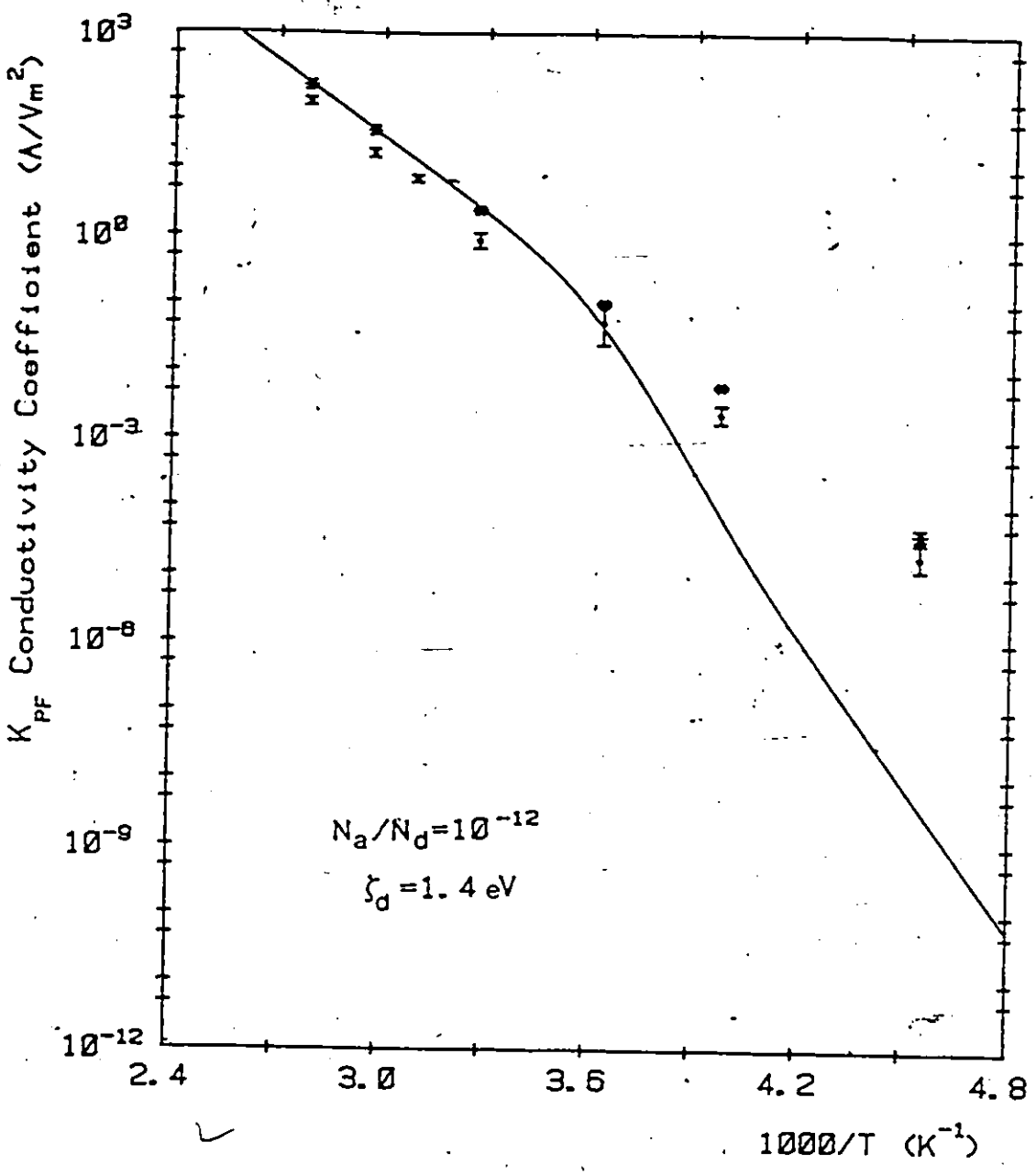

Although the ß-T curves for the hydrogen annealed samples, (Figure <41>, page 125) exhibited a change in slope suggestive of a change in compensation, no corresponding break in this curve is apparent. The solid line is the prediction based on the fitting parameters used in the ß-T plots.

when intermediately compensated donors are present. Instead K_{pf} must be rigorously defined as $\mu q/d$ times the value of n(T) extrapolated from the Poole Frenkel bias regime to zero bias, denoted $n_{ex}(T)$. Under either of the uncompensated or partially compensated conditions, $n_o(T)$ is equal to $n_{ex}(T)$. Under partly partially compensated conditions, however, they are not. To find $n_{ex}(T)$, values of equation <107> must be calculated for a series of voltages with ζ_d replaced with $\zeta_{do} - \Delta\zeta_d$. Recall that the magnitude of the one dimensional Poole Frenkel barrier lowering, $\Delta\zeta_d$, is related to the applied bias via equation <84> found on page 62, and repeated here for convenience:

$$\Delta\zeta_d = \sqrt{\frac{q^3 V}{\pi\varepsilon\varepsilon_o d}} \qquad \text{<84>}$$

Note that values of ε, d and ζ_{do} must be assumed. The values used and the rationale behind their choice will be discussed shortly. Also note that this equation is not valid for very low electric field strengths where a full three dimensional approach is necessary. These effects, which only add a low field ohmic portion to the curves have been omitted to highlight the effect under study. Figure <46> gives a plot of the calculated carrier density as a function applied voltage. For conditions corresponding to the temperature range where the activation energy of carrier density exhibits a transition between $\gamma = 1$ and $\gamma = 2$ conditions, ln(n) vs $\sqrt{V}$ has two approximately straight segments with slopes differing by approximately a factor of two.

Figure <46> Voltage Dependence Of Carrier Density

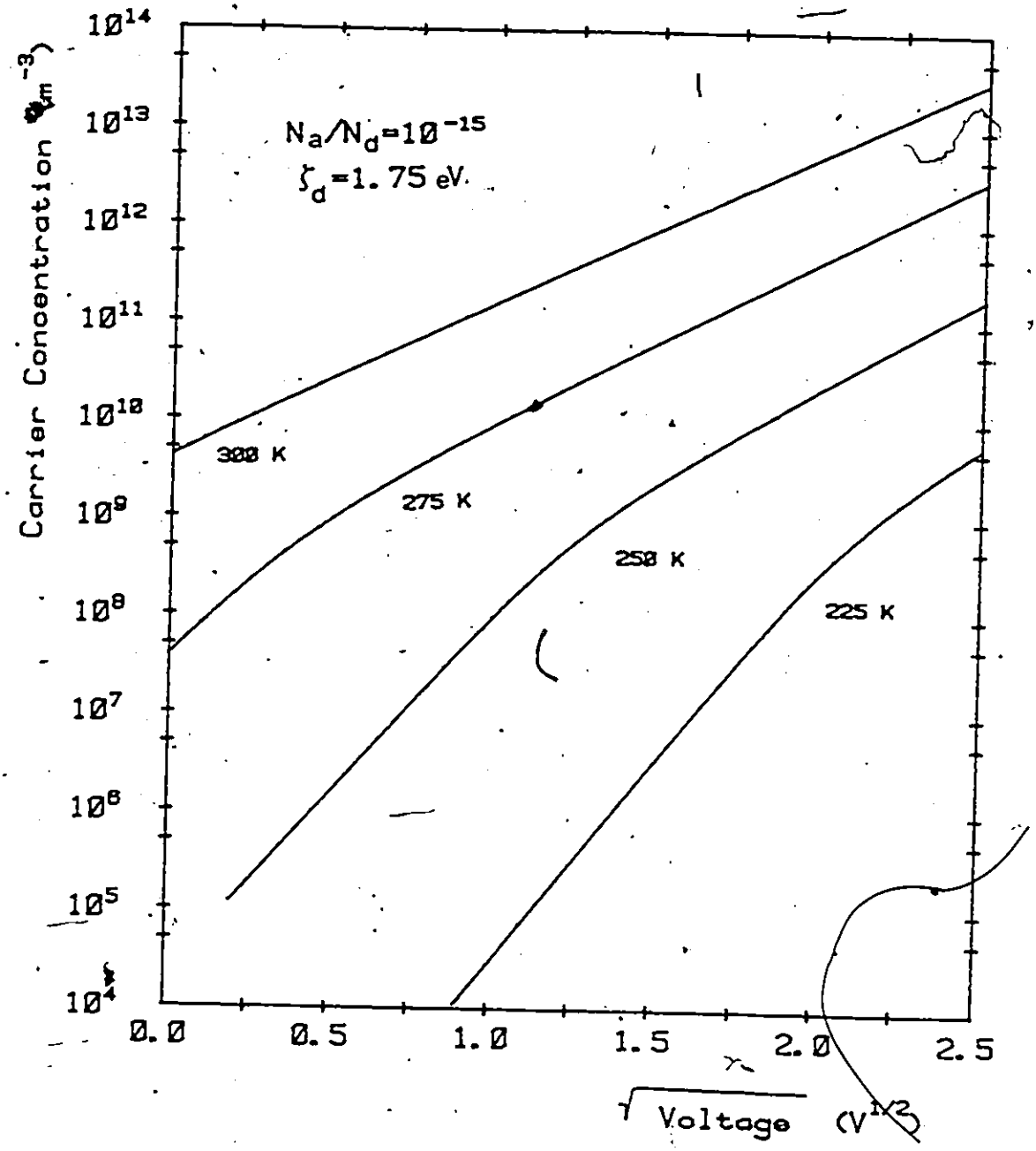

Carrier density, as described by equation <107>, page 72, is plotted against $\sqrt{\text{voltage}}$ for a range of temperatures. The donor energy was chosen to 1.75 eV. The N_a to N_d ratio was 10^{-15}. Note there are two nearly straight portions, corresponding to the two linear portions on the Poole Frenkel plots of J-V-T (Figures <35-37>, following page 122).

These curves are strongly reminiscent of the J-V-T plots of Figures <35-37> in the region where the one dimensional Poole Frenkel conduction formula is expected to hold. This also implies that for intermediately compensated conditions $n_{ox}(T)$ (and thus the true K_{pf}) is larger than $n_o(T)$ (and the incorrect K_{pf} that may be calculated from it).

The effect can be easily explained under the model of the intermediately compensated donor. As the electric field increases, and the donor levels begin to empty, the degree of compensation decreases, and thus the slope of a ln(n) vs $\sqrt{V}$ curve must decrease from a value corresponding to $\gamma = 1$ to one appropriate to $\gamma = 2$. Evidently, γ which relates the slope of the ln(n) (or ln(J/V)) vs $\sqrt{V}$ curve to the physical properties of the oxide and was previously thought to be constant for a given device, is not only temperature dependent, but also bias dependent! When the predicted K_{pf} is calculated using the $n_{ox}(T)$ extrapolated from the same bias region as that over which the experimental Poole Frenkel coefficients were calculated, good agreement between theory and experiment is achieved for the unheated and vacuum baked samples. The fit to the hydrogen annealed data is significantly poorer. The values used are given in the captions, and are summarized in Table X at the end of this section, page 145.

In a similar fashion, the anomalous temperature dependence of β can be explained. Again, values of n(V,T) are generated for

specific values of $\overline{N_d}$, N_a, ζ_{do}, ϵ, and d. Since J/V is proportional to n, β is equal to the slope of a ln(n) vs $\sqrt{V}$ curve. Then γ can be calculated from its original definition: that is, γ equals the ratio of the constant,

$$\frac{1}{kT}\sqrt{\frac{q^3}{\epsilon\epsilon_o \pi d}}$$

to β. Because it is dimensionless, results of the calculation have wider application when expressed in terms of γ. Its temperature behavior is shown in Figure <47>. The transition spans a temperature range of approximately 200°C. For a limited range of approximately 50° within that span, the function is nearly linear. Because β changes so smoothly with temperature, activation energy plots will appear normal, but give completely erroneous results because the temperature dependence of γ was inadvertently included. It is no surprise that ζ_d calculated in this manner does not vary with voltage with the correct constant of proportionality. In a similar fashion, a β vs 1/T curve constructed for that region would be accidently linear with an anomalously high slope. β rises too rapidly at low temperatures because γ is also dropping. The solid curves shown on Figures <39-41> demonstrate that the model presented here not only fits the K_{pf} temperature dependence, but also the temperature dependence of β using the same fitting parameters. Also, an unambiguous value of ϵ which fits the entire temperature range may be calculated for the vacuum baked and unheated samples. This

Figure <47> Temperature Dependence of Compensation Index

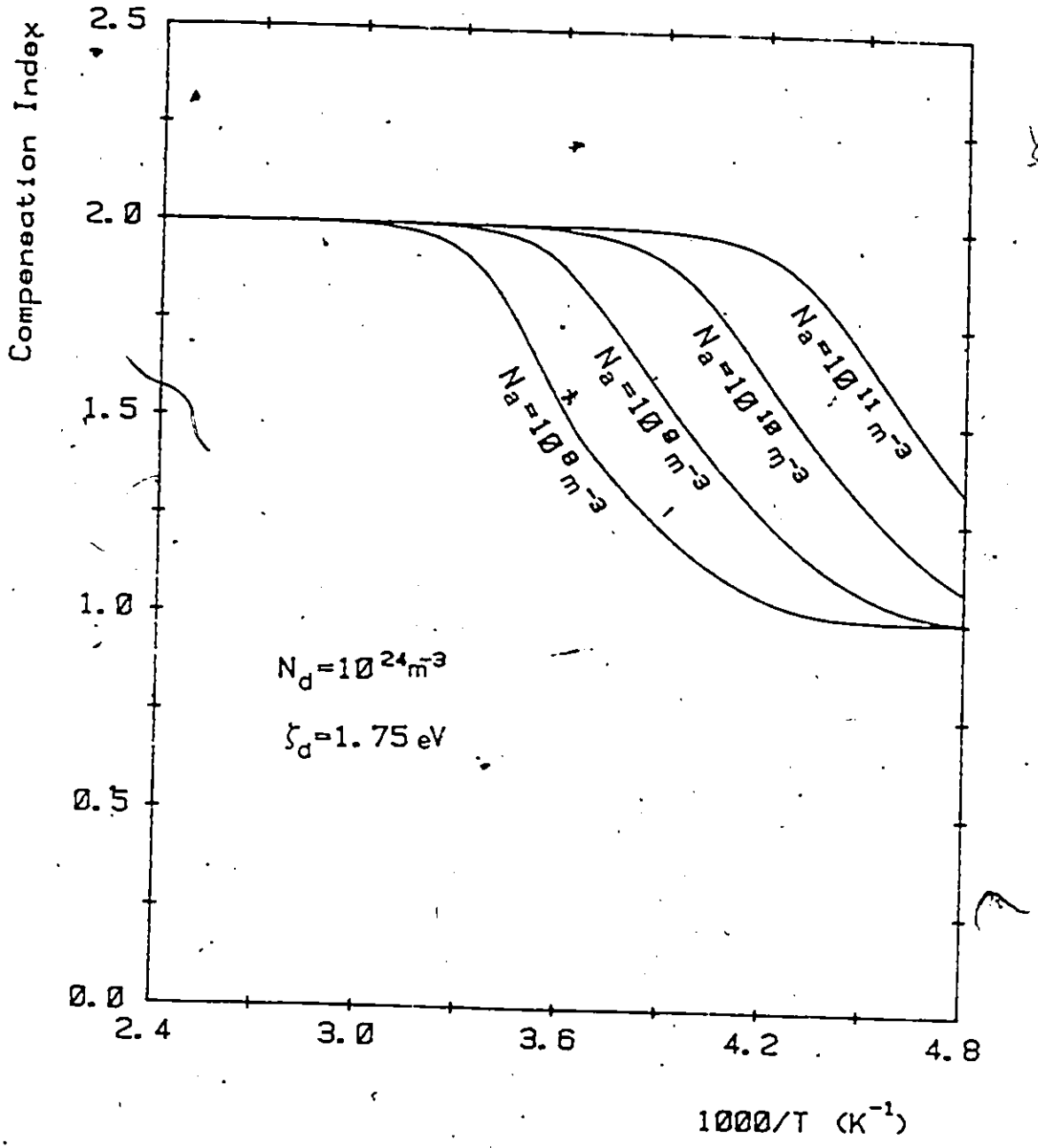

The effective compensation index can be calculated from equation <107>, page 72, for experimental bias conditions. Note that it varies smoothly over a range of 200°C from $\gamma = 1$ to $\gamma = 2$ conditions.

is 3.52 ± .07 (i.e. $\hat{n}$ = 1.87 ± .04) ← consistent with earlier optical measurements. See Table VII, page 114.

The shape of the β vs 1/T curves for the hydrogen annealed sample is similar to those of the unheated and vacuum baked samples even though corresponding break points in the K_{pf} vs 1/T and J/V vs $\sqrt{V}$ curves are not apparent. The anomalously low values of β indicate that either ϵ or d for these oxides are larger than what was determined in macroscopic optical measurements on unheated samples. Note that if d were assumed to be unchanged, then the ϵ that fits the observed β-T curves is 24 ± 5. This is equal to the static dielectric constant for Ta_2O_5 (157). Such agreement may be coincidental, or it may indicate that ionic Poole Frenkel conduction is taking place. Recall that for such a process Poole Frenkel like J(V) behavior is observed except that β then depends on the static dielectric constant (159-161). There is not enough data to decide what conduction process is most appropriate for these oxides.

The numerical values for the other parameters in equation <107> are arrived at in the following fashion:

1) Donor depth: The steepness of the ln(K_{pf}) vs 1/T plots and the width of the transition in the β vs 1/T curves is a strong function of ζ_{do}, so that this value can be estimated without knowledge of N_a or N_d. An interactive fitting program was written to allow user directed variations in ζ_{do} (and all other

fitting parameters) and comparison of the sum of the residual errors between predictions and theory. Convergence to a satisfactory fit could be rapid with careful choice of seed values. The value attained in this manner for ζ_{do} for both the vacuum baked and unheated samples is 1.75 ± .05 eV, and 1.40 ± .05 eV for the hydrogen annealed sample. An independent estimate of ζ_{do} is readily attained from the temperature dependence of the low field ohmic region. In light of the model proposed here, it is apparent that over the temperatures used to calculate the ohmic region's activation energy, $\gamma \cong 2$. Therefore the energy depth of the level responsible for the ohmic conduction is 2x.86 eV = 1.72 ±.08 eV. for the vacuum baked and unheated samples and 1.4 ±.1 eV for the hydrogen annealed samples. The shallow level has been observed in Ta_2O_5 films by other researchers (69,237), but the deeper one is new. It is believed that the optimization process employed by this laboratory to produce tantalum pentoxide with larger than normal conductivity levels may have enhanced a naturally occurring, but usually low density level, or has introduced a new, impurity related level.

2) Donor to acceptor density ratio: The temperature of the transition point between the two straight line portions of the n(T) and therefore the $K_{pf}(T)$ curves is a strong function of N_d/N_a. The value of N_d merely shifts the n curves vertically on such a plot. Once the transition temperature is identified, the

ratio is read off a graph such as Figure <48>, generated for a specific ζ_{do}.

3) Donor density: The value used is arbitrary. However, other researchers have applied a wide variety of analysis techniques to anodic Ta_2O_5 and have independently arrived at a doping concentration of $10^{24} m^{-3}$ even though the films differed in preparation, and conductivity behavior (51, 58, 59, 110, 137). This value may be universal for this material, for much the same reasons that amorphous semiconductors were thought to be intrinsically undopable (238). Impurities are simply tied up somewhere in the loose atomic structure where they are not electrically active.

4) Electron mobility: From the $K_{pf}(T)$ plots an estimate of electron mobility may be made (in the vacuum baked and unheated samples only, since the values of d and ϵ are in question for the hydrogen annealed samples). The values calculated, which depend on the exact value of N_d, are on the order of $10^{-1} m^2/Vs$ for all reasonable estimates (see Table X). They are fully consistent with electron propagation in the conduction band, and are in agreement with the results of Thomas (59).

The success of the model permits an interpretation of the observed J-V behavior in terms of impurities and their probable sources. To begin with, conduction in these films is now assured to be a bulk phenomenon. The sources of conduction electrons are

Figure <48> Dependence of the Compensation Index on Acceptor Density

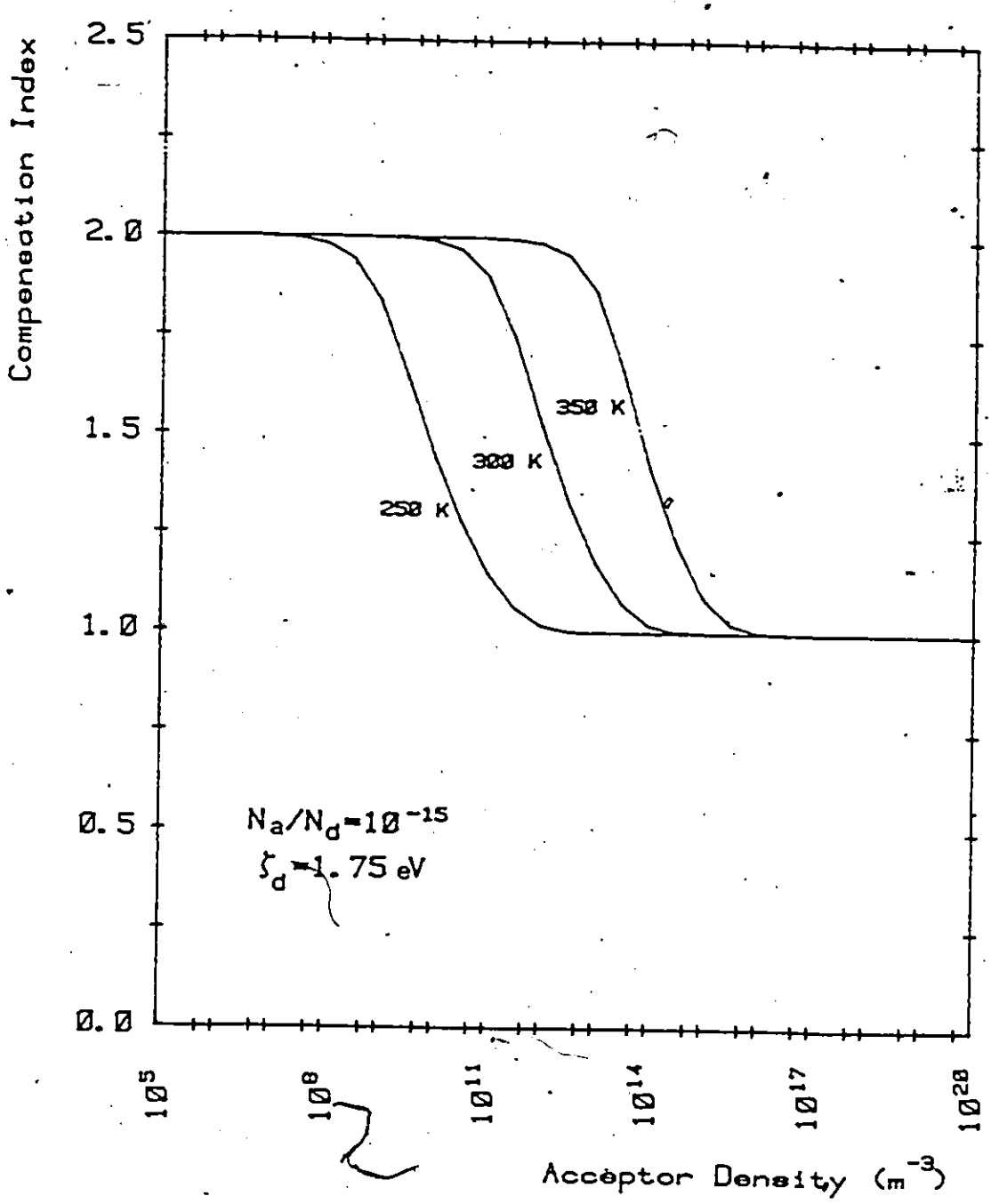

This graph recasts the data presented in figure <42>, after page 134 and <47> after page 139 to show the abrupt drop in γ at a fixed temperature as acceptor density is increased. This feature facilitates the accurate determination of the donor to acceptor density ratio.

partially ionized donors distributed throughout the oxide having an energy depth of 1.75 eV in unheated and vacuum baked samples. Conduction electrons (or ions) which dominate the hydrogen annealed samples have a different activation energy of 1.4 eV. This work has shown that under certain conditions compensating acceptors are also present. The identity of these donors and acceptors may be surmised by correlating the observed changes in the compensation index, γ, with the physical mechanisms by which the different process conditions change conductivity. Consider the undoped, unheated oxide. It exhibits a compensation index of around 1.5, and an intermediate conductivity coefficient, K_{pf}. After vacuum baking this oxide, γ rises to 2, corresponding to uncompensated Poole Frenkel conditions, and K_{pf} increases by an order of magnitude. Both observations may imply the loss of acceptors. It is proposed that the acceptor driven off in vacuum baking is water (or -OH), a well known impurity in anodic oxides formed in aqueous solutions. It was mentioned in the introduction that Krembs, working with tritiated water, estimated a density of $10^{24} m^{-3}$ H atoms in anodized Ta_2O_5 (16), so there can be no doubt that this impurity is important.

Consider the unheated oxide once more. Now add nitrogen by reactively sputtering the parent tantalum. K_{pf} drops dramatically and γ falls to 1, corresponding to "complete" partial compensation. This can be accomplished by the addition of more acceptors, or the loss of donors. The expression of charge

neutrality makes both views equivalent. Nitrogen fits this role well. It may be introducing another acceptor in additon to water. However another hypothesis could be that the primary donor in Ta_2O_5 is an oxygen vacancy. As nitrogen replaces oxygen atoms in atomic arrangements that would normally lead to the creation of donors, the extra electrons become bound to the nitrogen instead of being excited to the conduction band. This would explain the drop in K_{pf} - there are fewer donors - and in γ - the ratio of acceptor density to donor density rises. The changes observed in the hydrogen annealed samples point to large increases in the dielectric constant and/or oxide thickness, and a substantial increase in the carrier concentration. The reducing atmosphere used would increase the number of donors if these were oxygen vacancies (but the donors at 1.75 eV and 1.40 eV could not both be simple oxygen vacancies), or could be introducing hydrogen as an ionic charge carrier.

Table X - Summary of Poole Frenkel Analysis

Parameter	Oxide Type		
	Unheated	Vacuum Baked	Hydrogen Annealed
ζ_d (eV) [1]	1.75±.05	1.75±.05	1.4 ±.1
[2]	1.72±.03	1.72±.02	1.41±.08
$\varepsilon = n^2$ [3]	3.61±.07	-	-
[4]	3.58±.03	3.47±.03	(24 ± 5)
d (nm) [3]	54.9±.5	-	-
N_a/N_d [5]	3×10^{-15}	1×10^{-15}	3×10^{-12}
N_d^+/N_a [6]	2.1	5.1	1.9
γ_{280K} [7]	1.5±.1	1.84±.09	(1.1±.3)
$\mu(m^2/Vs)$ [6] [8]	.16	.23	.17

Notes:

$N_c = 10^{25} m^{-3}$ at 300 K with $T^{3/2}$ dependence is assumed

[1] calculated from the slope of K-T data (Figures<43-45>)

[2] calculated from σ_o-T data (Figure <32>)

[3] measured by ellipsometry

[4] calculated form slope of β-T data, γ=2 (Figures <39-41>)

[5] parameter for best fit to K-T and β-T (Figures <39-41>&<43-45>) (error in $\log(N_a/N_d)$ is estimated to be ±.5)

[6] inferred from fitting parameters, for 300 K and zero bias

[7] calculated from anodic β and ε and d given above

[8] assuming $N_d = 10^{24} m^{-3}$, error in log(μ) is estimated to be ±.5

3. SPATIALLY NON-UNIFORM DONORS:

The preceding analysis is all for nought, if there is no explanation how a supposedly bulk conduction mechanism can be asymmetric: which β does one use to fit the $\gamma(T)$ curves, and which K_{pf} for the $n(T)$? In this section, an explanation, preserving the main tenets of Poole Frenkel conduction theory, is drawn from the J-V-T experiment and observations made by various researchers who have studied the physical and electrical properties of anodic Ta_2O_5. The first task, however is to review what is known empirically about the asymmetry. Then the existing explanations will be explored, and their predictions compared to the data. And finally, a model which passes the test will be presented.

The term "asymmetry" needs a more precise definition than what has been used thus far. One figure of merit is the so called rectification ratio, defined to be the ratio of current observed for a set "forward" voltage to that observed for that voltage applied in the "reverse" direction. In common practise, when the rectification ratio is between 1 and 10, the J-V behavior has been deemed to be symmetric. The films under study in this study might also qualify under that criterion: the rectification ratios observed are approximately 4 for the unheated samples, approximately 3 for the vacuum baked samples, and less than 2 for

the hydrogen annealed samples. In all three, the cathodic (i.e. tantalum negative bias) currents are greater than their anodic (tantalum positive bias) counterparts.

The next observation is that the rectification ratio is nearly constant throughout the Poole Frenkel regime - that is, a Poole Frenkel plot such as Figure <27>, which is found after page 116, shows the curves for each polarity become parallel at higher voltages. Figures <19>, following page 100, substantiates the observation over a wider range of voltage. Thus the major difference between polarities is in K_{pf}, not β. Figures <43-45>, found after page 135, of K_{pf} as a function of temperature show that the rectification ratio (as seen as the ratio of K(cathodic) to the K(anodic)) is also independent of temperature. This leads us to conclude that asymmetry cannot be due to a bias dependent activation energy; such a situation might arise if the potential wells around the donors showed a preferentially oriented distortion.

A corollary to the preceding observation is that β tends to be the same for each polarity. As mentioned before, this is only approximately true. Differences of up to 10% have been observed, with the anodic β being greater than the cathodic one (whereas the currents show the opposite trend). The large differences seen by Pulfrey, Wilcox and Young (13), a factor of two, is likely a manifestation of the Schottky to Poole Frenkel transition in the cathodic polarity. The variation of β with T, shown in Figures

<39-41>, after page 125, show that in the case of a difference, the difference is greater at lower temperatures. It could be that the transition from $\gamma = 1$ to $\gamma = 2$ takes place at a lower temperature for the cathodic polarity. Unfortunately, there is no data to confirm that the β's reconverge at even lower temperatures.

Another observation: Even though the activation energies calculated in the experimental section cannot be directly related to the donor ionization energy, because the temperature dependence of γ was unavoidably included in the calculation, its voltage dependence shown previously in Figure <38> after page 123, is representative. It is clear that the observed activation energy for a given cathodic voltage is less than that for the same size anodic voltage. The difference between the values is greater for the unheated samples than for the vacuum baked samples, whereas it is almost zero for the most highly symmetric hydrogen annealed samples. The first two sample types, which differ in rectification ratio, none the less have the same slope relating the square root of voltage to decrease in activation energy. Thus, any mechanism proposed to explain the asymmetry must not alter the voltage dependence of activation energy except for an offset in the square root of voltage.

Previous Models for Asymmetry:

The predominant explanation used by other workers for asymmetry is the internal field resulting from metal work function differences (86, 209, 239). However, as discussed with the J-V-T experiment results, the fact that the ohmic component is non-rectifying, or slightly rectifying in the opposite sense to that seen in the Poole Frenkel regime clearly discounts this approach. A variation on the model could be that the internal fields arise only in the non-ohmic regime as a consequence of polarization or ionic drift. Ionic drift would be irreversible, and could be detected by comparison of J-V characteristics of devices with different biasing histories. This comparison has been made and no evidence of ionic drift was detected. Polarization on the other hand, is reversible for small voltages. It is field dependent, which would explain its appearance only at high fields. A polarity dependence, however is difficult to justify.

In any case, the simple addition or subtraction of a voltage due to an internal field of any origin would fail to eliminate the apparent asymmetry for all current levels; the rectification ratio could not be constant at all currents as observed. Similarily, the activation energy plots versus the square root of voltage would be distorted by the addition of an internal field, not brought into coincidence.

To summarize: there is evidence that asymmetry is not due

to a simple internal field, arising from metal work function differences nor to ionic drift, nor from intrinsically distorted potential wells giving polarity dependent activation energies. Because the Poole Frenkel plots and the ζ_a vs $\sqrt{V}$ are linear, the possible causes of asymmetry are limited to mechanisms which do not distort these relationships. The following proposal meets the criterion by applying the Poole Frenkel effect itself to a spatially non-unuiform distribution of donors.

Consider the effect of Poole Frenkel barrier lowering on the non-uniform distribution of donors diagrammed in Figure <49>. The donors are concentrated in the upper half of the anodic oxide adjacent to the chromium top metallization. As the field strength increases, the Fermi energy rises to maintain equilibrium. However, because there are more donors in the upper half of the oxide, the Fermi level moves further upwards in that half. The result is that the original electric field has been augmented by an internal field whose magnitude increases with the number of electrons added to the conduction band by Poole Frenkel barrier lowering.

A crude analysis is now offered to estimate the size of the effect proposed. It is necessary to solve Poisson's equation for a representative donor distribution. To start then:

$$\psi'' = \frac{-\rho}{\varepsilon\varepsilon_o} \qquad \text{<133>}$$

where for uncompensated donors we have

$$\rho = q\sqrt{\frac{N_d(x)N_c}{2}}\cdot\exp\left[\frac{-q\,\zeta_d}{2kT}\right]\exp\left[\frac{1}{2kT}\sqrt{\frac{q^3\,\xi}{\pi\varepsilon\varepsilon_o}}\right] \qquad \text{<103'>}$$

Figure <49> Energy Band Diagram with Spatially Nonuniform Donors

Consider a Ta-Ta_2O_5-Cr device containing donors predominantly in the upper half of the insulator adjacent to the chromium.

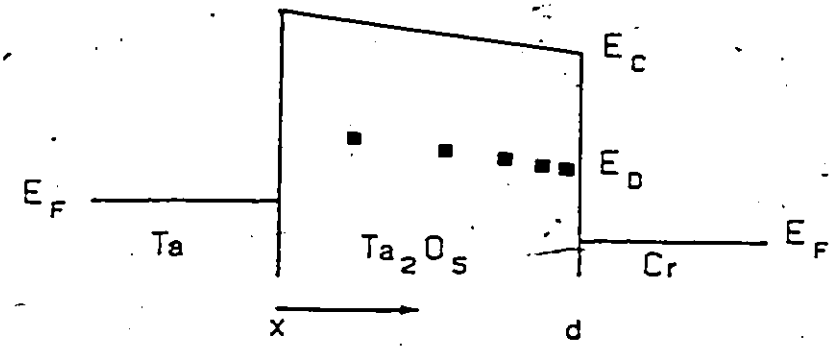

At low bias, while the donors remained filled, there is no internal field. Nonpolar ohmic behavior would be observed.

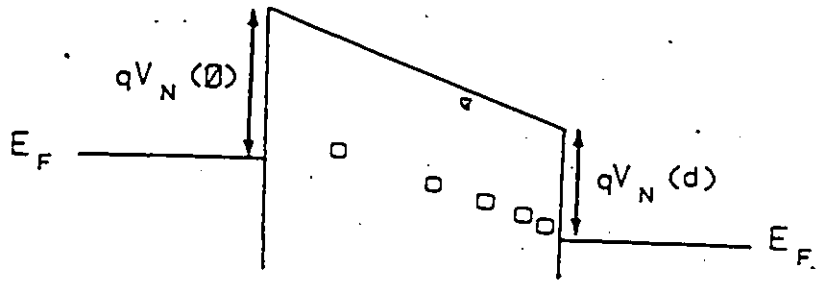

Under sufficiently high cathodic bias, the charging of the donors causes E_F to rise, but more so at $x = d$ than at $x = 0$. Therefore a potential $V_{in} = V_n(0) - V_n(d)$ is created.

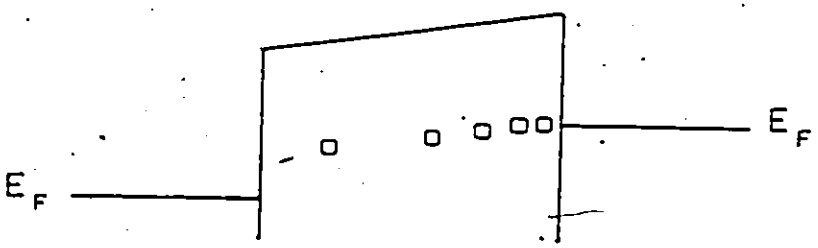

Under anodic bias, however, the same mechanism works against the applied field and leads to a lower current flow.

For brevity, write

$$n = n_o(x)\ \exp\left[\frac{a\sqrt{\xi}}{kT}\right] \qquad \text{<134>}$$

Furthermore, let $n_o(x) = 0$ for $0 < x < m$ - Region I

and N_o for $m < x < d$ - Region II

Therefore in Region I we have

$$\psi_I'' = 0 \qquad \text{<135>}$$

$$\psi_I' = c_1 \qquad \text{<136>}$$

$$\psi_I = c_1 x + c_2 \qquad \text{<137>}$$

In Region II, we can write

$$\psi_{II}'' = -\frac{q N_o}{\varepsilon\varepsilon_o} \exp\left[\frac{a\sqrt{\xi}}{kT}\right] \qquad \text{<138>}$$

To first order, let $\xi(x)$ be nearly constant. This will be true in the case of small donor densities, and will be justified more generally by numerical analysis given later. Thus

$$\psi_{II}' = -\frac{q N_o}{\varepsilon\varepsilon_o}\left[\exp\left[\frac{a\sqrt{\xi}}{kT}\right]\right]x + b_1 \qquad \text{<139>}$$

$$\psi_{II} = -\frac{q N_o}{2\varepsilon\varepsilon_o}\left[\exp\left[\frac{a\sqrt{\xi}}{kT}\right]\right]x^2 + b_1 x + b_2 \qquad \text{<140>}$$

The boundary conditions are such that

1) $\psi_I(0) = 0$, which sets $c_2 = 0$

2) $\psi_{II}(d) = -(V+V_{in})$, which fixes b_2 which respect to b_1

3) $\psi_I'(m) = \psi_{II}'(m)$, which sets c_1 in terms of b_1

4) $\psi_I'(m) = \psi_{II}'(m)$, which sets c_1 with respect to b_1 and b_2.

The final solutions are given as:

$$\psi_I = -\left[\frac{V+V_{in}}{d}\right]x - \frac{q\,N_o}{\varepsilon\varepsilon_o}\exp\left[\frac{\alpha}{kT}\sqrt{\xi}\right]\left[m - \frac{(d^2+m^2)}{2d}\right]x \qquad \langle 141\rangle$$

$$\psi_{II} = -\left[\frac{V+V_{in}}{d}\right]x - \frac{q\,N_o}{2\varepsilon\varepsilon_o}\exp\left[\frac{\alpha}{kT}\sqrt{\xi}\right]\left[x^2 - \frac{(d^2+m^2)}{d}x + m^2\right] \qquad \langle 142\rangle$$

$$\psi_I' = -\left[\frac{V+V_{in}}{d}\right] - \frac{q\,N_o}{\varepsilon\varepsilon_o}\exp\left[\frac{\alpha}{kT}\sqrt{\xi}\right]\left[m - \frac{(d^2+m^2)}{2d}\right] \qquad \langle 143\rangle$$

$$\psi_{II}' = -\left[\frac{V+V_{in}}{d}\right] - \frac{q\,N_o}{\varepsilon\varepsilon_o}\exp\left[\frac{\alpha}{kT}\sqrt{\xi}\right]\left[x - \frac{(d^2+m^2)}{2d}\right] \qquad \langle 144\rangle$$

In both regions, the electric field which is equal to $-\psi'$, is almost constant, being equal to the parallel plate value $(V+V_{in})/d$, and a correction term. If we let $N_d = 10^{24}/m^3$, $N_c = 10^{25}/m^3$, $N_a = 10^9\ /m^3$, and $\zeta_d = 1.75$ eV, the correction term can be calculated for a typical Ta_2O_5 device at 10 V bias to be 10^9 times smaller than the constant term. Thus it is well justified to take ξ constant. The step function chosen here for the donor distribution is an extreme. For smoother $n_o(x)$ distributions, the correction term will be even smaller.

The final step is to show how this result can lead to asymmetry. The result

$$\xi = \frac{\Delta V}{d} \qquad \langle 145\rangle$$

does not appear to offer any improvement over the "internal field" solution proposed by other researchers. Those models were

unable to explain the coexsistence of non-rectifying ohmic and asymmetric Poole Frenkel conduction regimes. Progress can be made, however, by examining the voltage dependence of V_{in}

By definition:

$$n = N_c \exp\left[\frac{E - E_c}{kT}\right] = N_c \exp\left[\frac{-q\ V_n(x)}{kT}\right] \qquad \langle 146 \rangle$$

$$V_{in} = V_n(d) - V_n(0) = \frac{kT}{q} \ln\left[\frac{n(d)}{n(0)}\right] \qquad \langle 147 \rangle$$

Thus V_{in} depends on the doping density at the end points only.

To calculate the magnitude of V_{in}, we cannot use the simple distribution used in the first example because $n(0)=0$ has certain unpleasant consequences in a logarithmic expression. It is also unphysical. If nothing else there is the intrinsic carrier concentration due to thermal excitation across the gap. Only in the purest semiconductor crystals are intrinsic conditions attained. Therefore it is probable in amorphous Ta_2O_5 that there are other sources of carriers with a total density of n_i. Let us assume that they are traps which do not experience Poole Frenkel barrier lowering. Therefore $n(x)$ has the form

$$\begin{aligned} n(x) &= n_i && \text{for } 0 < x < m \\ &\cong n_i + n_o \exp\left[\frac{a\sqrt{\xi}}{kT}\right] && \text{for } m < x < d \end{aligned} \qquad \langle 148 \rangle$$

Thus

$$V_{in} = \frac{kT}{q} \ln\left[\frac{n_i + n_o}{n_i} \exp\left[\frac{a\sqrt{\xi}}{kT}\right]\right] \qquad \langle 149 \rangle$$

for all biases wherein the one dimensional Poole Frenkel formula

is valid , and at very high bias

$$V_{in} \approx \frac{kT}{q} \ln\left[\frac{n_o}{n_i}\right] + \frac{a}{q}\sqrt{\xi} \qquad \langle 150 \rangle$$

Since no zero bias current leakage due to n_i in excess of what the Onsager model predicts for low bias Poole Frenkel behavior was observed, the upper limit on n_o/n_i can be estimated to be 0.1. This implies that at this limit V_{in} at zero bias is .002 V, and thus would not be observable. At a higher voltage, say 5 V, these same numbers give $V_{in} = .20$ V. Thus the difference in electric field for the forward and reverse directions is 8%. Continuing to use representative values for the Poole Frenkel coefficients, a rectification ratio of 1.5 is calculated, in good agreement with observation. Because V_{in} increases with bias, the rectification ratio is nearly constant, as observed. The model also predicts the observation of a slightly larger anodic β, because the relative magnitudes of V to V_{in} increases slowly at high bias.

The calculations just described are approximate, because there is a finite coupling between V_{in} and ξ. V_{in} depends on the number of carriers, which depends on the electric field, which depends on V_{in}. In addition, we used the assumption that ξ was constant, to prove ξ was constant in the preliminary example. An exact numerical analysis was performed to verify these results. The technique, known as a finite difference method, is in wide spread use in semiconductor device modelling (240). A potential

distribution is calculated by an iterative procedure which proceeds from an approximate solution to an arbitrarily exact solution of Poisson's equation for potential. The first step is to divide the device into a finite number of segments. The potential at each point is written as a function of the conditions at adjacent points. For example, to find the local carrier density from a given emission enhancement formula such as the Onsager equation <93b>, found on page 65, the electric field is estimated to be the difference in potential between the two adjacent points, divided by twice the mesh spacing. M such expressions are written out, where M is the total number of interior mesh points. A Taylor expansion is then employed to write each equation in terms of the most recent estimate of the potential at that point, plus a small error term in the potential. The expressions used in this thesis are necessarily different than those used for diodes, transistors, and the like, which are published in the literature and form the foundation of such modelling programs as MINIMOS, and SPICE (241). Because Poole Frenkel barrier lowering links carrier density to the derivative of potential, and not potential itself as in diodes, new finite difference expressions were needed. These are given in Appendix I. The M linear equations for the M error terms are solved simultaneously by a Gauss-Seidel algorithm, executed on an Apple IIe. For each iteration, the new potential estimate is calculated from the sum of the previous one, and the error terms.

PART IV - DISCUSSION

Convergence for a mesh spacing of 1 nm, and a tolerance in the potential of .01% was fast; usually within 5 passes. An outline of the algorithm is also given in Appendix I.

The results of these exact calculations are given in Figure <50>. It is clear that the asymmetry is of the correct magnitude and varies with bias in the expected manner.

The implications of this model to the interpretation of the J-V-T behavior of the three types of samples are these: The donors responsible for conduction in the case of the unheated samples are more predominantly located in the upper portions of the oxide than in the vacuum baked samples; whereas the hydrogen annealed samples conduct by virtue of a different donor uniformly distributed throughout the oxide. It has already been suggested that there is sufficient justification for proposing nonuniform distribution of impurities in the anodic oxides. While asymmetry has been reported even when care is taken to exclude electrolyte incorporation, the knowledge that anodization proceeds from the center, leaving a demarcation that is detected by TEM and ellipsometric techniques, leaves open to doubt that anodic films are ever homogeneous. The work presented here is the first self consistent model to explain how such a distribution affects J-V-T behavior.

Figure <50> Calculated J-V Plots for Nonuniform Donor Distribution

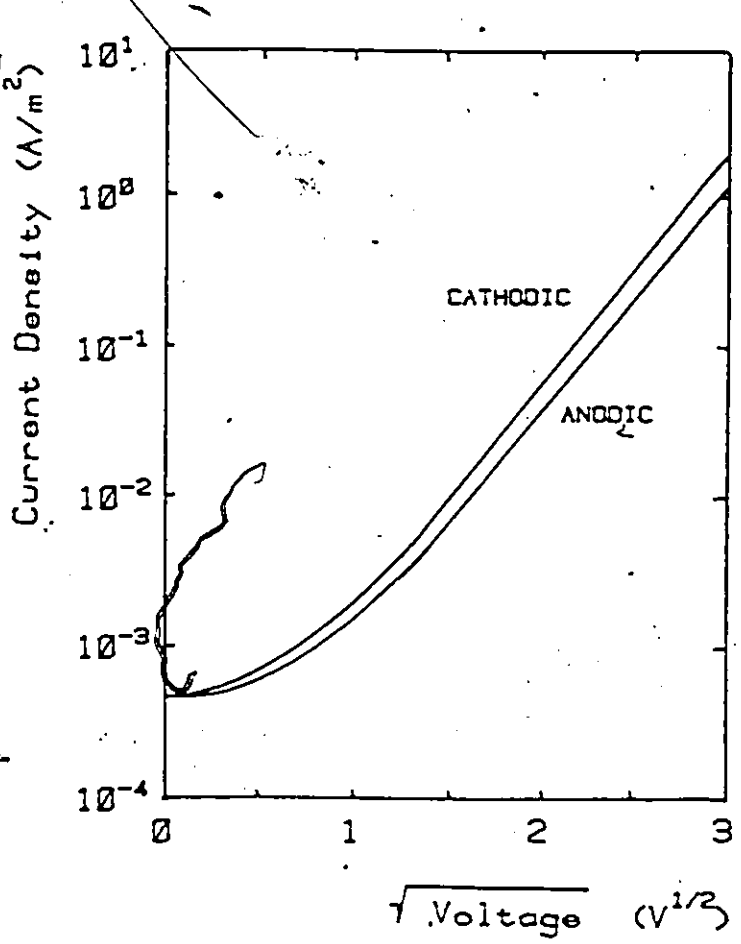

Results of numerical calculations using the alogrithm outlined in the appendix. are shown here. For a ratio of n_i/n_o of 10, and a β of 3.45, J-V behavior is predicted that shows nonpolar ohmic behavior near zero bias, and asymmetric Poole Frenkel behavior for larger bias. The rectification ratio ia nearly constant in this latter region, with a value of 1.4.

4. CONCLUSIONS:

The nonlinear conductivity exhibited by anodic oxides of tantalum and tantalum nitride has been explained in terms of an extended Poole Frenkel conduction model. Evaluation of the current density for electric fields up to 10^8 V/m as a function of the physical properties of the films under investigation has verified the predictions of the theory. Specifically, the following predicted relationships were confirmed:

J-V as a function of device area (4 μm^2 to > 1000 μm^2)

J-V as a function of device thickness (40 nm to 65 nm)

J-V as a function of dielectric function (2.99 to 3.61)

In the process of confirming Poole Frenkel conduction theory, the five main alternative conduction models, space charge limited conduction, polaron and variable range hopping conduction, and the punch through and imperfect insulator Schottky barrier models, were conclusively ruled out.

The J-V behavior for temperatures between -55°C and 145°C, wherein conductivity varied by over eight orders of magnitude, was also fitted to a new extended Poole Frenkel model. The J-V-T behavior, which would appear to be anomalous under the pre-existing Poole Frenkel theories, has been shown by the analysis presented here to be due to an intermediately compensated donor density. This analysis was also able to explain the appearance of a second Poole Frenkel region occurring at low

bias levels. Both effects are related to the change in compensation as temperature is raised, or donors are ionized by increasing electric fields. Similar unexplained J-V-T anomalies have been reported in the literature.

The often observed asymmetry in anodic film devices such as the ones studied in this work was shown to be due to a spatially non-uniform distribution of the dominant Poole Frenkel donors. Numerical analysis has quantified this effect, in good agreement with observation. This explanation is significantly better than previous attempts in that the predicted rectification ratio is only slightly dependent on current, as observed; activation energy plots are not distorted; and non-rectifying ohmic components at low field levels are permitted.

The extended theory has permitted the interpretation of the J-V behavior of anodic oxides processed under a variety of conditions. Nitrogen doping of the parent tantalum film has been shown to increase compensation by either introducing acceptors or reducing the donor density. Vacuum baking appears to remove an acceptor, probably due to water. Hydrogen annealing generates a shallow donor (1.4 eV) in sufficient numbers to dominate the deeper one (1.75 eV) seen in the unheated and vacuum baked films. Both heat treatments smooth out the spatial distribution of the donors, although some nonuniformity remains after vacuum baking.

APPENDIX

Appendix I: The Finite Difference Algorithm for Nonuniform Distribution of Poole Frenkel Donors

Consider an insulator with two impurity levels:

1) a trap like level, evenly distributed with a density of n_i, that does not experience Poole Frenkel barrier lowering.

2) a donor level, located in the outer section of the insulator with a density of n_o at zero bias.

If all other sources of carriers are assumed to be much smaller than these two, Poisson's equation may be solved approximately as follows:

given: $n = n_i$ for $0 < x < m$ <151>

$$n = n_i + n_o \exp\left(\frac{\alpha\sqrt{\xi}}{kT}\right) \quad \text{for } m < x < d \qquad \text{<152>}$$

where α is a constant defined in equation <84>, page 62

ξ is the electric field

then for $0 < x < m$

$$\psi_I'' = \frac{-q}{\varepsilon\varepsilon_o} n_i \qquad \text{<153>}$$

$$\psi_I' = -\left(\frac{V_{in} + V}{d}\right) + \frac{q}{2\varepsilon\varepsilon_o}\left(n_i(d-2x) + n_o \exp\left(\frac{\alpha\sqrt{\xi}}{kT}\right)\left(d - \frac{m^2}{d} - 2m\right)\right) \qquad \text{<154>}$$

$$\psi_I = -\left(\frac{V_{in} + V}{d}\right)x + \frac{q}{2\varepsilon\varepsilon_o}\left(n_i(xd-x^2) + n_o \exp\left(\frac{\alpha\sqrt{\xi}}{kT}\right)\left(d - \frac{m^2}{d} - 2m\right)x\right) \qquad \text{<155>}$$

Similarly for $m < x < d$

$$\psi''_{II} = \frac{-q}{\varepsilon\varepsilon_o}\left[n_i + n_o \exp\left[\frac{\alpha\sqrt{\xi}}{kT}\right]\right] \quad \langle 156 \rangle$$

$$\psi'_{II} = -\left(\frac{V_{in} + V}{d}\right) + \frac{q}{2\varepsilon\varepsilon_o}\left[n_i(d-2x) + n_o \exp\left[\frac{\alpha\sqrt{\xi}}{kT}\right](d - \frac{m}{d}^2 - 2x)\right] \quad \langle 157 \rangle$$

$$\psi_{II} = -\left(\frac{V_{in} + V}{d}\right)x + \frac{q}{2\varepsilon\varepsilon_o}\left[n_i(dx - x^2) + n_o \exp\left[\frac{\alpha\sqrt{\xi}}{kT}\right](d - \frac{m}{d}^2 - x)x\right] \quad \langle 158 \rangle$$

These results are approximate; to arrive at analytical solutions, ξ was assumed to be nearly constant in the integration steps, when, in fact, the above results demonstrate that $\xi = -\psi'$ does have a small x dependence. This x dependence represents a small error term which can be evaluated by a finite difference algorithm. The central premise of such a technique is that the carrier concentration at any given point in the device is specified by the local potential distribution. i.e.

$$n_{II}(x) = n_i + n_o \exp\left[\frac{\alpha\sqrt{\xi(x)}}{kT}\right]$$

$$= n_i + n_o \exp\left(\frac{\alpha}{kT}\frac{\sqrt{\psi'_{II}(x-\delta x) - \psi'_{II}(x+\delta x)}}{2\delta x}\right) \quad \langle 159 \rangle$$

in the limit $\delta x \to 0$

APPENDIX

Using the approximate Ψ', given in equations <154> and <157>, we may replace equation <152> with the more accurate equation <159> for the carrier distribution. This may lead in turn to a more accurate expression for $\psi(x)$, but this step can no longer be done analytically.

To show how $\psi(x)$ is obtained from the modified $n(x)$ distribution, it is usually convenient to change notation at this point. For simplicity, it is customary to divide the device into M+2 segments, and then specify the potential at each of the M interior mesh points. In this example the mesh points are equally spaced, with a separation h, but this need not be so in every case. Thus for an arbitary point N:

$$\Psi''(N) = \frac{\Psi'(N^+)-\Psi'(N^-)}{h}$$

$$= \frac{1}{h}\left(\frac{\Psi(N+1)-\Psi(N)}{h} - \frac{\Psi(N)-\Psi(N-1)}{h}\right)$$

$$= \frac{\Psi(N-1)-2\Psi(N)+\Psi(N+1)}{h^2} \qquad \text{<160>}$$

In addition, Ψ may be expressed as a Taylor expansion, i.e.

$$\Psi(N) = \Psi^{o}(N) + \delta\Psi(N) \qquad \text{<161>}$$

APPENDIX

So that combining <153>, <156>, <160> and <161>, we have:

for $0 < x < m$

$$\delta\Psi(N-1) - 2\delta\Psi(N) + \delta\Psi(N+1) = C(N) = \frac{-qn_1h^2}{\varepsilon\varepsilon_o} - \Psi^o(N-1) + 2\Psi^o(N) - \Psi^o(N+1) \qquad <162>$$

and for $m < x < d$

$$\delta\Psi(N-1) - 2\delta\Psi(N) + \delta\Psi(N+1) = C(N) = \frac{-qh^2}{\varepsilon\varepsilon_o}\left[n_1 + n_o \exp\left[\frac{q\bar{\xi}}{kT}\right]\right] - \Psi^o(N-1) + 2\Psi^o(N) - \Psi^o(N+1) \qquad <163>$$

There are M such expressions, one for each of the M interior mesh points. The two end points are invariant: $\Psi(0) = 0$, and $\Psi(M+1) = V + V_{in}$. These form a tridiagonal system of linear equations:

$$\begin{vmatrix} -2 & 1 & 0 & 0 & \cdots & 0 \\ 1 & -2 & 1 & 0 & & \\ 0 & 1 & -2 & 1 & & \\ \vdots & & & \ddots & & \\ 0 & & & & 1 & -2 \end{vmatrix} \cdot \begin{vmatrix} \delta\Psi(1) \\ \\ \\ \\ \delta\Psi(M) \end{vmatrix} = \begin{vmatrix} C(1) \\ \\ \\ \\ C(M) \end{vmatrix} \qquad <164>$$

The unknowns to be found by solving these equations are the error terms in Ψ. Once the $\delta\Psi(n)$'s are found, the present guess for Ψ^k is improved by:

$$\psi^k(N) = \psi^{k-1}(N) + o\psi(N) \qquad <165>$$

New C(N)'s are calculated, and the process is repeated until the $\delta\Psi(N)$'s are arbitrarily small. Figure <51> gives a flowchart of the program.

The algorithm used to solve the equations <164> is the Gauss-Seidel method (242). This is an exact method which is particularly useful for solving sparse matrices (i.e. possessing few off diagonal elements) such as <164>. This property also reduces the memory needs, and thus brings the problem within the capabilities of an Apple //e. The method is outlined for a general 3 x 3 matrix as follows:

Consider: $a_1x + b_1y + c_1z = d_1$

$a_2x + b_2y + c_2z = d_2$

$a_3x + b_3y + c_3z = d_3$

If y and z can be given estimated values y_0 and z_0, then

$$x_1 = \frac{d_1 - b_1y_0 - c_1z_0}{a_1} \qquad <169>$$

Using this estimate of x, a better guess for y may be made:

$$y_1 = \frac{d_2 - a_2x_1 - c_2z_0}{b_2} \qquad <170>$$

Figure <51> Flowchart for the Finite Difference Algorithm

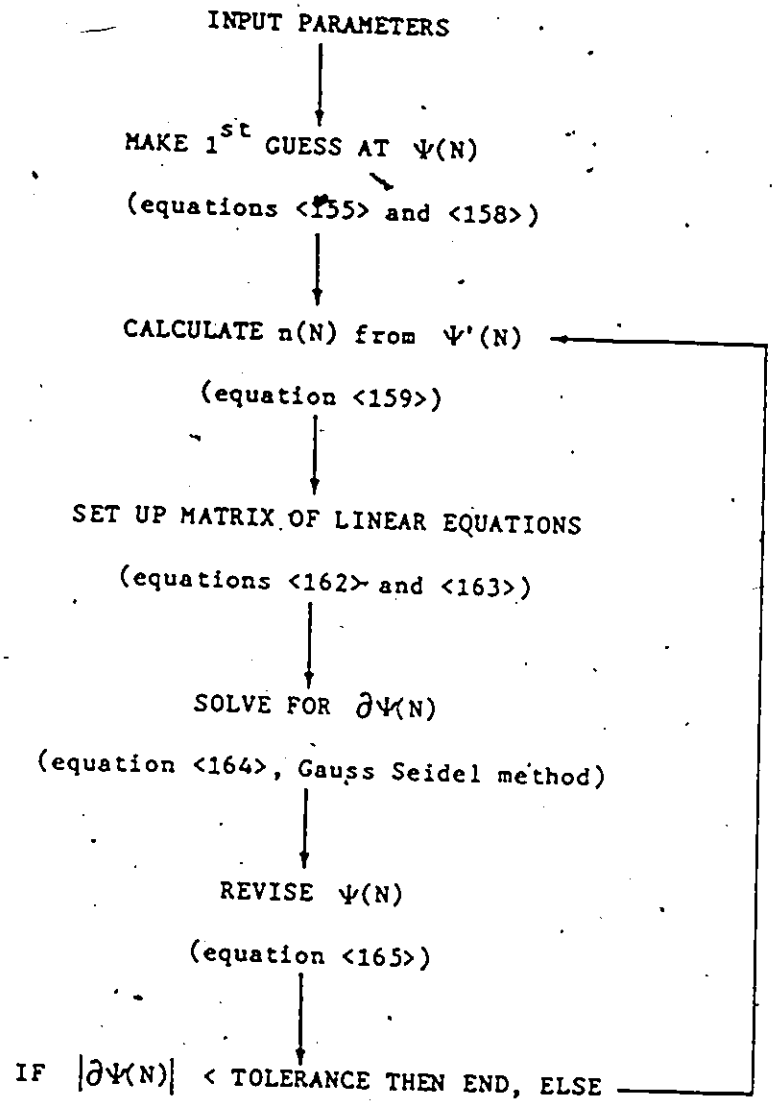

$$z_1 = \frac{d_3 - a_3x_1 - b_3y_1}{c_3} \qquad \langle 171 \rangle$$

With these x, y, and z estimates, new estimates are made using the general formulae for the k^{th} iteration:

$$x_k = \frac{d_1 - b_1y_{k-1} - c_1z_{k-1}}{a_1} \qquad \langle 172 \rangle$$

$$y_k = \frac{d_2 - a_2x_{k-1} - c_2z_{k-1}}{b_2} \qquad \langle 173 \rangle$$

$$z_k = \frac{d_3 - a_3x_{k-1} - b_3y_{k-1}}{c_3} \qquad \langle 174 \rangle$$

Convergence is assured if the diagonal element, the so called pivot point , is larger than the sum of all others in that column. Therefore row interchanges are employed to produce this condition. A second technique to reduce instability is point relaxation, whereby each new x_k is generated from a weighted average of x_{k-1} and the value produced by equation <172>. Convergence is determined by examining the size of the change in values between the last two iterations.

REFERENCES

(1) L.Young, ANODIC OXIDE FILMS (Academic Press, London and New York, 1961)

(2) S.R.Morrison, ELECTROCHEMISTRY AT SEMICONDUCTOR AND OXIDIZED METAL ELECTRODES, (Plenum Press, New York and London, 1980)

(3) Reference (1), page 90

(4) W.D.Westwood, N.Waterhouse and P.S.Wilcox, TANTALUM THIN FILMS, (Academic Press, London, New York and San Francisco, 1975) 293

(5) J.P.S.Pringle, "A Very Precise Sectioning Method for Measuring Concentration Profiles in Anodic Tantalum Oxide", Journal Electrochemical Society, 119 (1972) 482-491

(6) J.G.Simmons, "Conduction in Thin Dielectric Films", J.Phys.D: Appl.Phys., 4 (1971) 615-620

(7) M.Lampert and P.Mark, CURRENT INJECTION IN SOLIDS, (Academic Press, New York and London, 1970) 113-139

(8) H.K.Henisch and J.C.Manifacier, "Macroscopic Aspects of Carrier Transport in Thin Films", Thin Solid Films, 89 (1982) 3-11

(9) L.I.Maisel and R.Glang, HANDBOOK OF THIN FILM TECHNOLOGY, (McGraw-Hill, New York, 1970) 13-7

(10) H.Birey, "Thickness-Dependence of the Dielectric Constant and Resistance of Al_2O_3 Films", J.Appl.Phys., 48 (1977) 5209-5912

(11) M.W.Jones and D.M.Hughes, "Electrical Conduction in Anodic Tantalum Oxide Films", J.Phys.D: Appl.Phys., 7 (1974) 112-119

(12) A.K.Jonscher and P.A.Walley, "Electrical Conduction in Non-Metallic Amorphous Films", J.Vac.Sci.Tech., 6 (1969) 662-669

(13) F.Nazar and M.Atiq, "High-Field Conduction Mechanism Changes in Anodic WO_3 and Ta_2O_5 Films", Int.J.Electronics, 51 (1981) 165-171

(14) D.M.Smyth, G.A.Shirn, and T.B.Tripp, "Heat Treatment of Anodic Oxide Films on Tantalum, I", Journal Electrochemical Society, 110 (1963) 1264-1276

(15) D.A.Vermilyea, "Annealing Anodic Ta_2O_5 Films, Changes in Dissolution Behavior and X-Ray Scattering", Journal Electrochemical Society, 104 (1957) 485-488

(16) G.M.Krembs, "Residual Tritiated Water in Anodized Tantalum Films", Journal Electrochemical Society, 110 (1963) 938-940

(17) L.Masing, J.E.Orme and L.Young, "Optical Properties of Anodic Oxide Films on Tantalum, Niobium, and Tantalum and Niobium Alloys and The Optical Constants of Tantalum", Journal Electrochemical Society, 108 (1961) 428-438

(18) H.Takahashi, H.Konno, K.Fujimoto, and M.Nagayama, "Distribution of Anions in Oxide Films Anodically Formed on Aluminum in a Phosphate Solution", Electrochemical Society Extd. Abs., 81-1 (1981) 93-95

(19) T.Kamei and E.Matsuzaki, "Properties of Anodic Oxide Films Prepared on Nitrogen Doped Tantalum Films", Thin Solid Films, 77 (1981) 259-270

(20) K.Shimisu, G.E.Thompson, and G.C.Wood, "The Electrical Breakdown During Anodizing of Aluminum in Borate Solutions", Electrochemical Society Extd. Abs., 81-1 (1981) 105-106

(21) C.J.Dell'Oca and L.Young, "Ellipsometric Studies of Anodic Oxide Films Formed on Tantalum in Dilute Phosphoric Acid", Journal Electrochemical Society, 117 (1970) 1545-1548

(22) D.A.Vermilyea, "Flaws in Anodic Ta_2O_5 Films", Journal Electrochemical Society, 110 (1965) 250-262

(23) C.A.Mead, "Anomalous Capacitance of Thin Film Dielectric Structures", Phys.Rev.Lett., 6 (1961) 545-546

(24) D.Mohler and R.Hirst, "Dielectric Characteristics of Tantalum Anodic Films as Related to Film Structure", Journal Electrochemical Society, 108 (1961) 347-350

(25) N.Schwartz and N.N.Axelrod, "Asymmetric Conduction in Thin Film Tantalum/Tantalum Oxide/Metal Structures", Proc. Electrochemical Society Symp. on Electrolyte Rectification and Conduction Mechanisms in Anodic Oxide Films, (1967) 228-230

(26) D.A.Vermilyea, "Conduction and Rectification in Anodic Oxide Films", J.Appl.Phys., 36 (1965) 3663-3071

(27) M.Kleefstra, "L'Effet-Valve Du Tantale", Annales de Radioelectricite, 17 (1962) 223-226

(28) N.Schwartz and M.Gresh, "Effect of Ambients and Contact Area on the Asymmetric Conduction of Anodic Tantalum Oxide Films", Journal Electrochemical Society, 112 (1965) 295-300

(29) D.M.Smyth, and G.A.Shirn, "Conduction and Stoichiometry in Heat Treated, Anodic Oxide Films", Proc. Electrochemical Society Symp. on Electrolyte Rectification and Conduction Mechanisms in Anodic Oxide Films, (1967) 75-99

(30) J.P.S.Pringle, "Transport Numbers of Metal and Oxygen during the Anodic Oxidation of Tantalum", Journal Electrochemical Society, 120 (1973) 398-407

(31) Y.Sasaki, "P-i-n Junction in the Anodic Oxide Film of Tantalum", J.Phys.Chem.Solids, 13 (1960) 177-186

(32) D.M.Smyth, G.A.Shirn, and T.B.Trip, "The Heat Treatment of Anodic Oxide Films on Tantalum, III", Journal Electrochemical Society, 111 (1964) 1331-1336

(33) Reference (4), pages 76-84

(34) M.Read and C.Altman, "A New Structure in Tantalum Thin Films", Appl.Phys.Lett., 7 (1965) 51-52

(35) Reference (4), page 317

(36) F.Vratny, B.H.Vromen and A.J.Harendza-Harinxma, "Anodic Tantalum Oxide Dielectrics Prepared from Body-Centered-Cubic Tantalum and Beta Tantalum", Electrochem Tech, 5 (1967) 283-287

(37) D.Gerstenberg, "Properties of Anodic Films Formed on Reactively Sputtered Tantalum", Journal Electrochemical Society, 113 (1966) 542-547

(38) P.K.Reddy and S.R.Jawalekar, "Improved Properties of TaN-$Ta_2O_xN_y$-Al Capacitors", Thin Solid Films, 64 (1979) 71-76

(39) Reference (4), chapter 3, pages 96-200

(40) D.R.Baraff, J.R.Long, B.K.MacLaurin, C.J.Miner and R.W.Streater, "The Optimization of Metal-Insulator-Metal Nonlinear Devices for Use in Multiplexed Liquid Crystal Displays", IEEE Trans. Electron Devices, ED-28 (1981) 736-739

(41) C.J.Miner, R.W.Streater, B.K.MacLaurin and W.D.Westwood, "Optical Properties and Poole Frenkel Conduction in Anodic Films on Sputtered Tantalum and Tantalum Nitride", Electrochemical Society Extd. Abs., 81-1 (1981) 148-150

(42) J.Klerer, W.H.Orr, and D.Farrell, "The Effect of Moisture upon the Tantalum Oxide Thin Film Capacitors", Proc. Electronics Components Conference (1966) 348-360

(43) A.Climent, J.M.Martinez-Duart, and C.Palacio, "Dielectric Properties of Anodic Tantalum Oxide Grown on Sputtered Tantalum Nitride", Thin Solid Films, 58 (1979) 315-319

(44) J.M.Sanz and S.Hofmann, "Quantitative Evaluation of AES Depth Profiles of Thin Anodic Oxide Films (Ta_2O_5/Ta, Nb_2O_5/Nb)", Surface and Interface Analysis, 5 (1983) 210-216

(45) H.Bispinck, O.Ganschow, L.Wiedmann, and A.Benninghoven, "Combined SIMS, AES, and XPS Investigation of Tantalum Oxide Layers", Appl.Phys.A, 18 (1979) 113-117

(46) D.A.Vermilyea, "The Crystallization of Anodic Tantalum Oxide Films in the Presence of a Strong Electric Field", Journal Electrochemical Society, 102 (1955) 207-214

(47) N.F.Mott and E.A.Davis, ELECTRONIC PROCESSES IN NON-CRYSTALLINE MATERIALS, (Claredon Press, Oxford, 1971)

(48) Reference (1), page 193

(49) Reference (4), page 260

(50) Reference (4), chapter 6, pages 289-405

(51) R.Angle and H.Talley, "Electrical and Charge Storage Characteristics of the Tantalum Oxide - Silicon Dioxide Device", IEEE Trans. Elec. Devices, ED-25 (1978) 1277-1283

(52) D.Smith and L.Young, "Optical and Electrical Properties of Thermal Tantalum Oxide on Silicon", IEEE Trans. Elec. Devices, ED-28 (1981) 22-27

(53) J.R.Szedon, and R.M.Handy, "Characterization, Control and Use of Dielectric Charge Effects in Silicon Technology", J.Vac.Sci.Tech, 6 (1969) 1-12

(54) H.Matsumoto, S.Tanaka and T.Yabumoto, "DC Electroluminescence on MIS Structures in Thin Films", Japanese J.Phys., 17 (1978) 1543-1548

(55) T.Kallfass and E.Lueder, "High Voltage Thin Film Transistors Manufactured with Photolithography and with Ta_2O_5 as the Gate Oxide", Thin Solid Films, 61 (1979) 259-264

(56) S.Seki, T.Ungami, and B.Tsujiyama, "p-Channel TFT's using Magnetron Sputtered Ta_2O_5 Films as Gate Insulators", IEEE Trans. Elec. Devices Lett, EDL-5, (1984) 197-198

(57) C.J.Miner and R.W.Streater, "Liquid Crystal Puts on a Big Display", Telesis, 3 (1982) 20-25

(58) F.C.Aris and T.J.Lewis, "Steady State Transient Conduction Processes in Anodic Tantalum Oxide", J.Phys.D: Appl.Phys., 6 (1973) 1067-1083

(59) J.H.Thomas, "An Analysis of Conduction in Anodic Ta_2O_5", 1975 Annual Report : Conference on Electrical Insulation and Dielectric Phenomena, 413-417

(60) D.L.Bowman, "Photoconductivity and Photo Hall Measurements on High Resistivity GaP", J.Appl.Phys., 38 (1967) 568-572

(61) R.R.Parsons, J.C.Dyment and G.Smith, "Differential Electron Beam Induced Current Studies of GaAs-GaAlAs Heterojunctions", J.Appl.Phys., 50 (1979) 50-55

(62) Wm.Shockley, ELECTRONS AND HOLES IN SEMICONDUCTORS, (D.Van Nostrand Company, Inc., Princeton, 1950) 54-65

(63) J.H.Thomas, "Photoconductivity in Anodic Ta_2O_5 Formed on Nitrogen Doped Tantalum Films", J.Appl.Phys., 45 (1974) 5349-5355

(64) F.M.Nazar, M.Y.Zaheer, and W.H.Bokhari, "Photoconduction in Anodic Tantalum Oxide Films", Int. J. Electronics, 54 (1983) 447-452

(65) A.K.Jonscher, "Electronic Properties of Amorphous Dielectric Films", Thin Solid Films, 1 (1967) 213-234

(66) P.Skeath, I.Lindau, P.W.Chye, C.Y.Su, W.E.Spicer, "Investigation of the Mechanism for Schottky Barrier Formation by Group III metals on GaAs (110)", J.Vac.Sci.Tech., 16 (1979) 1143-1148

(67) G.D.O'Clock Jr., and L.D.Feisel, "Performance of Ta-Ta_2O_5-Au Metal Insulator Metal Devices", Appl.Phy.Lett., 44 (1984) 642-644

(68) V.Kadary and N.Klein, "Electrical Breakdown During the Anodic Growth of Tantalum Pentoxide", Journal Electrochemical Society, 127 (1980) 139-151

(69) J.H.Thomas, "Defect Photoconductivity of Anodic Ta_2O_5 Films", Appl.Phys.Lett., 22 (1973) 406-408

(70) S.M.Gubanski and D.M.Hughes, "Conduction Processes in Anodic Tantalum Oxide Thin Films with Gold Counter Electrodes", Thin Solid Films, 52 (1978) 119-127

(71) T.W.Hickmott, "Electroluminescence and Conduction in $Nb-Nb_2O_5-Au$ Diodes", J.Appl.Phys., 37 (1966) 4380-4388

(72) S.M.Sze, PHYSICS OF SEMICONDUCTOR DEVICES, 2nd Edition, (Wiley Interscience, New York, 1981) Chapter 5

(73) J.G.Simmons and G.S.Nadkarni, "Non-Steady State Phenomena in Defect Thin Film Metal-Insulator-Metal Systems Containing Schottky Barriers", J.Solid State Chem., 12 (1975) 341-348

(74) J.G.Simmons, "Transition from Electrode-Limited to Bulk-Limited Conduction Processes in Metal-Insulator-Metal Systems", Phys.Rev., 166 (1968) 912-920

(75) R.I.Frank and J.G.Simmons, "Space Charge Effects on Emission Limited Current Flow in Insulators", J.Appl.Phys., 38 (1967) 832-840

(76) D.L.Pulfrey, A.H.M.Shousha and L.Young, "Electronic Conduction and Space Charge in Amorphous Insulating Films", J.Appl.Phys., 41 (1970) 2838-2843

(77) M.Hacskaylo, "A Relationship Between the Schottky Emission Mechanism and the Energy Bands of Thin Film Metal-Insulator-Metal Configuration", J.Appl.Phys., 35 (1964) 2943-2947

(78) W.E.Flannery and S.R.Pollack, "Electron Transfer Processes Through Tantalum-Tantalum Oxide Diodes", J.Appl.Phys., 37 (1966) 4417-4422

(79) S.Namba et al., Rika Gaku Kenkjusho Hokoku, 40 (1964) 92-106 (as quoted in (78))

(80) C.A.Mead in BASIC PROBLEMS IN THIN FILM PHYSICS, R.Neidermayer and H.Mayer (eds) (Vandenhoek and Reprecht, Gottingen, 1966) (as qouted in 65)

(81) T.E.Hartman, J.C.Blair, and R.Bauer, "Electrical Conduction Through SiO_2 Films", J.Appl.Phys., 37 (1966) 2468-2474

(82) H.Hirose and Y.Wada, "Non Ohmic Conduction in Vacuum Deposited SiO_2Films", Japanese J.Appl.Phys., 4 (1965) 639-644

(83) Y.Inagaki, K.Adachi and S.Nitta, "Electrical Conduction Properties of Evaporated SiO_2 Films", Elec. Eng. in Japan, 80, no.2, (1970) 88-94

(84) M.Stuart, "Conduction in Silicon Oxide Films", British J.Appl.Phys., 18 (1967) 1637-1640

(85) M.Stuart, "Electrode Limited to Bulk Limited Conduction in Silicon Oxide Films", Phys.Stat.Sol., 23 (1967) 595-597

(86) H.Matsumoto, A.Suzuki, and T.Yabumoto, "Effect of Heat Treatment on the Coefficient β for the Poole Frenkel Effect and the Conduction in Ta_2O_5 Films", Japanese J.Appl.Phys., 19 (1980) 71-77

(87) P.L.Young, "dc Electronic Conduction in the Ta_2O_5 Films, II - Highly Imperfect Films", J.Appl.Phys., 47 (1976) 242-247

(88) J.Antula, "Method for Doping Thin Insulating Films and the Comparison Between the Electrical Characteristics of Undoped and Doped Films", J.Appl.Phys., 42 (1971) 2081-2084

(89) G.O'Clock, "Current Transport, Effective Dielectric Constant and Temperature of Ta_2O_5 Thin Films", Appl.Phys.Lett., 19 (1971) 403-405

(90) D.L.Pulfrey, P.S.Wilcox and L.Young, "Dielectric Properties of Ta_2O_5 Thin Films", J.Appl.Phys., 40 (1969) 3891-3898

(91) J.H.Sanchez-Lassise and J.R.Yeargan, "Conduction Mechanisms in Very Thin Silicon Nitride Films", Journal Electrochemical Society, 120 (1973) 423-425

(92) M.McColl and C.A.Mead, "Electron Current Through Thin Mica Films", Trans. Metallurgical Soc. AIME, 233 (1965) 502-511

(93) P.R.Emtage and W.Tantraporn, "Schottky Emission Through Thin Insulating Films", Phys.Rev.Lett., 8 (1962) 267-268

(94) T.C.McGill, S.Kurtin, L.Fishbone, and C.A.Mead, "Contact Limited Currents in Metal-Insulator-Metal Structures", J.Appl.Phys., 41 (1970) 3831-3839

(95) M.Lampert and P.Mark, CURRENT INJECTION IN SOLIDS, (Academic Press, New York and London, 1970)

(96) Reference (95), pages 25-27

(97) Reference (95), chapter 14

(98) Reference (95), pages 116-121

(99) A.Many and G.Rakavy, "Theory of Transient Space-Charge-Limited Currents in Solids in the Presence of Trapping", Phys.Rev., 126 (1962) 1980-1988

(100) J.Lindmayer, "Current Transients in Insulators", J.Appl.Phys.,36 (1965) 196-201

(101) H.Pfleiderer, W.Kruhler, M.Moller and R.Plattner, "A SCLC Model Including Diffusion", J.Noncrystalline Solids, 59&60 (1983) 485-488

(102) D.A.Edwards and P.L.Jones, "The Effects of Finite Contact Energy Barriers and Traps on Space Charge Limited Currents in Thin Insulators", Solid State Electronics, 21 (1978) 1163-1170

(103) M-A.Nicolet, "Unipolar Space Charge Limited Current in Solids with Non Uniform Spacial Distribution of Shallow Traps", J.Appl.Phys., 37 (1966) 4224-4235

(104) J.Sworakowski, "Space Charge Limited Currents in Solids with Non-Uniform Spatial Trap Distribution", J.Appl.Phys., 41 (1970) 292-295

(105) E.Sciri and R.Chabicovsky, "Conduction Phenomena in Nb-Nb_2O_5-Au Thin Film Structures Fabricated by Various Techniques", Vacuum, 27 (1975) 299-304

(106) G.Taylor and B.Lalevic, "Threshold Switching in Polycrystalline TiO_2 Thin Films", J.Appl.Phys., 48 (1977) 4410-4412

(107) P.R.Mason and V.Nathoo, "Characteristics Derived from Transient Current Measurements in Thin R.F. Sputtered Al_2O_3 Films", J. Phys.C : Solid State Phys., 11 (1978) 1391-1399

(108) M.Nakamura, J.Yamazaki, W.Endou and Y.Nishimura, "An Analysis of Voltage Bias Characteristics of Tantalum Thin Film Capacitor", Electronics and Communications in Japan, 55-C, no.4 (1972) 107-111

(109) I.F.M.Walker, "Conduction Mechanisms in Tantalum Thin Film Capacitors", Electrochemical Society Symp. Electrolytic Rectification and Conduction Mechanisms in Anodic Oxides, (1967) 63-74

(110) P.Mackus, A.Suli, M.I.Torok, and I.Hevesi, "Carrier Transport in the V_2O_5-n-Si System", Thin Solid Films, 42 (1977) 17-32

(111) Reference (47), pages 39-43

(112) C.Kittel, INTRODUCTION TO SOLID STATE PHYSICS, 5th Edition, (John Wiley & Son, New York, 1976) 542-545

(113) X.C.Deng, X.H.Liu, K.Bohringer, and S.Kalbitzer, "Hopping and Band Transport in Amorphized Semiconductors", Appl.Phy.A, 33 (1984) 29-35

(114) M.Ortuno and M.Pollak, "An Extended Theory for Hopping Transport in a-Ge and a-Si", J.Non-Crystalline Solids, 59 & 60 (1983) 53-56

(115) P.Viscor, "Comment on Two-Dimensional Variable-Range Hopping Conduction in Group IV Amorphous Semiconductors", Solid State Commun., 32 (1979) 281-284

(116) G.Desrousseaux, A.Carlan, H.Schaffer, and R.Faure, "Hopping Conduction in Carbon Films", Thin Solid Films, 89 (1982) 76

(117) R.M.Hill, "Hopping Conduction in Amorphous Solids", Phil.Mag., 24 (1971) 1307-1325

(118) I.G.Austin and M.Sayer, "Hopping Conduction at High Electric Fields in Transition Metal Ion Glasses", J.Phys.C: Solid State Phys., 7 (1974) 905-924

(119) M.Pollak, and I.Riess, "A Percolation Treatment of High Field Hopping Transport", J.Phys.C: Solid State Phys., 9 (1976) 2339-2352

(120) B.G.Bagley, "The Field Dependent Mobility of Localized Electronic Carriers", Solid State Commun., 8 (1970) 345-348

(121) B.I.Shklovskii, "Hopping Conduction in Semiconductors Subjected to a Strong Electric Field", Sov.Phys.Semi., 6 (1973) 1964-1967

(122) B.I.Shklovskii, "Nonohmic Hopping Conduction", Sov.Phys.Semi., 10 (1976) 855-860

(123) Reference (47), pages 50-52

(124) Reference (47), page 21

(125) I.G.Austin and N.F.Mott, "Polarons in Crystalline and Non-Crystalline Materials", Advances in Physics, 18 (1969) 41-102

(126) N.F.Mott, "Conduction in Glasses Containing Transition Metal Ions", J.Noncrystalline Solids, 1 (1968) 1-17

(127) J.Schnakenberg, "Polaronic Impurity Hopping Conduction", Phy.Stat.Sol., 28 (1968) 623-633

(128) M.Pollak, "On the Frequency Dependence of Conductivity in Amorphous Solids", Phil.Mag., 23 (1971) 519-540

(129) S.R.Elliott, "A Theory of AC Conduction in Chalcogenide Glasses", Phil.Mag., 36 (1977) 1291-1304

(130) N.F.Mott, "States in the Gap of Non-crystalline Semiconductors", J.Phy.C: Solid State Phys., 13 (1980) 5433-5421

(131) M.Pollak and T.H.Geballe, "Low Frequency Conductivity Due to Hopping Processes in Silicon", Phys.Rev., 122 (1961) 1742-1753

(132) M.Pollak, "Temperature Dependence of ac Hopping Conductivity", Phys.Rev., 138 (1965) A1822-A1826

(133) H.Böttger and V.V.Bryksin, "Hopping Conductivity in Ordered and Disordered Solids", Phys.Stat.Sol. (b), 78 (1976) 9-56 and 415-451

(134) I.I.Fischuk and V.N.Rudko, "Low Frequency Conductivity in Disordered Systems Due to Variable Range Hopping", J.Phys.C: Soild State Phys., 13 (1980) L493-L497

(135) A.J.SpringThorpe, "The Electrical and Optical Properties of Single Crystal NiO and CoO", PhD Thesis, Sheffield University, Sheffield, England, 1967

(136) N.A.Savinova, "Electrical Conduction in Amorphous and Crystalline Tantalum Pentoxide", Sov.Phys.Solid State, 21 (1979) 1665-1667

(137) V.V.Bryksin, M.N.D'yakonov, and S.D.Khanin, "Hopping Transport in Noncrystalline Tantalum Pentoxide", Sov.Phys.Solid State, 22 (1980) 818-822

(138) M.S.Frost and A.K.Jonscher, "The Electrical Properties of Silicon Monoxide", Thin Solid Films, 29 (1975) 7-185

(139) D.F.Barbe and D.S.Herman, "Transport Processes in Amorphous Cr_2O_3 Films", J.Appl.Phys., 41 (1970) 3116-3120

(140) A.K.Jonscher "The Universal Dielectric Response: A Review of Data and Their New Interpretation", PHYSICS OF THIN FILMS, Vol.11, (Academic Press, Inc., New York, 1980) 205-317

(141) G.E.Pike, "ac Conductivity of Scandium Oxide and a New Hopping Model for Conductivity", Phys.Rev.B, 6 (1972) 1572-1580

(142) A.Mansigh, J.K.Vaid and R.P.Tandon, "ac Conductivity of Vanadium Phosphate Glasses", J.Phys.C: Solid State Phys., 8 (1975) 1023-1033

(143) M.Meaudre, R.Meaudre, J.Tardy and B.Tribollet, "Correlation between Conductivity, Electron Spin Resonance and Optical Absorption in RF Sputtered SiO_2 Films", Journal de Physique, 42 (1981) C4 1013-1016

(144) M.Meaudre, and R.Meaudre , "AC Conductivity in RF Sputtered SiO_2 Films" Phil.Mag.B, 40 (1979) 401-410

(145) D.Mangalaraj, M.Radhakrishnan, and C.Balasubramanian, "Dielectric and ac Conduction Properties in Ion Plated Aluminum Nitride Thin Films", J.Phys.D: Appl.Phys., 15 (1982) 467-472

(146) D.Schalch, A Scharmann, and H.Weber "Electrical Conduction in Reactively Sputtered Silicon Nitride Films at Medium Field Strengths", Phys.Stat.Sol.(a), 64 (1981) 159-167

(147) M.Meunier, J.F.Currie, M.R.Wertheimer, A.Yelon, "Electrical Conduction in Biotite Micas", J.Appl.Phys., 54 (1983) 898-905

(148) A.S.Barriere, J.Richon, S.Lofti and G.Gevers, "Electrical Charge Transfer between Localized States in Insulating Thin Films", Thin Solid Films, 89 (1982) 77-82

(149) W.Keller and K.Wunstel, "Thermal Donors in Silicon: Consistent Interpretation of Hall Effect and Capacitance Transient Spectroscopy", Appl.Phys.A, 31 (1983) 9-12

(150) W.Keller, G.Pensl and M.Schulz, "Experimental Study of the Poole Frenkel Effect on the Si:Tl Acceptor", Physica, 116B (1983) 244-251

(151) T.Changhua, H.Mingzhen, and W.Yangyuan, "Field Asssisted Thermally Stimulated Current of Mobile Ions in a Dielectric Layer of a Metal Oxide Semiconductor Structure", J.Appl.Phys., 54 (1983) 4398-4404

(152) S.J.Fox, "Decay of Surface Potential in Electrophotography: Single Carrier Case", J.Appl.Phys., 45 (1974) 610-617

(153) K.J.Donovan and E.G.Wilson, "Photocarrier Creation in One Dimension", Phil.Mag.B, 44 (1981) 31-45

(154) A.K.Jonscher and C.H.Loh, "Poole Frenkel Conduction in High Alternating Electric Fields", J.Phys.C: Solid State Phys., 4 (1971) 1341-1347

(155) J.Frenkel, "On Pre-Breakdown Phenomena in Insulator and Electronic Semiconductors", Phys.Rev., 54 (1938) 647-648

(156) A.G.Milnes, DEEP IMPURITIES IN SEMICONDUCTORS, (Wiley Interscience, New York, 1973) 3

(157) Reference (4), page 358

(158) Reference (1), Chapter 7

(159) J.P.Lacharme and J.O.Isard, "Ionic Jump Processes and High Field Conduction in Glasses", J.Noncrystalline Solids, 27 (1978) 381-397

(160) C.A.Hogarth and M.A.Ghauri, "The Electrical Properties of Cadmium Zinc Phosphate Glasses at Higher Electric Fields", Int.J.Electronics, 52 (1982) 201-207

(161) M.A.Ghauri and F.M.Nazar, "High Field Conductivity in Cadmium Zinc Phosphate Glasses", Int.J.Electronics, 56 (1984) 25-30

(162) G.A.N.Connell, D.L.Camphausen, and W.Paul, "Theory of Poole Frenkel Conduction in Low Mobility Semiconductors", Phil.Mag., 26 (1972) 541-551

(163) J.L.Hartke, "The Three Dimensional Poole Frenkel Effect", J.Appl.Phys., 39 (1968) 4871-4873

(164) R.M.Hill, "Poole Frenkel Conduction in Amorphous Solids", Phil. Mag., 23 (1971) 59-86

(165) M.Ieda, G.Sawa, and S.Kato, "A Consideration of the Poole Frenkel Effect on Electric Conduction in Insulators", J.Appl.Phys., 42 (1971) 3737-3740

(166) L.Onsager, "Initial Recombination of Ions", Phys.Rev., 54 (1938) 554-557

REFERENCES

(167) D.M.Pai, "Electric Field Enhanced Conductivity in Solids", J.Appl.Phys., 46 (1975) 5122-5126

(168) V.Adamec and J.H.Calderwood, "Electric Field Enhanced Conductivity in Dielectrics", J.Phys.D: Appl.Phys., 10 (1977) L79-L81.

(169) D.M.Pai and R.C.Enck, "Onsager Mechanism of Photogeneration in Amorphous Selenium", Phy.Rev.B, 11 (1975) 5163-5174

(170) J.P.Crine and A.Yelon, "Photogeneration and Transport of Carriers in Atactic Polystyrene", J.Appl.Phys., 51 (1980) 2106-2114

(171) J.Plans, M.Zielinski, T.Swiderski and M.Kryszewski, "Application of the Onsager Theory to Thermally Stimulated Currents", J.Appl.Phys., 53 (1982) 3103-3109

(172) P.C.Arnett and N.Klein, "Poole Frenkel Conduction and the Neutral Trap", J.Appl.Phys., 46 (1975) 1399-1400

(173) P.A.Martin, B.G.Streetman and K.Hess, "Electric Field Enhanced Emission from Non-Coulombic Traps in Semiconductors", J.Appl.Phys., 52 (1981) 7409-7415

(174) W.Teubner and B.Fromm, "Some Remarks on the Poole Frenkel Effect for Centers with Screened Potential", Phys.Stat.Sol.(a), 41 (1977) K47-K49

(175) W.Bobe and L.Fritzch, "Poole Frenkel Effect on Centers with Screened Coulomb Potential", Phys.Stat.Sol.(b), 61 (1974) K35-K39

(176) L.Hrivnak, "A Note on the Utilization of the Poole Frenkel Effect for the Determination of the Shape of Trap Potential Wells", Phys.Stat.Sol.(b), 101 (1980) K173-K176

(177) H.Kahnt and F.Schirrmeister, "Electric Field Dependent Conductivity in Amorphous Semiconductors", Phys.Stat.Sol.(b), 115 (1983) 171-179

(178) D.M.Taylor and T.J.Lewis, "Electric Conduction in Polyethylene Terephthalate and Polyethylene Films", J.Phys.D: Appl.Phys., 4 (1971) 1346-1357

(179) J.M.Marshall and G.R.Miller, "Field Dependent Carrier Transport in Non-crystalline Semiconductors", Phil.Mag., 27 (1973) 1151-1168

(180) M.R.Belmont, "The Capture Cross Section of a Dipole Trap", Thin Solid Films, 28 (1975) 149-156

(181) G.Vincent, A Chantre and D.Bois, "Electric Field Effect on the Thermal Emission of Traps in Semiconductors", J.Appl.Phys., 50 (1979) 5484-5487

(182) R.A.Smith, SEMICONDUCTORS, 2nd ed., (Cambridge University Press, Cambridge, 1978) 86-94

(183) P.Mark and T.E.Hartman, "On Distinguishing Between the Schottky and Poole Frenkel Effect", J.Appl.Phys., 39 (1968) 2163-2164

(184) J.R.Yeargan and K.L.Taylor, "The Poole Frenkel Effect with Compensation Present" J.Appl.Phys., 39 (1968) 5600-5604

(185) A.K.Jonscher, "Electronic Conduction in Dielectric Films", Journal Electrochemical Society, 116 (1969) 217C-226C

(186) A.K.Jonscher, "Electronic Conduction in Amorphous Semiconductors", J.Vac.Sci. & Tech., 8 (1971) 135-144

(187) A.K.Jonscher and A.A.Ansari, "Photocurrents in Silicon Monoxide Films", Phil.Mag., 23 (1971) 205-223

(188) J.G.Simmons, "Poole Frenkel and Schottky Effect in Metal - Insulator - Metal Systems", Phys.Rev., 155 (1967) 657-660

(189) J.G.Simmons and G.W.Taylor, "Dielectric Relaxation and Its Effect on the Thermal Electric Characteristics of Insulators", Phys.Rev.B, 6 (1972) 4804-4814

(190) W.G.Trodden, as quoted in Reference (65)

(191) A.Sapega, "Charge Transport Through the Cadmium-Selenium Interface", PhD Thesis, Worcester Polytechnic Institute, Worcester, Massachusetts, USA, 1972

(192) C.J.Miner, Bell-Northern Research internal report, Feb. 1979

(193) A.Sapega and H.P.D.Lanyon, "Charge Transport Through the Cadmium-Selenium Interface", Phys.Stat.Sol.(a), 11 (1972) 713-719

(194) B.G.Tagiev, E.S.Guseinova and V.A.Gadzhiev, "Frenkel's Mechanism of Thermoelectric Ionization in Single Crystals of Gallium.Selenide", Phys.Stat.Sol., 36 (1969) 75-80

(195) M.Morita, K.Tsubouchi and N.Mikoshiba, "Electronic Conduction in Epitaxial Aluminum Nitride Films on Silicon", Japanese J.Appl.Phys., 21 (1982) 728-730

(196) J.W.Gibson and R.E.Thomas, "Secondary Electron Emission and Conductivity Mechanisms of Epitaxial MgO Films", Appl.Surf.Sci., 14 (1982-83) 56-72

(197) A.K.Jonscher, "Free Carrier Poole Frenkel Effect in Crystalline Solids", J.Phys.C: Solid State Phys., 3 (1970) 1159-1162

(198) David Emin, "Electrical and Optical Properties of Amorphous Thin Films", POLYCRYSTALLINE AND AMORPHOUS THIN FILMS AND DEVICES, ed. L.L.Kazmerski, (Academic Press, New York, 1980) 17-36

(199) J.Robertson, "Electronic Structure of Amorphous Semiconductors", Advances in Physics, 32 (1983) 361-452

(200) A.Servini and A.K.Jonscher, "Electronic Conduction in Evaporated SiO_x Films", Thin Solid Films, 3 (1969) 341-365

(201) R.C.Hughes, "High Field Electron Properties of SiO_2", Solid State Electronics, 21 (1978) 251-258

(202) Reference (72), page 44

(203) N.Klein, private communications, Summer 1981

(204) P.Wilcox, "A Dielectric Loss Model Based on Interfacial Electron Tunnelling", Can.J.Phys., 50 (1972) 912-924

(205) G.A.Brown, W.C.Robinette Jr., and H.G.Carlson, "Electrical Characterization of Silicon Nitride Films Prepared by Silane Ammonia Reaction", Journal Electrochemical Society, 115 (1968) 948-955

(206) S.M.Sze, "Current Transport and Maximum Dielectric Strength of Silicon Nitride Films", J.Appl.Phys., 38 (1967) 2931-2956

(207) I.T.Johansen, "Electrical Conductivity in Evaporated Silicon Oxide Films", J.Appl.Phys., 37 (1966) 499-507

(208) C.L.Standley and L.I.Maissel, "Some Observations on Conduction Through Thin Tantalum Oxide Films", J.Appl.Phys., 35 (1964) 1530-1534

(209) C.A.Mead, "Electron Transport Mechanisms in Thin Insulating Films", Phys.Rev., 128 (1962) 2088-2093

(210) J.C.Schug, A.C.Lilly Jr., and D.A.Lowitz, "Schottky Currents in Dielectric Films", Phys.Rev.B, 1 (1970) 4811-4818

REFERENCES

(211) P.L.Young, "D.C. Electrical Conduction in Thin Ta_2O_5 Films I. Bulk Limited Conduction", J.Appl.Phys., 47 (1976) 235-2412

(212) S.M.Hu, D.R.Kerr, and L.V.Gregor, "Evidence of Hole Injection and Trapping in Silicon Nitride Films Prepared by Reactive Sputtering", Appl.Phys.Lett., 10 (1967) 97-99

(213) A.K.Sinha and T.E.Smith, "Electrical Properties of Si-N_x Films Deposited on Silicon from Reactive Plasma", J.Appl.Phys., 49 (1978) 2756-2760

(214) M.D.Aggarwal, S.Ashok and S.J.Fonash, "Characterization of Si-N_x Films Prepared by Reactive Ion Beam Sputtering", J.Elect.Mat., 11 (1982) 491-504

(215) M.Meaudre and R.Meaudre, "Low Electric Field Poole Frenkel Effect in R.F. Sputtered SiO_x Films", Thin Solid Films, 61 (1979) 83-88

(216) P.A.Timson and P.Wickens, "The Conduction Process in Silicon Oxide", Thin Solid Films, 5 (1970) R55-R58

(217) G.Jouve et J.Goube, "Conduction Electronique dans les Couches Minces d'Oxyde Anodique Formes sur le Titane", Thin Solid Films, 59 (1979) 361-372

(218) M.Maeda and Y.Arita, "Electrical Properties and Their Thermal Stability for Silicon Nitride Films Prepared by Plasma Enhanced Deposition", J.Appl.Phys., 53 (1982) 6852-6856

(219) H.Krause, "Poole Frenkel Currents in Thermally Grown SiO_2 Films", Phys.Stat.Sol.(a), 74 (1982) K121-K154

(220) Y.Vidadi, S.A.Saraddinov and A.K.Zeinally, "Frenkel-Poole Effect in Phthalocyanine", Sov.Tech.Phys.Lett., 8 (1982) 133-134

(221) C.M.Vodenicharov and M.B.Vodenicharova, "Schottky and Pool-Frenkel Mechanisms of Conductivity in Thin Solid Film Me-GeS-Me Systems", Phys.Stat.Sol.(a), 57 (1980) 483-487

(222) S.Gogi and K.Barua, "D.C. Electrical Properties of Vacuum Deposited CdTe Films", Thin Solid Films, 92 (1982) 227-230

(223) C.Paracchini and G.Schinachi, "Electronic Conduction in Rare Earth Doped CdF_3 Insulating Crystals", J.Phys.C: Solid State Phys., 15 (1982) L627-L630

(224) J.Tyczkowski and M.Kryszewski, "Poole Frenkel Centres in Dielectrics / Kind and Space Density in Plasma Polymerized Organosilicon Films", Phys.Stat.Sol.(a), 78 (1983) 259-265

(225) M.S.Yun, M.Ozaki, K.Yoshino, and Y.Inuishi, "Electrical Conductivity and Photoconductivity in Polymethylpentene", Japanese J.Appl.Phys.I, 22 (1983) 1810-1814

(226) R.Bahri, "Solution Grown Thin Polystyrene Films: I. D.C. Electrical Conduction", J.Phys.D: Appl.Phys., 15 (1982) 677-687

(227) S.J.Ingrey, W.D. Westwood, F.C.Livermore, R.J.Boynton, and B.K.MacLaurin, "Birefringent Waveguides in Thermally Oxidized Nitrogen Doped Sputtered Tantalum Films", Thin Solid Films, 35 (1976) 1-9

(228) S.Maniv, and W.D.Westwood, "Discharge Characteristics For Magnetron Sputtering of Al in Ar and Ar/O_2 Mixtures", J.Vac.Sci.Tech., 17 (1980) 743-751

(229) W.D.Westwood and A.G.Sadler, "Optical Constants of Sputtered Ferrite Films", Canadian.J.Phys., 49 (1971) 1103-1113

(230) K.Barwinkel and H.J.Schmidt, "Numerical Analysis of Normal Reflectance Data as Applied to the Study of Oxide Films on Copper", Thin Solid Films, 59 (1979) 373-383

(231) S.Kumagi and L.Young, "Ellipsometric Investigation of the Optical Properties of Anodic Oxide Films on Tantalum", Journal Electrochemical Society, 111 (1964) 1411-1416

(232) N.Terao, "Structure of Tantalum Nitride", Japanese J.Appl. Phys., 10 (1971) 248-259

(233) M.H.Rottersman and M.J.Bill, "Properties of Planar Magnetron Sputtered Tantalum Films", Thin Solid Films, 61 (1979) 281-288

(234) Reference (4), page 293

(235) J.S.Blakemore, SEMICONDUCTOR STATISTICS, (Pergamon Press, 1962)

(236) A.T.Hunter, et al., "Compensation in Undoped, Liquid Encapsulated Czochralski GaAs", Technical Program of the 1983 Electronic Materials Conference, Burlington, Vermont, June 1983, Paper F-2

(237) V.A.Laleko, and P.A.Raikerus, "Irreversible Changes in Conductivity of Oxide Films on Tantalum in Strong Electric Fields", Sov.Phys.Tech.Phys., 27 (1982) 90-91

(238) L.L.Kazmerski, POLYCRYSTALLINE AND AMORPHOUS THIN FILMS AND DEVICES, (Academic Press, New York, 1980)

(239) H.Ekrut and A.Hahn, "Polarity Dependent Tunneling Conductance of $Ta/Ta_2O_5/Ag$ Junctions", J.Appl.Phys., 51 (1980) 1686-1691

(240) M.Kurata, NUMERICAL ANALYSIS FOR SEMICONDUCTOR DEVICES, (Lexington Books, Lexington, Massachusetts, 1979)

(241) G.Tarr, course notes for "Surface Controlled Semiconductor Devices" given by the Department of Electrical Engineering, Carleton University, Winter 1983

(242) A.Miller, BASIC PROGRAMS FOR SCIENTISTS AND ENGINEERS, (Sybex, Berkeley, 1981) 106